Supramolecular Polymers from Oligophosphodiesters Containing Squaraine or Cyanine Chromophores

Inaugural dissertation

of the Faculty of Science,

University of Bern

presented by

Larysa Markova

from Ukraine

Supervisor of the doctoral thesis:

Prof. Dr. Robert Häner

Department of Chemistry and Biochemistry, University of Bern

Supramolecular Polymers from Oligophosphodiesters Containing Squaraine or Cyanine Chromophores

Inaugural dissertation

of the Faculty of Science,

University of Bern

presented by

Larysa Markova

from Ukraine

Supervisor of the doctoral thesis:

Prof. Dr. Robert Häner

Department of Chemistry and Biochemistry, University of Bern

Accepted by the Faculty of Science

Bern, 03.11.2020

The Dean

Prof. Dr. Zoltan Balogh

Acknowledgements

First of all, I would like to thank Robert for giving me the opportunity to do my Ph.D. thesis in his group.

I am very thankful for the external referee Prof. Dr. Claudia Höbartner and the chairman of the defense Prof. Dr. Norbert Polacek for agreeing to evaluate my work.

During my Ph.D., I was lucky to have two very friendly and high-moral labmates, Giovanni Picca and Henrik Peters. Thank you, guys, for your help and time.

Thanks to Henrik for his help in the writing section about gold nanoparticles, proofreading my thesis, suggestions, and useful discussions.

My thanks to Oleh Vybornyi for his help in the preparation of AFM images.

Of course, my work would not be possible without the support of my friends, Yevgeniya Kovalova and Dina Erzina. Thank you, girls, for our scientific and near-scientific discussions.

My growth and development were not possible without my students. Together with you, I studied and became wiser.

Last but not least, my gratitude to all with whom I worked in Robert's group during 2011–2012 and 2016–2020.

Table of Contents

V

Chapter 1. General Introduction

1.1 Supramolecular Polymers

Many organic compounds for various applications have been synthesized, but the search for new functional materials continues. From the viewpoint of functional materials, supramolecular polymer chemistry is relatively new and opens a whole area of research.

Supramolecular polymers (SPs) are polymeric arrays of monomeric units that are brought together by reversible and highly directional interactions, resulting in polymeric properties in dilute and concentrated solutions, as well as in bulk [1]. Several noncovalent and reversible interactions can lead to the formation of supramolecular polymers [2]. The typical are van der Waals interactions, π–π interactions, electrostatic interactions, and hydrogen bonds [3].
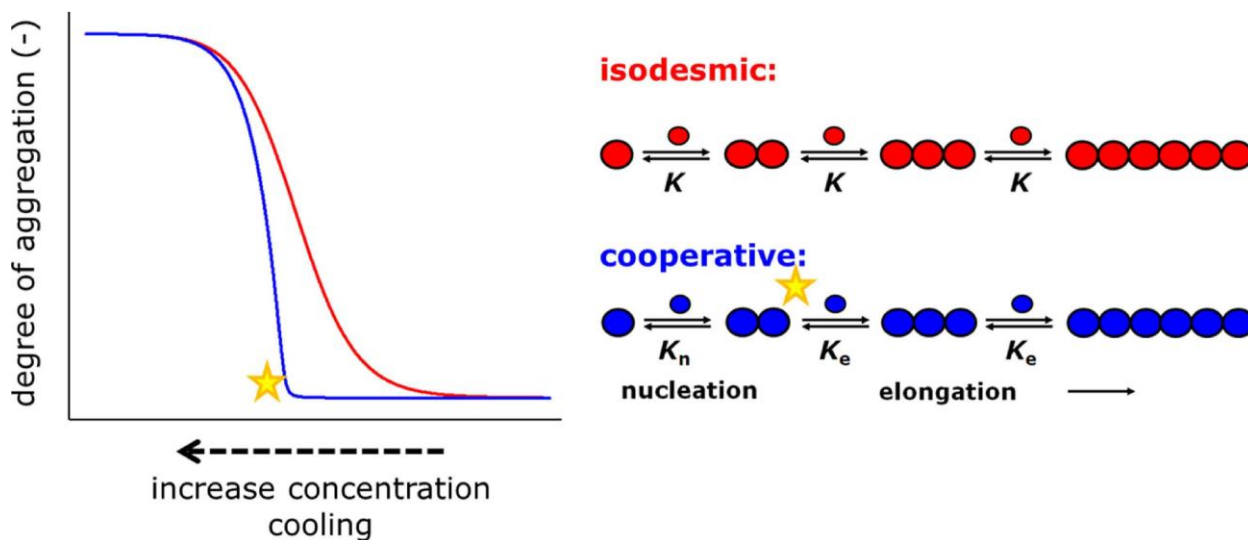
Figure 1.1. Two possible mechanisms of the supramolecular polymerization [4].

Supramolecular polymerization can be described by one of the following mechanisms: 1) stepwise or isodesmic polymerization and 2) nucleation–elongation or cooperative polymerization [4] (Figure 1.1). The isodesmic polymerization is characterized by the reversible formation of a single noncovalent bond identical at all steps of the polymerization process. The binding constant (K) remains unchanged for each reversible step in the assembly pathway [5, 6]. In the cooperative

polymerization, the first phase is the formation of the nucleation center; monomers associate with constant K_n at each step. The second phase is the elongation, the process where the monomers are added to the nucleus. Here, this process happens stepwise as well but with the constant K_e that is higher than K_n [5, 7]. The polymerization mechanisms are characterized by sigmoidal or near-sigmoidal dependence of the degree of aggregation from concentration or temperature. Both mechanisms are displayed in Figure 1.1. Such dependence can be assumed as one of the signs formation of the supramolecular polymers.

The structure of the monomeric building blocks influences the mechanism of the supramolecular polymerization and final morphology of the SPs. As a rule, the polymers are formed according to the isodesmic mechanism when π-stacking is the main driving force of the self-assembly process. The introduction of additional non-covalent forces, for example, H-bonding, is a powerful method to induce cooperativity [8]. Supramolecular polymers often adopt a helical geometry when their formation caused by cooperative polymerization. For example, if the monomeric units are disc-shaped, they lack the freedom of fast rotational motion in the SPs due to strong intermolecular interactions. As a result, the preferred conformation is helical [4].

The SPs form structures with well-defined morphology and can be visualized by microscopic methods such as atomic force microscopy (AFM), transmission electron microscopy (TEM), and scanning electron microscopy (SEM). The simplest examples of the helical structures are nanofibers [9, 10], nanoribbons [11, 12], and nanotubes [13, 14]. Also, the SPs can self-assemble into spheres [15], vesicles [16, 17], nanorods [18], and nanosheets [19], as illustrated in Figure 1.2.

Since SPs are such dynamic systems, their composition continuously changes due to continuous reorganizing and replacing of the building blocks. The main properties of the SPs are caused by the dynamic nature of the non-covalent bonds, such as self-healing [20, 21], stimuli-responsiveness [22, 23], adaptability to their environment [24], and recyclability [25].

Both reversible properties and architecture of the SPs play key roles in the determination of possible application areas. Supramolecular polymerization can be used for the creation of the materials for optoelectronics, self-healing materials, as well as for biological and medical applications [2].
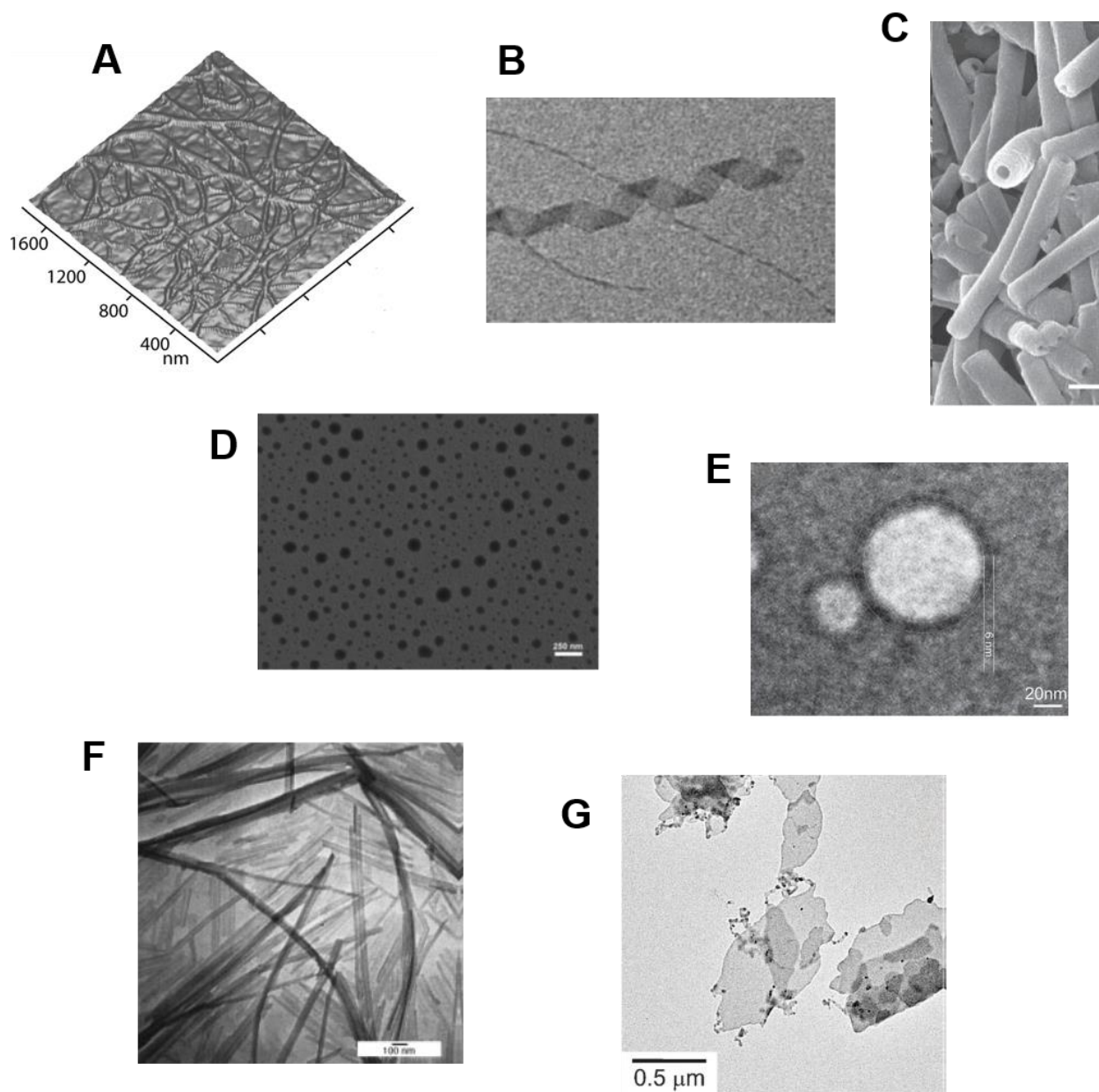
Figure 1.2. A variety of morphologies that SPs can adopt. A: AFM image of nanofibers [9]. B: TEM image of nanoribbons [11]. C: SEM image of nanotubes [13]. D: TEM image of nanospheres [15]. E: TEM image of vesicles [16]. F: TEM image of nanorods [18]. G: TEM image of nanosheets [19].

Optoelectronics can create organic semiconductors with optimized properties by controlled co-assembly of the electron donor and electron acceptor molecules. The desired structures are columnar or helical architectures with alternating donor and acceptor moieties [26, 27]. Other known applications of the materials developed by supramolecular chemistry include

electrochromic polymers for electronic paper, smart windows, photoluminescent polymers for organic light-emitting diodes, plastic solar cells, and organic white-light-emitting polymers.

The concept of supramolecular self-healing materials relies on the ability of noncovalent, transient bonds to generate networks that can heal the damaged sites. Chemical, physical, or thermal stress can induce a mechanic deformation in the fragment of the polymer due to the breaking of local non-covalent bonds. In turn, these bonds recover since they are dynamic and reversible. Supramolecular self-healing materials are characterized by multiple reversible healing cycles. The polymeric networks can be formed by hydrogen bonds, π-π interactions, via ionomers, and coordinative bonds [20]. The examples of the self-healing materials are supramolecular thermoplastic elastomers, dynamic supramolecular hydrogels, and polymer glasses [28],

Applications of supramolecular polymers in biology and medicine include drug delivery [29–31], gene transfection [32, 33], protein delivery [34, 35], bioimaging and diagnostic [36, 37], tissue engineering [38, 39], regenerative medicine [40, 41], and biomimetic chemistry [42–44]. The SPs must meet several specific requirements in order to be applied in biomedical applications, such as excellent biodegradability and biocompatibility, responsiveness to various physiological stimuli in human cells, tissues, organs, targeting, and bioactivity. However, the main requirement is aqueous compatibility since many biochemical reactions and biological processes occur in an aqueous environment [42].

The rational design and description of SPs compatible with an aqueous environment demand special attention regarding the hydrogen bonds of water. In aqueous medium, large nonpolar surfaces impose strong hydrophobic interactions; their strength grows approximately linearly with the size of the nonpolar surface. Polar and charged groups provide solubility in an aqueous medium; they are strongly solvated, contributing to the steric bulk of the aqueous assemblies. The electrostatic repulsion between equally charged groups counterbalances the attractive interactions between hydrophobic moieties. Water, as a highly polar medium, screens electrostatic interactions that lead to the weakening of the attraction between charged groups. In an aqueous environment, the strength of the hydrogen bonds decreases [45].

In general, supramolecular polymers chemistry opens broad perspectives to develop new materials with unique properties that no one other materials can provide. The properties of the SPs are entirely different from the properties of monomers. The possibility of applying SPs in biomedicine is particularly attractive even if this area requests water-compatible materials whose creation and description pose significant challenges.

1.2 Squaraine- and Cyanine-Based Compounds as Building Blocks for SPs

1.2.1 Structure and Properties of the Squaraines and Cyanines

Both squaraine and cyanine dyes belong to the family of polymethines. This chromophore system contains the chain of conjugated double bonds with nitrogen-containing heterocyclic or carbocyclic moieties at the end positions of the polymethine chain (Figure 1.3 and Figure 1.4). While squaraines have a zwitterionic structure, cyanines are positively charged [46].

Squaraine dyes are 1,3-disubstituted derivatives of the 3,4-dihydroxycyclobut-3-ene-1,2-dione (squaric acid). Squaric acid can be substituted directly (Type A) or via a methine bridge (Type B) (Figure 1.3). Squaraines can have unsymmetrical ($X^1{\neq}X^2$) or symmetrical structure ($X^1{=}X^2$) [47]. Furthermore, one of the oxygen atoms of the square core can be acceptor-substituted [48, 49].

The structure of the squaraine molecule is resonance-stabilized. The data of the IR spectroscopy reveal [50] that in symmetrical squaraines, the positive charge delocalizes over the four-membered ring system (Figure 1.3). Besides, the symmetrical Type B squaraines preferably adopt the trans-conformation [51, 52]. In this work, for convenience, the real distribution of the charges and adopted conformation are only presented when it is necessary for discussion.

The structure of the cyanines (cyanine dyes) is characterized by the number of vinylene units in the polymethine chain (n) (Figure 1.4). The dyes with $n = 0, 1, 2, 3$ called mono-, tri-, penta-, and heptamethine cyanines, accordingly. The number n determines the stability of the dye and spectral region where the dye absorbs light.

Type A

Unsymmetrical squaraine dyes   Symmetrical squaraine dyes

Type B

Unsymmetrical squaraine dyes   Symmetrical squaraine dyes

Unsymmetrical acceptor-substituted   Symmetrical acceptor-substituted
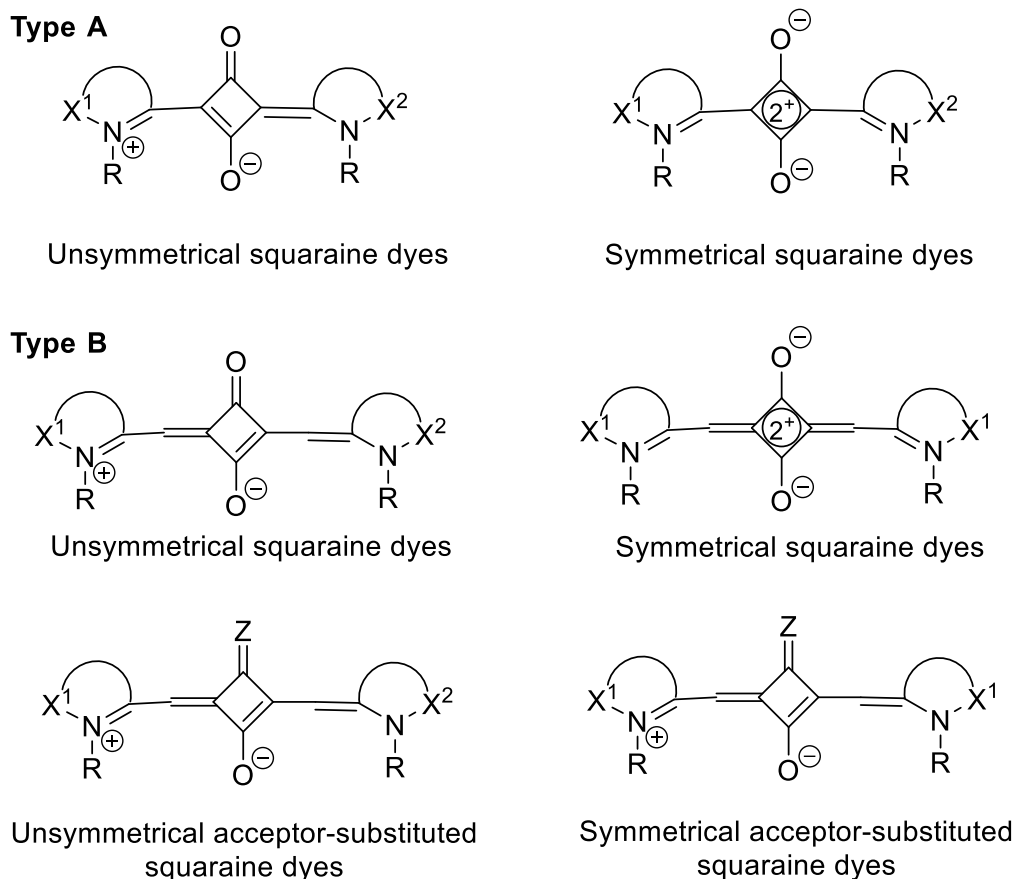squaraine dyes   squaraine dyes

Figure 1.3. The general structure of the squaraine dyes and distribution of the charges in unsymmetrical and symmetrical squaraines.
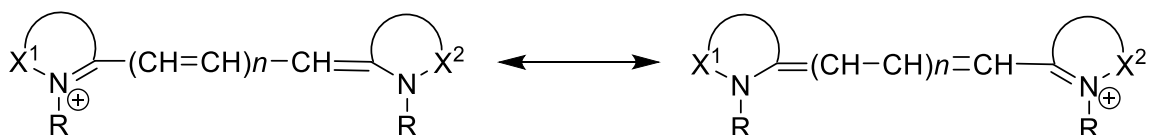
Figure 1.4. The general structure of the cyanine dyes.

Squaraines and cyanines (starting from trimethines) exhibit a strong absorption with high extinction coefficients (up to 260 000 $M^{-1}cm^{-1}$) in the red and near IR region (550–1050 nm) [53–55]. In biomedical applications, long-wavelength fluorescent dyes remarkably decrease the interference caused by the self-absorption and autofluorescence of biomolecules, increase detection selectivity and sensitivity, and reduce damage to the human body [56]. Therefore, squaraines and cyanines are valuable compounds for biology and medicine [57].

The squaraines have some advantages over cyanines. The cyclobutene moiety of the chromophore "rigidly" fixes the links of the polymethine chain. This significantly increases the stability of the squaraines [58]. Besides, fluorescence characteristics of the squaraines, such as quantum yield and fluorescence lifetime, are more sensitive to the microenvironment [59, 60]. Many biomedical analyses are based on measuring changes in the fluorescent characteristics of labels or probes, dyes covalently or non-covalently attached to an analyzed biological object. The more the signal changes, the more sensitive the analysis is. Therefore, squaraines are more attractive for applications based on the measurement of fluorescence.

Another essential property of the squaraines and cyanines is the ability to form aggregates [61–64]. In contrast to well-ordered supramolecular polymers, the aggregates consist of irregular clusters [3]. Squaraines and cyanines are conjugated systems and can form π-stacking interaction between electron-rich and electron-deficient regions of neighboring dye molecules, respectively [65]. Hydrogen bonds, hydrophobic-hydrophilic interactions, van der Waals force, an electrostatic force can also promote aggregation, depending on the dye's structure and the composition of the microenvironment.

The formation of the aggregates leads to the changes in the absorption of the dye, which are caused by exciton interaction between molecules. The dyes can form *H-* and *J*-type dimers and higher aggregates [64, 66]. According to the theory of excitons [66] (Figure 1.5), *H*-aggregates are characterized by a new blue-shifted absorption band in the UV-Vis spectrum. They indicate that the transition dipole moments of the chromophores are oriented parallel. Opposed to this, *J*-aggregates are revealed by a new red-shifted band in the absorption spectrum since the dipoles are organized in a "head-to-tail" fashion. If the absorption spectrum contains both *H-* and *J-* bands (the band of a monomer splits into hypsochromic and bathochromic constituents), then the transition dipole moments arrange obliquely.
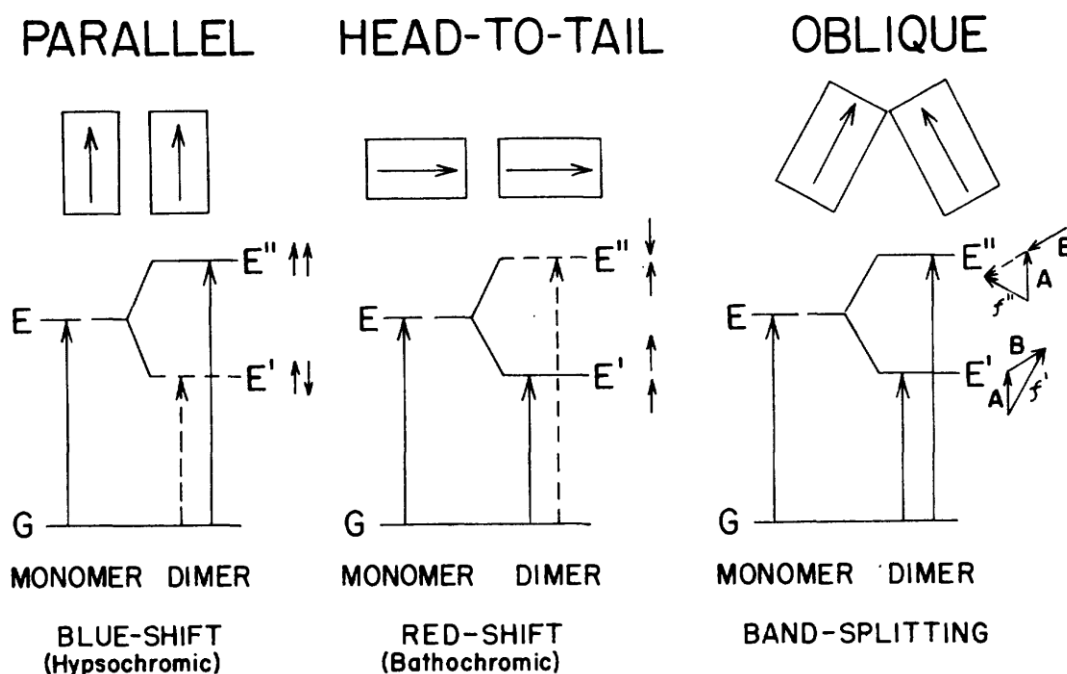
Figure 1.5. Exciton band structure diagrams in molecular dimers with various geometrical arrangements of transition dipole [66]. G: ground state. E: excited state. Solid arrows represent allowed energy transitions. Dashed arrows indicate forbidden energy transitions. Parallel: *H*-aggregate. Head-to-tail: *J*-aggregate.

1.2.2 Self-Assembly of the Squaraines into SPs

The self-assembly of the squaraine compounds described in solutions, thin films, and on surfaces [67–70]. Various approaches have been applied to promote a supramolecular organization in the solution: a combination of "poor" and "good" solvents, increasing the monomer concentration, temperature changes, or the introduction of assembly-promoting additives. In some cases, unusual stimuli such as ultrasound favor the self-assembly process [71].

Ajayaghosh and coworkers [72] performed one of the first works describing squaraine-based SPs. They have demonstrated that in $CHCl_3$/CH_3CN solution, covalently linked squaraine dimers **1a–1c** bind to Ca^{2+} ions to form extended one-dimensional supramolecular arrays where the squaraine dimers arrange in an *H*-like motif (Figure 1.6).
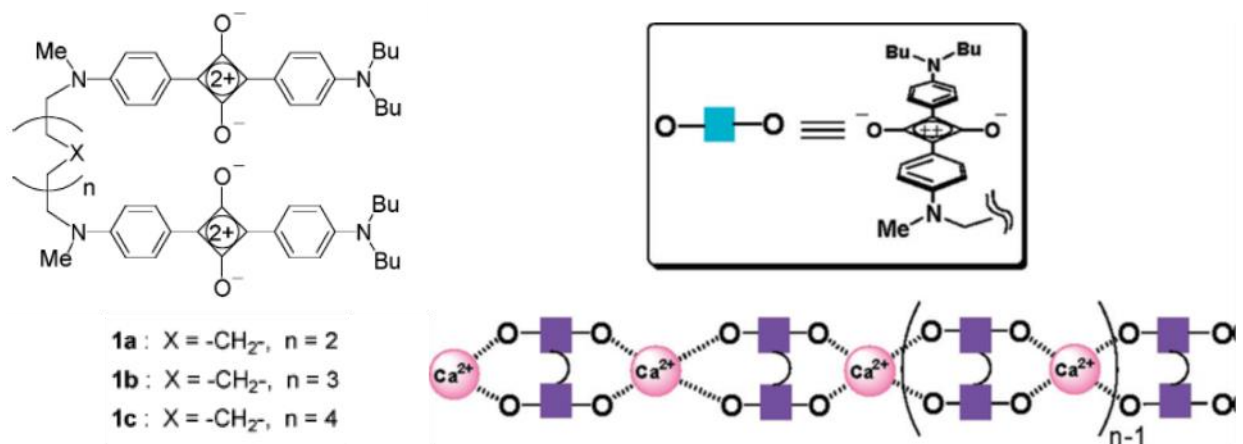
8

Figure 1.6. The linear arrangement of the squaraine units in the one dimensional SPs [72].

In subsequent studies, Ajayaghosh and coworkers presented other examples of the self-assembly of squaraine-based compounds in the presence of Ca^{2+} ions. Catechol-linked squaraine dimer **2** forms spherical micelles in acetonitrile. The micelles reorganize to thermodynamically stable cylindrical rods, as illustrated in Figure 1.7 [73]. Tripodal squaraine dyes self-assemble into nanosized fibers in the presence of Ca^{2+} or Mg^{2+} ions in acetonitrile solution [74].
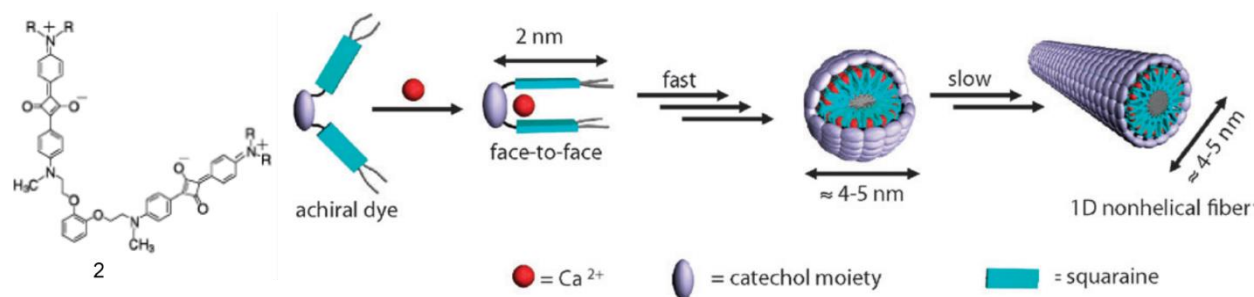

Figure 1.7. Schematic representation of Ca^{2+}-induced self-assembly processes leading to spherical and extended micellar structures [73].

The Würthner group made a noticeable contribution to the study of the supramolecular polymerization of squaraines. It was reported that pyrrole-based squaraine **3** forms extended fiber-like structures in toluene or methylcyclohexane (Figure 1.8). In these assemblies, the squaraine molecules arrange in face-to-face π-stacks, which are stabilized by dispersive interactions and H-bonds. The supramolecular polymerization is described by a cooperative mechanism [75].

Simultaneously, a series of 7-halogenquinolinium-based dicyanomethylene ring-substituted squaraines self-assemble in toluene according to the isodesmic model [76]. The dyes of this series demonstrate the example of noncovalent interactions between halogens and arenes, which, together with π-π stacking and dipole-dipole interplay, drive the polymerization process.
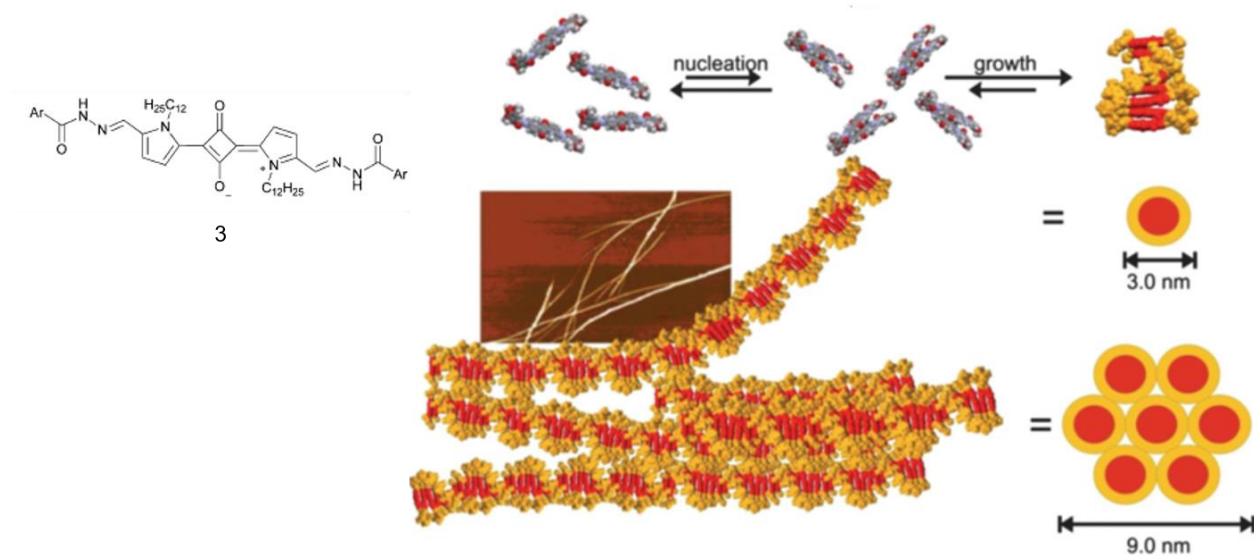

Figure 1.8. Supramolecular polymerization of the pyrrole-based squaraine **3** [75].

The aforementioned supramolecular polymers were created in organic solvents. In aqueous mediums, nonetheless, the SPs of squaraines are hardly known and have only been documented in a few instances [61, 67, 77]. To generate aggregates in aqueous media, water or aqueous acetonitrile or dimethylsulfoxide solutions were used. Some of the studied aggregates are chiroptically active and demonstrate responsiveness to temperature and pH. Considering that microscopic methods have not investigated the morphology of the aggregates, it is not possible to assign these structures to supramolecular polymers.

Self-assembly of amphiphilic aryl-squaramide **4** is a rare example of SPs formation in aqueous medium by compound bearing squaraine core [78]. In phosphate-buffered saline (PBS) or 0.1 M NaOH (pH = 7–8), the aryl-squaramides form well-defined nanofibers. The driving force of the supramolecular polymerization is dipolar π-π interactions between the squaramide rings and the phenyl moieties (Figure 1.9).
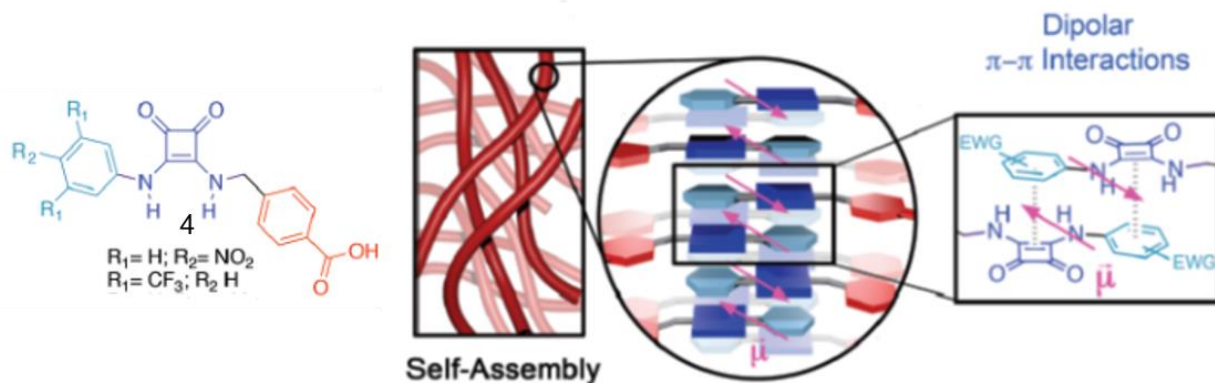
Figure 1.9. Schematic representation of the self-assembly of squaramide **4** in aqueous medium via dipolar π–π interactions. [78].

The squaraine assemblies designed for biomedical applications very often base on copolymer systems. Hydrophobic phospholipid bilayers of liposomes (nanovesicles) with embedded squaraine dyes are promising materials for the near-infrared fluorescence and photoacoustic tomography dual-modular imaging [79]. Formation of the copolymers of squaraine and ATP on the surface of the silica nanoparticles can be used as an assay for ATP [80]. Further, supramolecular assemblies of squaraine and β-cyclodextrin were proposed to detect the thiol-containing amino acids in water [81].

In general, squaraine-based compounds can self-assemble into supramolecular polymers. The typical morphologies of squaraine-based SPs are nanovesicles and nanofibers. A promising approach for creating squaraine-containing SPs in aqueous media is the copolymerization of squaraines with other molecules or the utilization of amphiphilic squaraines as building blocks for supramolecular polymers.

1.2.3 Cyanine-Based SPs

In contrast to squaraines, the aggregation [64, 82], self-assembly [83–85], and supramolecular polymerization [86–88] of the cyanines are well described. It should be mentioned, the first *J*-aggregates were found and studied for pseudoisocyanine more than 80 years ago [89, 90].

For self-assembly in aqueous media, amphiphilic cyanine dyes are of particular interest. The amphiphilic character is superimposed to the dye molecules by covalently adding both

11

hydrophobic alkyl chains and hydrophilic acid groups as substituents [91]. The morphology of the nanostructures formed by amphiphilic cyanine dyes depends on the molecular structure of the chemical substituents of the dye chromophore. The most prominent structural motif is a tubular structure [85, 92]. Self-assembly of cyanine amphiphilic dye **5** into a double-walled tubule is illustrated in Figure 1.10 [93].
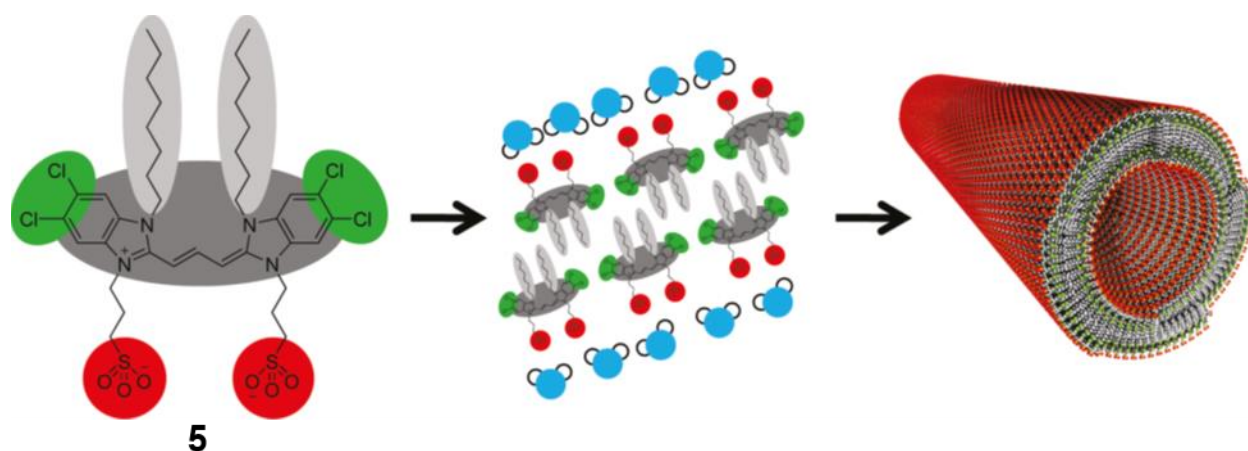

Figure 1.10. Chemical structure of cyanine dye **5**, simple sketch of bilayer formation in water, and 3-D schematic of a helical, double-walled tubule [93].

Another way to create amphiphilic cyanine-containing monomers for self-assembly in aqueous solutions is to prepare block copolymers (BCPs) [94, 95]. A BCP is a system that consists of two or more chemically distinct and typically immiscible blocks that are covalently bound together [96]. The properties and assembly behavior of a block copolymer are dependent on the chemical composition of its component monomers, the length of each block, and the length of the blocks ratio [97].

BCPs containing cyanine molecules showed good characteristics for application in cancer theranostic [98, 99]. Thus, conjugates of cyanine and methoxy poly(ethylene glycol)$_{5k}$-*block*-poly(L-aspartic acid sodium salt)$_{10}$ form nanomicelles that can be used for near-infrared fluorescence imaging-guided photothermal therapy [98]. BCPs constructed from cyanine, polycarborane, polycaprolactone, and poly(ethylene glycol)methyl ether methacrylate self-

assemble into nanomicelles that work as a boron neutron capture therapy agent and near-infrared imaging system [99].

1.3 Synthesis and Self-Assembly of the DNA and DNA-Related Compounds

Self-assembly, the spontaneous association of components into organized structures using noncovalent interactions, is the chief method that nature uses to achieve the complexity of the organization. Of the natural self-assembling molecules, DNA is arguably the most remarkable. DNA has the most predictable and programmable interactions of any natural or synthetic molecule. Currently, the DNA is not just a molecule that stores and transmits genetic information but also a highly promising template for organizing nanomaterials in a programmable way [100, 101].

The classic DNA is a right-handed helical structure consisting of two complementary oligonucleotides [102, 103] (Figure 1.11A). Each DNA strand formed from four repeating and alternating nucleosides — adenosine (A), guanosine (G), cytidine (C), and thymidine (T) that are linked in a strand via phosphodiester groups. (Figure 1.11B). 5-Carbon deoxyribose sugars of the nucleosides with phosphodiester groups form the backbone of the oligonucleotide,
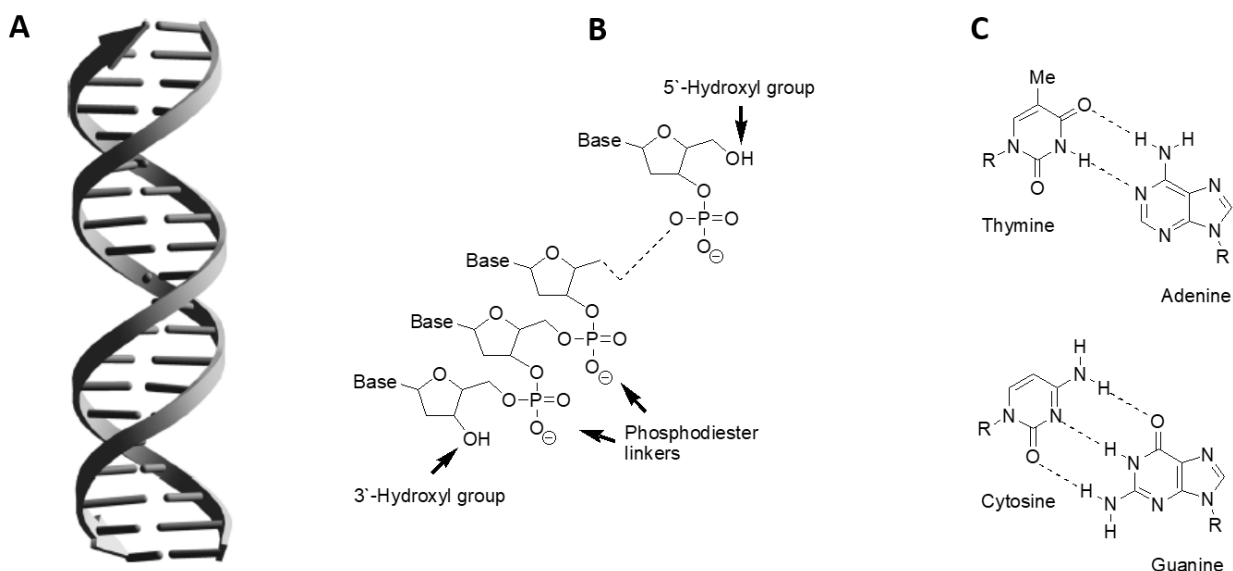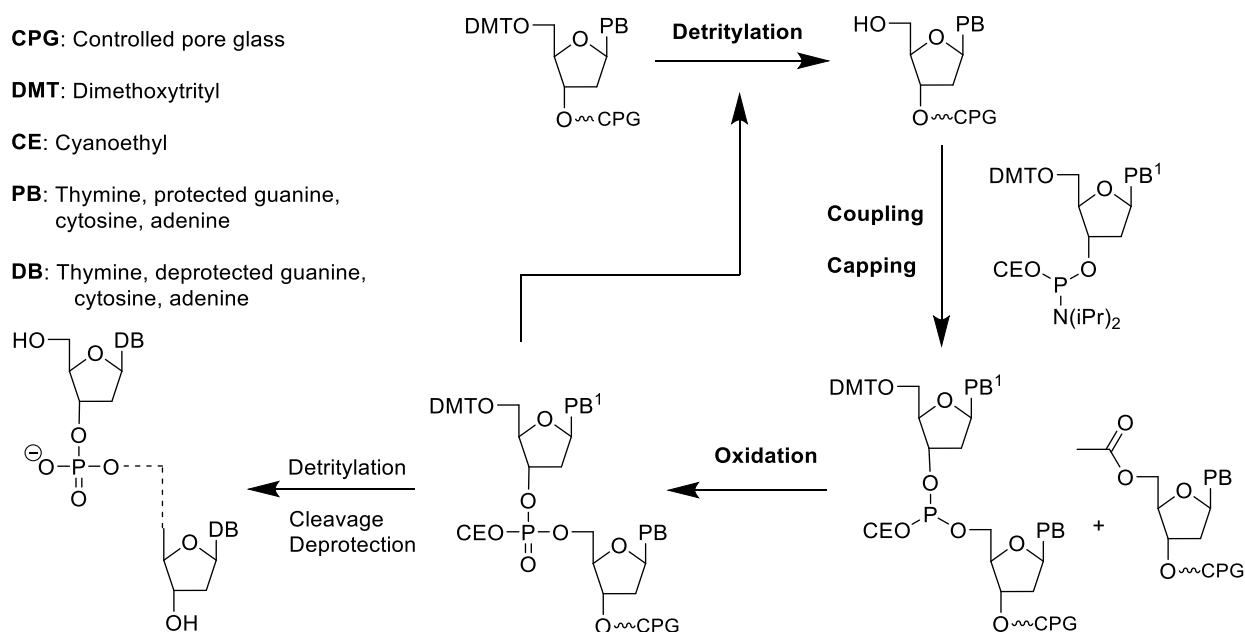

Figure 1.11. A: Schematic DNA double helix [103]. B: Structure of the oligonucleotide strand. C: Formation of hydrogen bonds between complementary base-pairs.

The double-stranded helix is formed and stays stable due to hydrogen bonds between facing nucleobases and aromatic π-π stacking of adjacent nucleobases [104]. Hydrogen bonds are formed between complementary bases of the opposing oligonucleotide strands: two bonds connect thymine and adenine, and three bonds connect cytosine and guanine (Figure 1.11C). Intermolecular aromatic stacking occurs mostly between bases within one strand of the helix, although there is also a contribution of stacking between bases in opposite strands of a duplex. Intrastrand base-stacking serves to preorganize a single strand for binding a target strand. Upon heating, the noncovalent bonds destroy, and the helix dissociates into two single strands; this process is called thermal denaturation. When the complementary strands are cooled in aqueous solution, the double-stranded helix forms again; this process is called hybridization.

The structure and organization of DNA were described more than 65 years ago by Watson and Crick [102]. Since that, the methods for the preparation of the synthetic oligonucleotides were continuously improved [105]. Currently, the solid-phase phosphoramidite approach is the most widely applied [106]. This method bases on the use of the phosphoramidites of adenosine, guanosine, cytidine, and thymidine [107]. To be incorporated into oligonucleotide sequences, the nucleosides must contain two hydroxy groups. In phosphoramidite, one hydroxy group is protected (for example, by 4,4'-dimethoxytrityl, DMT), and the other converted into a monoamide of a phosphodiester. The oligonucleotide synthesis was significantly simplified with the development of the automated DNA synthesizers.

The synthesis consists of the sequential addition of the nucleotides to the growing oligomer sequence [108]. The synthesis is going in the direction from the 3'-end to the 5'-end, and the first nucleotide is covalently attached to the solid support via 3'-position. Every addition is a cycle that includes four steps: detritylation, coupling, capping, and oxidation (Scheme 1.1). Initially (step 1), it is necessary to remove the dimethoxytrityl protecting group from the hydroxy group and make the last one available for the next nucleoside (step 2). The reaction between nucleosides usually occurs with high yield; however, 1–2% of the oligonucleotide with the number of units (n-1) remains unreacted. Therefore, the next step (step 3) is directed on the deactivation by acylation of the shorter oligonucleotide. The last step (step 4) in the cycle is the oxidation of the internucleotide phosphite linker to phosphate. After the synthesis, the oligonucleotide strand is cleaved from the

support by treatment with base. During the synthesis, the primary amine groups of the adenine, guanine, and cytosine must be protected. The final procedure is the deprotection of these nucleobases, which is, typically, combined with the cleavage from the support.

CPG: Controlled pore glass

DMT: Dimethoxytrityl

CE: Cyanoethyl

PB: Thymine, protected guanine, cytosine, adenine

DB: Thymine, deprotected guanine, cytosine, adenine

Scheme 1.1. Solid-phase synthesis of the oligonucleotides using the phosphoramidite approach. Adapted from [108].

The phosphoramidite method and application of the automated DNA synthesizers allow to relatively simply prepare oligophosphodiesters containing not only natural monomers but also artificial molecules or functionalizing groups. The most important here is that the oligophosphodiesters are created with well-defined positioning and the number of unnatural molecules in the sequence.

Several possibilities for the modification of the DNA single-strand exist, as illustrated in Figure 1.12 [109–111]. The functional group of interest can introduce into the nitrogenous bases of the nucleosides [112], or the bases can completely substitute by other molecules [113]. Upon conversion to phosphoramidites, such nucleosides are used for the synthesis of the oligonucleotides. The phosphodiester linkers can be entirely or partly replaced by alternative groups [114, 115]. Modifications can be added to the 3'- or 5'-termini of the strand via phosphodiester linkers [116, 117]. The oligonucleotides can be synthesized with changes in the

backbone when artificial molecules are incorporated into the nucleotide sequence instead of ribose [118–120]. Furthermore, oligomers constructed only from synthetic molecules can be obtained by using phosphoramidite chemistry [121, 122].

Figure 1.12. Possible DNA modifications that are accessible via phosphoramidite chemistry.

Currently, a variety of synthetic labels and modifiers for the phosphoramidite synthesis are commercially available [123]. While cyanine phosphoramidites and even cyanine-modified oligonucleotides can be purchased from different commercial sources, squaraine phosphoramidites are not commercially available, however. To our best knowledge, squaraine phosphoramidite has only been reported once [124].

The phosphoramidite chemistry and automated DNA synthesis have opened access to various compounds, structures, and materials for various applications [101, 125, 126]. For this work, the most important aspect is that DNA and DNA-related compounds, such as modified

oligonucleotides and phosphodiester-linked oligomers, represent valuable building blocks for the creation of the nanostructures and supramolecular architectures.

Interactions of complementary nucleobases drive the assembly of DNA. The driving forces are extremely selective. Therefore, the assembly of DNA is programmable and allows to generate addressable nanostructures in one (1D), two (2D), and three (3D) dimensions [100]. To create a 1D structure, a minimal set of two complementary oligonucleotides is sufficient. More complicated 2D and 3D architectures require several DNA single strands. Two main approaches are used in the preparation of the 2D and 3D structures [100]. The first one utilizes the origami principle [127]: one long ssDNA stapled by many short strands and, thus, arranged in the desired geometry (Figure 1.13A). The second approach [128, 129] uses tiles of the short strands; the short oligonucleotides have sticky ends (complementary nucleotide overhangs) or parts that result in the formation of multihelical 2D or 3D objects upon hybridization (Figure 1.13B). The practical value of the DNA nanostructures is their ability to organize other molecules or particles at the nanoscale level with precise position to each other.
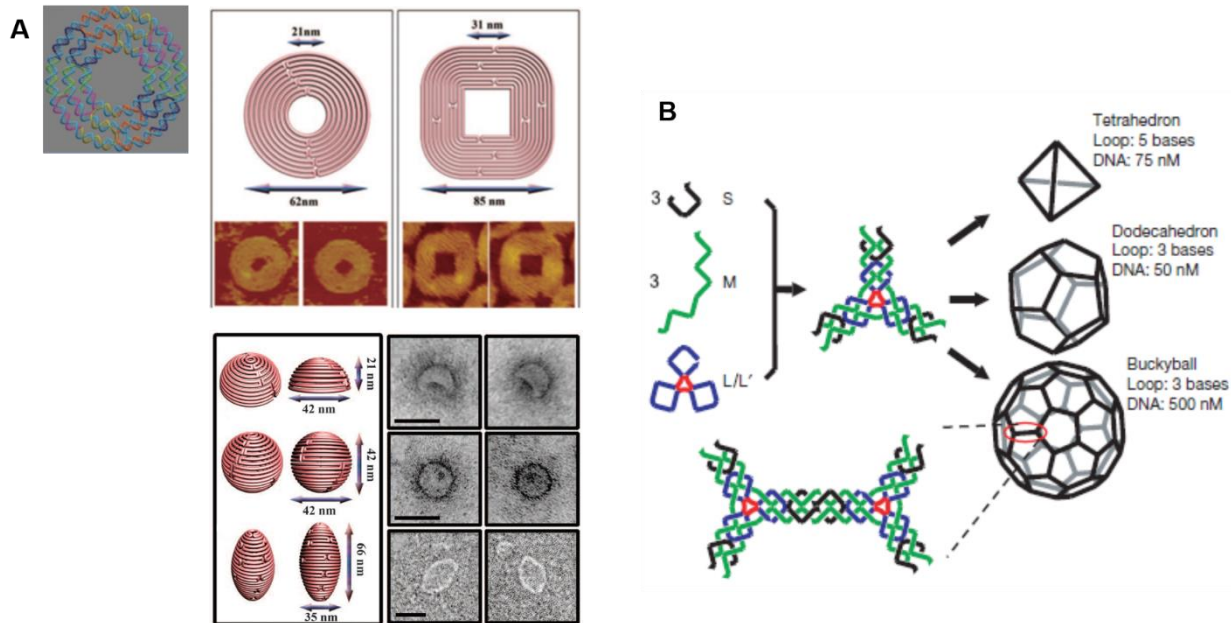
Figure 1.13. A: Applying the origami principle to create curled 2D and 3D DNA nanostructures, adapted from [127]. B: Building of the 3D DNA polyhedral architectures using three-point-star motifs (tiles) [128].

DNAs modified by organic, inorganic, and polymeric structures represent systems where the predictable and programmable nature of DNA is combined with the supramolecular interactions, originated from artificial molecules [130]. In these systems, self-assembly can be caused not only by the hybridization of the complementary nucleobases but also by intermolecular forces that appear between molecules conjugated with DNA. These "dual" interactions result in the formation of hybrid architectures with new functional and structural properties [131, 132].
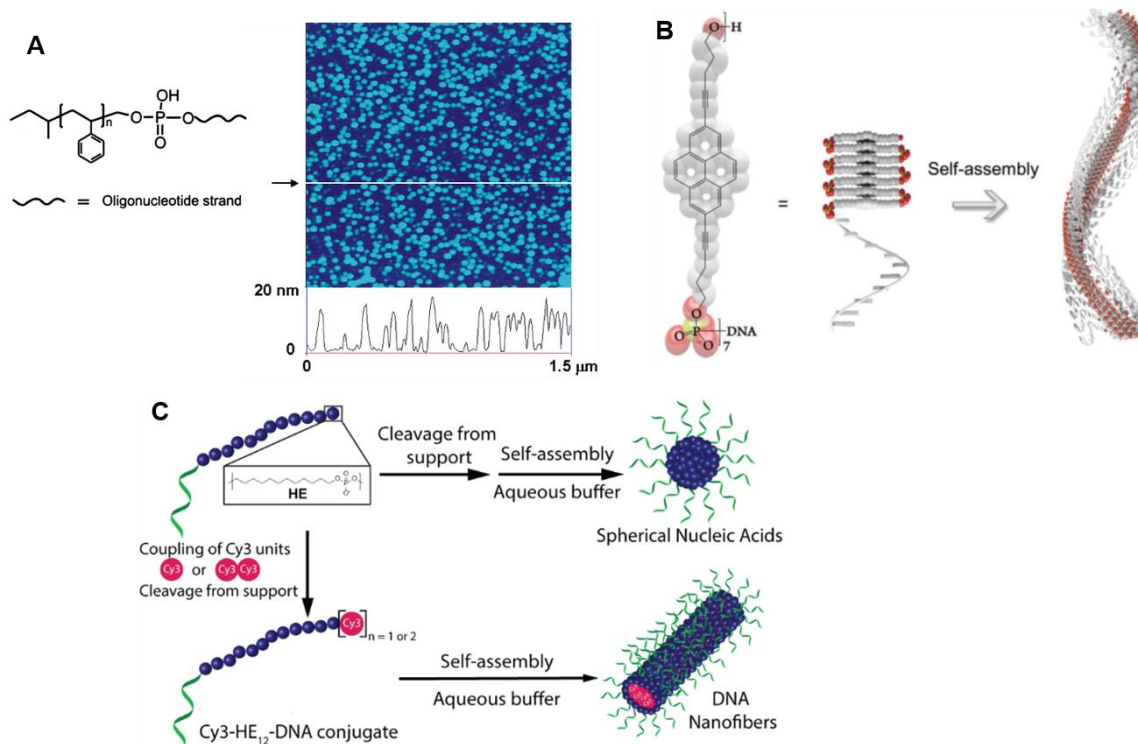
Figure 1.14. Self-assembly of DNA copolymers into SPs. A: Vesicles of polystyrene-DNA, adapted from [133]. B: Ribbon of pyrene-DNA [134]. C: Sphere of hexaethylene-DNA and nanofiber of cyanine-hexaethylene-DNA [94].

The intermolecular non-covalent interactions between the synthetic molecules covalently linked to DNA can be the main driving force of the self-assembly. The DNA-conjugates represent diblock copolymers (or DNA block copolymers) consisting of DNA part and part of artificial molecules [97]. The DNA copolymers self-assemble into ordered structures in a wide range of morphologies, including spheres, fibers, vesicles, and ribbons. For example, polystyrene-DNA copolymers form vesicles [133], pyrene-DNA conjugates adopt ribbon-like geometry [134], hexaethylene-DNA hybrids self-assemble in spheres [94], and cyanine-hexaethylene-DNA copolymers yield nanofibers [94] (Figure 1.14).

Phosphodiester-linked non-nucleosidic oligomers are systems where the DNA part is absent. Thus, the self-assembly of such structures is caused only by non-covalent interactions of the molecules making up the oligomer. The combination of hydrophobic molecules with hydrophilic phosphodiester linkers is a promising approach for creating amphiphilic structures, the potential monomers for SPs in aqueous media. The formation of supramolecular polymers in aqueous media has been described for phosphodiester-linked dimers of anthracene [135], trimers of pyrene [136], and phenanthrene [137] (Figure 1.15). Oligomers containing longer pyrene chains (8 or 14 pyrene units), oligopyrenotides, form assemblies that exhibit remarkable structural analogies to DNA [122].
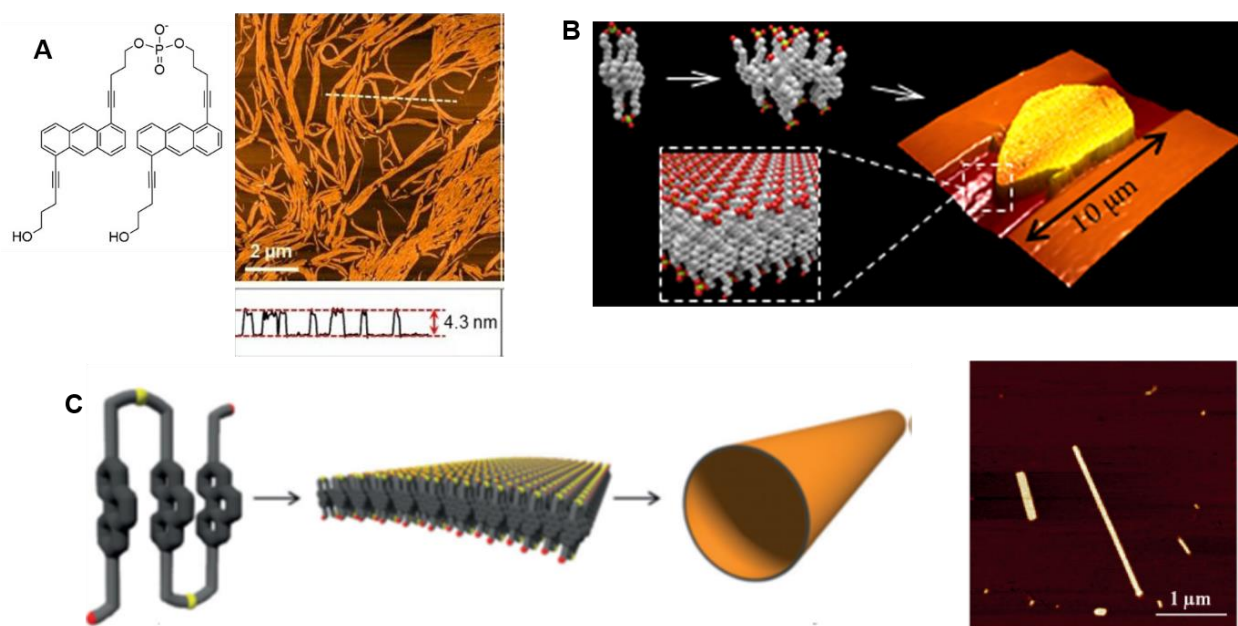
Figure 1.15. SPs formed by phosphodiester-linked oligomers. A: Nanotubes of anthracene dimers, adapted from [135]. B: Nanosheet of pyrene trimers [136]. C: Nanotubes of phenanthrene trimers [137].

In general, DNA-conjugates and phosphodiester-linked oligomers have demonstrated that their self-assembly in aqueous solutions can yield supramolecular polymers. In the vast majority of cases, aromatic or polycyclic aromatic hydrocarbons were used to create building-blocks for SPs. The SPs based on oligonucleotides or oligomers containing charged molecules are almost not known. There are no examples of SPs formed by squaraine-containing oligophosphodiesters, while supramolecular polymers of cyanine (Cy3) DNA-conjugates have been described only recently [94] (Figure 1.14C).

Chapter 2. Supramolecular Polymers Based on Squaraine Chromophores

2.1 Introduction

The aim of this work is the creation of long-wavelength water-compatible supramolecular polymers. Such nanostructures are especially interesting since they can be potentially applied in biology and medicine. Squaraine dyes absorb and emit light in the near-infrared region. Nonetheless, the squaraine molecule is not water-soluble. A possible solution to this challenge is developing amphiphilic structures that would include a hydrophobic squaraine part and a hydrophilic, preferably biocompatible part. These structures can be produced by a combination of squaraines and DNA or squaraines and phosphodiester groups. Phosphoramidite chemistry and automated DNA synthesizers make the synthesis of such oligophosphodiesters possible.

Whole libraries of structures can be prepared by variation of the length and composition of the DNA and squaraine parts. However, only compounds with the well-defined design are potential building blocks for SPs. Over the last decade, several constructions showing supramolecular polymerization behavior in aqueous buffers were developed in our group [135, 138, 139] (Figure 2.1).
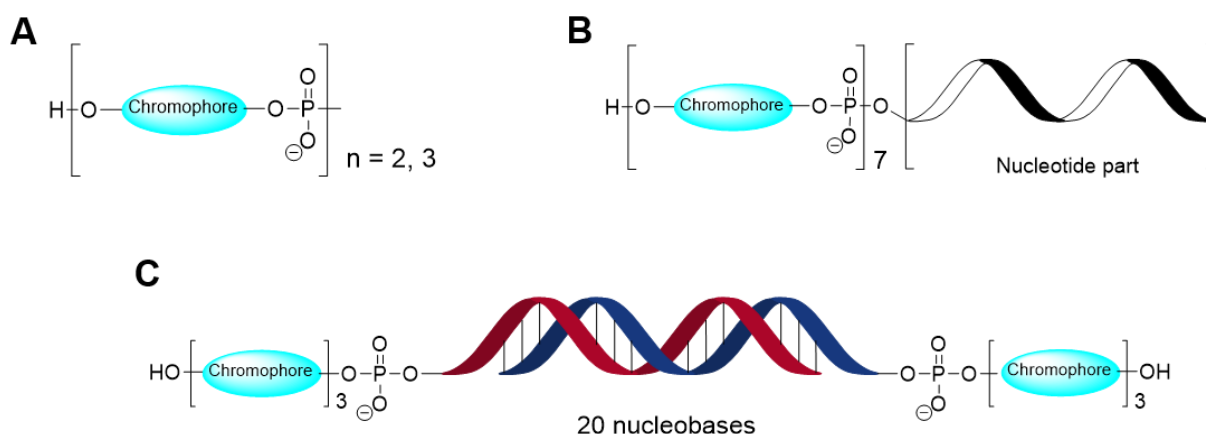
Figure 2.1. Design of oligophosphodiesters that have demonstrated the ability to form SPs in aqueous solutions. A: Short phosphodiester-linked oligomers. B: DNA-conjugates. C: DNA duplex with overhangs.

The first type of monomers — short (dimers or trimers) phosphodiester-linked oligomers [135, 137, 140] — has already been discussed in Chapter 1, section "Synthesis and Self-Assembly of the DNA and DNA-Related Compounds." The supramolecular polymers based on these units adopt different morphologies, including nanosheets and nanotubes (Figure 1.15). Some of the oligomers serve as copolymers in the self-assembly of light-harvesting supramolecular systems [137, 141].

The next class of monomers is conjugates of DNA with chromophores. In this case, the formation of the SPs and their morphology depend on both the length of the DNA and the chromophore parts. On the example of pyrene molecules, it has been shown that the DNA-conjugates built from ten nucleotides and seven pyrenes self-assemble into nanoribbons. In contrast, copolymers with four and one pyrene units form no elongated SPs [138]. Conjugates of one nucleotide and seven pyrenes yield sheets; prolongation of the nucleotide part leads to the formation of supramolecular fibers [142]. Also, the supramolecular process can be sensitive to a complementary oligonucleotide strand in the sample and, thus, yield nanostructures with other morphology [143]. In addition, the DNA part available for hybridization enables further functionalization of the SPs, for example, by nanoparticles [134].

Finally, the DNA duplex formed by two complementary 20-mer oligonucleotides with chromophore overhangs at both ends can also serve as a building block for the SPs. Experiments conducted on the duplex-containing phenanthrenes demonstrated the self-assembly of such a system into large vesicles [139].

The described constructions of the supramolecular monomers are reference points in the rational design of the squaraine-based units for SPs. In this section, we describe the synthesis of the oligophosphodiesters — phosphodiester-linked squaraine oligomers and DNA-squaraine conjugates — and study their supramolecular polymerization in aqueous ethanol solutions.

2.2 Results and Discussion

2.2.1 Synthesis of the Squaraine-Containing Oligophosphodiesters

To obtain squaraine-based monomers for water-compatible SPs, we took into account the experience of our group (see Chapter 2, section "Introduction"). We synthesized several squaraine (Sq)-containing oligophosphodiesters whose structures and yields after isolation are shown in Table 2.1. The chemical structure of the squaraine unit is shown in Figure 2.2. The list of the oligophosphodiesters includes phosphodiester-linked squaraine homo-oligomers containing three (**SqTr**) and six (**SqHex**) squaraine units, DNA–squaraine conjugates consisting of ten nucleotides and a variable squaraine part (one (**Sq1** and **cSq1**), three (**Sq3** and **cSq3**), and six (**Sq6** and **cSq6**) squaraine molecules), as well as conjugates constructed from 20 nucleobases and three squaraine units at terminus positions (**Sq3-ON20** and **cSq3-ON20**).
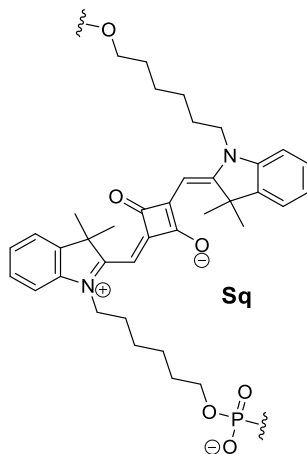
Figure 2.2. The structure of the squaraine unit.

The synthesis of the oligomers performed via phosphoramidite chemistry using a DNA synthesizer. Squaraine phosphoramidite for the synthesis was prepared according to a published procedure [124].

Table 2.1. Name, sequence, and yield of the squaraine-containing oligophosphodiesters.

Name	Sequence	Yield, %
SqTr	Sq-Sq-Sq	21%
SqHex	Sq-Sq-Sq-Sq-Sq-Sq	11%
Sq1	Sq-CTC ACG GAA G – 3'	16%
cSq1	Sq-CTT CCG TGA G – 3'	15%
Sq3	Sq-Sq-Sq-CTC ACG GAA G – 3'	11%
cSq3	Sq-Sq-Sq-CTT CCG TGA G – 3'	10%
Sq6	Sq-Sq-Sq-Sq-Sq-Sq-CTC ACG GAA G – 3'	12%
cSq6	Sq-Sq-Sq-Sq-Sq-Sq-CTT CCG TGA G – 3'	13%
Sq3-ON20	Sq-Sq-Sq-CTT CCT TGC ATC GGA CCT TG – 3'	20%
cSq3-ON20	Sq-Sq-Sq-CAA GGT CCG ATG CAA GGA AG – 3'	14%

While planning the synthesis of the modified oligonucleotides on the DNA synthesizer, the most important is the correct choice of nucleobase protection and deprotection conditions. The choice depends on the stability of the artificial molecules used for the synthesis. The squaraine chromophore decomposes when concentrated ammonium hydroxide (the commonly applied solution) is used for deprotection and remains chemically stable upon deprotection with 50 mM potassium carbonate in methanol (UltraMild deprotection solution, GlenResearch) [124] (Figure 2.3). Using the potassium carbonate solution requires specially protected nucleobases — phenoxyacetyl-protected dA, 4-isopropyl-phenoxyacetyl-protected dG, and acetyl-protected dC. Also, phenoxyacetic anhydride must be used instead of acetic anhydride in the capping solution. This modification eliminates the possibility of an exchange of the protecting group on the dG with acetate from the acetic anhydride capping mix [123].

The squaraine homo-oligomers **SqTr** and **SqHex** consist of only non-nucleosidic molecules. Therefore, their synthesis performed with commonly applied reagents (standard conditions, see Chapter 2, "Experimental Section"), but the cleavage from the support was conducted in potassium carbonate solution to avoid the destruction of the squaraine chromophores. This allowed synthesis squaraine trimer **SqTr** with a yield of 21% and squaraine hexamer **Sq6** with a yield of 13%.
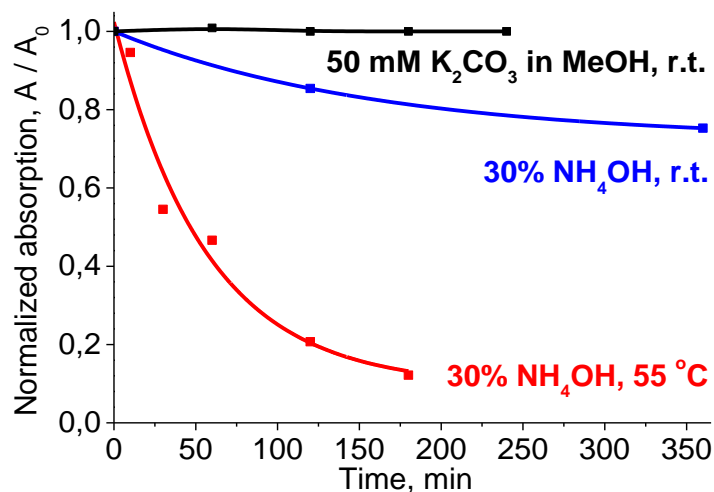
Figure 2.3. The decay of the long-wavelength absorption band of the squaraine chromophore after treatment by 30% NH₄OH (r.t. and 55ºC) and K_2CO_3 in MeOH (r.t.). A/A_0 – relative absorption, where A_0 is the absorption intensity at the starting point, and A is the absorption intensity at the respective time-point.

Oligonucleotides **Sq1**, **cSq1**, **Sq3**, **cSq3**, **Sq6**, and **cSq6** contain both squaraine and nucleotide parts. These structures synthesized according to the UltraMild protocol with yields 10–16%. The yield of the oligonucleotides depends on the quality of the squaraine phosphoramidite. We also found that the impurities in capping and oxidizing solutions, which appear during their utilization, can dramatically decrease the yield of the squaraine-modified oligonucleotides. Squaraine phosphoramidite and the isopropyl-phenoxyacetyl protected dG are the most sensitive to the impurities: the decrease in the rate of incorporation of these units observed after 1–2 days of using freshly opened reagents. Thus, the UltraMild synthesis of the squaraine-modified oligonucleotides requires fresh reagents.
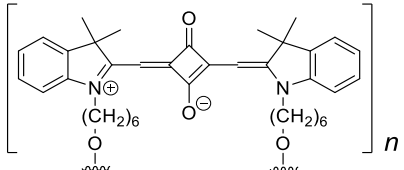
During the synthesis of the relatively long strands **Sq3-ON20** and **cSq3-ON20**, we attempted to abandon the UltraMild protocol and apply the standard conditions. The application of dmf-protected dG and benzyl-protected dA is not compatible with the potassium carbonate deprotection solution; on the other hand, the Sq molecule decomposes in concentrated ammonium hydroxide. The answer to this problem was found in using *t*-butylamine/methanol/water (1:1:2) solution for the deprotection [117]. The oligonucleotides **Sq3-ON20** and **cSq3-ON20** were isolated with yields of 20% and 14%, accordingly, which is in the same range as the other synthesized squaraine oligomers (Table 2.1).

2.2.2 Supramolecular Polymers of Phosphodiester-Linked Squaraine Oligomers

In this section, we describe the aggregation and supramolecular polymerization of the squaraine oligomers — **SqTr** and **SqHex** — in aqueous ethanol solutions containing sodium chloride (NaCl) and 10 mM of phosphate buffer (PB, pH=7.0). In the oligomers, three (**SqTr**) or six (**SqHex**) units are linked via phosphodiester groups.

In the beginning, we studied spectral properties of the trimer **SqTr** and hexamer **SqHex** in ethanol, the solvent in which the non-aggregated state of the oligomers is expected. Absorption [λ(Abs)] and fluorescence maxima [λ(Fl)], molar absorptivities (ε), and fluorescence quantum yields (Q.Y.s) are given in Table 2.2. The spectral characteristics of squaraine diol **SqMon** [124] were added for comparison.

Table 2.2. Spectral properties of the squaraine oligomers in ethanol at concentration $c = 1\ \mu M$, λ(Ex) = 590 nm.

Name	Structure	λ(Abs), nm (ε, M^{-1} cm^{-1})	λ(Fl), nm	Q.Y., %
SqMon	$n=1$	260 (11 000) 632 (258 000)	641	27.3
SqTr	$n=3$	260 (33 000) 632 (774 000)	648	6.3
SqHex	$n=6$	260 (66 000) 632 (1 548 0000)	654	3.2

The oligomers **SqTr** and **SqHex** absorb light in the same spectral region as monomer **SqMon** (Figure 2.4A). The maximum of the main absorption band was determined at 632 nm for all squaraine compounds. The absorption spectra contain a blue-shifted shoulder at 594 nm. For the oligomers, the intensity of the shoulder is about two times higher than for monomer (Figure 2.4B).
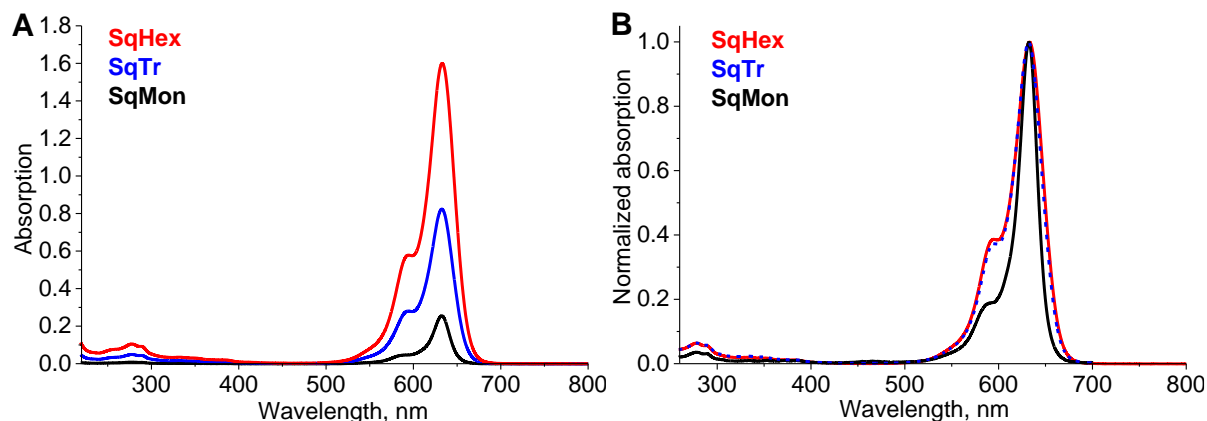
Figure 2.4. A: Absorption spectra of the squaraine oligomers **SqTr** (blue) and **SqHex** (red) in comparison with the spectrum of squaraine diol **SqMon** (black). B: Normalized absorption spectra. Conditions: ethanol, $c = 1$ μM.

The synthesized oligomers exhibit extra high molar absorptivities in the long-wavelength region. Taken into count that the absorptivity of **SqMon** is 258 000 M^{-1}cm^{-1} [124], the absorptivities of **SqTr** and **SqHex** can be calculated as 774 000 M^{-1}cm^{-1} and 1 548 0000 M^{-1}cm^{-1}, respectively.

The studied squaraine compounds emit light in the region between 541 nm and 654 nm, with quantum yields 3.2–27.3% (Table 2.2, Figure 2.5). The Q.Y.s decrease with increasing oligomer length: **SqMon** (27.3%) > **SqTr** (6.3%) > **SqHex** (3.2%). The significant reduction of the Q.Y.s together with an increase of the absorption of the blue-shifted shoulder in the UV-Vis spectrum can be caused by the formation of weakly or completely non-fluorescent *H*-aggregates.
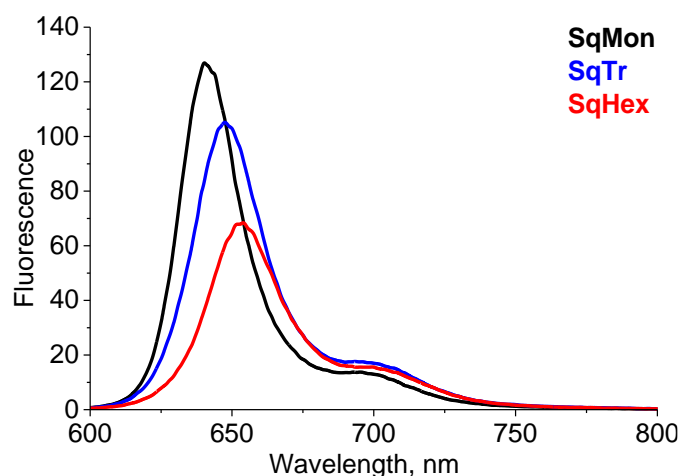
Figure 2.5. Fluorescence spectra of the squaraine oligomers **SqTr** (blue) and **SqHex** (red) in comparison with the spectrum of squaraine monomer **SqMon** (black). Conditions: ethanol, $c = 1$ μM, λ(Ex) = 590 nm.

To determine whether the aggregation is intramolecular or intermolecular, the absorption spectra of the oligomers were measured in a wide range of concentrations. The shape and position of the long-wavelength absorption band of **SqTr** are almost similar in 3.5×10^{-5} M to 10^{-7} M concentration range (Figure 2.6A), which indicates the absence of the intermolecular interactions and confirms folding due to intramolecular forces. The same conclusions can be made for ethanol solutions of oligomer **SqHex** with concentrations between 2.2×10^{-5} M and 10^{-6} M (Figure 2.6B).
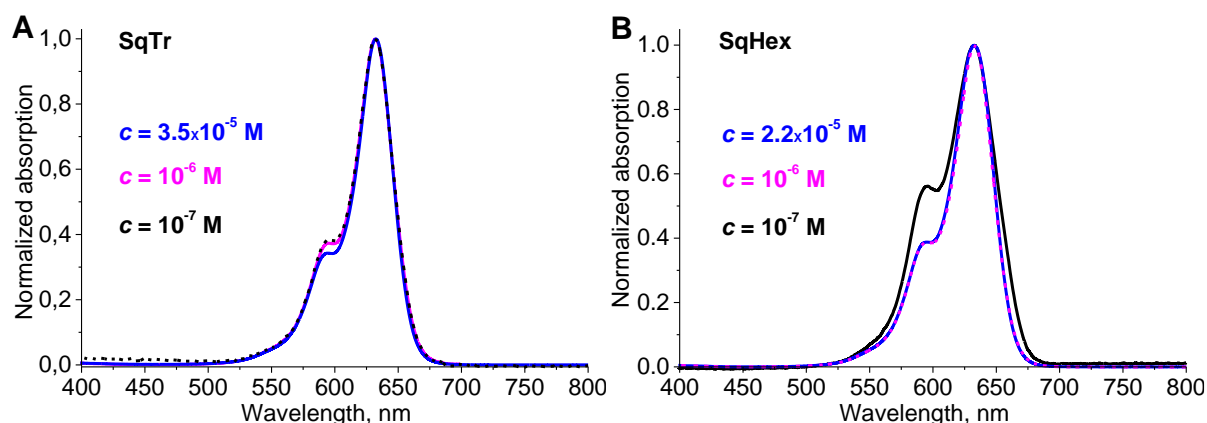
Figure 2.6. Normalized absorption spectra of the oligomers measured in ethanol solutions with a concentration between 10^{-5} M and 10^{-7} M. A: **SqTr**. B: **SqHex**.

Next, we studied the spectral characteristics of the squaraine oligomers in aqueous solutions (Figure 2.7). As a reference point, we chose solutions containing 1 μM of oligomer, 10 mM of PB, and 100 mM of NaCl. The absorption and fluorescence spectra were investigated depending on the percentage of ethanol in the solution. The appearance of *H*- and *J*- bands in the absorption spectra and decrease in the fluorescence intensity indicate the formation of aggregates, *i.e.* potential supramolecular polymers (SPs).

The shape of the absorption spectrum and the intensity of the fluorescence strongly depend on the concentration of ethanol in a solution. At ethanol concentrations of 2–20% by volume, the absorption spectrum of **SqTr** shows a splitting of the main band (M, around 633 nm) on more long-wavelength *J*-band (about 658 nm) and more short-wavelength *H*-band (around 590 nm). According to the exciton theory of Kasha, this phenomenon indicates an oblique orientation of the transition dipole moments of chromophores in aggregates [66, 144]. In the range of ethanol

concentrations of 20–30%, the *J*-band has completely disappeared. Starting from 30% of EtOH in the mixture, the intensity of the *H*-band decreases, and the intensity of the main band starts to increase. The absorption spectrum of **SqHex** demonstrates a similar response to the change of ethanol quantity in the solution. However, the quenching of the *J*-band was observed when the concentration of ethanol was at 25–35%.
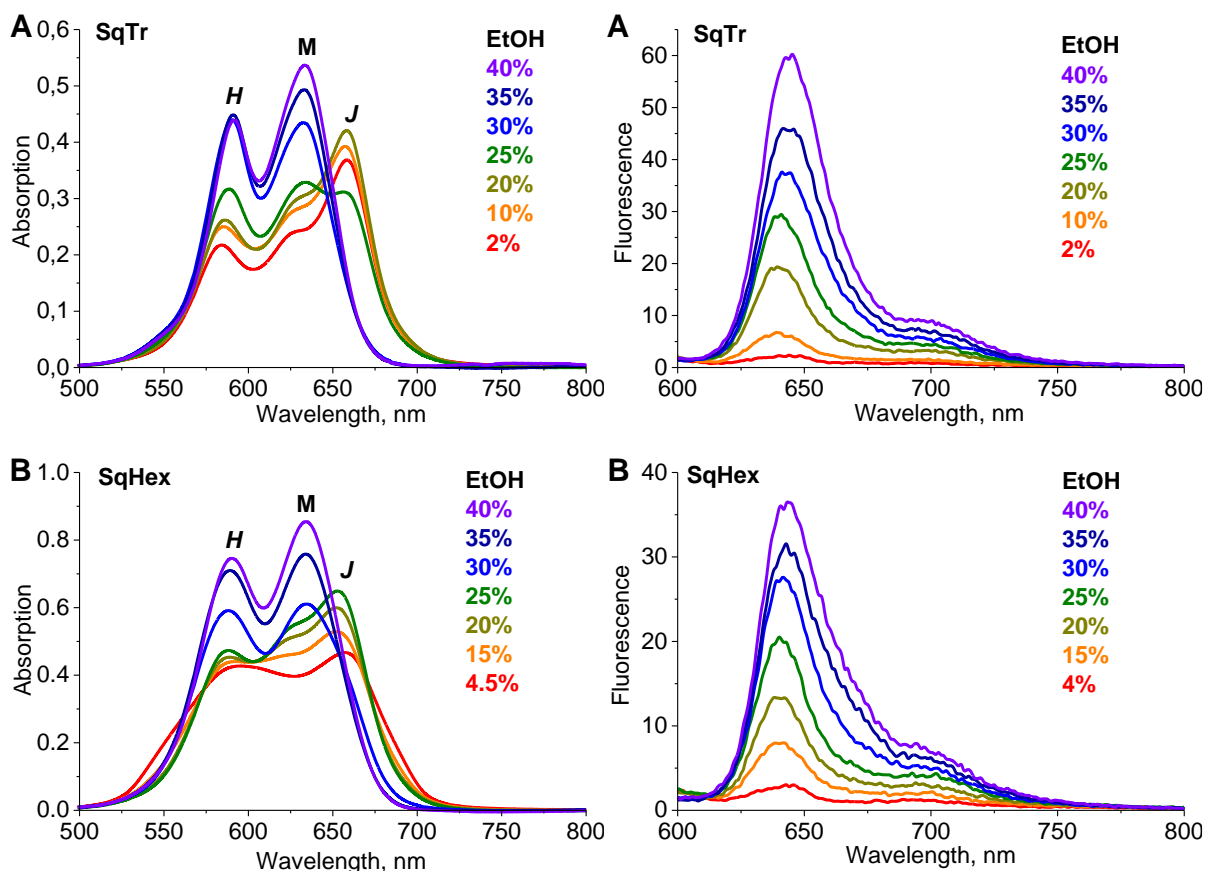
Figure 2.7. Absorption (left) and fluorescence (right, λ(Ex) = 585 nm) spectra of the oligomers **SqTr** (A) and **SqHex** (B) depending on the concentration of ethanol in the solutions. Conditions: conc. of oligomer 1 μM, 100 mM NaCl, 10 mM PB. Heating-cooling runs with a rate of 10 ºC/min were performed before the measurements.

The fluorescence of the oligomers is almost undetectable when the concentration of ethanol is 2% (**SqTr**) and 4% (**SqHex**). The fluorescence intensity increases proportionally to the quantity of ethanol in the solution caused by the decomposition of non-fluorescent aggregates.

Finally, we studied the supramolecular properties of the above-described aggregates. To determine whether the *H*-aggregates or the aggregates with split absorption bands are supramolecular

polymers, we investigated the temperature dependence of their absorptions. In the thermal experiments, the samples were cooled from 75 ºC to 20 ºC with a rate of 0.5 ºC/min. In the case of supramolecular polymerization, the temperature-absorption dependence adopts a characteristic sigmoidal or quasi-sigmoidal appearance. Furthermore, the supramolecular polymers represent large regular objects that can be visualized by microscopic methods. For the sake of convenience, temperature-dependent assembly–disassembly experiments will be referred to as 'thermal experiments.'

H-aggregates of oligomers **SqTr** and **SqHex** show no signs of SP formation. The dependence of absorption from temperature is close to linear (Figure 2.8, top). The aggregates are small and irregular as established by atomic force microscopy (Figure 2.8, bottom).
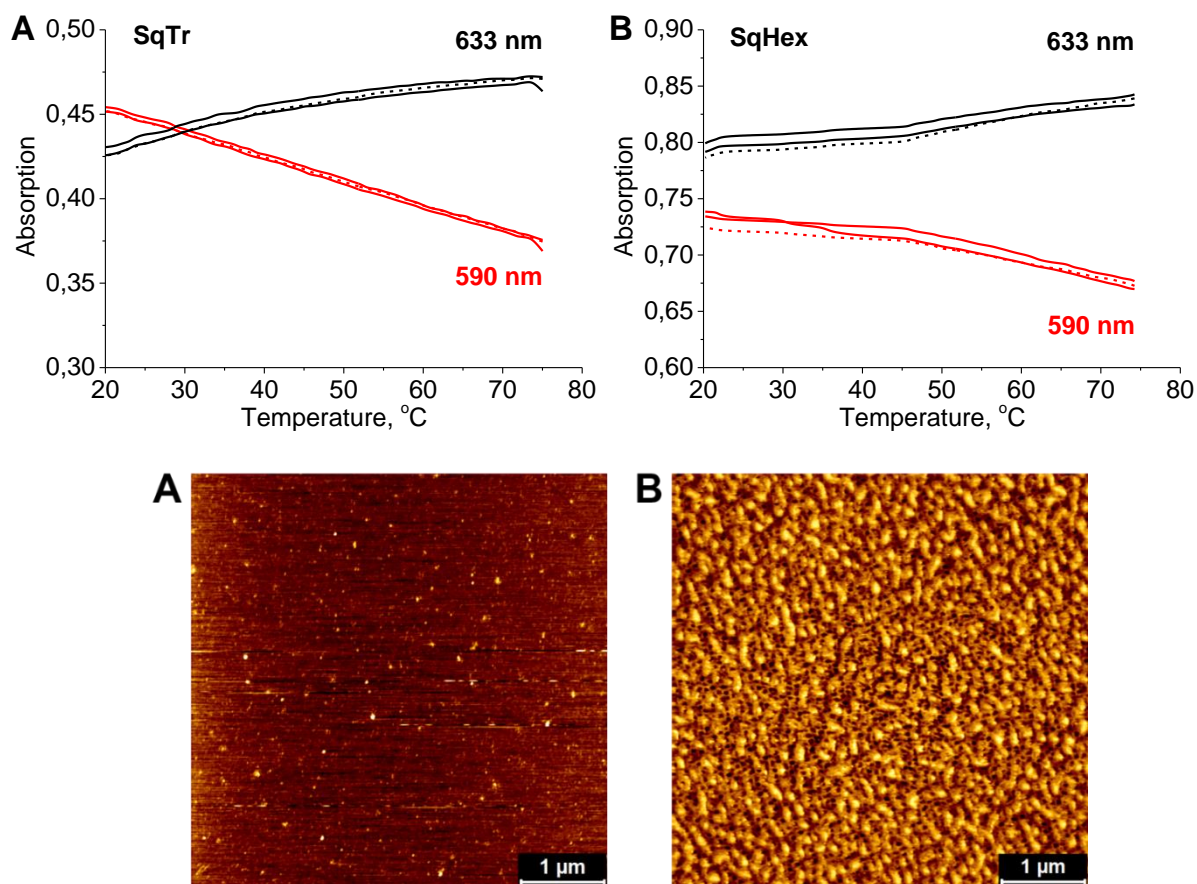
Figure 2.8. Data for *H*-aggregates of **SqTr** (A) and **SqHex** (B). Top: Temperature-dependent UV-Vis absorption spectrum of **SqTr** and **SqHex** registered at 590 nm (red) and 633 nm (black). Solid lines — cooling, dashed lines — heating. Bottom: The view of the nanostructures formed by **SqTr** and **SqHex**. Conditions for **SqTr**: conc. 1 µM, 30% EtOH, 100 mM NaCl, 10 mM PB. Conditions for **SqHex**: conc. 1 µM, 35% EtOH, 100 mM NaCl, 10 mM PB.
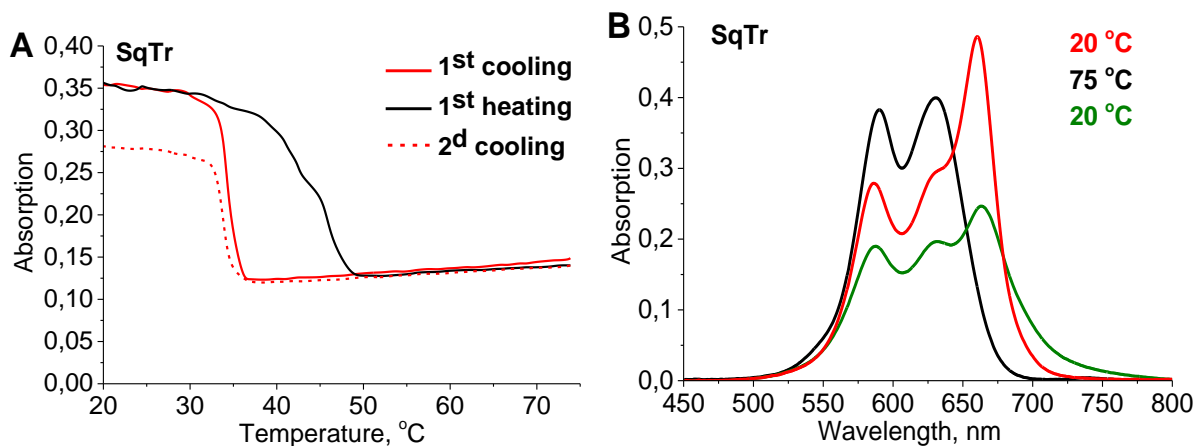
Figure 2.9. Supramolecular polymerization of the **SqTr**. A: Thermal experiment (registration at 660 nm) demonstrated precipitation during the self-assembly process. Solid red line — 1ˢᵗ cooling, solid black line — heating, dashed red line — 2d cooling. B: Absorption spectrum measured at 20 °C before the beginning of the experiment (red), at 75 °C before the first cooling (black), and at 20 °C after the second cooling run (green). Conditions: 1 µM **SqTr**, 20% EtOH, 75 mM NaCl, 10 mM PB.

In contrast to the *H*-aggregates, the aggregates with a split absorption band can self-assemble to SPs. Temperature-responsive SPs of **SqTr** associate when the sample contains 15–25% EtOH (conc. **SqTr** 1 µM, NaCl variable and depends on EtOH concentration, PB 10 mM) as can be determined with temperature-dependence experiments (Figure 2.9A). At lower concentrations of ethanol, the aggregates do not dissociate with increasing temperature; at higher concentrations of EtOH, the SPs do not assemble. Oligomer **SqHex** forms thermally-responsive SPs when the amount of ethanol in the aqueous solution is between 20 and 25% (conc. NaCl variable).

The process of supramolecular polymerization of **SqTr** and **SqHex** is accompanied by the precipitation of the formed nanostructures. After heating–cooling runs, the intensity of the long-wavelength band is noticeably lowered, as demonstrated for oligomer **SqTr** in Figure 2.9B. Thus, the SPs of the oligomers are only partially reversible.

Atomic force microscopy was used to determine the morphology of SPs. The samples were deposed on a mica substrate modified with (3-aminopropyl)-triethoxysilane (APTES). This method is commonly used for the visualization of DNA [145, 146]. In aqueous solutions, the DNA attaches to the substrate due to interactions between positively charged amino-groups of the modified mica and negatively charged phosphodiester groups of the duplex. Although the squaraine oligomers contain phosphodiester groups, large objects of interest were not observed on

the APTES-modified mica. Besides, no nanostructures with regular morphology were found on unmodified mica. Thus, SPs of squaraine oligomers **SqTr** and **SqHex** cannot be visualized by AFM on the mica substrate.

2.2.3 Supramolecular Polymers of Squaraine-Modified Oligonucleotides

In this section, we describe aggregation and supramolecular polymerization of the squaraine-modified oligonucleotides **Sq1**, **cSq1**, **Sq3**, **cSq3**, **Sq6**, and **cSq6**. The DNA-squaraine conjugates contain ten nucleotides and a variable squaraine part; the number after "Sq" determines the number of units in the squaraine segment. The oligonucleotide sequences in the line **Sq1**, **Sq3**, and **Sq6** are identical. In pairs **Sq1** and **cSq1**, **Sq3** and **cSq3**, and **Sq6** and **cSq6**, the oligonucleotide parts are complementary (Table 2.3).

Absorption and fluorescence characteristics of the squaraine-modified oligonucleotides measured in ethanol at concentration 1 µM (absence of intermolecular aggregation is assumed) are given in Table 2.3.

Table 2.3. Spectral properties of the squaraine-modified oligonucleotides in ethanol ($c = 1$ µM, λ(Ex) = 590 nm).

Name	Structure	λ(Abs), nm	λ(Fl), nm	Q.Y., %
Sq1	Sq-CTC ACG GAA G – 3'	633	641	33
cSq1	Sq-CTT CCG TGA G – 3'	634	643	32
Sq3	Sq-Sq-Sq-CTC ACG GAA G – 3'	633	643	9.7
cSq3	Sq-Sq-Sq-CTT CCG TGA G – 3'	634	647	9.6
Sq6	Sq-Sq-Sq-Sq-Sq-Sq-CTC ACG GAA G – 3'	633	647	4.4
cSq6	Sq-Sq-Sq-Sq-Sq-Sq-CTT CCG TGA G – 3'	634	652	4.5

The absorption spectra of the squaraine-modified oligonucleotides consist of a long-wavelength band with a maximum at 633–634 nm, caused by squaraine absorption, and a band situated in the ultraviolet region at about 260 nm that appears due to transitions in both the squaraine ($\varepsilon = 11\,000$ M^{-1} cm^{-1}) and the oligonucleotide parts (Figure 2.10A).

31
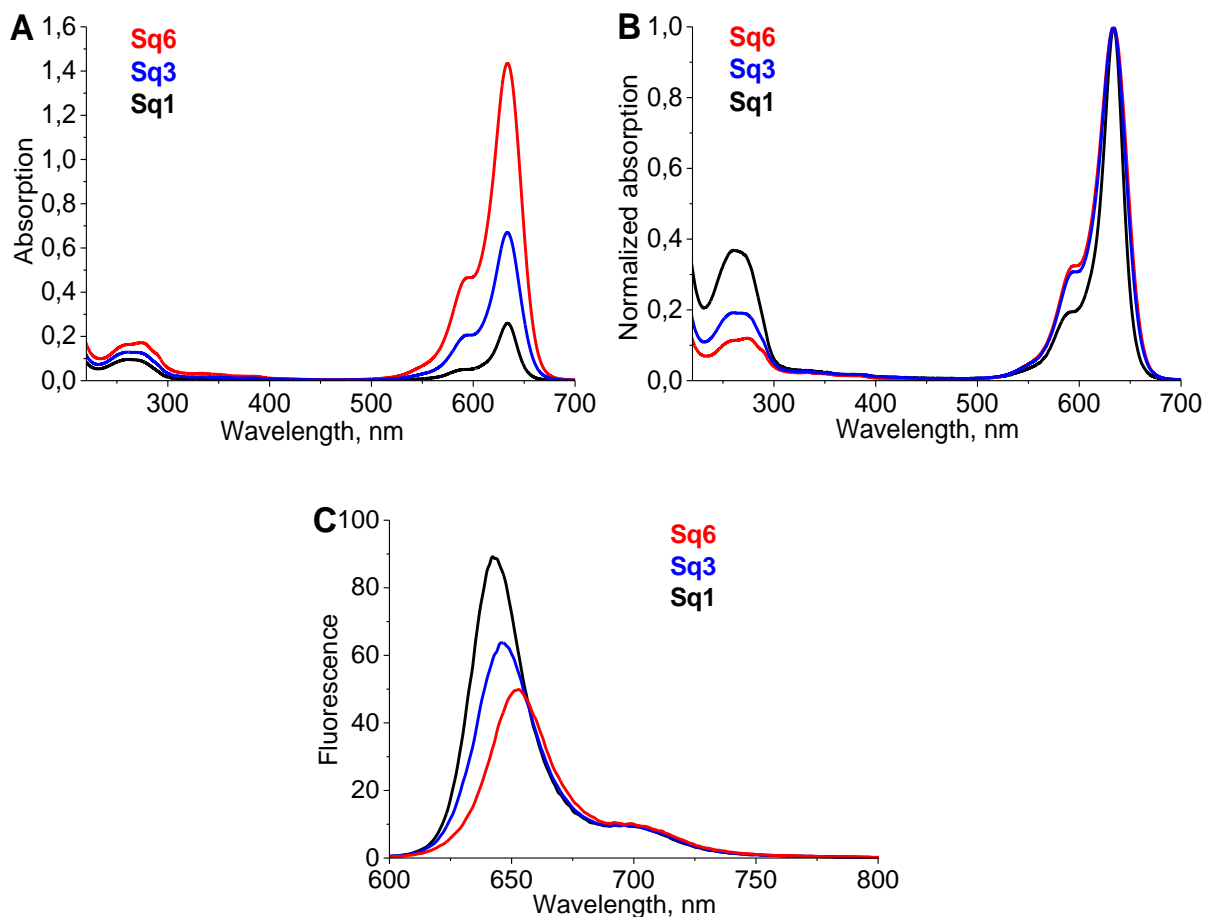
Figure 2.10. Absorption (A), normalized absorption (B), and fluorescence (C) spectra of the squaraine-modified oligonucleotides **Sq1** (black), **Sq3** (blue), and **Sq6** (red). Conditions: ethanol, c = 1 µM.

Similarly to the phosphodiester-linked squaraine trimer **SqTr** and hexamer **SqHex** (section "Supramolecular Polymers of Phosphodiester-Linked Squaraine Oligomers," Table 2.2), prolongation of the squaraine chain in the modified oligonucleotides leads to a bathochromic shift of the fluorescence bands. Also, the fluorescence quantum yield decreases from 33% for **Sq1** to 9.7% for **Sq3**, and to 4.4% for **Sq6**. The decreasing of Q.Y.s and increase of the absorption intensity at 594 nm (Figure 2.10B) are signs of aggregation of the oligonucleotides **Sq3** and **Sq6** in *H*-type fashion. Most likely, the aggregation is caused by intramolecular interactions of the squaraine molecules as it was shown for squaraine oligomers **SqTr** and **SqHex**.

In comparison with oligomers **SqTr** and **SqHex**, the Q.Ys of the modified oligonucleotides **Sq3** and **Sq6** are 1.4–1.5 times higher (Table 2.2 and Table 2.3). This effect can be explained by a

change in the polarity of the microenvironment [147]. In oligomers **SqTr** and **SqHex**, the squaraine chromophores are surrounded only by polar molecules of ethanol while in DNA-conjugates, the chromophores are partially shielded from the polar environment by their nucleotide chain. In the excited state, polar squaraine chromophores interact with polar EtOH molecules, which leads to non-radiative loss of energy. Due to polarity differences in the microenvironment, the loss of energy is higher for oligomers **SqTr** and **SqHex**.

The nucleotide sequence (CTTCCGTGAG or CTCACGGAAG) does not noticeably influence the absorption and fluorescence characteristics of the DNA-squaraine conjugates. In pairs **Sq1** and **cSq1**, **Sq3** and **cSq3**, and **Sq6** and **Sq6**, the spectral-fluorescence properties are closely similar.

The aggregation properties and supramolecular polymerization of the squaraine-modified oligonucleotides have been studied in aqueous solutions containing ethanol, sodium chloride, and 10 mM of phosphate buffer (pH = 7.0). Heating–cooling runs with a rate of 10 ºC/min were performed before measurements when aggregation properties were studied. The annealing rate of 0.5 ºC/min was applied in thermal experiments.

In the first part, we investigated the impact of the squaraine segment's length on their ability to the aggregation and form SPs.

UV-Vis spectroscopy measurements indicated that modified oligonucleotide **Sq1** containing only one squaraine molecule shows no well-defined type of aggregation under any of the screened conditions (conc. of **Sq1** up to 6.5 µM, conc. of NaCl up to 300 mM, 15% EtOH, 10 mM PB, pH = 7.0). The band pattern of a spectrum recorded in ethanol (for which a non-folded state of **Sq1** is expected) reveals an almost perfect overlay with the one recorded in aqueous ethanolic solution (Figure 2.11A). The thermal denaturation experiments show no significant changes in the absorbance of the sample during the heating-cooling cycles (Figure 2.11B).
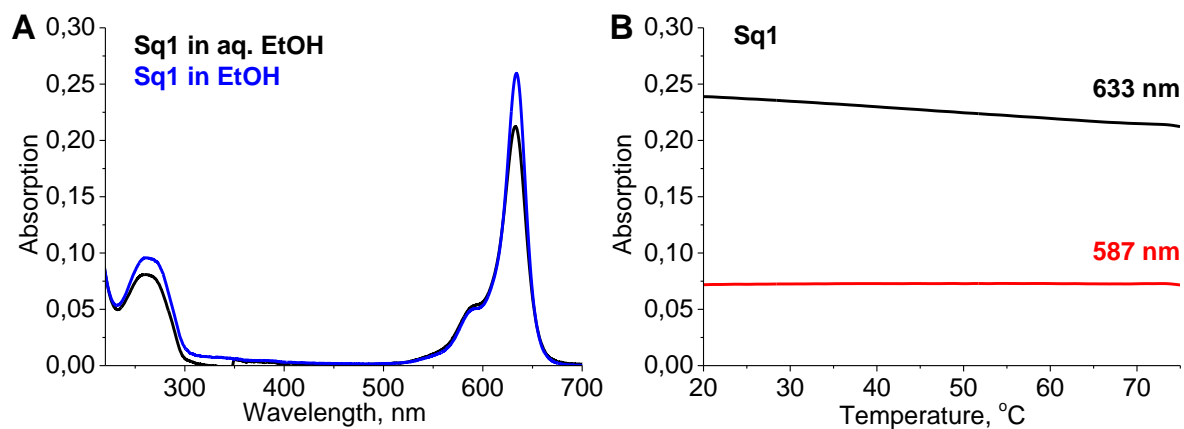
Figure 2.11. A: Absorption spectra of **Sq1** in aqueous media (black) and pure ethanol (blue). B: Temperature-dependent absorption of **Sq1** at 587 nm (red), and 633 nm (black). The solid lines represent the cooling cycle. Conditions: 1 µM **Sq1**, 15% EtOH, 100 mM NaCl, 10 mM PB.
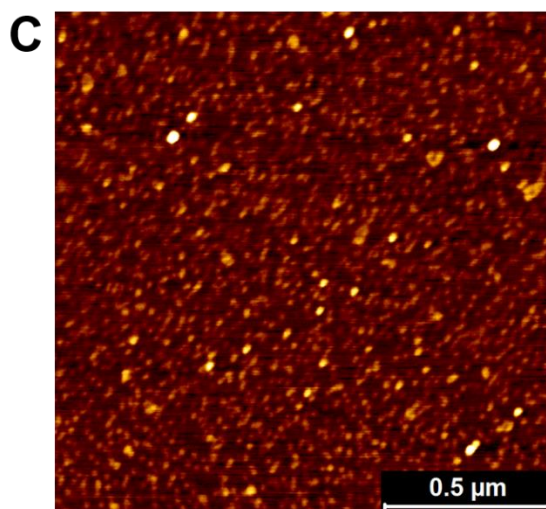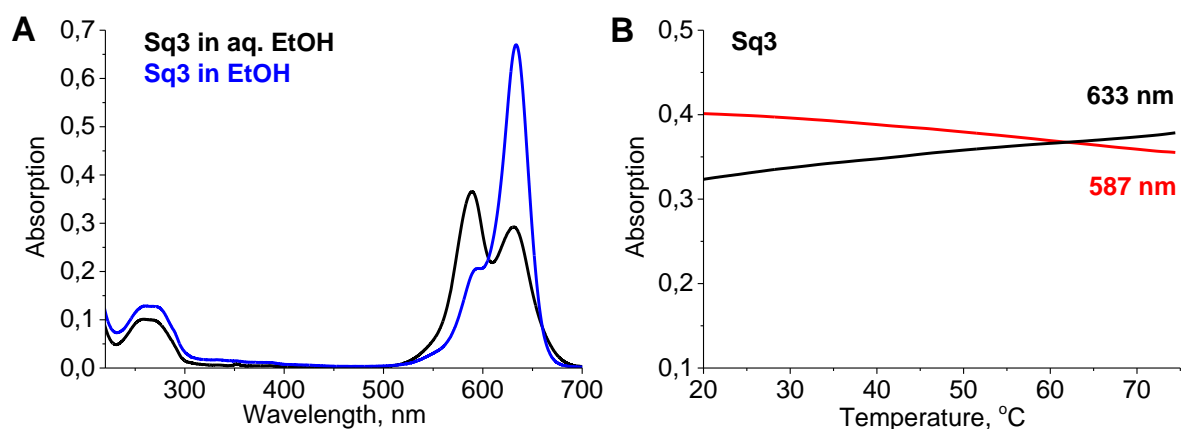
Figure 2.12. A: Absorption spectra of **Sq3** in aqueous media (black) and pure ethanol (blue). B: Temperature-dependent UV-Vis absorption of **Sq3** at 587 nm (red) and 633 nm (black). Solid lines represent the cooling cycle. C: AFM image of **Sq3** aggregates. Conditions: 1 µM **Sq3**, 15% EtOH, 100 mM NaCl, 10 mM PB.

34

Oligonucleotide **Sq3** containing three squaraine units demonstrates (Figure 2.12A) an additional blue-shifted peak around 589 nm in the UV-Vis absorption spectrum (conc. of **Sq3** up to 5.5 μM, NaCl up to 300 mM, EtOH 15%, PB 10 mM). This is in agreement with data indicating the formation of *H*-aggregates in which the transition dipole moments of the squaraine chromophores are arranged in a parallel fashion [66, 144]. Under the heating–cooling runs, the absorption spectrum of **Sq3** changes insignificantly, the absorption's temperature-dependence is non-sigmoidal within the measured temperature range (Figure 2.12B). AFM visualizes the *H*-aggregates of **Sq3** on APTES-modified mica, where they appear as irregular objects (Figure 2.12C).

DNA-squaraine conjugates **Sq6** containing six squaraines can form *H*-aggregates, nanostructures characterized by split absorption bands, and various transition structures (Figure 2.13). The type of aggregate depends on the concentration of EtOH and NaCl in the solution. *H*-aggregates associate mainly when the sample contains 100 mM of NaCl (conc. **Sq6** 1 μM, 10 mM PB) (Figure 2.13A). Increasing the NaCl concentration to 300 mM under otherwise identical conditions allows to obtain aggregates with a well-resolved split band (Figure 2.13B).

Another parameter that significantly influences the shape of the absorption spectrum and the type of aggregate is the annealing rate. For example, slowing of the cooling rate from 10 ℃/min to 0.5 ℃/min (Figure 2.13C) for a sample containing 15% of ethanol and 300 mM of NaCl results in a change the aggregation type: instead of *H*-aggregates, the aggregates with a split band are formed.
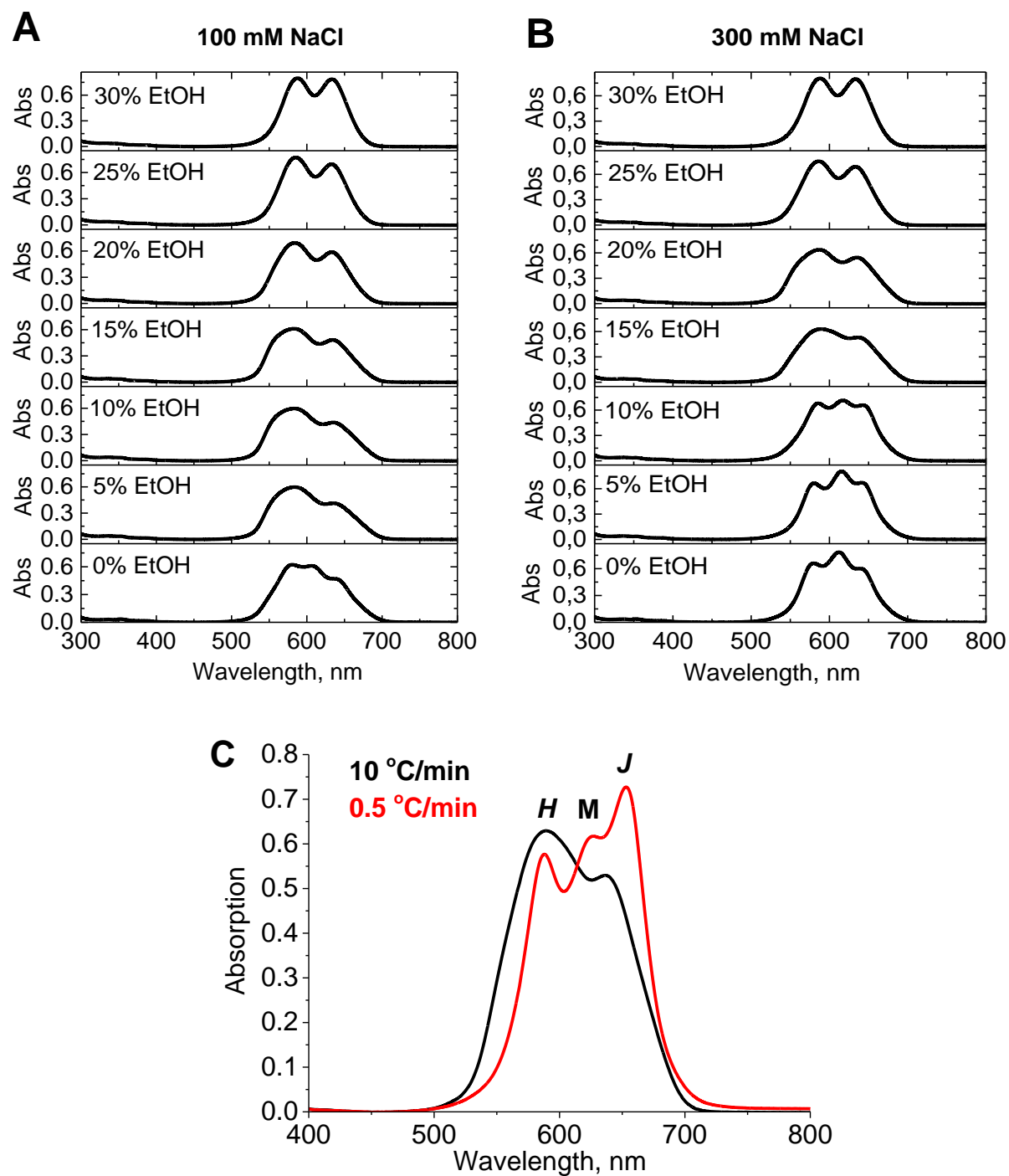
Figure 2.13. Influence of different parameters on the aggregation of **Sq6**. A: Impact of EtOH. Conditions: 1 μM strand, 100 mM NaCl, 10 mM PB, for EtOH, see the legend on the picture. B: Impact of EtOH. Conditions: 1 μM strand, 300 mM NaCl, 10 mM PB, for EtOH, see the legend on the picture.C: Influence of annealing rate. Cooling runs with a rate 10 °C/min (black) or 0.5 °C/min (red) was performed before the measurements. Conditions: 1 μM strand, 15% EtOH, 300 mM NaCl, 10 mM PB.

The *H*-aggregates of **Sq6** are characterized by a blue-shifted absorption band at around 585 nm (Figure 2.14A). These nanostructures do not show spectral features of the supramolecular polymers (Figure 2.14B) and appear on the AFM images as small irregular objects (Figure 2.14C).
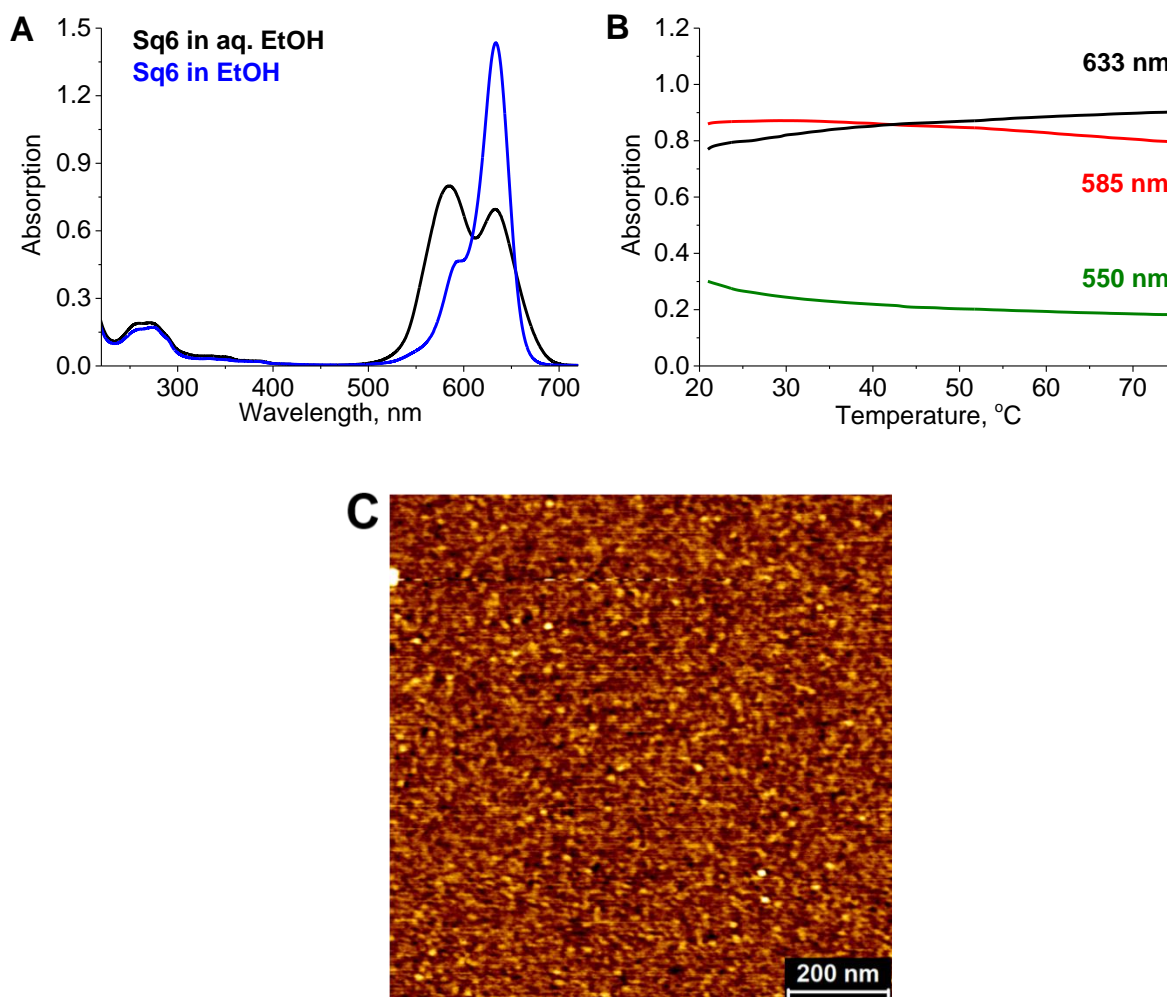
Figure 2.14. The spectral and microscopic characteristics of the *H*-aggregates of **Sq6**. A: UV-Vis spectra measured in aqueous media (black) and pure ethanol (blue). B: Temperature-dependent UV-Vis absorption of **Sq6** at 550 nm (green), 585 nm (red), and 633 nm (black). Solid lines represent the cooling cycle. C: AFM image. Conditions: 1 μM **Sq6**, 25% EtOH, 100 NaCl, 10 mM PB.

Based on experience obtained upon an investigation of the squaraine oligomers **SqTr** and **SqHex**, we assumed that the aggregates with a split absorption band represent supramolecular polymers. Indeed, the oligonucleotide **Sq6** was found to form well-defined nanostructures. Intermolecular folding is accompanied by the splitting of the long-wavelength band in the UV-Vis absorption

spectrum. Such behavior is in agreement with an oblique orientation of transition dipole moments of the squaraine molecules.

The formation of supramolecular polymers by **Sq6** was tested by varying different parameters. In the presence of 15% EtOH by volume, squaraines start to aggregate (with the splitting of the absorption band) in 125 mM NaCl aqueous solution. A further increase of the salt concentration to 300 mM resulted in a more pronounced splitting of the absorption bands. Even higher concentrations of salt (>400 mM NaCl) prompted the precipitation of aggregates (Figure 2.15)
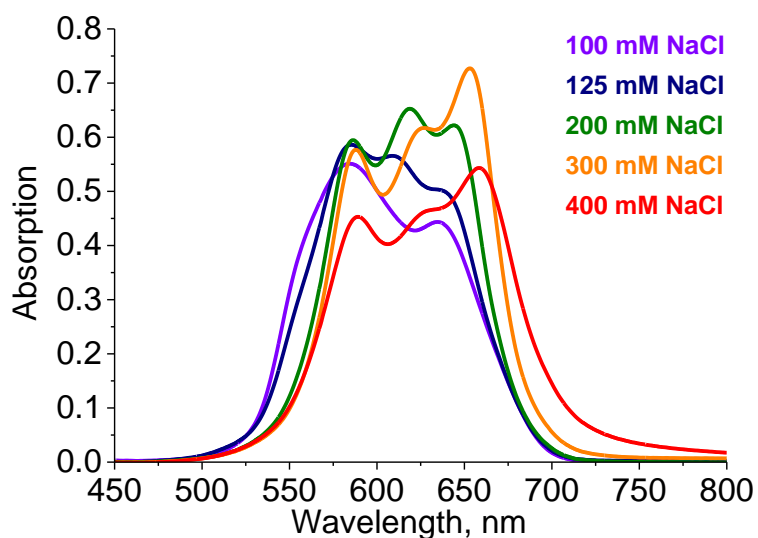
Figure 2.15. The absorption spectra of oligomer **Sq6** were recorded for different NaCl concentrations. Conditions: 1 µM **Sq6**, 15% EtOH, 10 mM PB, for NaCl, see the legend on the right. Annealing rate of 0.5 °C/min.

In thermal experiments, the assemblies formed in solutions with a concentration of NaCl ≥ 200 mM (15% EtOH) exhibit an absorption curve shape (monitoring at λ_{abs} = 660 nm), which is in agreement with a supramolecular polymerization process (Figure 2.16A). A large hysteresis (~20 °C) exists between the assembly and disassembly processes. Hysteresis is often observed for cooperative self-assembly processes when a large kinetic barrier in the assembly or disassembly pathway is present [5].

The splitting mentioned above of the absorption band is best seen by comparing UV-Vis spectra of the sample taken at different temperatures. It occurs in the temperature range from 50 °C to 30 °C (Figure 2.16B). Simultaneously, a distinct signal of exciton-coupling appears in the long-

wavelength region of the CD spectra (Figure 2.16C), revealing the formation of the chiroptically active SPs. Importantly, the fluorescence of **Sq6**-SPs is almost no detectable; the Q.Y. of **Sq6**-SPs was calculated to be less than 1%.
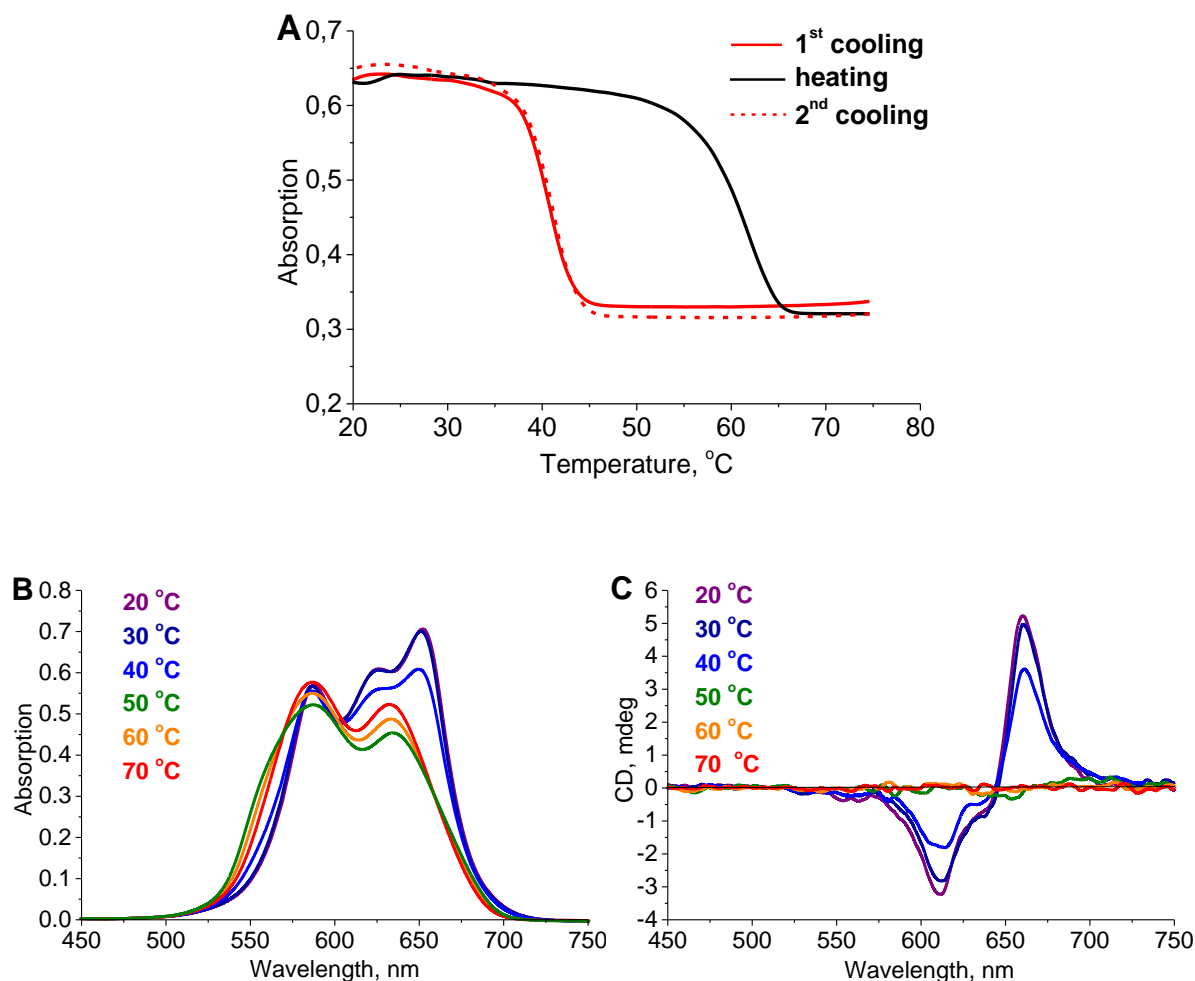
Figure 2.16. A: Cooling and heating runs recorded at 660 nm showing reversible self-assembly processes; solid red: 1st cooling ramp; solid black: heating ramp; dashed red: 2nd cooling ramp. B: Temperature-dependent UV-Vis absorption spectra. C: Temperature-dependent CD spectra. Conditions: 1 µM **Sq6**, 15% EtOH, 300 mM NaCl, PB.

AFM measurements reveal the presence of well-defined objects. The dimensions of the observed structures exhibit a uniform height of about 4 nm with a width of 50 to 100 nm, and a length of up to 500 nm. Similar results were obtained from TEM images (Figures 2.17A and 2.17B).
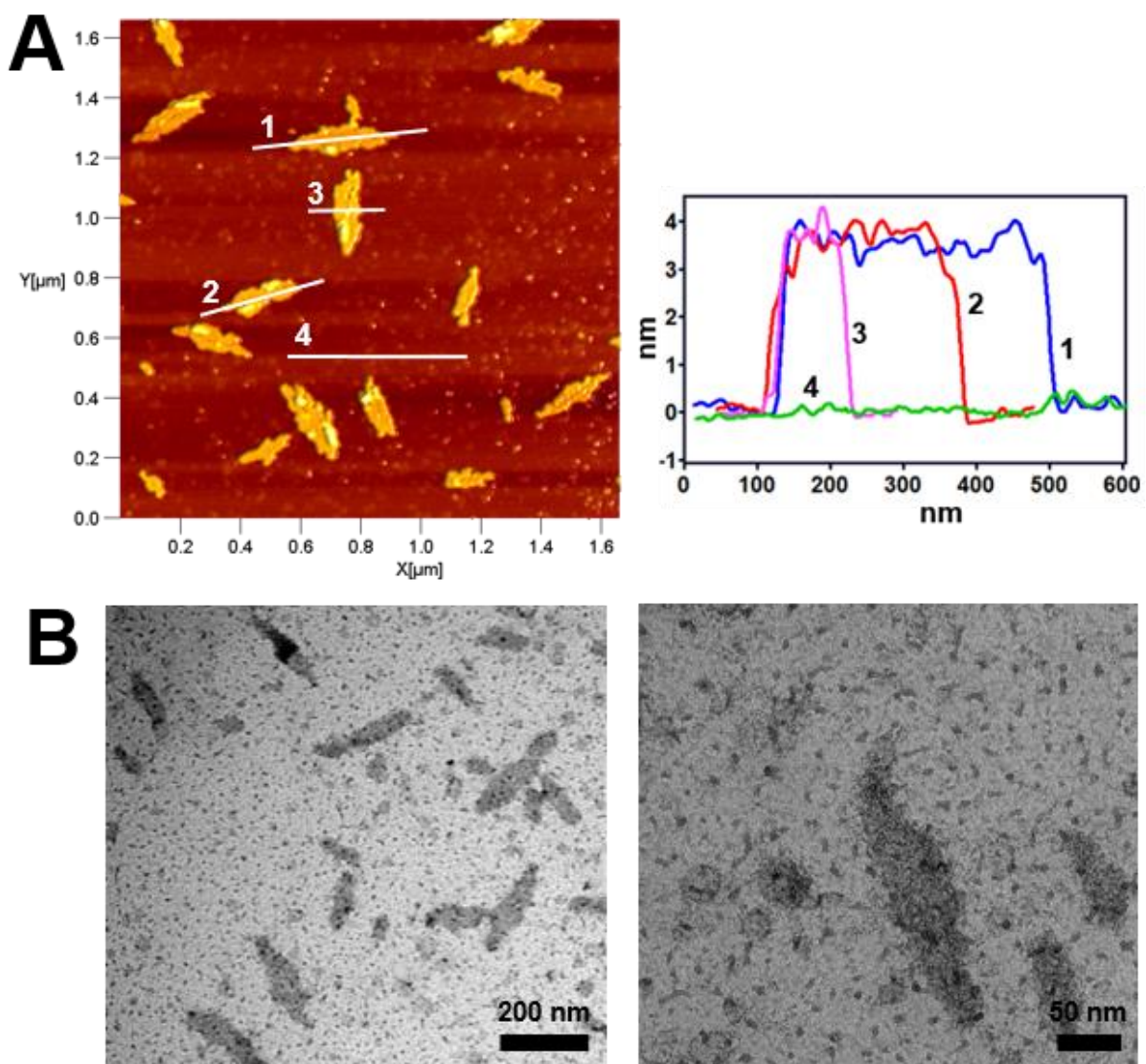
Figure 2.17. A: AFM image of the supramolecular polymers formed by oligomer **Sq6** (deposited on APTES-modified mica) and height histogram of SPs. B: TEM images (carbon-coated copper grid). Conditions: 1 µM **Sq6**, 15% EtOH, 300 mM NaCl, 10 mM PB.

In pairs **Sq6** and **cSq6**, **Sq3** and **cSq3**, and **Sq1** and **cSq1**, the oligonucleotides demonstrate the same aggregation behavior and the identical ability to undergo supramolecular polymerization. Thus, the nucleotide composition does not noticeably influence the aggregation and polymerization processes.

Further, we studied the supramolecular polymerization of **Sq6** in the presence of the complementary sequence CTTCCGTGAG – 3'. Hybridization of the nucleotide part of oligomer **Sq6** with the complementary (not modified) strand **cNM** (Scheme 2.1) or the squaraine-modified strand **cSq6** (Scheme 2.2) can influence the self-assembly process and leads to the formation of SPs of different morphology. In the hybrids **Sq6*cNM** and **Sq6*cSq6**, two types of interactions are possible: squaraine–squaraine interactions and hybridization of complementary DNA strands (Scheme 2.1 and 2.2).
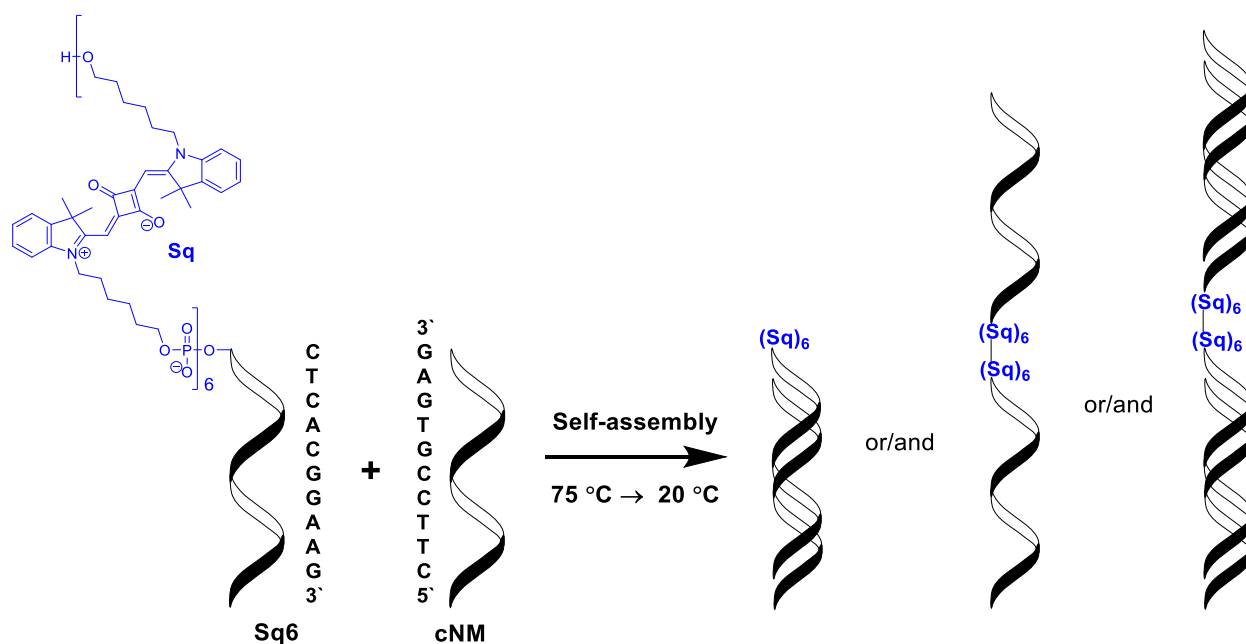
Scheme 2.1. Possible intermolecular interactions in the hybrid **Sq6*cNM**.
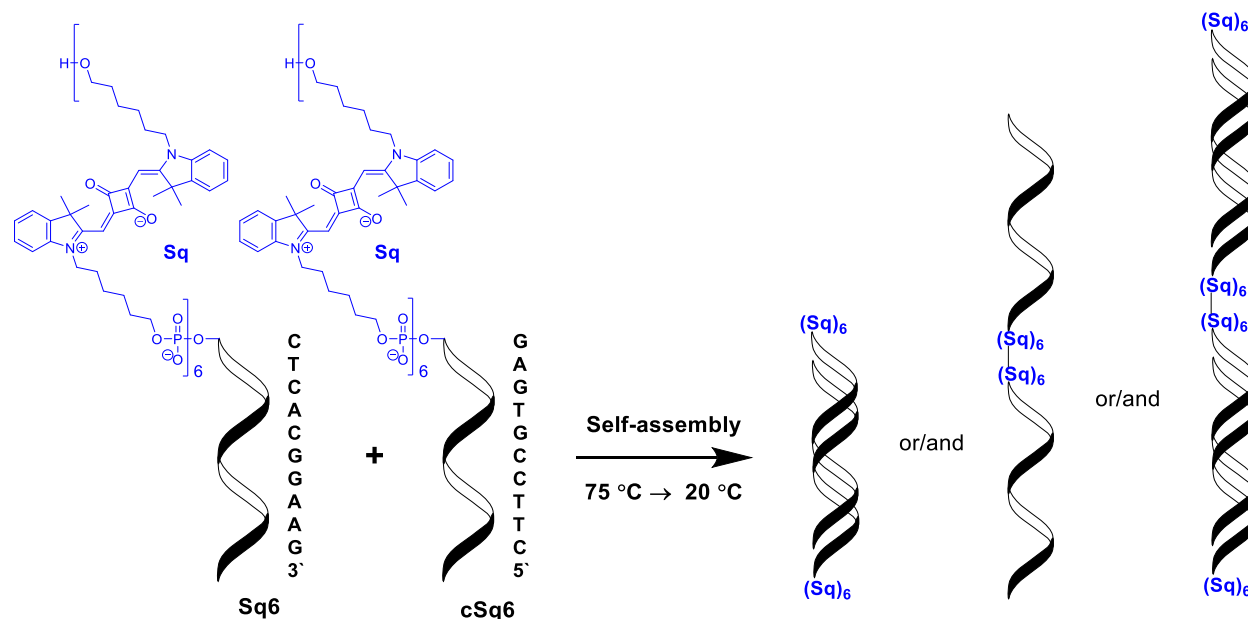
Scheme 2.2. Possible intermolecular interactions in the hybrid **Sq6*cSq6**.

As described above, the squaraine-modified oligonucleotides **Sq6** form SPs in aqueous solution (15% EtOH, 300 mM NaCl, 10 mM PB). However, the mixture of **Sq6*cNM** in the same conditions does not form the SPs. This is clear from the lack of sigmoidal temperature-dependence of the absorption at 260 nm and 660 nm, respectively, in the temperature range of interest (Figure 2.18A) as well as the absence of large regular objects as found in AFM investigations (Figure 2.18B). These findings confirm that hybridization occurs under the indicated conditions and reveals the absence of squaraine–squaraine interactions.
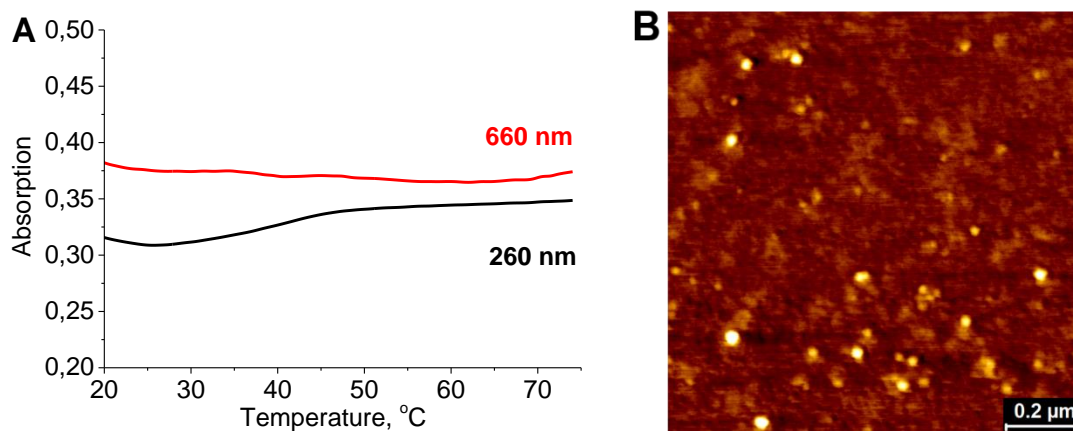
Figure 2.18. A: Cooling run recorded at 260 nm (black) and 660 nm (red). B: AFM image of the hybrid **Sq6*cNM**. Conditions: 1 µM **Sq6**, 1 µM **cNM**, 15% EtOH, 300 mM NaCl, 10 mM PB.

To obtain SPs of **Sq6*cNM**, we tested different conditions. The most interesting results were found for the solution containing 10% EtOH and 250 mM NaCl. Two sigmoidal transitions were revealed in the absorption as a function of temperature experiments (Figure 2.19A). The first one is observed between 40 °C and 60 °C and the second one below 30 °C. Most likely, the first transition is the result of the squaraine–squaraine interactions, while the second event also involves the hybridization of the complementary DNA strands. Thus, the sigmoidal transition at higher temperatures is observed only at 660 nm, where only the squaraine units absorb light, while at lower temperatures, the transition is also detected at 260 nm (absorption mainly by nucleobases).
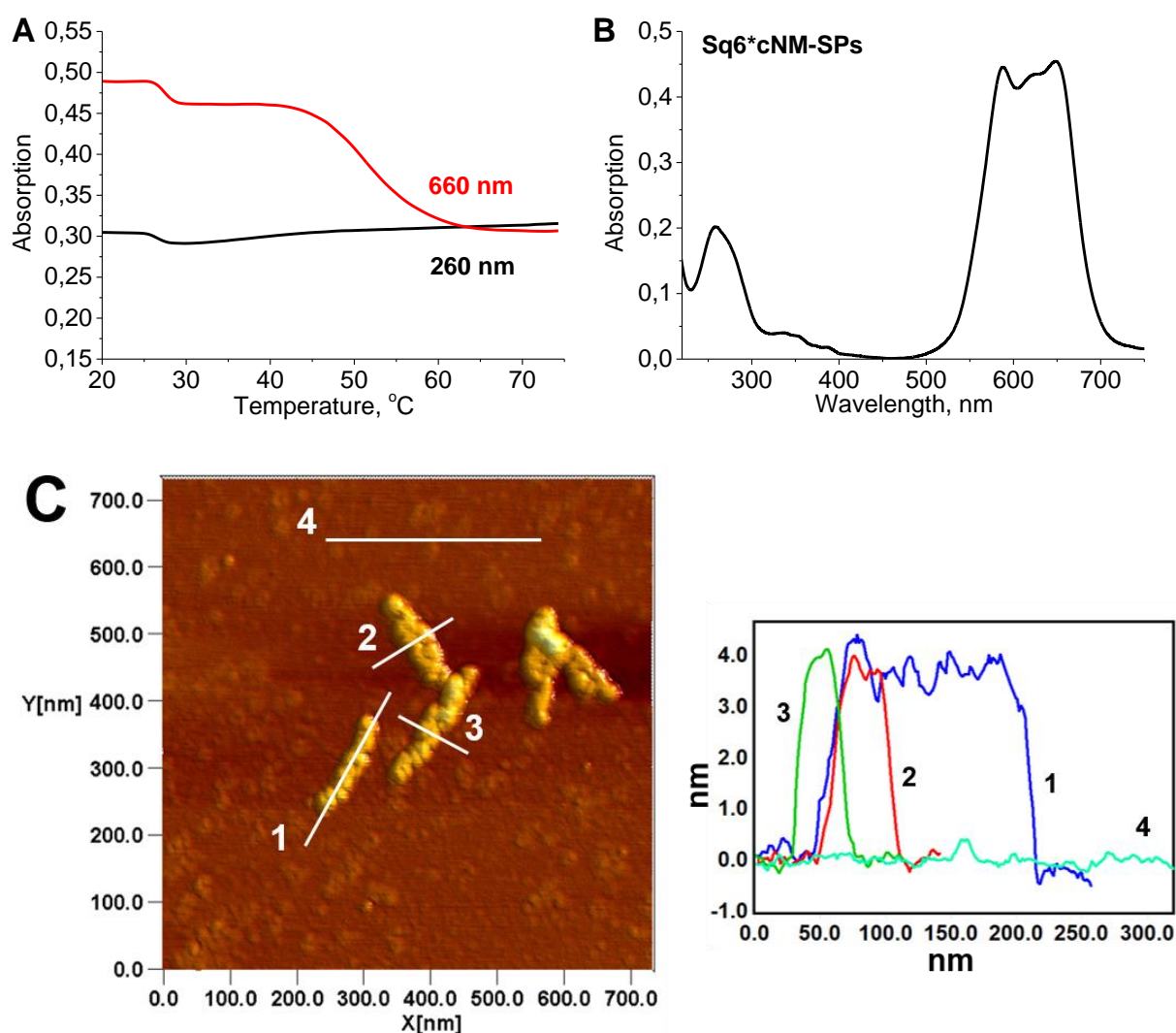
Figure 2.19. A: Cooling run recorded at 260 nm (black) and 660 nm (red), showing two sigmoidal transitions. B: UV-Vis absorption spectrum of the SPs. C: AFM image of the SPs and height histogram of SPs. Conditions: 1 µM **Sq6**, 1 µM **cNM**, 10% EtOH, 250 mM NaCl, 10 mM PB.

Like in the case of the oligomer **Sq6**, the dipole moments of the squaraine molecules in the supramolecular polymers of the hybrid **Sq6*cNM** are oriented obliquely (Figure 2.19B). However, the morphology of the SPs formed by the hybrid **Sq6*cNM** is different (Figure 2.19C). The **Sq6*cNM**-SPs are more uniform than **Sq6**-SPs. Their width is between 40 nm and 50 nm, and they are 150–200 nm long.

The process of supramolecular polymerization of hybrid **Sq6*cSq6** depends on the percentage of ethanol present in the medium. If the solution contains 20–25% of ethanol, the main driving force for intermolecular interactions originates from DNA base pairing (Figure 2.20 A). Furthermore, this process was also accompanied by the precipitation of the formed SPs (Figure 2.20B, decrease in absorbance).
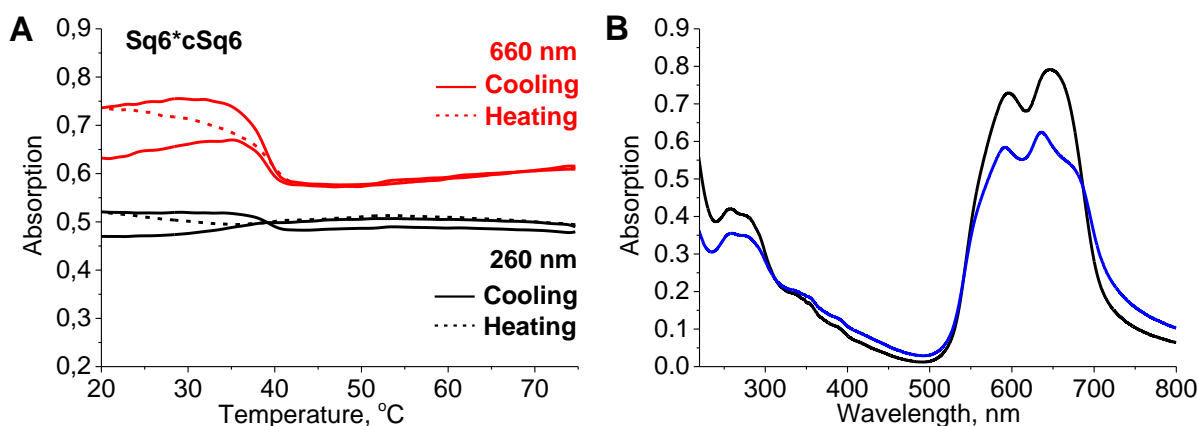
Figure 2.20. A: Cooling and heating runs recorded at 260 nm (black) and 660 nm (red) for hybrid **Sq6*cSq6**, showing the contribution of the nucleotide–nucleotide interactions in the self-assembly process. Solid lines: cooling cycles, dashed lines: heating cycle. B: The UV-Vis absorption spectra before (black) and after (blue) heating-cooling runs. Conditions: 1 μM **Sq6**, 1 μM **cSq6**, 20% EtOH, 100 mM NaCl, 10 mM PB,.

If the amount of ethanol in a solution containing **Sq6*cSq6** decreases to 10%, the base-pairing plays a minor role, and the main driving force for the self-assembly process is the interactions between the squaraine molecules (Figure 2.21A). The UV-Vis absorption spectrum is changed in the same way as for single-strand **Sq6** upon increasing NaCl concentration (Figures 2.15 and 2.21B). The AFM images of the SPs formed by hybrid **Sq6*cSq6** are shown in Figure 2.22. The objects with different morphology ranging from little nanospheres and short nanofibers to large and more complicated nanostructures visualize on a mica surface.
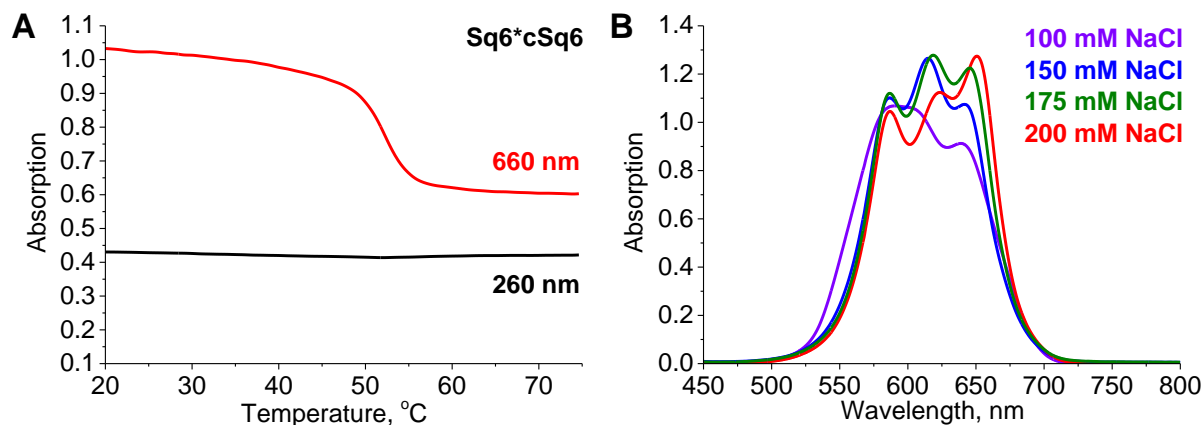
Figure 2.21. A: Cooling run recorded at 260 nm (black) and 660 nm (red) for hybrid **Sq6*cSq6**, showing the negligible contribution of the nucleotide–nucleotide interactions in the self-assembly process. Conditions: 1 µM of each strand, 10% EtOH, 200 mM NaCl, 10 mM PB. B: Absorption spectra of **Sq6*cSq6** recorded for different NaCl concentrations. Conditions: 1 µM of each strand, 10% EtOH, 10 mM PB, for NaCl, see the legend on the right.
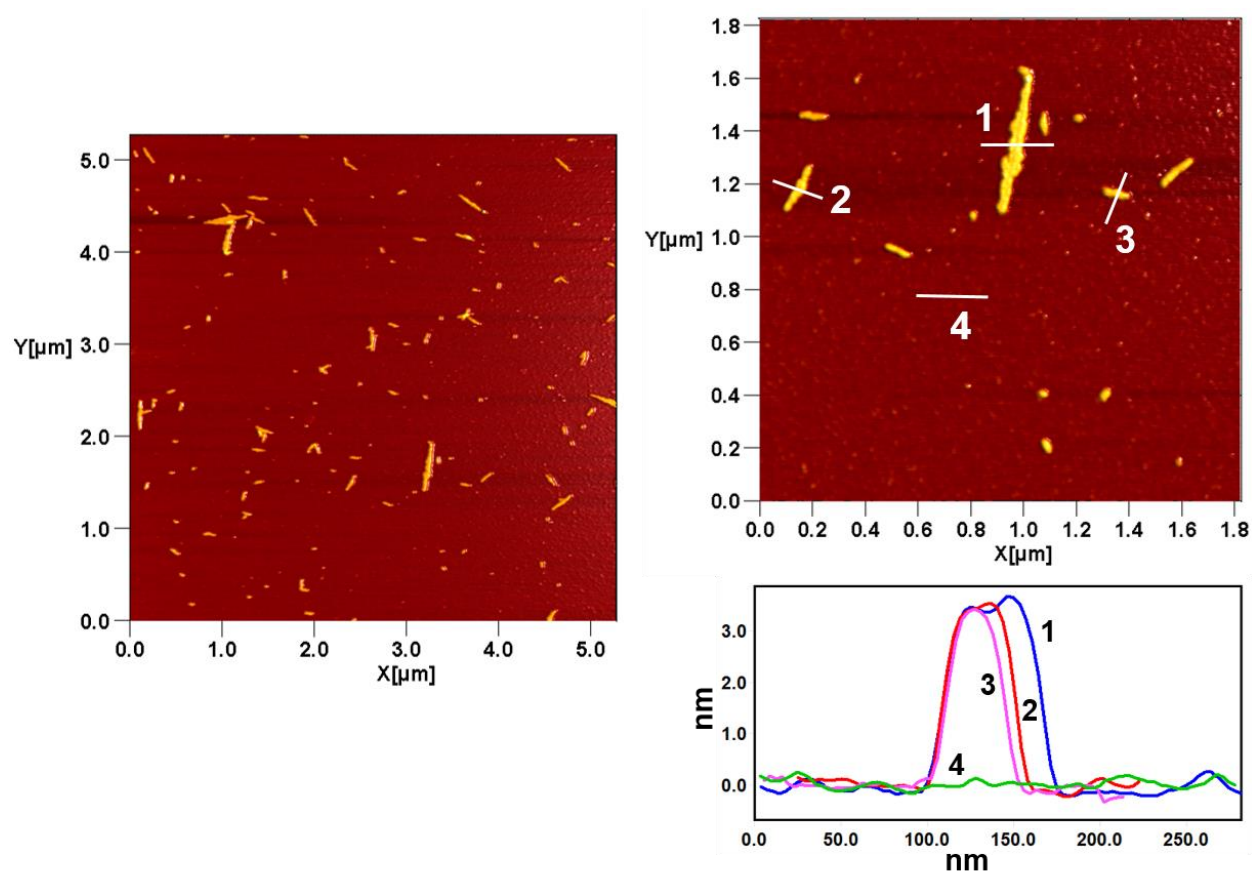
Figure 2.22. AFM images of the SPs formed by the hybrid **Sq6*cSq6** and height histogram of SPs. Conditions: 1 µM **Sq6**, 1 µM **cSq6**, 10% EtOH, 200 mM NaCl, 10 mM PB.

2.2.4 DNA Duplex with Squaraine Overhangs

In this section, we describe aggregation and supramolecular polymerization of the duplex **SqDup** formed by complementary 5'-end squaraine-modified oligonucleotides **Sq3-ON20** and **cSq3-ON20**. The oligonucleotides are built from 20 nucleotides and three squaraine units (Figure 2.23). Such type systems were reported self-assemble into large vesicles in an aqueous ethanol solution containing spermine tetrahydrochloride [139].

Figure 2.23. The structure of the duplex **SqDup** formed by squaraine-modified strands **Sq3-ON20** and **cSq3-ON20**.

Absorption and fluorescence characteristics of the squaraine-modified oligonucleotides **Sq3-ON20** and **cSq3-ON20** measured in ethanol at a concentration 1 µM (the absence of intermolecular interactions is expected) given in Table 2.4. Absorption and fluorescence spectra are shown in Figure 2.24.

Table 2.4. Spectral-luminescence properties of the oligonucleotides **Sq3-ON20** and **cSq3-ON20** in ethanol (strand concentration: 1 µM, λ(Ex) = 590 nm).

Name	Structure	λ(Abs), nm	λ(Fl), nm	Q.Y., %
Sq3-ON20	Sq-Sq-Sq-CTT CCT TGC ATC GGA CCT TG – 3'	633	644	9.9
cSq3-ON20	Sq-Sq-Sq-CAA GGT CCG ATG CAA GGA AG – 3'	633	644	8.5
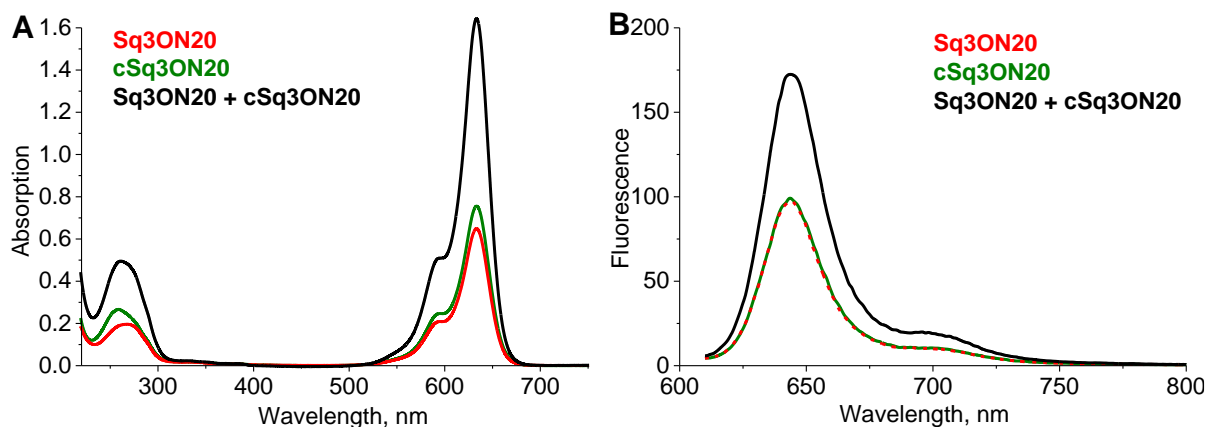
Figure 2.24. Absorption (A) and fluorescence (B) spectra of the oligonucleotides **Sq3-ON20** (red) and **cSq3-ON20** (green) and their mixture (black) in ethanol. Conditions: c = 1 µM, λ(Ex) = 590 nm.

The oligonucleotides **Sq3-ON20** and **cSq3-ON20** demonstrate almost identical spectral properties (Table 2.4, Figure 2.24). The long-wavelength absorption and fluorescence maxima were determined at 633 nm and 644 nm, correspondingly. Quantum yields are slightly different (9.9% for **Sq3-ON20** and 8.5% for **cSq3-ON20**).

The mixture of the oligonucleotides **Sq3-ON20** and **cSq3-ON20** gives the same shape of the absorption and fluorescence spectra as individual strands (Figure 2.24). Thus, no squaraine–squaraine interactions or hybridization occur in ethanol.

The aggregation properties of the oligonucleotide mixture **Sq3-ON20** and **cSq3-ON20** were studied in aqueous ethanol solutions containing 0.1 mM of spermine and 10 mM of phosphate buffer. Heating–cooling runs with a rate of 10 ℃/min were performed before the measurements.

In aqueous ethanol solutions (Figure 2.25) containing 0.1 mM spermine, the intermolecular interactions between **Sq3-ON20** and **cSq3-ON20** lead to noticeable changes in the absorption spectrum. At concentrations of EtOH in sample $c \geq 35\%$, a clear monomer band with a maximum around 592 nm, and a band of *H*-aggregates with absorption at 634 nm are observed. At lower concentrations of EtOH, the intensity of both peaks is comparable, and the bands become significantly broader. The appearance of new higher- and lower-energy transitions in the UV-Vis spectrum reveals the formation of new nanostructures.
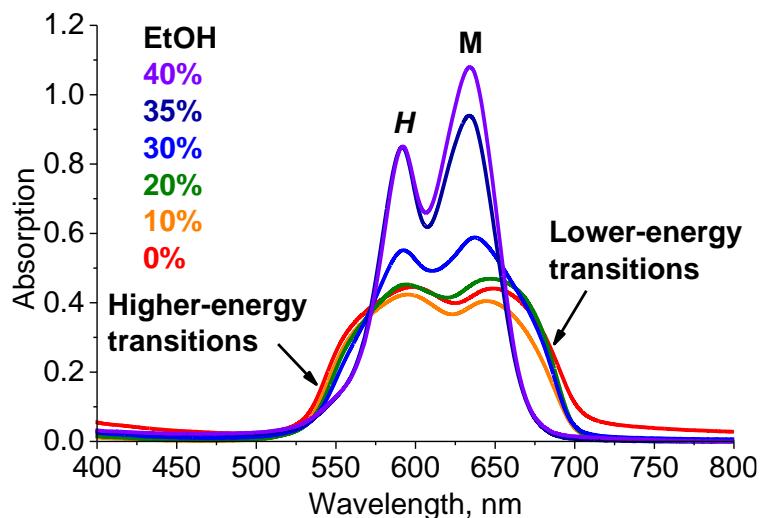
Figure 2.25. Absorption spectra of the mixture of oligonucleotides **Sq3-ON20** and **cSq3-ON20** depending on the ethanol concentration in solution. Conditions: conc. of strand 1 μM, 0.1 mM spermine, 10 mM PB.

Similarly to the *H*-aggregates of the squaraine oligomers **SqTr** and **SqHex** (Chapter 2, section "Supramolecular Polymers of Phosphodiester-Linked Squaraine Oligomers") and the squaraine-modified oligonucleotides **Sq3** and **Sq6** (Chapter 2, section "Supramolecular Polymers of Squaraine-Modified Oligonucleotides"), the *H*-aggregates of the mixture of **Sq3-ON20** and **cSq3-ON20** formed in the solutions with an ethanol concentration above 30% show a featureless temperature-dependence of the absorption at 633 nm (Figure 2.26A). Thus, no squaraine–squaraine interactions are found. At the same time, the absorption at 260 nm has a sigmoidal behavior that is caused by the hybridization of the nucleotide sequences.

In the solutions with EtOH percentage of 10–20%, the self-assembly process yields SPs that are completely reversible. The supramolecular polymerization is accompanied by a significant change of the absorption at 633 nm upon decreasing temperature (Figure 2.26B). Hysteresis is insignificant and amounts to 3 °C.
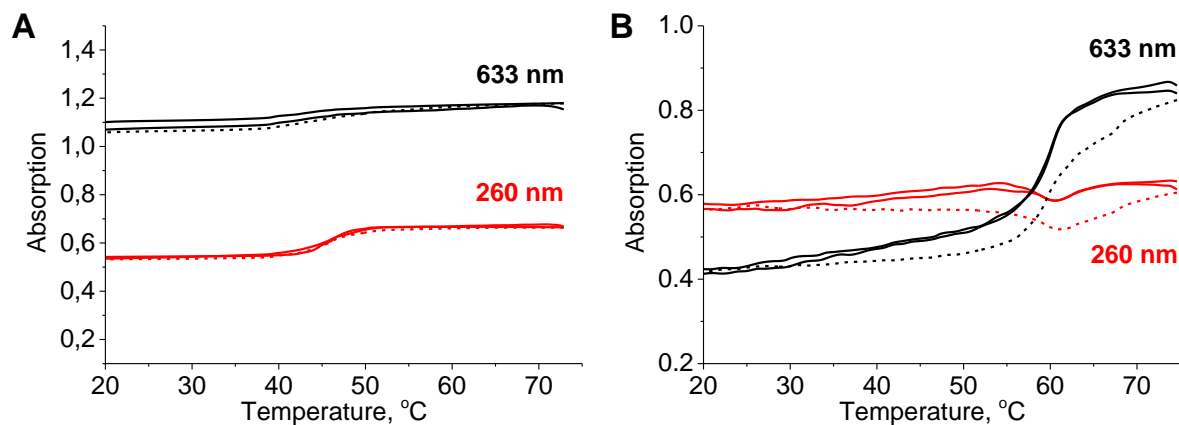
Figure 2.26. Cooling (solid lines) and heating (dashed lines) runs recorded at 260 nm (red) and 633 nm (black). A: 35% EtOH in the sample. B: 15% EtOH in the sample. Conditions: conc. of **Sq3-ON20** and **cSq3-ON20** 1 μM, 0.1 mM spermine, 10 mM PB. Heating and cooling rate of 0.5° C/min.

Like duplexes with phenanthrene overhangs [139], duplexes with squaraine overhangs self-assemble to large vesicular structures (Figure 2.27 and 2.28). Round-shaped objects are well visualized by AFM (Figure 2.27) and TEM (Figure 2.28). According to TEM, the diameter of the formed vesicles is up to 250 nm
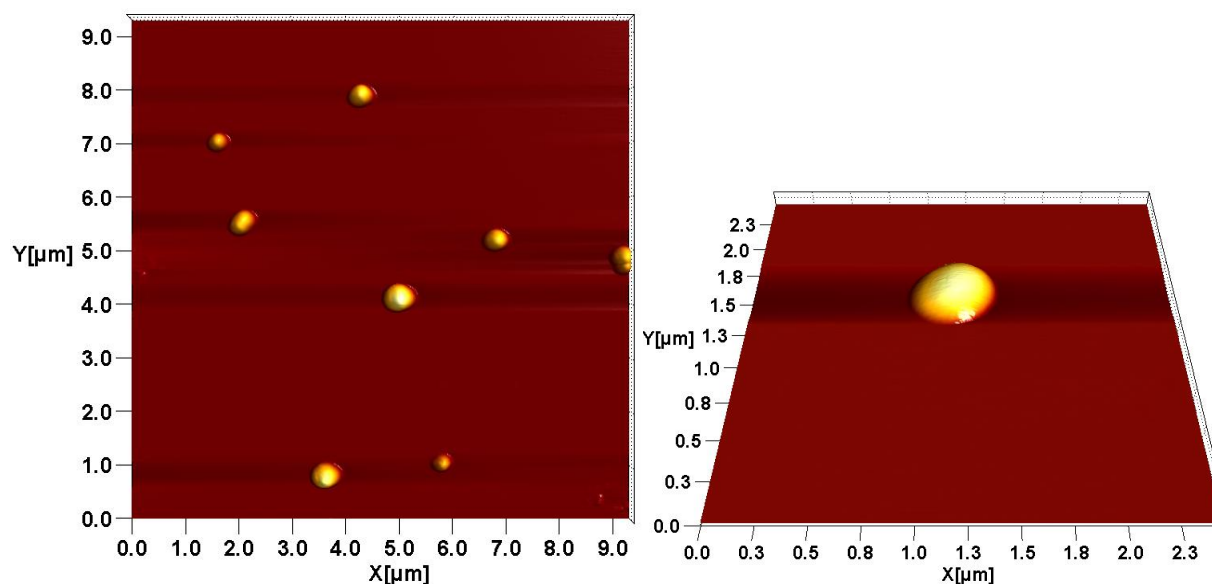
Figure 2.27. AFM images of **SqDup**-SPs. Conditions: conc. of **Sq3-ON20** and **cSq3-ON20** 1 μM, 0.1 mM spermine, 10 mM PB.
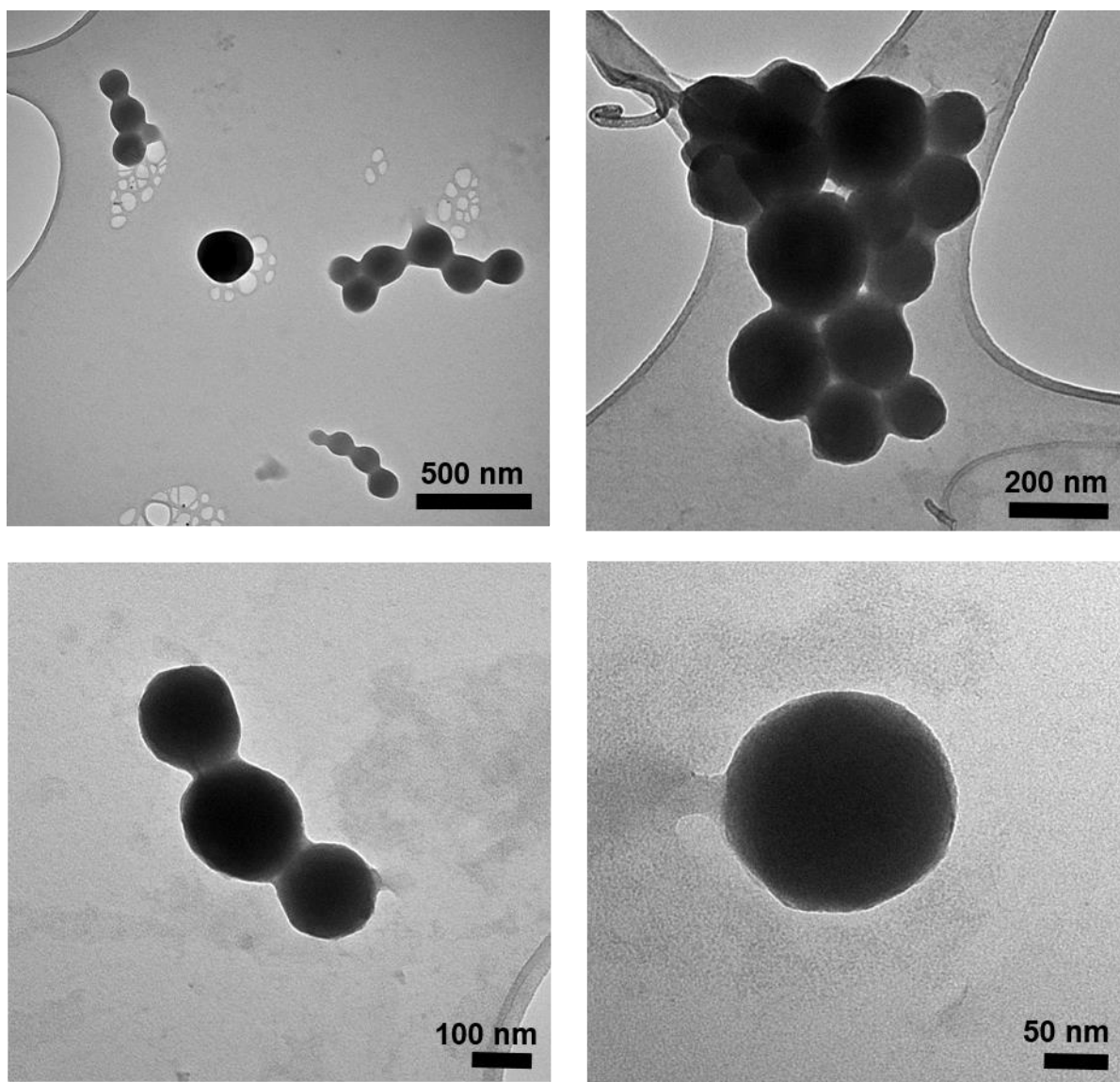
Figure 2.28. TEM images of **SqDup**-SPs. Conditions: conc. of **Sq3-ON20** and **cSq3-ON20** 1 μM, 0.1 mM spermine, 10 mM PB.

2.2.5 Functionalization of the SPs by Gold Nanoparticles

The goal of this part of the project is to demonstrate the possibility of the functionalization of the supramolecular polymers formed from squaraine-modified oligonucleotides **Sq6**. The possibility of functionalization is studied on the example of gold nanoparticles (AuNPs) since they are easily visualized by TEM. AuNPs are arguably the most extensively studied members of the metal nanoparticle groups and have attracted considerable interest and driven a variety of potential

applications in catalysis [148, 149], biology [150, 151], and optics [152–154]. Their application in biology and medicine is especially interesting. AuNPs can be applied in photodynamic therapy [155, 156], photothermal therapy [157, 158], x-ray imaging [159, 160], delivery applications [161, 162], and sensing [163–165].

In this section, we describe the rational synthesis of the AuNPs with a diameter of 5 nm and sulfur-containing oligonucleotides for attachment to the AuNPs. Also, we test three different approaches to the functionalization of the SPs and define the advantages and disadvantages of each of them. The outcomes of the functionalization were followed by TEM analysis.

Preparation of the Gold Nanoparticles.

As was described above (see Chapter 2, section "Supramolecular Polymers of Squaraine-Modified Oligonucleotides"), squaraine-modified strands **Sq6** self-assemble into supramolecular polymers in aqueous media with sufficiently high salt concentration (15% EtOH, 300 mM NaCl, 10 mM PB). At these conditions, AuNPs (5 nm) prepared according to the citrate reduction method [134, 166, 167] form a black precipitate indicative of the formation of colloidal gold.

The literature revealed ways in which salt resistance of the AuNPs can be improved [168–171]. The particles with higher monodispersity have a lower tendency to form aggregates [168, 169]. Good stability of AuNPs against the high electrolyte concentration achieves when they are stabilized by the use of ligands with superior passivation properties such as short oligonucleotide strands [170]. To prepare highly monodisperse nanoparticles with an average size of 5 nm, we used K_2CO_3–$NaBH_4$ mixture for the reduction of $HAuCl_4$ in the presence of bis(*p*-sulfonatophenyl)phenylphosphine (BSPP) as a passivating ligand [171]. In order to functionalize gold nanoparticles (approaches 2 and 3, see "*Functionalization of the SPs by AuNPs" below*), target nucleotide sequences were attached to their surface. The remaining BSPP ligands were exchanged by hexathymine oligonucleotide chain **T6-SS**, as shown in Scheme 2.3.
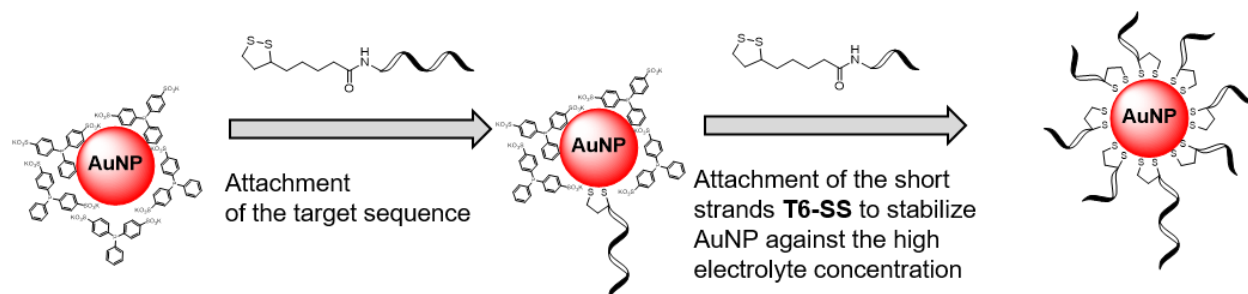
Scheme 2.3. Functionalization (for simplicity, one attached oligonucleotide shown) and stabilization of the AuNPs.

Synthesis of the Sulfur-Containing Oligonucleotides.

The most known method used for the attachment of oligonucleotides to AuNPs is exploiting the gold's affinity to sulfur-containing end-groups of modified oligonucleotides [172, 173]. In the literature, we found two different ways [171, 174] in which sulfur can be introduced into the terminus position of the oligonucleotide.

According to the first method [174], the disulfide group is added to the strand during the synthesis using disulfide-modified support and then reduced to give the free thiol (Scheme 2.4A). However, during storage, the oligonucleotides tend to dimerize as a result of disulfide formation. As a result, two oligonucleotides instead of just one functionalize the AuNPs (Scheme 2.4B).
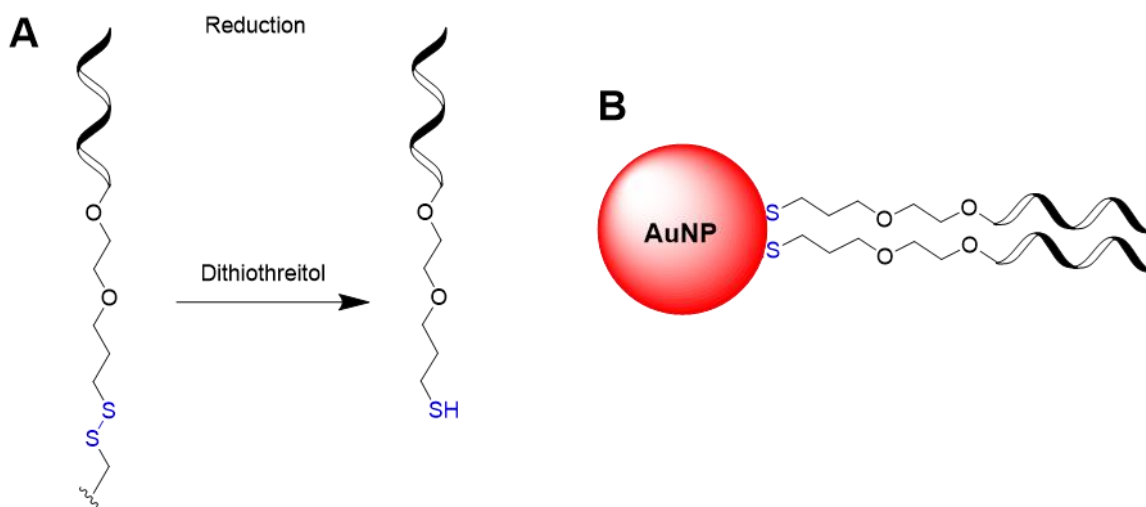
Scheme 2.4. A: Last step in the synthesis of the thiol-modified oligonucleotides. B: The dimer functionalized with an AuNP.

The second method [171] consists of the synthesis of the amino-modified oligonucleotide and its post-synthetic reaction with *N*-hydroxysuccinimide ester of thioctic acid (Scheme 2.5A). In this case, dimerization does not occur, and a single strand is involved in forming the bond with the AuNP (Scheme 2.5B).

In the case of the functionalization of SPs by AuNPs, coverage of the nanoparticles by more than one oligonucleotides must be avoided. This prevents particles from bridging several polymers. Therefore, the sulfur-containing oligonucleotides used in this work (Table 2.5) were synthesized by the post-synthetic approach via conjugation with thioctic acid.
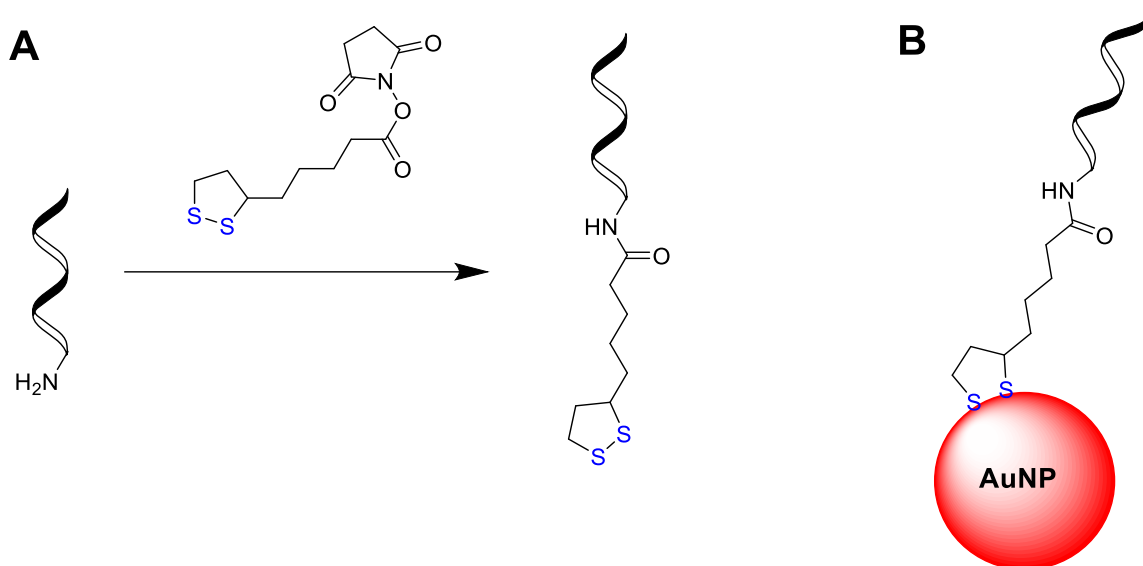
Scheme 2.5. A: Synthesis of the sulfur-containing oligonucleotide from an amino-modified strand via post-synthetic reaction with *N*-hydroxysuccinimide ester thioctic acid. B: The oligonucleotide functionalized with AuNP.

Table 2.5. Name and structures of the sulfur-containing oligonucleotides used in this work.

Name	Structure
Sq6-SS	Sq-Sq-Sq-Sq-Sq-Sq-CTC ACG GAA G-Thioctic acid – 3'
Sq6T10-SS	Sq-Sq-Sq-Sq-Sq-Sq-CTC ACG GAA GTT TTT TTT TT-Thioctic acid – 3'
T6-SS	5' – TTT TTT-Thioctic acid – 3'
cNM-SS	5' – Thioctic acid-CTT CCG TGA G – 3'
NC-SS	5' – Thioctic acid-ATT GAA GTC C – 3'
cNMT10-SS	5' – Thioctic acid-TTT TTT TTT TCT TCC GTG AG – 3'
NCT10-SS	5' – Thioctic acid-TTT TTT TTT TAT TGA AGT CC – 3'

Functionalization of the SPs by AuNPs.

As described above, squaraine–squaraine interactions are the predominant force for forming SPs from oligonucleotides **Sq6**. Hence, the DNA strands in **Sq6**-polymers are expected to be accessible for AuNPs or complementary DNA strands.

The main idea of the first approach to the functionalization of SPs by AuNPs is illustrated in Scheme 2.6. For the formation of the SPs, instead of using oligonucleotide **Sq6**, we proposed to use its sulfur-containing analog **Sq6-SS**. The functionalization occurs upon incubation of the disulfide-coated polymers with AuNPs stabilized by BSPP. For this approach, AuNPs stabilized by **T6-SS** are unusable since the surface of AuNP must contain binding sites accessible to the SP.
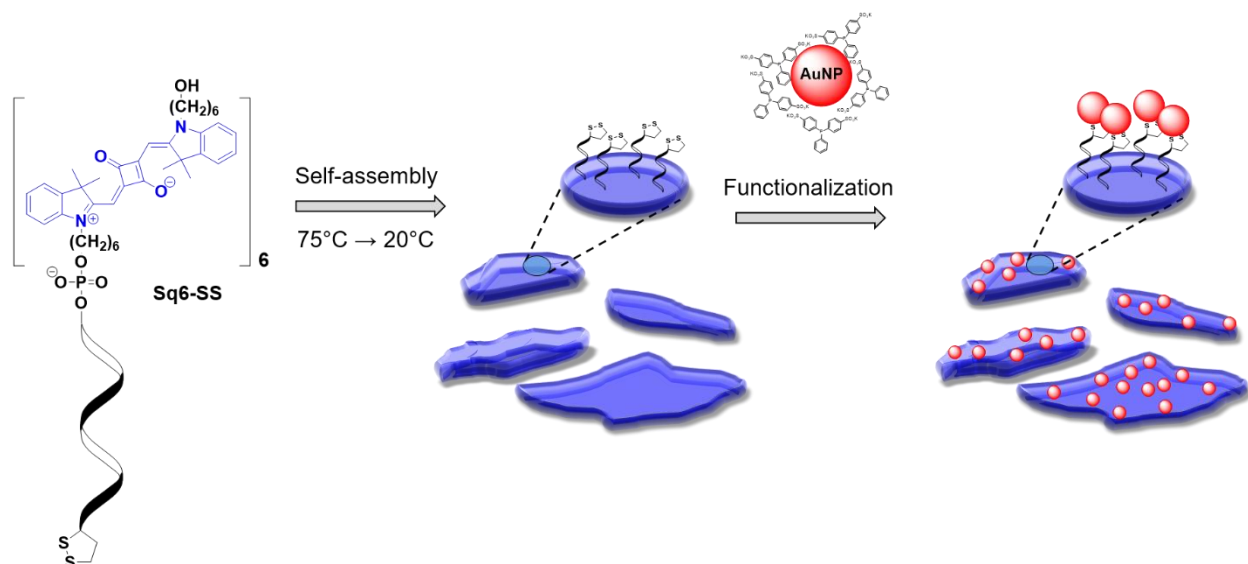
Scheme 2.6. Functionalization of the SPs by AuNPs. Approach 1.

Spectral characteristics of the **Sq6-SS**-polymers and **Sq6**-polymers are closely similar. Cooling profiles in the thermal experiment demonstrate the characteristic curve in the same range of temperatures (Figure 2.29A). The absorption spectrum of the SPs formed by **Sq6-SS** repeats the spectrum of **Sq6**-polymers (Figure 2.29B). Besides, disulfide-coated polymers also form flakes-like objects (Figure 2.29C).
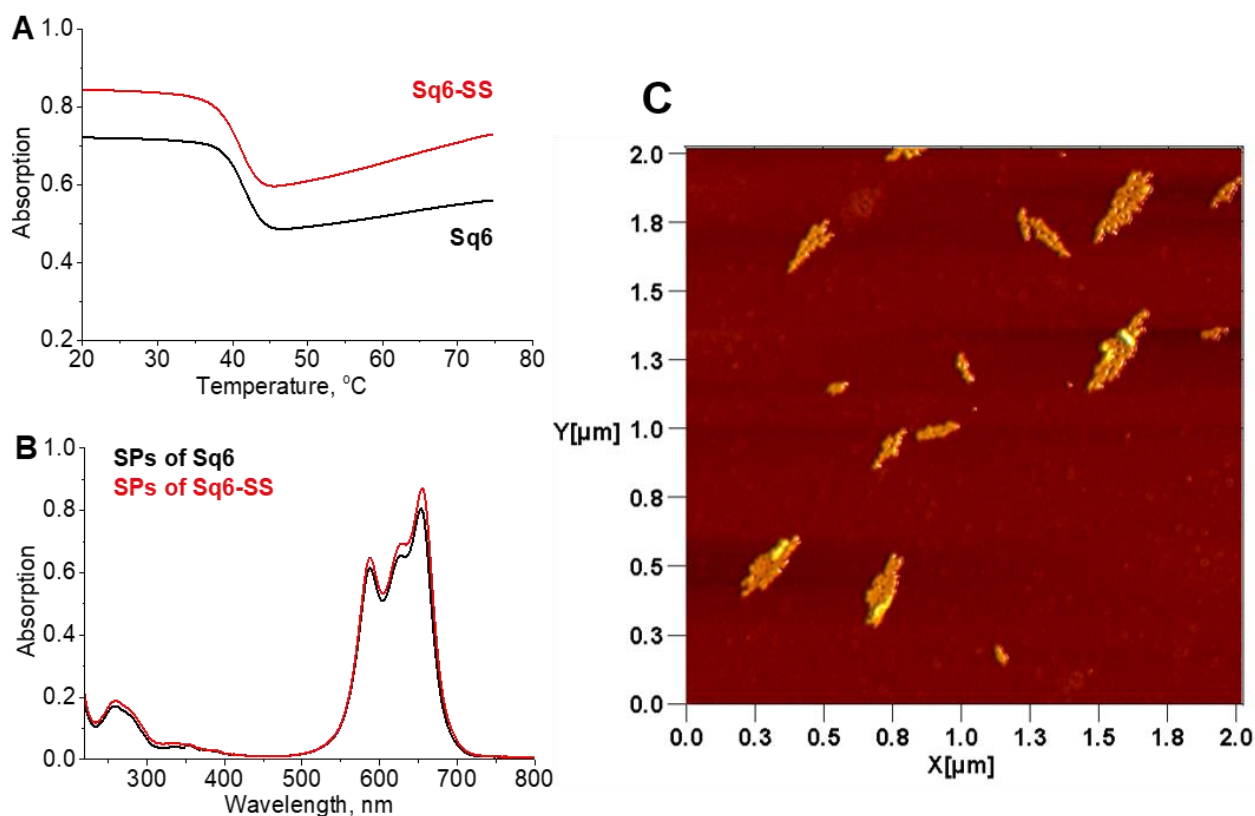
Figure 2.29. A: Cooling profile (registration at 660 nm) of **Sq6-SS** (red) and **Sq6** (black) upon the formation of the SPs. B: Absorption spectra **Sq6-SS**-polymers (red) and **Sq6**-polymers (black). C: AFM image of the SPs formed by **Sq6-SS**. Conditions: 1 µM oligo, 15% EtOH, 300 mM NaCl, 10 mM PB.

After incubation of **Sq6-SS**-polymers with AuNPs, the sample was investigated by TEM on a carbon-coated copper grid. On the substrate, the most typical observation was regions with large congestion of the AuNPs (Figure 2.30).

The control experiment conducted for the AuNPs stabilized by BSPP demonstrated that the nanoparticles precipitate under shaking in a solution containing 15% EtOH, 300 mM NaCl, and 10 mM PB. This explains the results obtained by TEM, where aggregates of the particles were observed instead of functionalized SPs. Consequently, the first approach cannot be used for the functionalization of **Sq6**-SPs by AuNPs.
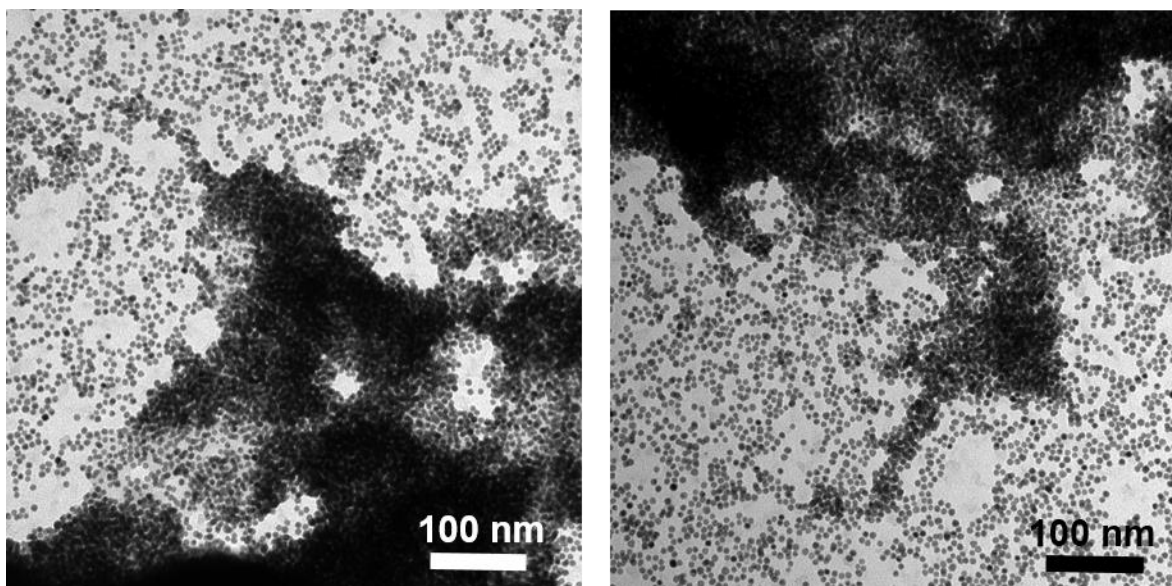
Figure 2.30. TEM images of the sample obtained after incubation of the **Sq6-SS**-polymers with AuNPs (Approach 1).

The main idea of the second approach was to prepare SPs from a mixture of two strands: squaraine-modified oligonucleotide **Sq6** and its analog containing a nanoparticle **Sq6**-AuNP (Scheme 2.8). **Sq6**-AuNPs were prepared according to Scheme 2.3: first, strands **Sq6-SS** were attached to the AuNP surface; then, the surface of **Sq6**-AuNPs was passivated by **T6-SS**. Control experiments conducted for the thus prepared **Sq6**-AuNPs demonstrated that in the aqueous ethanol solution containing 15% EtOH, 300 mM NaCl, and 10 mM PB, the particles remained non-aggregated during and after heating–cooling runs.

After preparation, the polymers formed from **Sq6** and **Sq6**-AuNP were deposited on the TEM grid for analysis. SPs are well visualized as grey "clouds" while AuNPs appear as black dots (Figure 2.31). The particles cover the polymers only partially.

We assumed that the random coverage of the surface of SPs by AuNPs could be caused by steric hindrances created by large enough particles of gold. Therefore, the SPs mainly consist of unfunctionalized oligonucleotides **Sq6**. Au-modified strands **Sq6**-AuNP are only incorporated when there is no steric hindrance, for example, in fragments with defects or at the edge positions of the SPs. Also, random coverage can occur due to electrostatic repulsion. Since the AuNPs are DNA-covered, they have a high negative charge density on the ligand shell.
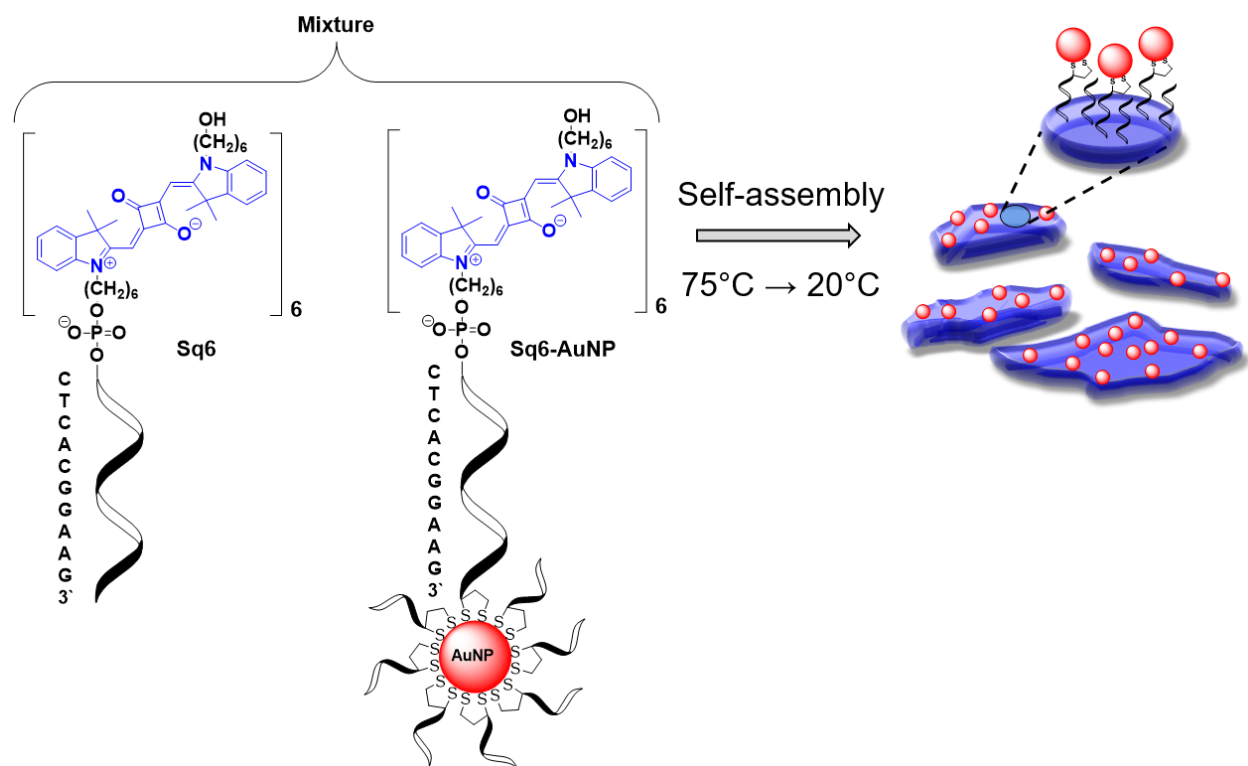
Scheme 2.8. Functionalization of the SPs by AuNPs. Approach 2. AuNP is attached to strand **Sq6-SS**.
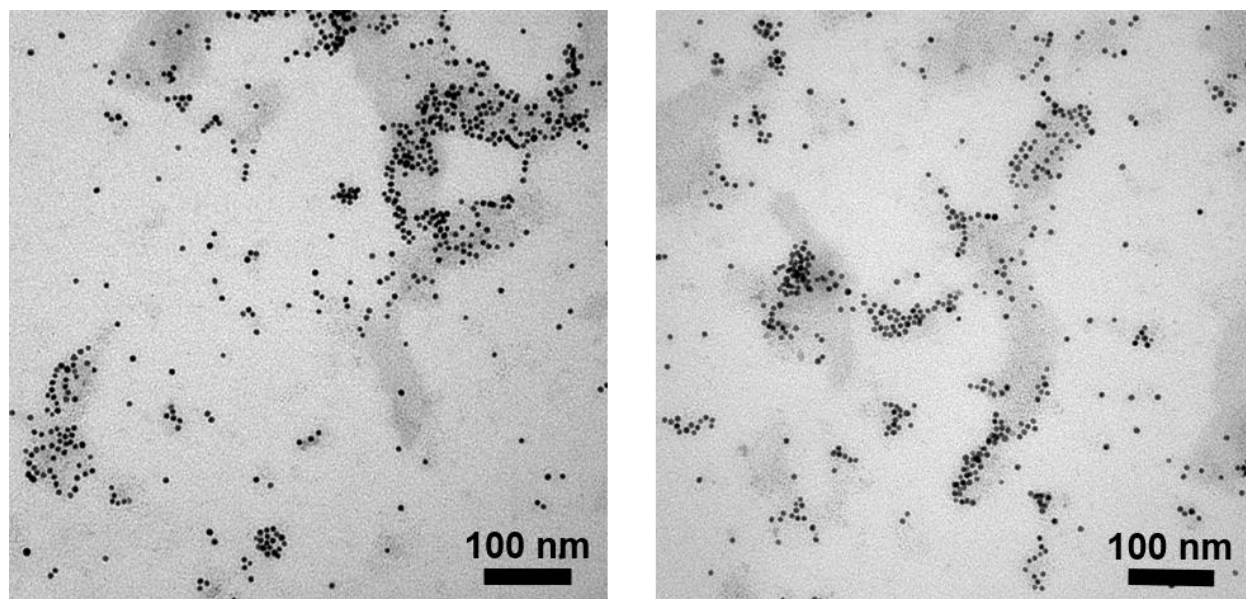
Figure 2.31. TEM images of the SPs functionalized with AuNPs, according to Scheme 2.8.

To verify these hypotheses, we synthesized oligonucleotide **Sq6T10-SS** with a nucleotide chain prolonged by 10 units, prepared SPs from the mixture of **Sq6** and **Sq6T10**-AuNP (Scheme 2.9), and analyzed the obtained sample by TEM (Figure 2.32). Prolongation of the nucleotide chain allows to arrange AuNPs at a more remote location from the SPs and, thus, avoid the steric hindrance between AuNPs upon the formation of polymers. However, even such a modification did not allow to prepare SPs equally covered by AuNPs. The results were similar as for the above-described experiment: AuNPs concentrated in some regions of the SPs (Figure 2.32). This speaks in favor of the fact that it is electrostatic repulsion that causes the random coverage of the surface of SPs by AuNPs.
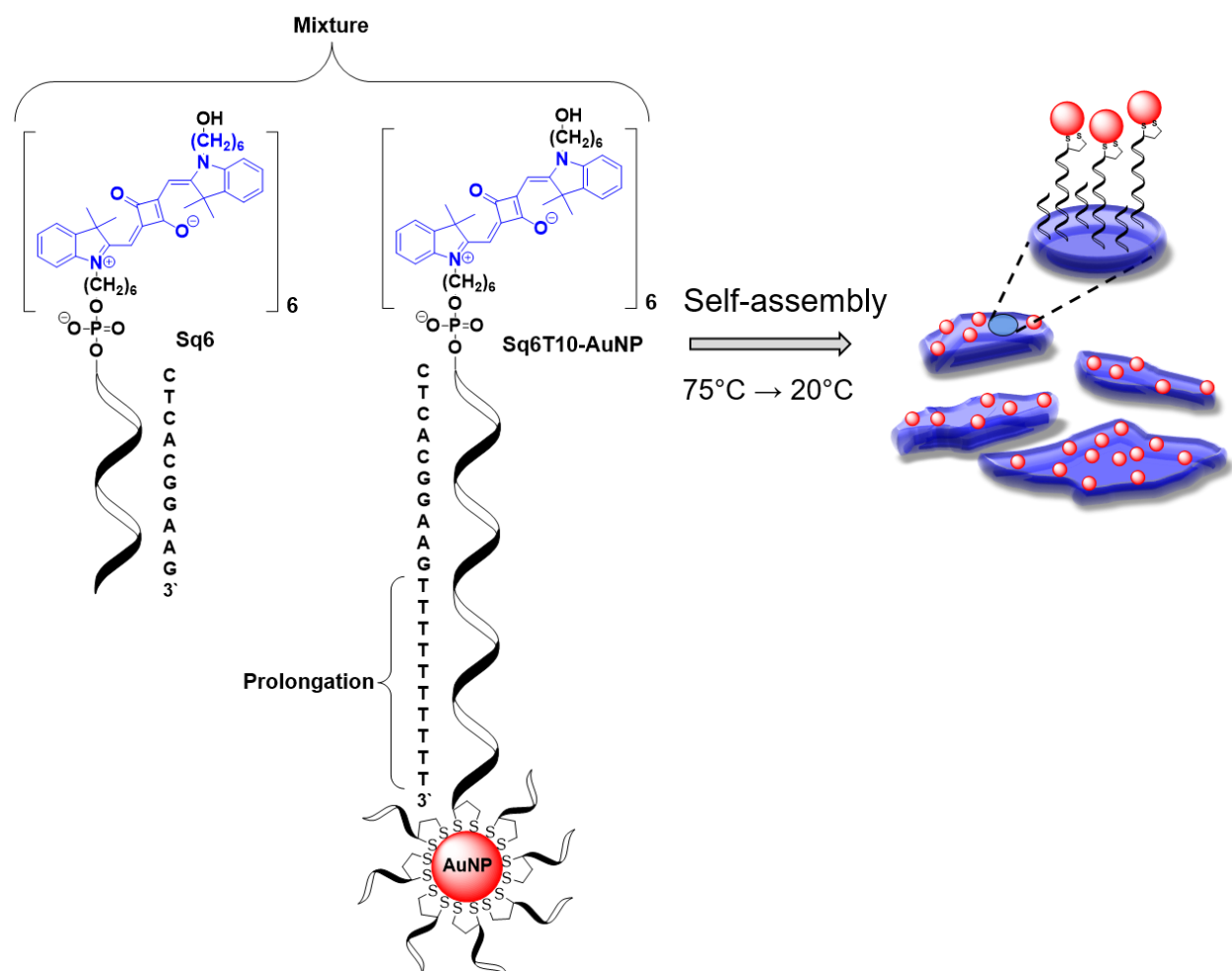
Scheme 2.9. Functionalization of the SPs by AuNPs. Approach 2. AuNP is attached to prolonged strand **Sq6T10-SS**.
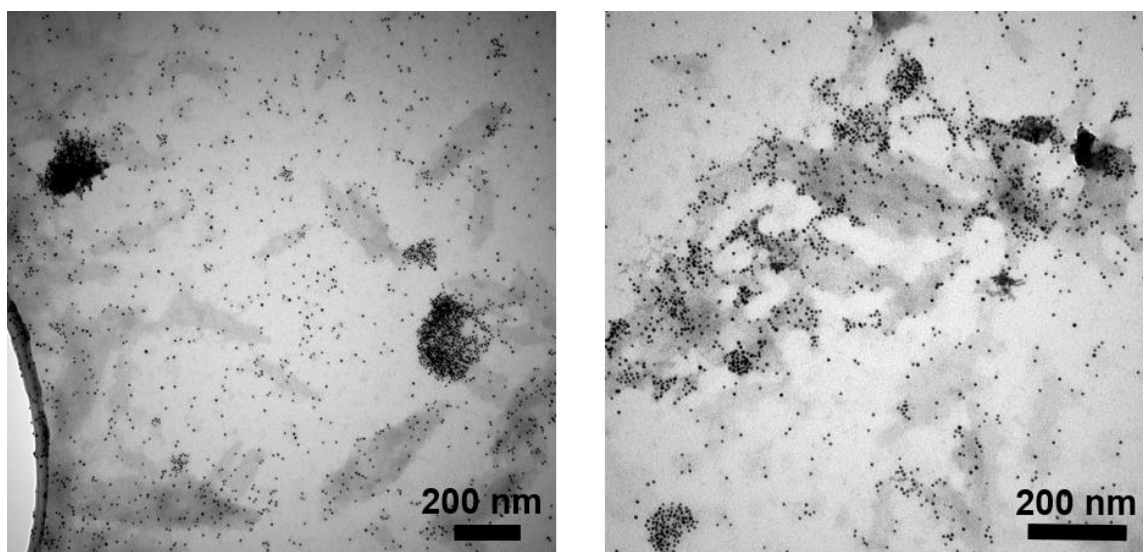
Figure 2.32. TEM images of the SPs functionalized with AuNPs by Scheme 2.9.

The third approach bases on the utilization of hybridization (Scheme 2.10). First, the SPs were formed from squaraine-modified oligonucleotides **Sq6**. Then, nucleotides of the **Sq6**-polymers hybridized sequence specifically to the nucleotides attached to AuNP. The nanoparticles were functionalized and stabilized according to Scheme 2.3.
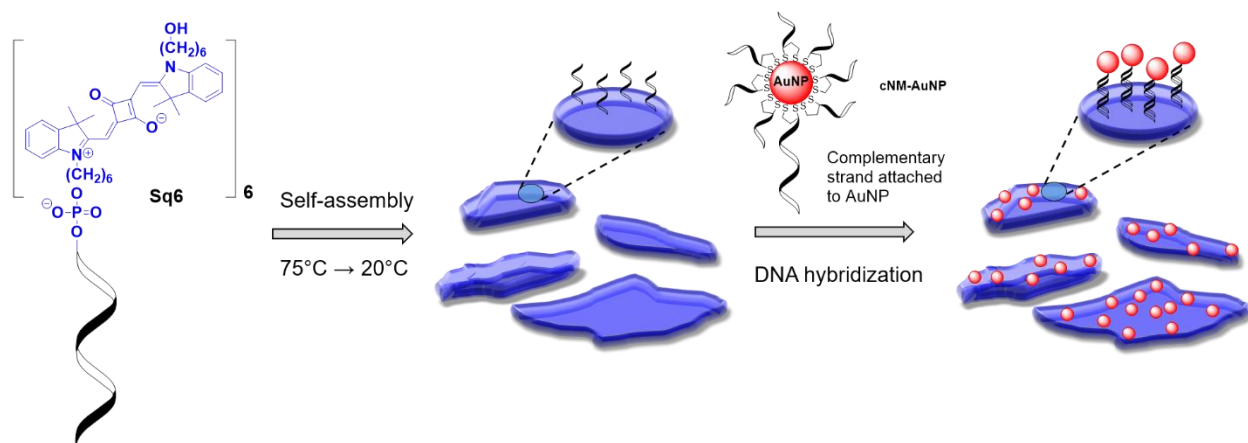
Scheme 2.10. Functionalization of the SPs by AuNPs. Approach 3. AuNP is attached to complementary oligonucleotide strand **cNM-SS**.

The preformed **Sq6**-polymers were incubated with AuNP-modified oligonucleotide **cNM**-AuNP (for structure see Table 2.5). As a result, almost complete disassembly of the initial supramolecular

polymers occurred. On the TEM grid (Figure 2.33A), we observed little fragments of the **Sq6**-SPs without well-defined shapes or bulks of large fragments plentifully covered by AuNPs. Most likely, the nanoparticles start to disrupt the SPs after attachment to their surface. This is confirmed by the results of the control experiment where the AuNPs modified by non-complementary strand **NC-**AuNPs were used instead of **cNM**-AuNP. In the control experiment, the flakes-like shaped SPs and randomly distributed **NC**-AuNPs appeared on the grid (Figure 2.33B).
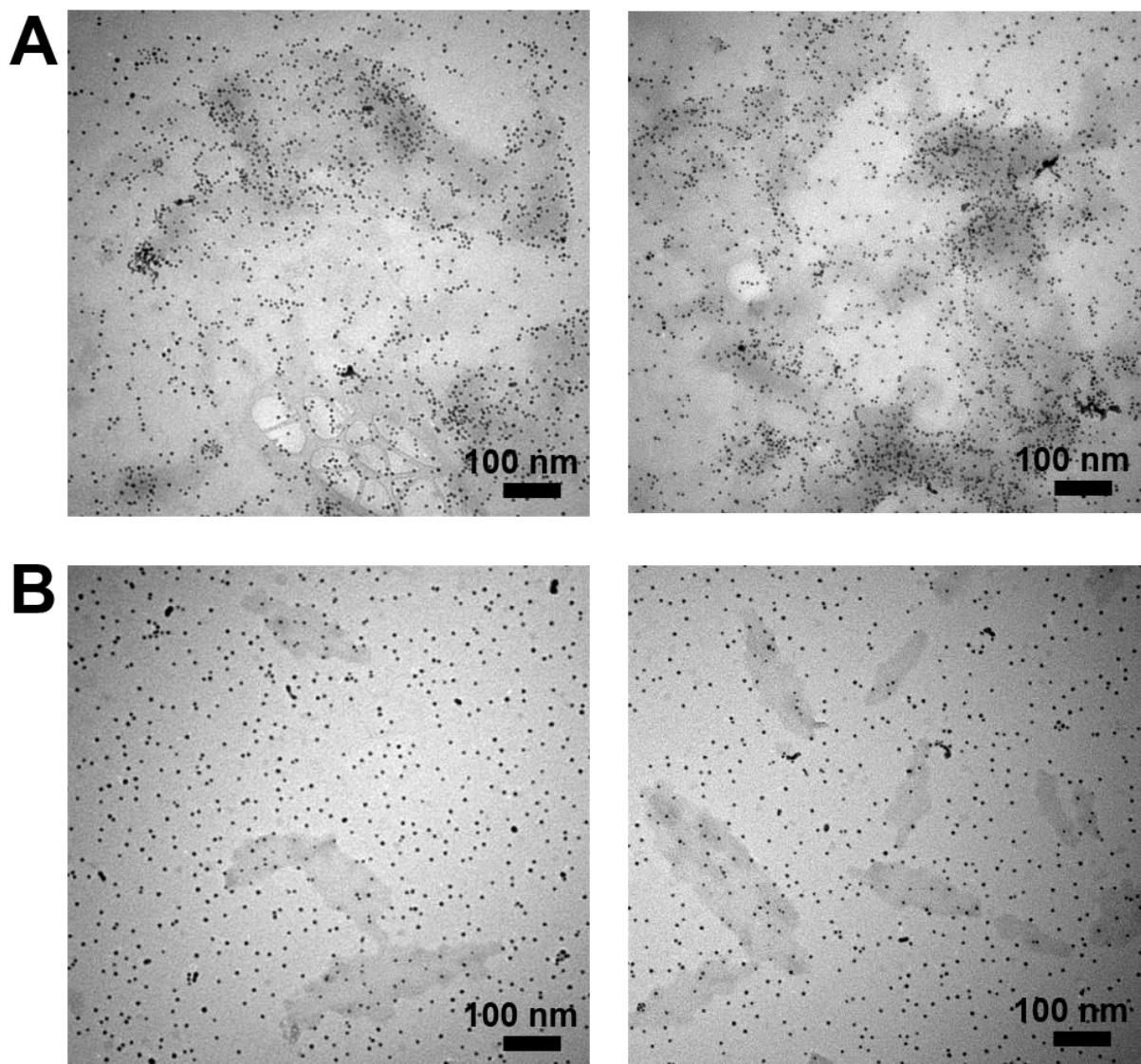
Figure 2.33. A: TEM images of **Sq6**-SPs treated with **cNM**-AuNPs (Scheme 2.10). B: Control experiment. **Sq6**-SPs were treated with **NC**-AuNPs.

To avoid disruption of the supramolecular polymers, we inserted additional 10 nucleotides into the structure of oligonucleotide attached to AuNPs (Scheme 2.11). In this way, it is possible to attach the AuNPs at a more remote location from the SPs and prevent their interactions.
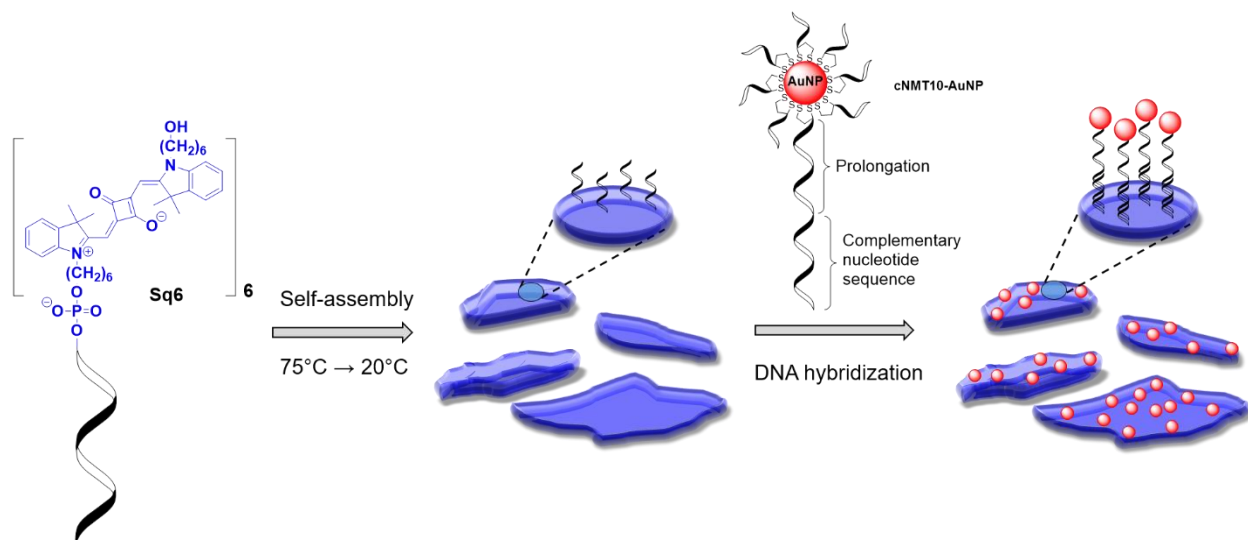
Scheme 2.11. Functionalization of the SPs by AuNPs. Approach 3. AuNP is attached to prolonged strand **cNMT10-SS** containing the complementary sequence.

After incubation of **Sq6**-polymers with **cNMT10**-AuNPs, TEM images (Figure 2.34A) show the attachment of AuNPs to the SPs. An approximation of the surface coverage (AuNP's per SP area) indicates values ranging from 4% to 14%. Control experiments with a non-complementary, AuNP-modified oligonucleotide (**NCT10**-AuNP) showed only a small number of randomly deposited AuNPs (Figure 2.34B). This sort of background deposition of AuNPs on the TEM grids always observed. We ascribe it to the presence of a relatively high concentration of NaCl. This is supported by control experiments that were performed in the absence of NaCl. TEM images revealed that no AuNPs were deposited on the grids under such conditions (Figure 2.35).
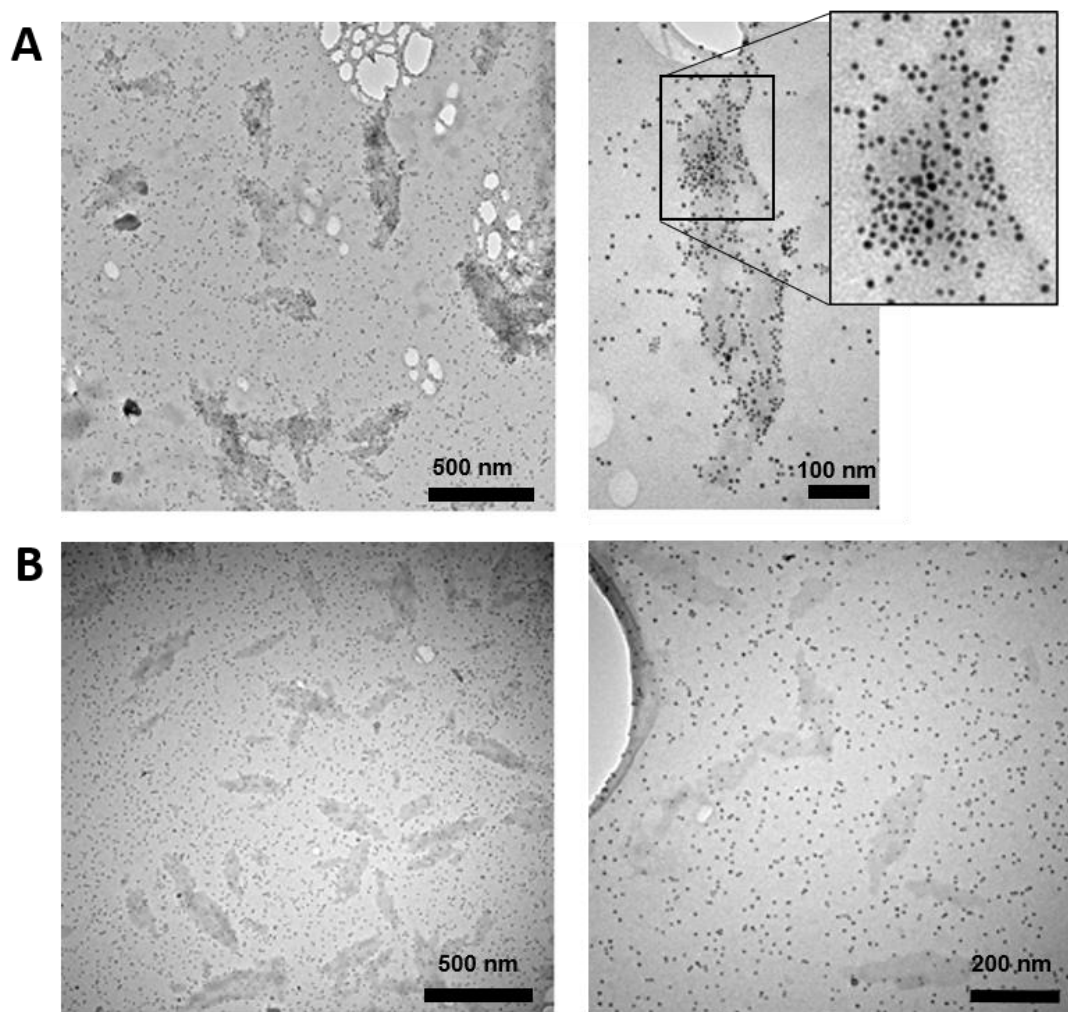
Figure 2.34. TEM images of **Sq6**-SPs treated with **cNMT10**-AuNPs (A) or **NCT10**-AuNPs (B).
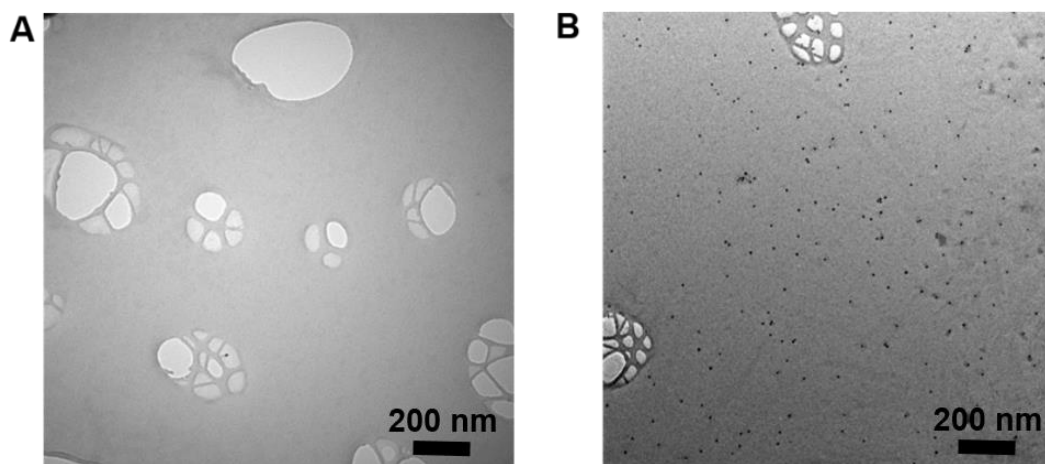
Figure 2.35. TEM images of the sample containing **cNMT10**-AuNPs suspended in water (A) or aqueous medium consisting of 15% EtOH, 300 mM NaCl, and 10 mM PB (B).

2.3 Conclusions

Oligophosphodiesters containing up to six squaraine units were successfully synthesized via solid-phase phosphoramidite chemistry and used to create long-wavelength water-compatible supramolecular polymers.

The squaraine trimer **SqTr** and hexamer **SqHex** demonstrate similar aggregation and supramolecular behavior in aqueous ethanol solutions containing NaCl and PB: at concentrations of EtOH more than 30–35%, they form *H*-type aggregates, while at lower EtOH concentrations, the oligomers self-assemble into SPs. In the SPs, the transition dipole moments of the squaraine molecules are oriented obliquely. Due to high hydrophobicity, the supramolecular polymers precipitate upon formation. The SPs of **SqTr** and **SqHex** were visualized by AFM on neither APTES-modified nor on unmodified mica substrates.

Squaraine-modified oligonucleotides **SqN** containing ten nucleotides and a variable length of the squaraine segment (N = 1, 3, 6) self-assemble to supramolecular polymers in aqueous media, depending on the conditions and the number of squaraine units. The formation of SPs results in the splitting of the long-wavelength absorption band of squaraine and is accompanied by a distinct exciton couplet in the CD spectrum. The fluorescence of SPs is almost undetectable. The SPs forms flake-like nanostructures. The presence of functional groups at the 3'-position of 5'-squaraine-modified oligonucleotides does not affect their ability to form SPs.

Duplexes constructed from 20 nucleotides with three squaraine overhangs form supramolecular polymers in aqueous ethanol solutions containing spermine tetrahydrochloride. The self-assembly results in large vesicular structures.

The SPs formed from squaraine-modified oligonucleotides can be further functionalized using sequence-specific deposition via DNA hybridization. This allows applications such as DNA- or RNA-addressed targeting and delivery devices based on our SPs.

2.4 Experimental Section

Synthesis of the Squaraine Phosphoramidite.

The synthesis of the squaraine phosphoramidite was adapted from a published procedure [124] with small changes to the original protocols and is shown in Scheme 2.12. The synthesis consists of four steps.
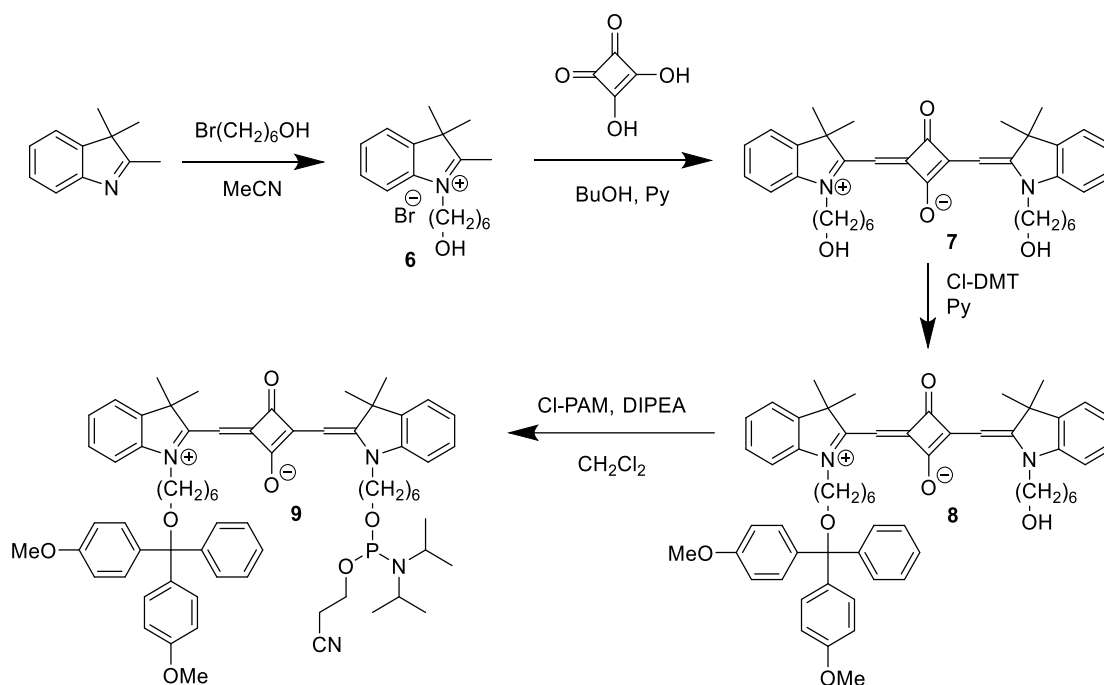
Scheme 2.12. Synthesis of squaraine phosphoramidite **9**.

Synthesis of compound **6**.

A mixture of 2,3,3-trimethylindolenine (4 g, 25.1 mmol) and 6-bromo-1-hexanol (5.46 g, 30.1 mmol) in acetonitrile (30 ml) was refluxed under argon for 30 hours. The solvent was removed under reduced pressure, and the residue was purified by column chromatography (Silica gel 60, 0–30% MeOH in CH_2Cl_2) to give the product **6**. R_f = 0.67 (Silica gel 60, 15% MeOH in CH_2Cl_2). λ(Abs) = 279 nm (MeOH). Yield: 3.64 g (43%).

^{1}H-NMR (300 MHz, DMSO, ppm): δ 8.03–7.94 (1H, m, arom H), 7.89–7.81 (1H, m, arom H), 7.66–7.59 (2H, m, arom H), 4.46 (2H, t, J = 7.72 Hz, NCH$_2$), 3.37 (2H, t, J = 5.93 Hz, CH$_2$OH), 2.86 (3H, s, 2-CH$_3$), 1.91–1.72 (2H, m, CH$_2$), 1.54 (6H, s, 3-CH$_3$), 1.49–1.29 (6H, m, CH$_2$).

^{13}C-NMR (75 MHz, DMSO, ppm): δ 196.41, 141.87, 141.04, 129.37, 128.93, 123.52, 115.48, 60.43, 54.14, 47.58, 40.35, 40.08, 39.80, 39.52, 39.24, 38.96, 38.69, 32.17, 27.25, 25.74, 25.10, 22.01, 14.06.

ESI-MS (pos., MeOH): mass calc. for C$_{17}$H$_{26}$NO$^+$ = 260.2009; mass found = 260.2002.

Synthesis of compound **7**.

Compound **6** (950 mg, 2.79 mmol) was dissolved in pyridine (10 ml). Then 3,4-dihydroxy-3-cyclobutene-1,2-dione (150 mg, 1.32 mmol) and 1-butanol (10 ml) were added. The mixture was stirred at 110 °C for 5 hours. The solvent was removed under reduced pressure, and the residue was purified by column chromatography (Silica gel 60, 0–8% MeOH in CH$_2$Cl$_2$) to give the diol **7** as a blue powder. R$_f$ = 0.39 (Silica gel 60, 7% MeOH in CH$_2$Cl$_2$). Yield: 340 mg (43%).

^{1}H-NMR (300 MHz, DMSO, ppm): δ 7.51 (2H, d, J = 7.35 Hz, arom H), 7.40–7.25 (4H, m, arom H), 7.16 (2H, t, J = 6.87 Hz, arom H), 5.80 (2H, s, CH), 4.36 (2H, t, J = 5.18 Hz, OH), 4.07 (4H, t, J = 6.5 Hz, NCH$_2$), 3.38 (4H, t, J = 5.56 Hz, CH$_2$OH), 1.81-1.55 (4H, m, CH$_2$), 1.68 (12H, s, 3-CH$_3$), 1.50-1.26 (12H, m, CH$_2$).

^{13}C-NMR (75 MHz, CDCl$_3$, ppm): δ 178.63, 170.27, 142.42, 142.29, 127.89, 123.85, 122.41, 109.45, 86.66, 62.56, 49.37, 43.19, 32.50, 27.10, 26.25, 26.21, 24.93.

ESI-MS (pos., MeOH): mass calc. for C$_{38}$H$_{48}$N$_2$O$_4$ = 596.3614; mass found = 596.3601.

Synthesis of compound **8**.

4,4'-Dimethoxytrityl chloride (320 mg, 0.947 mmol) was added to a solution of the squaraine diol **7** (565 mg, 0.947 mmol) in anhydrous pyridine (12 ml). The mixture was stirred overnight at room temperature and under argon. The solvent was removed under reduced pressure, and the residue

was purified by column chromatography (Silica gel 60, 0–4% MeOH in CH_2Cl_2/EtOAc/Et_3N, 49/49/2, v/v/v) to yield the compound **8**. R_f = 0.65 (Silica gel 60, 7% MeOH in CH_2Cl_2). Yield: 390 mg (37%).

^{1}H-NMR (300 MHz, DMSO, ppm): δ 7.52 (2H, d, J = 7.53 Hz, arom H), 7.40–7.11 (15H, m, arom H), 6.87 (4H, d, J = 9.04 Hz, arom H), 5.80 (1H, s, CH), 5.79 (1H, s, CH), 4.35 (1H, t, J = 5.18 Hz, OH), 4.15–3.96 (4H, m, NCH_2), 3.71 (6H, s, OCH_3), 3.38 (2H, t, J = 5.84 Hz, C$\underline{H}_2$OH), 2.93 (2H, t, J = 6.21 Hz, CH_2DMT), 1.80–1.60 (4H, m, CH_2), 1.67 (6H, s, 3-CH_3), 1.66 (6H, s, 3-CH_3), 1.58–1.47 (2H, m, CH_2), 1.46–1.25 (10H, m, CH_2).

^{13}C-NMR (75 MHz, $CDCl_3$, ppm): δ 179.22, 179.11, 170.23, 170.15, 158.40, 145.45, 142.55, 142.46, 142.33, 136.78, 130.10, 128.30, 127.88, 127.80, 126.68, 123.81, 122.42, 117.57, 113.09, 109.47, 109.40, 86.73, 86.62, 85.79, 77.58, 77.16, 76.74, 63.30, 62.64, 55.30, 49.41, 49.36, 45.91, 43.79, 43.14, 32.51, 30.07, 27.15, 27.13, 26.28, 26.24, 26.15, 24.88.

ESI-MS (pos., CH_2Cl_2): mass calc. for $C_{59}H_{66}N_2O_6$ = 898.4921; mass found = 898.4888.

Synthesis of compound **9**.

To a solution of compound **8** (390 mg, 0.434 mmol) and diisopropylethylamine (226 µL, 1.3 mmol) in anhydrous dichloromethane (8 ml), 2-Cyanoethyl-*N*,*N*-diisopropylchlorophosphor-amidite (145 µL, 0.651 mmol) was added under argon atmosphere. The mixture was stirred at room temperature for 2 hours. The mixture was partially concentrated under reduced pressure and purified by column chromatography (Silica gel 60, 50–100% EtOAc in hexane containing 1% of Et_3N). Note: use only freshly distilled Et_3N and anhydrous EtOAc and hexane. The fractions containing the product were combined and concentrated to a volume of about 2 mL. Cold (-28 °C) hexane (100 mL) was added, and the solution was kept at -28 °C for 2 hours. A blue precipitate was formed, the material was filtered off, and the product was dried under high vacuum to give phosphoramidite **9**. R_f = 0.57 (Silica gel 60, EtOAc containing 1% of Et_3N). Yield: 215 mg (45%).

^{1}H-NMR (300 MHz, $CDCl_3$, ppm): δ 7.46–7.07 (15H, m, arom H), 6.96 (2H, t, J = 7.82 Hz, arom H), 6.82 (4H, d, J = 8.85 Hz, arom H), 5.94 (2H, s, CH), 4.09-3.89 (4H, m, NCH_2), 3.89–

3.75 (2H, m, C$\underline{H}$CH$_3$), 3.77 (6H, s, OCH$_3$), 3.70–3.50 (4H, m, CH$_2$OP), 3.03 (2H, t, J = 6.5 HZ, CH$_2$ODMT), 2.62 (2H, t, J = 6.5 Hz, CH$_2$CN), 1.88–1.71 (4H, m, CH$_2$), 1.78 (12H, s, 3-CH$_3$), 1.68–1.55 (4H, m, CH$_2$), 1.51–1.37 (8H, m, CH$_2$), 1.22–1.10 (12H, m, CHC$\underline{H}_3$).

^{13}C-NMR (75 MHz, CDCl$_3$, ppm): δ 179.59, 179.49, 170.10, 170.05, 158.37, 145.43, 142.54, 142.28, 136.75, 130.08, 128.27, 127.84, 127.78, 126.65, 123.75, 122.38, 117.79, 113.06, 109.42, 86.61, 85.77, 77.58, 77.16, 76.74, 63.57, 63.34, 63.27, 58.52, 58.27, 55.27, 49.36, 43.76, 43.71, 43.15, 42.98, 31.18, 31.08, 30.04, 27.16, 27.12, 26.90, 26.25, 25.87, 24.78, 24.73, 24.69, 24.64, 20.50, 20.41.

^{31}P-NMR (121 MHz, CDCl$_3$, ppm): δ = 147.25.

ESI-MS (pos., CH$_2$Cl$_2$): mass calc. for C$_{68}$H$_{83}$N$_4$O$_7$P = 1098.5999; mass found = 1098.5958.

Solid Phase Synthesis of the Squaraine-Containing Oligophosphodiesters.

The syntheses of the squaraine homo-oligomers **SqTr** and **SqHex** and the squaraine-modified oligonucleotides **Sq1**, **cSq1**, **Sq3**, **cSq3**, **Sq6**, **cSq6**, **Sq3-ON20**, and **cSq3-ON20** were performed via automated oligonucleotide synthesis on a 394-DNA/RNA synthesizer (*Applied Biosystems*). The coupling time between nucleotide and squaraine and squaraine and squaraine was increased to 3 minutes.

Squaraine homo-oligomers **SqTr** and **SqHex** were synthesized according to the standard procedure: dmf-protected dG, benzyl-protected dA, acetyl-protected dC, CapA containing acetic anhydride. Universal support Glen Unisupport (GlenResearch) was used for the synthesis. Cleavage from the solid support and final deprotection were done by treatment with 50 mM potassium carbonate solution in methanol at room temperature for 4 hours.

For the syntheses of **Sq1**, **cSq1**, **Sq3**, **cSq3**, **Sq6**, and **cSq6**, the UltraMILD procedure (GlenResearch) was applied, using the corresponding phosphoramidites, solid-supports, and reagents (Cap A). The conditions for the cleavage and deprotection were the same as for **SqTr** and **SqHex**.

Oligonucleotides **Sq3-ON20** and **cSq3-ON20** were prepared by standard procedure. The cleavage and deprotection were done by treating a solution containing *t*-butylamine, methanol, and water (1:1:2, v:v:v) at 55 ºC for 16 hours.

The squaraine-containing oligophosphodiesters were purified by reverse-phase HPLC: column C4 polymer, 250 mm × 4.6 mm, Supelco; mobile phase A = (Et$_3$NH)OAc (0.1 M, pH 7.0), mobile phase B = MeCN; elution at 40 °C. For **SqTr**, **SqHex**, **Sq1**, **cSq1**, **Sq3**, **cSq3**, **Sq6**, and **cSq6**: gradient 40–100% B over 15 min; flow 0.5 ml/min. For **Sq3-ON20** and **cSq3-ON20**: gradient 0–100% B over 20 min; flow 1 ml/min.

Table 2.6. Name, sequence, chemical formula, and calculated and found mass (from the MS analysis) of the squaraine oligomers and oligonucleotides.

Name	Sequence	Chem. formula	Calc. mass	Found mass	Yield [nmol]
SqTr	(Sq)$_3$	C$_{114}$H$_{140}$N$_6$O$_{16}$P$_2$	1910.9801	1910.98	212
SqHex	(Sq)$_6$	C$_{228}$H$_{278}$N$_{12}$O$_{34}$P$_5$	3882.9082	3882.95	112
Sq1	Sq-CTCACGGAAG – 3'	C$_{135}$H$_{169}$N$_{43}$O$_{62}$P$_{10}$	3693.8770	3693.8836	160
cSq1	Sq-CTTCCGTGAG – 3'	C$_{135}$H$_{171}$N$_{37}$O$_{66}$P$_{10}$	3675.8538	3675.8598	150
Sq3	(Sq)$_3$-CTCACGGAAG – 3'	C$_{211}$H$_{263}$N$_{47}$O$_{74}$P$_{12}$	5010.5113	5010.5172	113
cSq3	(Sq)$_3$-CTTCCGTGAG – 3'	C$_{211}$H$_{265}$N$_{41}$O$_{78}$P$_{12}$	4992.4882	4992.4938	104
Sq6	(Sq)$_6$-CTCACGGAAG – 3'	C$_{325}$H$_{404}$N$_{53}$O$_{92}$P$_{15}$	6985.4629	6985.4792	116
cSq6	(Sq)$_6$-CTTCCGTGAG – 3`	C$_{325}$H$_{406}$N$_{47}$O$_{96}$P$_{15}$	6967.4397	6967.4600	130
Sq3-ON20	(Sq)$_3$-CTTCCTTGCATC-GGACCTTG – 3'	C$_{307}$H$_{389}$N$_{71}$O$_{141}$P$_{22}$	8006.9680	8006.9780	204
cSq3-ON20	(Sq)$_3$-CAAGGTCCGAT-GCAAGGAAG – 3'	C$_{310}$H$_{384}$N$_{92}$O$_{131}$P$_{22}$	8172.0443	8172.0680	138

Preparation of the Gold Nanoparticles.

The gold nanoparticles, with an average diameter of 5 nm, were prepared according to the literature [171]. Since HAuCl$_4$ is corrosive, a glass spatula was used to avoid its contact with metal. All glassware and magnetic stirring bars used in the preparation were thoroughly cleaned in aqua regia (HCl:HNO$_3$, 3:1, v:v), rinsed with distilled water, and dried in the oven before the use [169]. The

solutions of 4% $HAuCl_4$, 0.2 M K_2CO_3, and $NaBH_4$ were filtered through 0.2 µm syringe filters before the application. The molar absorptivity of the AuNPs applied for calculation of concentration was $10^7 \, M^{-1} \, cm^{-1}$ [169].

*Synthesis of the N-hydroxysuccinimide Ester (NHS-Ester) of Thioctic Acid **10** (Scheme 2.13) [170, 171].*
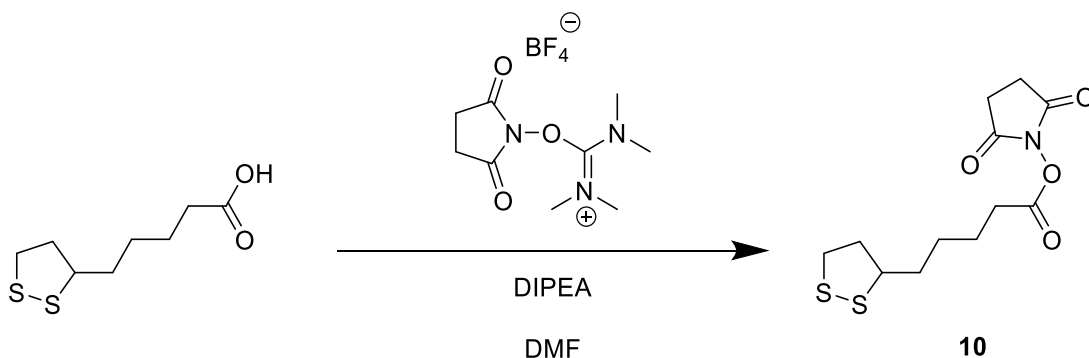
Scheme 2.13. Synthesis of NHS-ester of thioctic acid.

DIPEA (0.42 mL, 2.42 mmol) and *N,N,N′,N′*-tetramethyl-O-(*N*-succinimidyl)uronium tetrafluoroborate (TSTU, 290 mg, 0.969 mmol) were added to a solution of thioctic acid ((±)-α-lipoic acid; 100 mg, 0.485 mmol) in anhydrous DMF (1.5 mL). The mixture was stirred under argon at room temperature for one hour. Diethyl ether (40 mL) was added, and the mixture was kept at -30 °C for 16 hours. The liquid containing the crude product was decanted, and the solvents were evaporated under reduced pressure. The material was purified by column chromatography (on Silica gel 60, using EtOAc) to afford the product (100 mg, 68%).

^{1}H-NMR (300 MHz, DMSO, ppm): δ 3.68–3.56 (1H, m, CH_2), 3.25–3.06 (2H, m, CH, CH_2), 2.81 (4H, s, NHS), 2.68 (2H, t, *J* = 7.16 Hz, C$\underline{H}_2$COONHS), 2.48-2.35 (1H, m, CH_2), 1.96–1.79 (1H, m, CH_2), 1.79–1.53 (4H, m, CH_2), 1.54–1.38 (2H, m, CH_2).

ESI-MS (pos. mode, sample in MeCN): calc. mass for $C_{12}H_{17}NO_4S_2$ = 303.0599; mass found = 303.0596.

Amino-Oligonucleotides.

Amino-oligonucleotides **T6-NH2**, **cNM-NH2**, **NC-NH2**, **cNMT10-NH2**, and **NCT10-NH2** were purchased from Microsynth (Balgach, Switzerland).

Squaraine-modified amino-oligonucleotides **Sq6-NH2** and **Sq6T10-NH2** were prepared via automated oligonucleotide synthesis. The nucleotide–squaraine and squaraine–squaraine coupling time was increased to 3 minutes. The UltraMILD procedure (GlenResearch) was applied, using the corresponding phosphoramidites, 3'–amino-modified support (3'–NH$_2$-Mod C7 CPG) and reagents (Cap A). Cleavage from the solid support and final deprotection were done by treatment with 50 mM potassium carbonate solution in methanol at room temperature for 16 hours. The oligonucleotides were purified by reverse-phase HPLC: column C4 polymer, 250 mm × 4.6 mm, Supelco; mobile phase A = (Et$_3$NH)OAc (0.1 M, pH 7.0), mobile phase B = MeCN, gradient 40–100% B over 15 min; flow 0.5 ml/min; elution at 40 °C.

Table 2.7. Name, sequence, chemical formula, and calculated and found mass (from the MS analysis) of the amino-oligonucleotides **Sq6-NH2** and **Sq6T10-NH2**.

Name	Sequence	Chem. formula	Calc. mass	Found mass	Yield [nmol]
Sq6-NH2	(Sq)$_6$-CTCACGGAAG-NH$_2$ – 3'	C$_{332}$H$_{420}$N$_{54}$O$_{96}$P$_{16}$	7194.5445	7194.5610	57
Sq6T10-NH2	(Sq)$_6$-CTCACGGAAG-TTTTTTTTTT-NH$_2$ – 3'	C$_{432}$H$_{550}$N$_{74}$O$_{166}$P$_{26}$	10235.0050	10235.9309	338

Synthesis of the Thioctic Acid-Modified Oligonucleotides (Scheme 2.14).
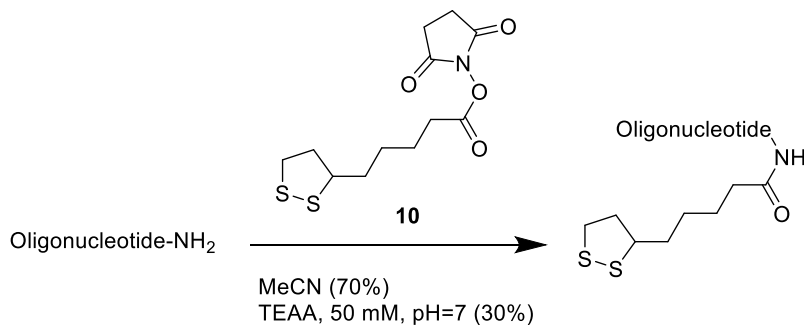
Scheme 2.14. Synthesis of the thioctic acid-modified oligonucleotides.

The amino-modified oligonucleotide **T6-NH2**, **cNM-NH2**, **NC-NH2**, **cNMT10-NH2**, **NCT10-NH2**, **Sq6-NH2** or **Sq6T10-NH2** was dissolved in 500 µL of a mixture of MeCN (70%) and TEAA (50 mM, pH = 7) (30%). The NHS-ester of thioctic acid **10** was added in a 200 equimolar excess [171]. The reaction was carried out in a lab-shaker at 25 °C overnight. To the reaction mixture, TEAA (2 mL, 0.1 M, pH = 7) was added. The solution was filtered via a 0.45 µm disposable syringe filter, and the crude product was purified by RP-HPLC. Mobile phase A = (Et₃NH)OAc (0.1 M, pH 7.0), mobile phase B = MeCN. Overall yields of 41–66% were achieved.

The purification of **T6-SS**, **cNM-SS**, **NC-SS**, **cNMT10-SS**, and **NCT10-SS**. Column: Clarity® 5 µm Oligo-RP, 250 mm × 4.6 mm, Phenomenex®; gradient 0% to 100% of solvent B within 20 min; flow rate = 1 mL/min; elution at 40 °C.

The purification of **Sq6-SS** and **Sq6T10-SS**. Column: C4 polymer, 250 mm × 4.6 mm, Supelco; gradient 40% to 100% of solvent B within 15 min; flow rate 0.5 ml/min; elution at 40 °C.

Table 2.8. Name, sequence, chemical formula, and calculated and found mass (from the MS analysis) of the thioctic acid-modified oligonucleotides.

Name	Sequence	Chemical formula	Mass. calc.	Mass. found
Sq6-SS	(Sq)₆-CTCACGGAAG-Thioctic acid – 3'	$C_{340}H_{432}N_{54}O_{97}P_{16}S_2$	7382.5775	7382.5910
Sq6T10-SS	(Sq)₆-CTCACGGAAGTTTTTTTTTT-Thioctic acid – 3'	$C_{440}H_{562}N_{74}O_{167}P_{26}S_2$	10423.0379	10423.9440
T6-SS	5' – TTTTTT-Thioctic acid	$C_{75}H_{107}N_{13}O_{45}P_6S_2$	2159.4351	2159.4396
cNM-SS	5' – Thioctic acid-CTTCCGTGAG – 3'	$C_{111}H_{150}N_{36}O_{64}P_{10}S_2$	3384.6407	3384.6416
NC-SS	5' – Thioctic acid-ATTGAAGTCC – 3'	$C_{112}H_{150}N_{38}O_{62}P_{10}S_2$	3392.6571	3392.6550
cNMT10-SS	5' – Thioctic acid-TTTTTTTTTTCTTCCGTGAG – 3'	$C_{211}H_{280}N_{56}O_{134}P_{20}S_2$	6425.1012	6425.1040
NCT10-SS	5' – Thioctic acid-TTTTTTTTTTATTGAAGTCC – 3'	$C_{212}H_{280}N_{58}O_{132}P_{20}S_2$	6433.1175	6433.1200

Functionalization of the SPs by AuNPs.

Approach 1.

The SPs were prepared from oligonucleotide **Sq6-SS** (1 µM **Sq6-SS**, 15% EtOH, 300 mM NaCl, 10 mM PB). The sample was heated to 75 °C and then cooled to 20 °C (with a rate of 0.5 °C/min). Then, the **Sq6-SS** polymers (1 eq.) and the AuNPs (0.05 eq.) were combined and kept in the lab-shaker (700 rpm) for 16 hours at room temperature.

Approach 2.

First, AuNP-modified oligonucleotides (**Sq6**-AuNPs or **Sq6T10**-AuNPs) were prepared. The general procedure to prepare the AuNP-modified oligonucleotides (Approaches 2 and 3) was as follows [170]: AuNPs (0.3 nmol) and the oligonucleotide (containing thioctic acid) (0.6 nmol) were incubated overnight at room temperature in 0.5 × TBE buffer containing 50 mM NaCl. Afterward, oligo **T6-SS** (30 nmol) was added, and the mixture was incubated for an additional 12 h. Then, the sample was centrifuged twice (12 000 rpm, 35 min), the supernatant was removed, and the remaining precipitate was diluted with Milli-Q water. Then, the SPs were prepared from a mixture of oligonucleotides **Sq6** and **Sq6**-AuNP (1 µM **Sq6**, 0.05 µM **Sq6**-AuNP, 15% EtOH, 300 mM NaCl, 10 mM PB) or **Sq6T10**-AuNP (conditions the same). The sample was heated to 75 °C and then cooled to 20 °C (with a rate of 0.5 °C/min).

Approach 3.

First, AuNP-modified oligonucleotides (**cNM**-AuNPs, **NC**-AuNPs, **cNMT10**-AuNPs, **NCT10**-AuNPs) were prepared in the way as described above in Approach 2. Next, the SPs were prepared from oligonucleotide **Sq6** (1 µM **Sq6**, 15% EtOH, 300 mM NaCl, 10 mM PB). The sample was heated to 75 °C and then cooled to 20 °C (with a rate of 0.5 °C/min). Finally, the **Sq6**-SPs (1 eq.) and the AuNP-modified samples (0.03 eq.) were combined and kept in the lab-shaker (700 rpm) for 16 hours at room temperature.

Chapter 3. SPs Based on Core-Substituted Squaraine Chromophores

3.1 Introduction

The goal of the project is to obtain new water-compatible squaraine-based monomers for SPs and investigate how the modifications in the squaraine chromophore influence its ability to form supramolecular polymers in an aqueous media.
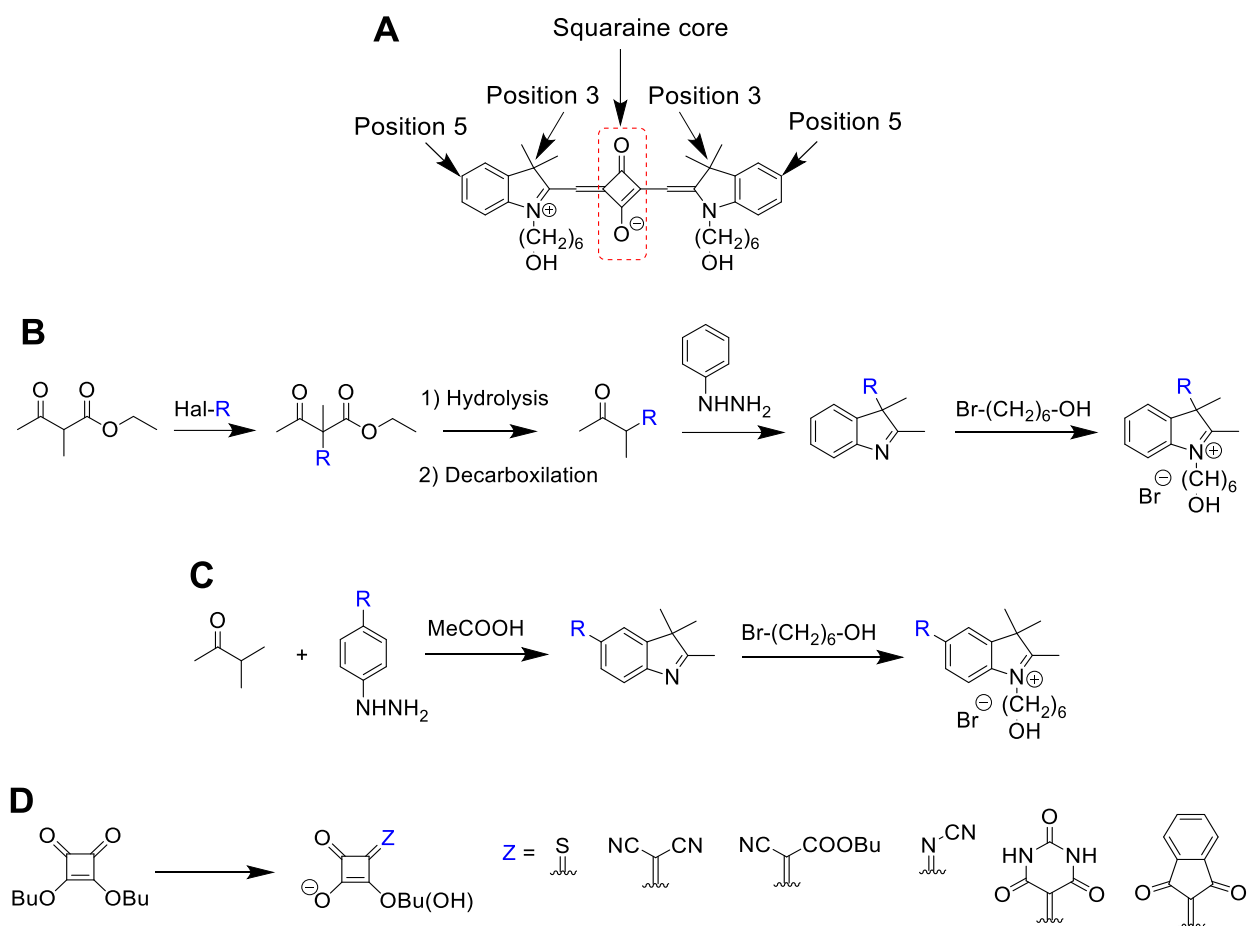
Scheme 3.1. A: Structure of the squaraine molecule containing two indolenine moieties. B: Synthesis of the indolenines with a substituent in position 3. C: Preparation of the indolenines modified in 5 position. D: Substitution of one oxygen in the squaraine ring.

There are several ways to introduce substituents into the squaraine molecule containing indolenine moieties. In the indolenine residue, positions 3 and 5 are the most synthetically available for modification (Scheme 3.1A). However, the synthesis of such indolenines, even from commercially available reagents, requires several steps (Scheme 3.1B and 3.1C). On the other hand, substituents can be easily introduced in the squaraine core via a one-step synthesis (Scheme 3.1D). Thus, the simplest way to prepare modified squaraines is to utilize derivatives of squaric acid for their synthesis. We found literature reports on ring-substituted squaraine dyes that contain sulfur, malononitrile, cyanoacetic ester, cyanamide, barbituric acid, or 1,3-indanedione residues instead of the oxygen (Scheme 3.1D) [48, 175, 176].

The introduction of substituents into the cyclobutene fragment leads to a change of conformation, planarity, electron density distribution in the squaraine chromophore, and, as a result, photophysical properties. Thus, unsubstituted oxy-squaraine adopts a *trans,anti(1)*-conformation, squaraines with a dicyanomethylene group have a *cis,syn*-conformation, and squaraines containing barbituric group have a *cis,syn(2)*-conformation (Figure 3.1) [49]. In contrast to oxy-squaraine, barbituric- and dicyanomethylene-squaraines are less planar. Also, the substitution of the oxygen atom causes a noticeable increase in the calculated dipole moments.

Figure 3.1. Conformation of the oxy-, dicyanomethylene-, and barbituric-squaraines [49].

Among the ring-substituted squaraines, the dyes with the dicyanomethylene group are the most extensively studied [177, 178]. These compounds found application in the near-infrared fluorescence and photoacoustic tomography imaging [79], as labels for proteins [176, 179] and parallel G-quadruplexes [180], and in solar cells [181, 182].

For supramolecular chemistry, squaraines modified with barbituric acid are, probably, the most attractive. Barbituric acids are promising building blocks for the preparation of supramolecular compounds due to their ability to form multiple hydrogen bonds [183]. The photophysical properties of the barbituric squaraines are well studied, and some of them were proposed for application in protein labeling [179] and photodynamic therapy [184].

In this section, we describe the synthesis of two novel squaraine phosphoramidites, which contain a dicyanomethylene or barbituric acid group in the squaraine core. We demonstrate the possibility of using these phosphoramidites to synthesize phosphodiester-linked trimers and modified oligonucleotides and study aggregation and supramolecular polymerization of the obtained oligophosphodiesters in aqueous media.

3.2 Results and Discussion

3.2.1 Synthesis of the Phosphoramidites and Oligophosphodiesters

The syntheses of the ring-substituted squaraine phosphoramidites were started from the preparation of dicyanomethylene and barbituric acid derivatives **11** and **12** of dibutyl squarate **13** (Scheme 3.2). The syntheses were performed according to the published procedures via condensation of dibutyl squarate with malononitrile in benzene [178, 185] or with barbituric acid in ethanol [179]. The derivative **11** was isolated with 97% yield; NMR and Mass spectrometry data were in good agreement with the proposed structure. However, the derivative **12** was isolated with a yield of more than 100%. Besides the main product **12**, NMR and Mass data revealed the presence in the sample of monosubstituted product **14** with unhydrolyzed butoxy group and disubstituted side product **15** (Scheme 3.2). Therefore, we added the butoxy-group hydrolyzation step (**14** was transformed into **12**) to the synthetic procedure and purification by column chromatography. Such modifications to the original protocol allowed to isolate the barbituric derivative **12** in 65% yield.

On the next step, the derivatives **11** and **12** were used to prepare corresponding squaraine dyes **16** and **17** (Scheme 3.3). Commonly used conditions for the synthesis of the symmetrical ring-

substituted squaraines are the condensation of the squaraine core-substituted derivative (1 eq.) with a quaternized heterocycle (2 eq.) in butanol–benzene [48] or butanol–toluene mixtures [49]. The dyes **16** and **17** were synthesized in butanol–toluene; the yield after isolation was 64% for dicyanomethylene squaraine **16** and 61% for barbituric squaraine **17**.
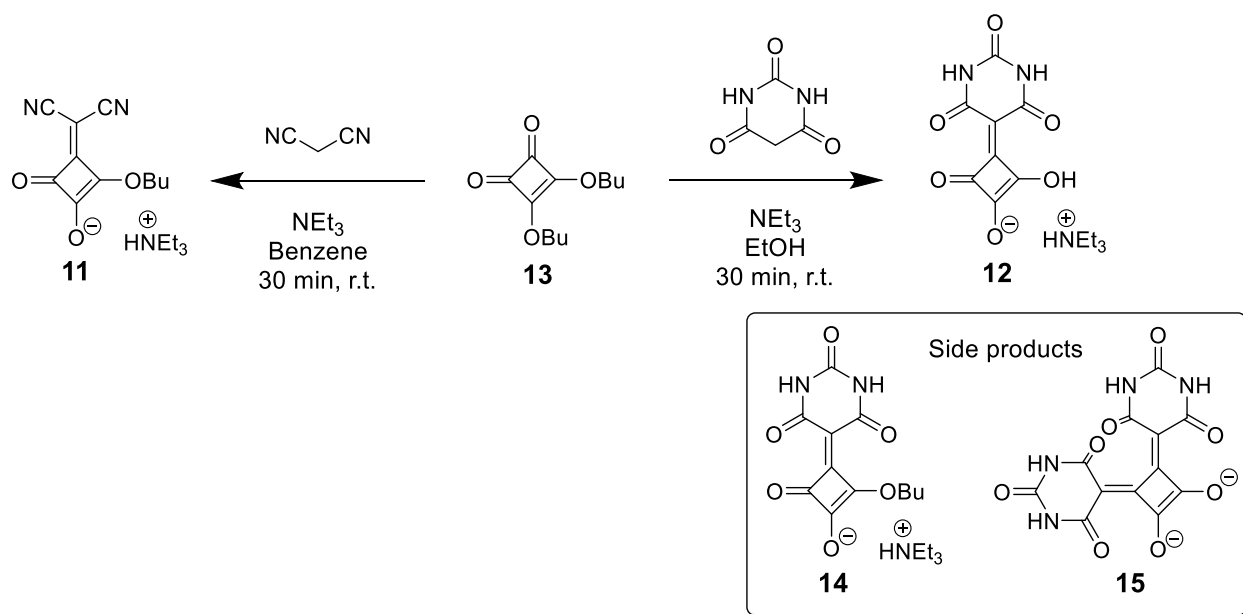
Scheme 3.2. Preparation of the dicyanomethylene **11** and barbituric acid **12** derivatives of dibutyl squarate.
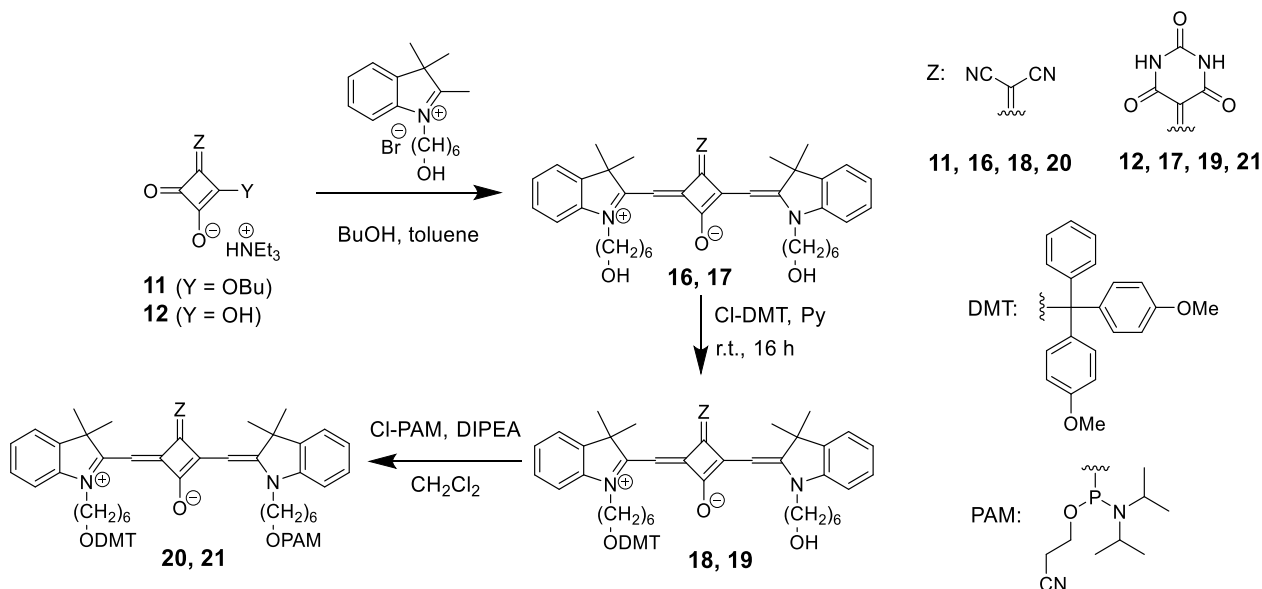
Scheme 3.3. Synthesis of the phosphoramidites of the ring-substituted squaraine dyes.

The last steps of the synthesis involved preparing mono-dimethoxytrityl derivatives **18** and **19** and corresponding phosphoramidites **20** and **21**. The syntheses were performed according to published procedures [124]. No deviation or unpredictable difficulties were observed.

Based on the results of Chapter 2, the most promising design of monomers for SPs is squaraine-modified oligonucleotides containing ten nucleotides and six squaraines. Also, phosphodiester-linked squaraine homo-oligomers can be valuable building blocks for SPs if no precipitation of the polymers is observed. Besides, the duplexes with squaraine overhangs self-assemble into SPs. In this section, we concentrated on the synthesis of the squaraine-modified oligonucleotides **CNSq6** and **BarbSq6** (for structures, see Figure 3.2 and Table 3.1). The availability of the oxy-squaraine phosphoramidite made it possible to synthesize oligonucleotide **CNOSq** where unsubstituted oxy-squaraines (*trans*-conformation) and dicyanomethylene-substituted squaraines (*cis*-conformation) are alternating [186]. Squaraine trimers **CNSqTr** and **BarbSqTr** were also prepared.
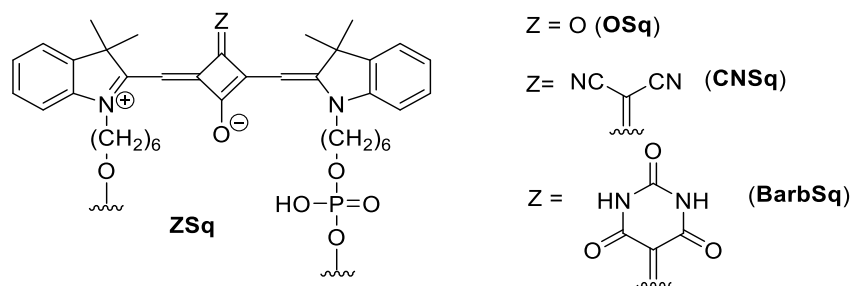
Figure 3.2. Structure of the oxy-, dicyanomethylene- and barbituric-squaraine units.

Table 3.1. Name, structure, and yield of the oligophosphodiesters containing ring-substituted squaraine dyes.

Name	Sequence	Yield, %
CNSqTr	CNSq-CNSq-CNSq	23
CNSq6	CNSq-CNSq-CNSq-CNSq-CNSq-CNSq-CTC ACG GAA G – 3'	18
CNOSq	CNSq-OSq-CNSq-OSq-CNSq-OSq-CTC ACG GAA G – 3'	11
BarbSqTr	BarbSq-BarbSq-BarbSq	4.9
BarbSq6	BarbSq-BarbSq-BarbSq-BarbSq-BarbSq-BarbSq-CTC ACG GAA G – 3'	1.8

Squaraine-modified oligonucleotides **CNSq6**, **CNOSq**, and **BarbSq6** were prepared under UltraMild conditions (GlenResearch). The necessity of applying the UltraMild protocol and, thus, UltraMild deprotection solution (potassium carbonate in methanol) is due to the sensitivity of the ring-substituted squaraine chromophores against basic conditions. It is known that the nitrile group hydrolyzes to the corresponding carboxylic acid in aqueous base solutions [187] and, therefore, concentrated ammonium hydroxide cannot be applied for the deprotection of oligophosphodiesters containing dicyanomethylene squaraine. The stability of the ring-substituted squaraines in metanolic potassium carbonate is shown in Figure 3.3. While the absorptivity of **BarbSq** remained almost unchanged during the treatment with K_2CO_3 in MeOH CN-squaraine lost about 20% of absorbance under the same conditions. Consequently, **CNSq** chromophore, even at UltraMild deprotection conditions, partially destroys. In concentrated ammonium hydroxide, the long-wavelength absorption band of both **BarbSq** and **CNSq** completely disappears within 20 minutes of treatment.

Squaraine homo-oligomers **CNSqTr** and **BarbSqTr** could be synthesized according to both UltraMild and standard protocol since there is no oligonucleotide part in their structures. We applied UltraMild conditions and universal support GlenUni (GlenResearch) for the synthesis. Cleavage and final deprotection were done in the abovementioned potassium carbonate solution.
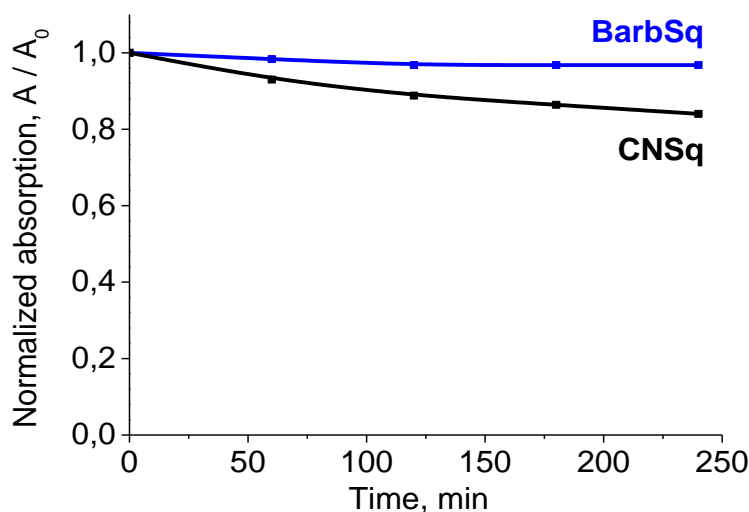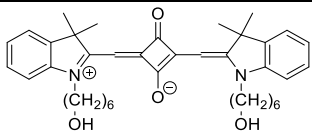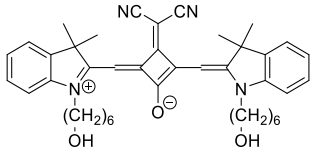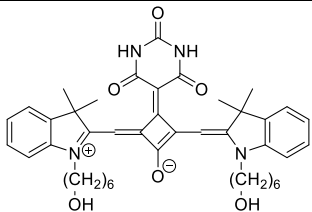
Figure 3.3. The decay of the long-wavelength absorption band of the ring-substituted squaraine dyes **16** (black) and **17** (blue) after treatment by K_2CO_3 in MeOH (4 h, r.t.). A/A_0 – relative absorbance, where A_0 is the absorption intensity at the starting point, and A_0 is the absorption intensity at the time-point.

Oligophosphodiesters **CNSqTr**, **CNSq6**, and **CNOSq** containing dicyanomethylene-squaraine were synthesized with yields of 11–23%. The yields of the strands with barbituric-squaraine **BarbSqTr** and **BarbSq6** were 2–5%. As clearly shown in Figure 3.3, the decomposition of the barbituric squaraine chromophore during the deprotection step can not be the reason for the low yields. Consequently, this phenomenon can be explained either by a low rate of incorporation of the phosphoramidite or by decomposition of the phosphoramidite during the synthesis under treatment by relatively aggressive CapA, CapB, oxidizing, or detritylation solutions. In order to completely elucidate the issue, additional investigations are necessary.

3.2.2 Spectral Properties of the Core-Substituted Squaraines

Spectral-luminescence properties of the dicyanomethylene (**CNSq**) and barbituric (**BarbSq**) ring-substituted squaraine dyes were studied in comparison with the same properties of unsubstituted oxy-squaraine **OSq** (Table 3.2, Figure 3.4). The spectral characteristics were obtained in ethanol at a concentration of 1 μM, where the non-aggregated state of the dyes was expected.

Table 3.2. Spectral-luminescence properties of the ring-substituted squaraine dyes **CNSq** and **BarbSq** in comparison with the unsubstituted oxy-squaraine **OSq**.

Name	Squaraine	λ(Abs), nm	ε, M^{-1} cm^{-1}	λ(Fl), nm	Q.Y., %
OSq [a]		632 260	258 000 11 000	640	27.3
CNSq [b]		676 380 260	190 000 34 000 11 500	694	25.8
BarbSq [a]		637 427 260	154 000 22 000 10 000	658	8.4

[a] Excitation at 590 nm
[b] Excitation at 630 nm
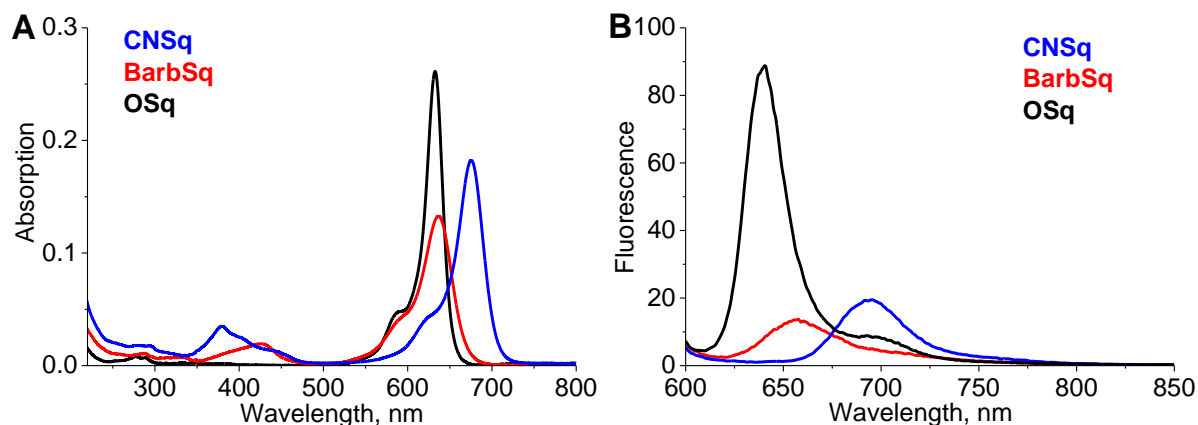
Figure 3.4. A: Absorption and B: fluorescence spectra of the ring-substituted squaraine dyes **CNSq** (blue) and **BarbSq** (red) in comparison with the unsubstituted oxy-squaraine **OSq** (black). Conditions: ethanol, concentration 1 μM, λ(Ex) = 590 nm.

In general, the substitution of the oxygen by dicyanomethylene or barbituric group causes a bathochromic shift of the absorption and fluorescence spectra and a significant decrease of the molar absorptivity and fluorescence quantum yield of the squaraine. Absorption spectra of the ring-substituted squaraines contain additional bands at 380 nm (**CNSq**) and 427 nm (**BarbSq**) with molar absorptivities 34 000 M^{-1} cm^{-1} and 22 000 M^{-1} cm^{-1}, accordingly. These bands appear due to electron transitions into substituted squaraine core.

3.2.3 Self-Assembly of the Phosphodiester-Linked Squaraine Trimers

In this section, we comparatively study spectral-luminescence properties, aggregation, and supramolecular polymerization of the phosphodiester-linked trimers containing oxy-squaraine **OSqTr**, dicyanomethylene-squaraine **CNSqTr**, and barbituric-squaraine **BarbSqTr** (Figure 3.5). The aggregation and polymerization behavior are investigated in aqueous media containing sodium chloride and phosphate buffer.

The spectral characteristics of the trimers measured in ethanol at concentration 1 μM are given in Table 3.3; absorption and fluorescence spectra are presented in Figure 3.6.
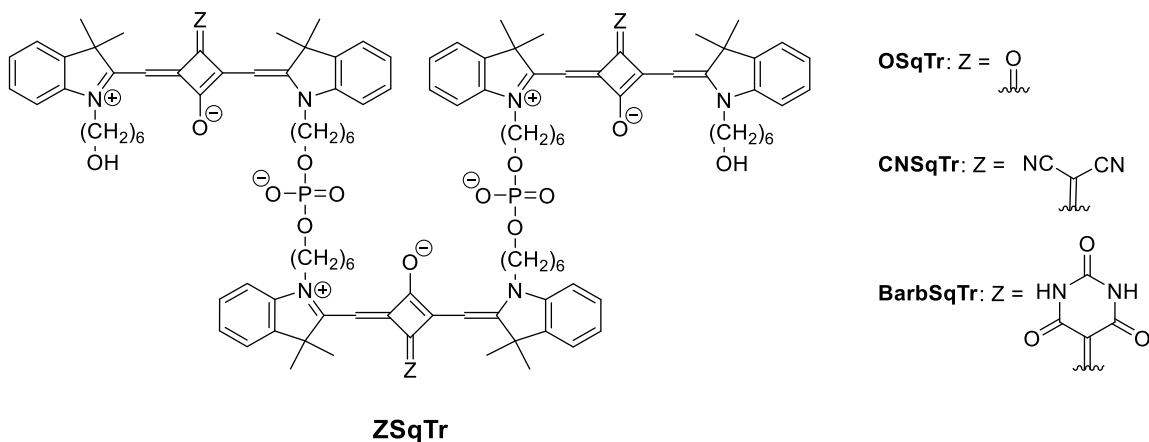
Figure 3.5. Structure of the squaraine trimers **OSqTr**, **CNSqTr**, and **BarbSqTr**.

Table 3.3. Spectral properties of the phosphodiester-linked trimers in ethanol.

Name	Structure	λ(Abs), nm	λ(Fl), nm	Q.Y., %
OSqTr [a]	OSq-OSq-OSq	632	648	6.3
CNSqTr [b]	CNSq-CNSq-CNSq	380, 675	696	4.5
BarbSqTr [a]	BarbSq-BarbSq-BarbSq	427, 631	657	1.5

[a] λ(Ext) = 590 nm
[b] λ(Ext) = 630 nm
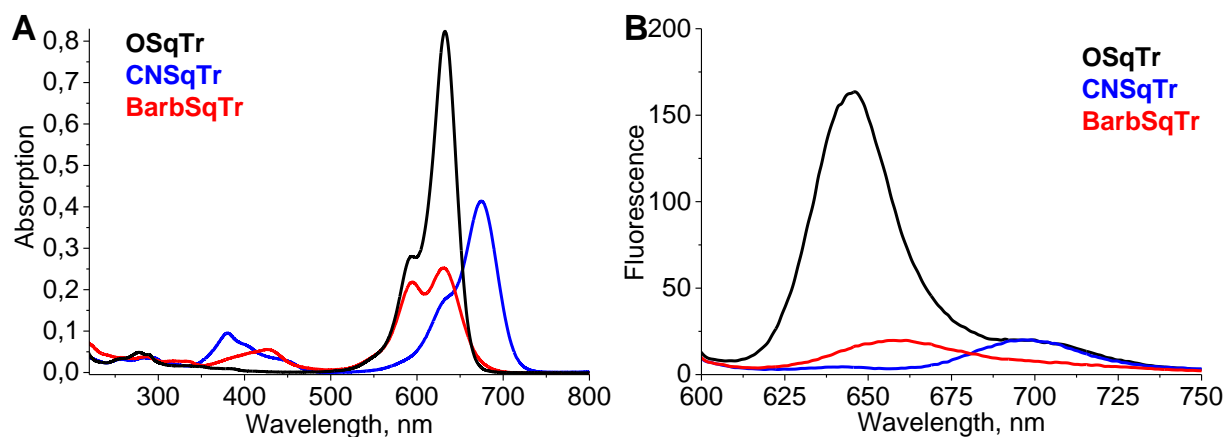
Figure 3.6. A: Absorption spectra of **OSqTr** (black), **CNSqTr** (blue), and **BarbSqTr** (red). B: Fluorescence spectra. Conditions: EtOH, 1 μM. λ(Ext) = 590 nm.

The squaraine trimers **OSqTr**, **CNSqTr**, and **BarbSqTr** absorb and emit light in similar spectral regions as the corresponding squaraine monomers (Table 3.2 and 3.3). However, their fluorescence quantum yields are 4–6 times lower than monomers. The fluorescence quenching is caused by the formation of slightly or non-fluorescent aggregates. The formation of *H*-aggregates is also confirmed by the emergence of new blue-shifted bands in the UV-Vis spectra. In the case of OSq- and CNSq-trimers, the blue-shifted band of the aggregates is overlapped with the short-wavelength absorption shoulder of squaraine chromophores. As a result, the intensity of the latter increases. In contrast to **OSqTr** and **CNSqTr**, **BarbSqTr** demonstrates a well-resolved band of *H*-aggregates with absorption around 594 nm. The Q.Y.s of the trimers are low and decrease in the line: **OSqTr** (6.3%) > **CNSqTr** (4.5%) > **BarbSqTr** (1.5%).

In aqueous solutions containing 25% (**BarbSqTr**) or 30% (**OSqTr** and **CNSqTr**) ethanol (1 µM strand, 100 mM NaCl, 10 mM PB), the squaraine trimers form *H*-type aggregates (Figure 3.7). The absorption bands of the *H*-aggregates are blue-shifted regarding the bands of the monomers and were identified at 591 nm, 622 nm, and 593 nm for **OSqTr**, **CNSqTr**, and **BarbSqTr**, accordingly.

At lower concentrations of EtOH in the aqueous solution, OSq-trimer demonstrates clear splitting of the absorption band of monomer into blue-shifted *H*-band and red-shifted *J*-band (Figure 3.7A). A well-resolved *J*-band with absorption around 700 nm was also identified in the UV-Vis spectrum of BarbSq-trimer (Figure 3.7C). At the same time, CNSq-trimer reveals no distinct type of aggregation. The formation of nanostructures by **CNSqTr** leads to the broadening of both the absorption band of the monomer and the *H*-aggregates (Figure 3.7B). Thus, the substitution of oxygen in the squaraine chromophore by the dicyanomethylene group or barbituric acid strongly affects the aggregation behavior of the squaraine trimer.
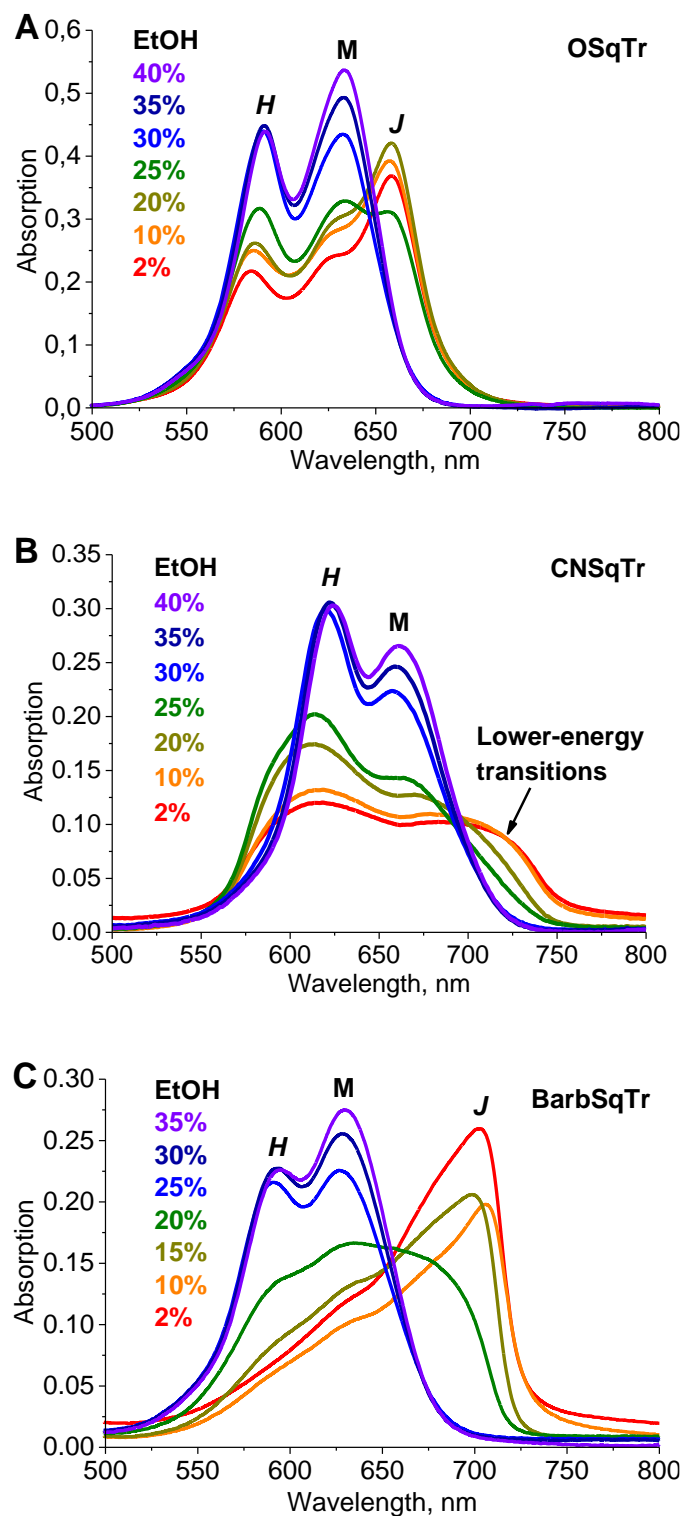
Figure 3.7. Aggregation of the squaraine trimers depending on the percentage of ethanol in aqueous solution. A: **OSqTr**. B: **CNSqTr**. C: **BarbSqTr**. Conditions: 1 μM trimer, 100 mM NaCl, 10 mM PB, for EtOH, see the legend on the left. Heating–cooling run (10 °C/min) was performed before the measurements.

During the investigation of the supramolecular polymerization of **OSqTr** (Chapter 2), we observed that only aggregates with a split absorption band self-assembled as supramolecular polymers. At the same time, *H*-aggregates demonstrated no signs of the SPs. Like **OSqTr**, the *H*-aggregates of **CNSqTr** and **BarbSqTr** do not demonstrate the characteristic curve in the thermal experiments (Figure 3.8). In all experiments, a linear dependence of absorption from temperature was observed.
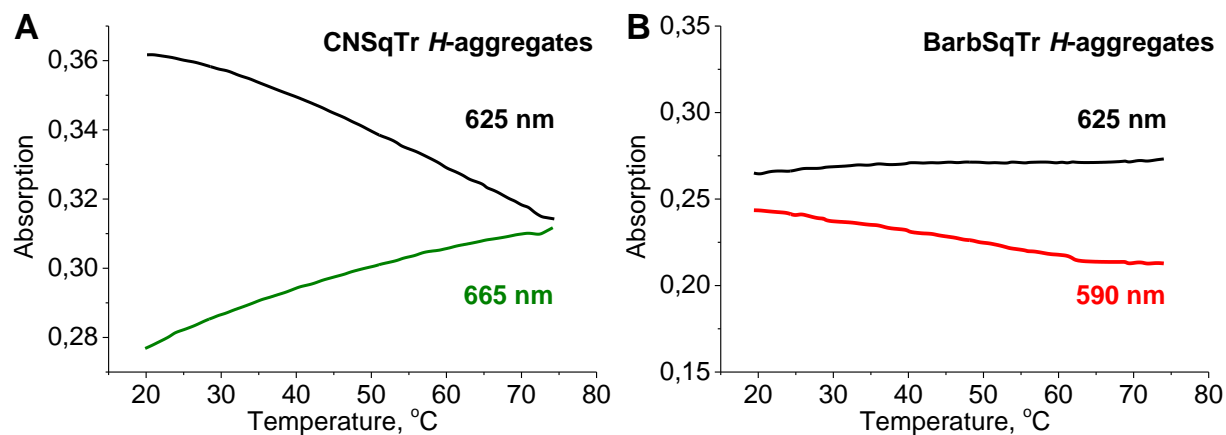
Figure 3.8. Cooling runs (rate: 0.5 °C/min) recorded at 590 nm (red), 625 nm (black), and 665 (green) for *H*-aggregates of squaraine trimers. A: **CNSqTr**. Conditions: 1 μM trimer, 30% EtOH, 100 mM NaCl, 10 mM PB. B: **BarbSqTr**. Conditions: 1 μM trimer, 25% EtOH, 100 mM NaCl, 10 mM PB.

In contrast to *H*-aggregates, the nanostructures formed by **CNSqTr** and **BarbSqTr**, which demonstrate lower-energy transitions in the UV-Vis spectrum, reveal a sigmoidal-shaped curve in the thermal experiments, indicating the formation of SPs (Figures 3.9A and Figure 3.10A). However, as the case with **OSqTr** (Figure 2.9), SPs from **CNSqTr** and **BarbSqTr** are only partially reversible and precipitate under formation. Besides, their UV-Vis spectra are broad and poorly structured (Figures 3.9B and Figure 3.10B), which indicates multiple electron transitions. Consequently, transition dipole moments of the substituted squaraine chromophores in the SPs adopt many orientations relative to each other.

To study the organization of the squaraine molecules in **CNSqTr**- and **BarbSqTr**-polymers, AFM and TEM analyses were applied. However, neither of these methods could provide a visualization of the SPs. AFM images of **CNSqTr**- and **BarbSqTr**-polymers deposited on both APTES-modified and unmodified mica contain almost no structures of interest. TEM images reveal no assemblies with repeated morphology.
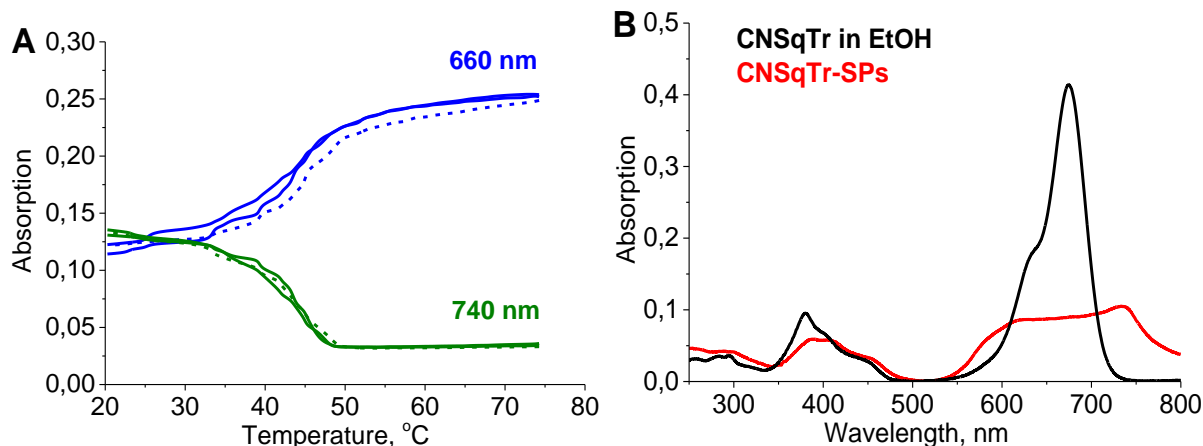
Figure 3.9. A: Cooling (solid lines) and heating (dashed lines) runs (rate: 0.5 °C/min) recorded at 660 nm (blue) and 740 nm (green) for **CNSqTr**. B: Absorption spectrum of the SPs formed from **CNSqTr** (red) compared to the spectrum obtained for **CNSqTr** in ethanol (black). Conditions: 1 µM strand, 25% EtOH, 200 mM NaCl, 10 mM PB.
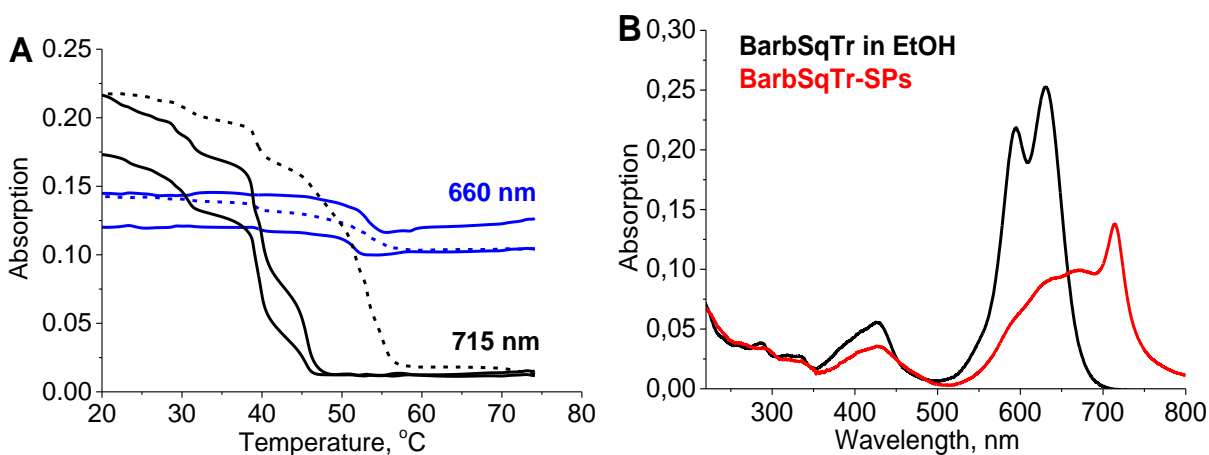
Figure 3.10. A: Cooling (solid lines) and heating (dashed lines) runs (rate: 0.5 °C/min) recorded at 660 nm (blue) and 715 nm (black) for **BarbSqTr**. B: Absorption spectrum of the SPs formed from **BarbSqTr** (red) compared to the spectrum obtained for **BarbSqTr** in ethanol (black). Conditions: 1 µM strand, 15% EtOH, 100 mM NaCl, 10 mM PB.

3.2.4 Self-Assembly of Squaraine-Modified Oligonucleotides

This section is dedicated to investigating spectral characteristics, aggregation, and supramolecular polymerization of the modified oligonucleotides containing ten nucleotides and six squaraine units (Figure 3.11). The properties of the strand with oxy-squaraines **OSq6**, dicyanomethylene-squaraines **CNSq6**, alternating oxy- and dicyanomethylene-squaraines **CNOSq**, and barbituric-squaraines **BarbSq6** are compared. The aggregation and polymerization are investigated in aqueous media containing sodium chloride and phosphate buffer.

Spectral characteristics of the squaraine-modified oligonucleotides measured in ethanol are given in Table 3.4. Absorption and fluorescence spectra are shown in Figure 3.12.
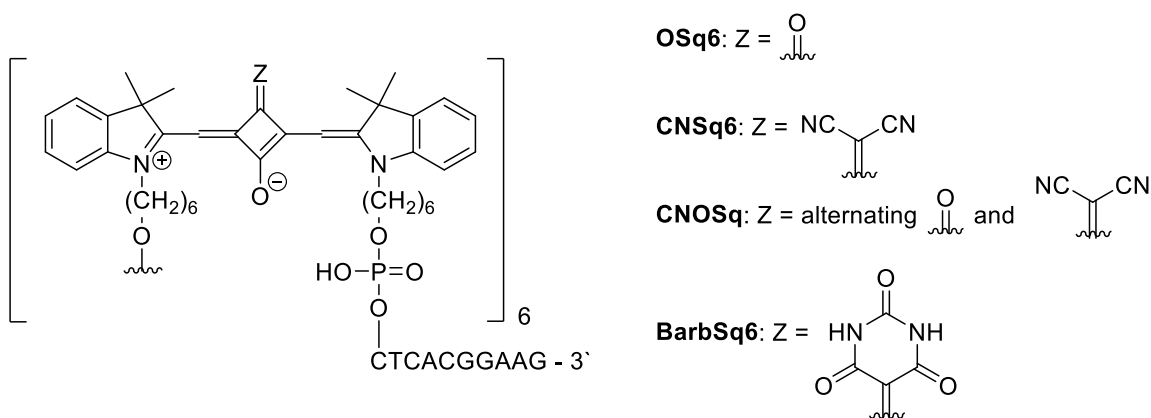
Figure 3.11. Structure of the squaraine-modified oligonucleotides.

Table 3.4. Spectral properties of the squaraine-modified oligonucleotides. EtOH, $c = 1$ μM.

Name	Structure	λ(Abs), nm	λ(Fl), nm	Q.Y., %
OSq6 [a]	(OSq)$_6$-CTC ACG GAA G – 3'	260, 633	647	4.4
CNSq6 [b]	(CNSq)$_6$-CTC ACG GAA G – 3'	260, 380, 677	699	1.6
CNOSq [b]	(CNSq-OSq)$_3$-CTC ACG GAA G – 3'	260, 380, 634, 679	697	2.9
BarbSq6 [a]	(BarbSq)$_6$-CTC ACG GAA G – 3'	260, 427, 635	662	0.7

[a] λ(Ext) = 590 nm
[b] λ(Ext) = 630 nm.
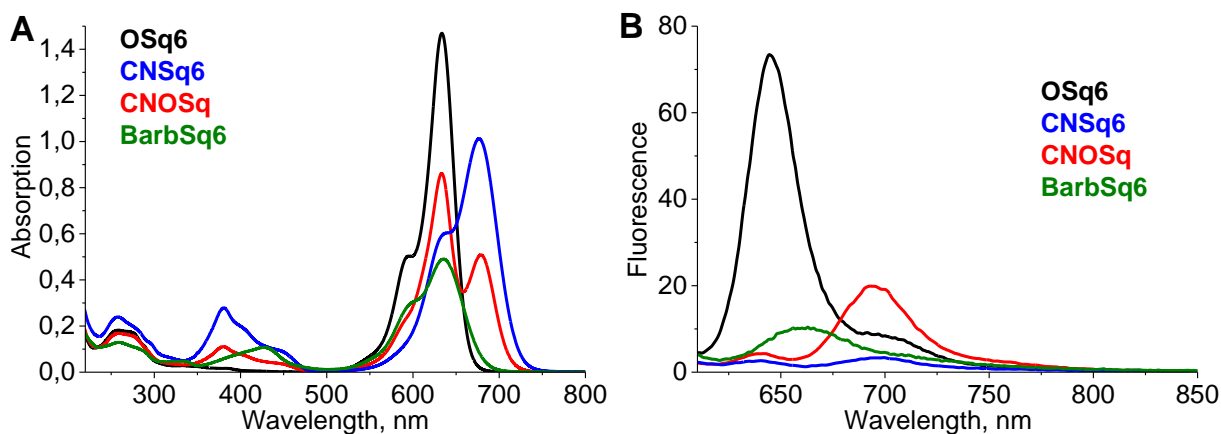
Figure 3.12. A: Absorption spectra. B: Fluorescence spectra. **OSq6**: black. **CNSq6**: blue. **CNOSq**: red. **BarbSq6**: green. Conditions: ethanol, $c = 1$ μM, λ(Ext) = 590 nm.

The absorption spectra of the squaraine-modified oligonucleotides consist of a band at 260 nm, caused by electron transitions in the nucleotide ($\varepsilon \approx 112\,000\ \text{M}^{-1}\ \text{cm}^{-1}$) and squaraine ($\varepsilon \approx 60\,000\ \text{M}^{-1}\ \text{cm}^{-1}$) parts, a band at 380 nm (**CNSq6** and **CNOSq**) or 427 nm (**BarbSq6**) that appears due to the transitions in the substituted squaraine core, and a band in the long-wavelength region (Figure 3.12A) Oligonucleotides **OSq6**, **CNSq6**, and **BarbSq6** demonstrate only one long-wavelength maximum (633 nm, 677 nm, and 635 nm, correspondingly), while the strand with alternating dicyanomethylene- and oxy-squaraines **CNOSq** gives two peaks corresponding to oxy-squaraine at 634 nm and dicyanomethylene-squaraine at 679 nm.

Fluorescence of the modified oligonucleotides was detected at 647-699 nm. While the Q.Y. of **OSq6** (4.4%) can be easily measured, the fluorescence of **BarbSq6** (0.7%) is almost undetectable. The fluorescence spectrum of **CNOSq** mainly contains the band of the dicyanomethylene squaraines at 697 nm while the fluorescence of the oxy-squaraines at 647 nm is almost absent (Figure 3.12B). We attribute this to an energy transfer from oxy- to dicyanomethylene-squaraines.

The quantum yields of the modified strands are 7–16 times lower than the Q.Y.s of the monomer dyes (Table 3.2 and 3.4). Most likely, the fluorescence quenching is caused by the formation of the non-fluorescent or weakly fluorescent intramolecular *H*-aggregates.

In aqueous solutions containing 100 mM NaCl and 0–40% EtOH (1 µM strand, 10 mM PB), the squaraine-modified oligonucleotides form only *H*-type aggregates. Increasing the NaCl concentration in the solution to 500 mM (1 µM strand, 15–20% EtOH, 10 mM PB) causes different responses in the UV-Vis spectra of **OSq6**, **CNSq6**, **CNOSq**, and **BarbSq6**. **OSq6** demonstrates a well-resolved splitting of the absorption band (Figure 3.13A). **BarbSq6** reveals a tendency to form a *J*-band (Figure 3.13D) while **CNSq6** and **CNOSq** show only an absorbance decrease in the *H*-bands at 602 nm and 590 nm, correspondingly (Figure 3.13B and 3.13C).
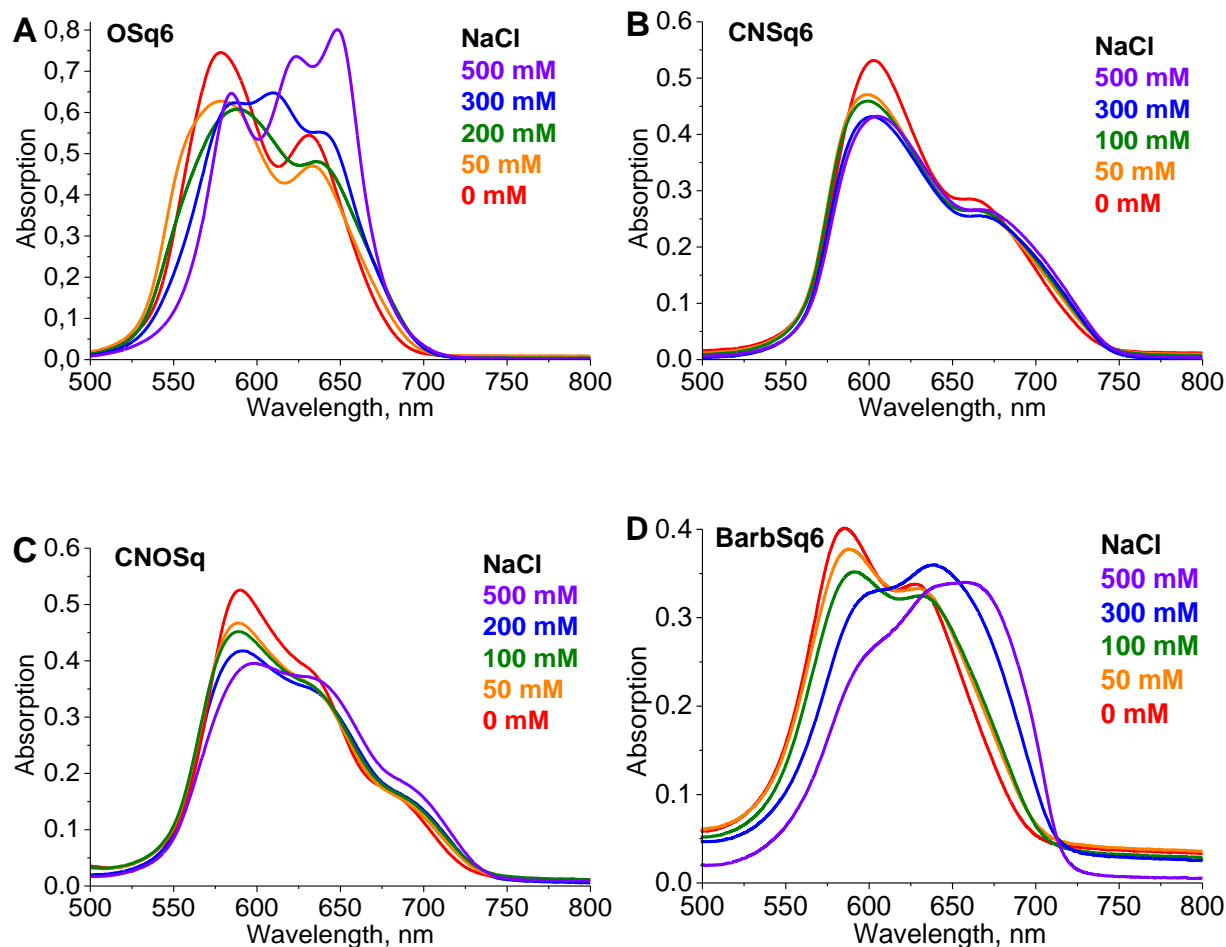
Figure 3.13. Aggregation of the squaraine-modified strands in aqueous solution depending on the NaCl concentration. A: **OSq6**. B: **CNSq6**. C: **CNOSq**. D: **BarbSq6**. Conditions: 1 µM strand, 15–20% EtOH, 10 mM PB, for NaCl, see the legend. Cooling runs with a rate of 10 °C/min were performed before the measurements.

Like the *H*-aggregates of all previously studied oligophosphodiesters, the *H*-aggregates of squaraine-modified oligonucleotides **CNSq6**, **CNOSq**, and **BarbSq6** self-assemble without signs of supramolecular polymerization as indicated by the absence of a characteristic sigmoidal curve in thermal experiments in the temperature range of interest (Figure 3.14).
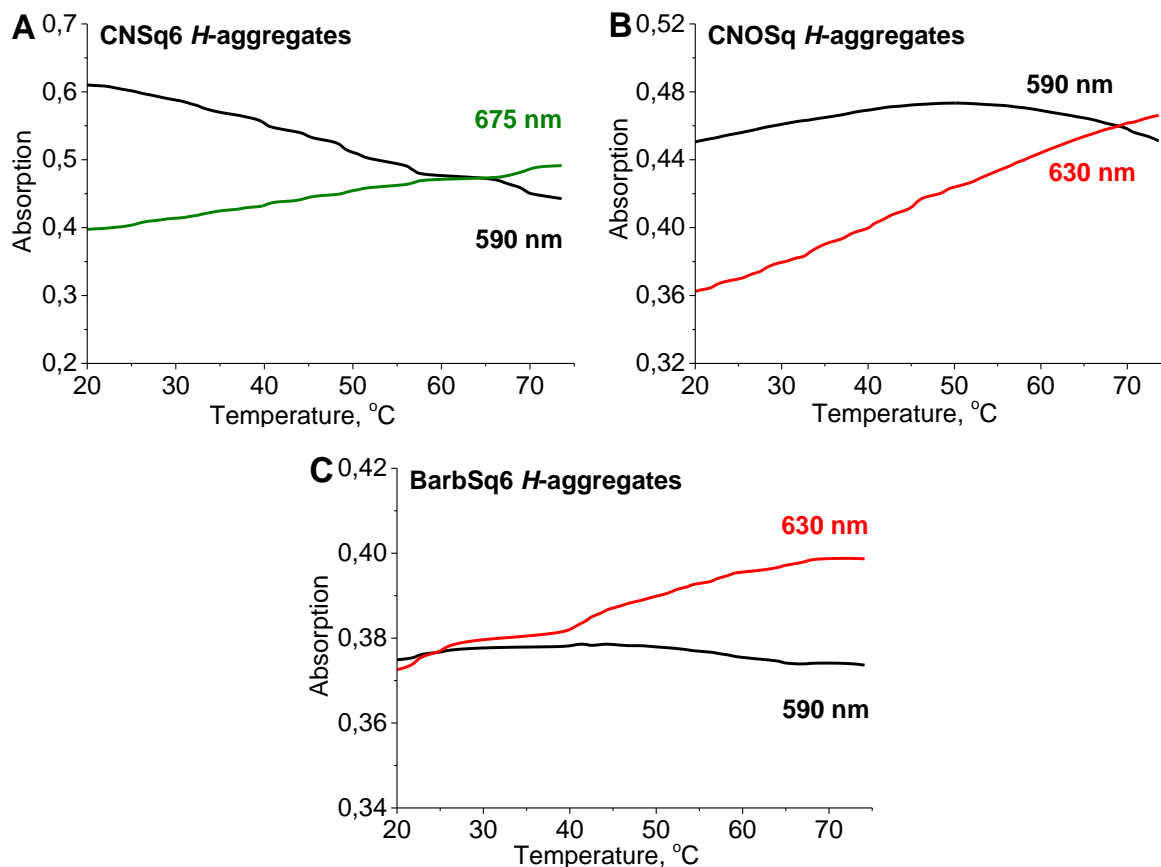
Figure 3.14. Thermal experiments (cooling rate 0.5 C °/min) for *H*-aggregates of **CNSq6** (A), **CNOSq** (B), and **BarbSq6** (C). The runs recorded at 590 nm (black), 630 nm (red), and 675 nm (green). Solid lines represent cooling runs. Conditions: 1 µM strand, 20% EtOH, 100 mM NaCl, 10 mM PB.

Slowing of the annealing rate from 10 °C/min to 0.5 °C/min allows to obtain SPs of **BarbSq6**, which demonstrate the splitting of the absorption band of the monomer into *H*- (595 nm) and *J*-bands (675 nm) (Figure 3.15A). The splitting is most pronounced when the sample contains 10% EtOH and 250 mM NaCl (1 µM **BarbSq6**, 10 mM PB.). The sigmoidal temperature dependence of the absorption in thermal experiments can best be observed at 675 nm.

BarbSq6-SPs show almost no detectable fluorescence (Q.Y. < 1%) and weak exciton coupled CD signal in the long-wavelength region of the spectrum ($\Delta\varepsilon(701\ nm) = +20\ M^{-1}\ cm^{-1}$, $\Delta\varepsilon(668\ nm) = -14\ M^{-1}\ cm^{-1}$).

AFM visualizes supramolecular polymers of **BarbSq6**. On APTES-modified mica, the polymers appear as nanodiscs with an average height of 1.5 nm and an average diameter of 40 ± 10 nm (Figure 3.16).
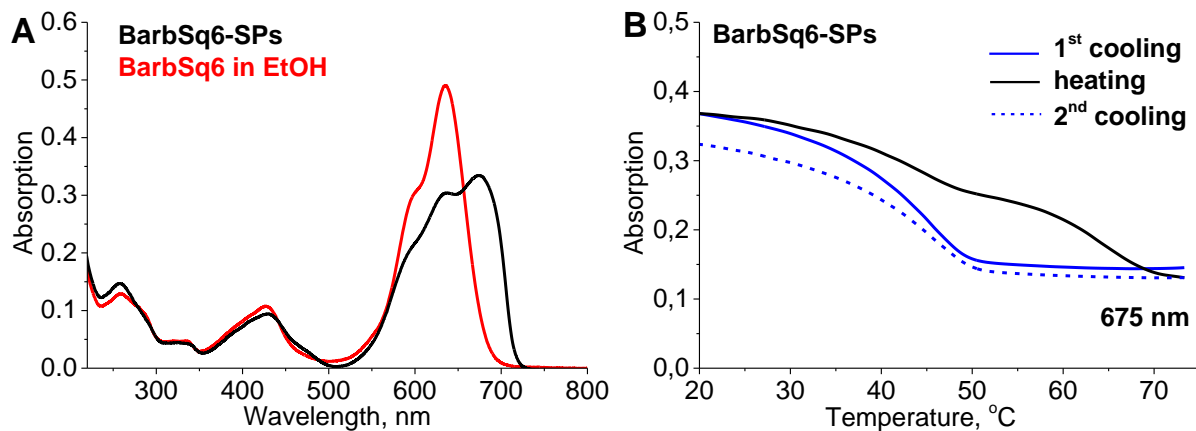
Figure 3.15. Characterization of the **BarbSq6**-SPs. A: Absorption spectrum of the SPs (black) in comparison with the spectrum of **BarbSq6** measured in EtOH (red). B: Heating–cooling runs (rate: 0.5 C/min) monitored at 675 nm. 1st cooling: solid blue. Heating: solid black. 2nd cooling: dashed blue. Conditions: 1 µM strand, 10% EtOH, 250 mM NaCl, 10 mM PB.
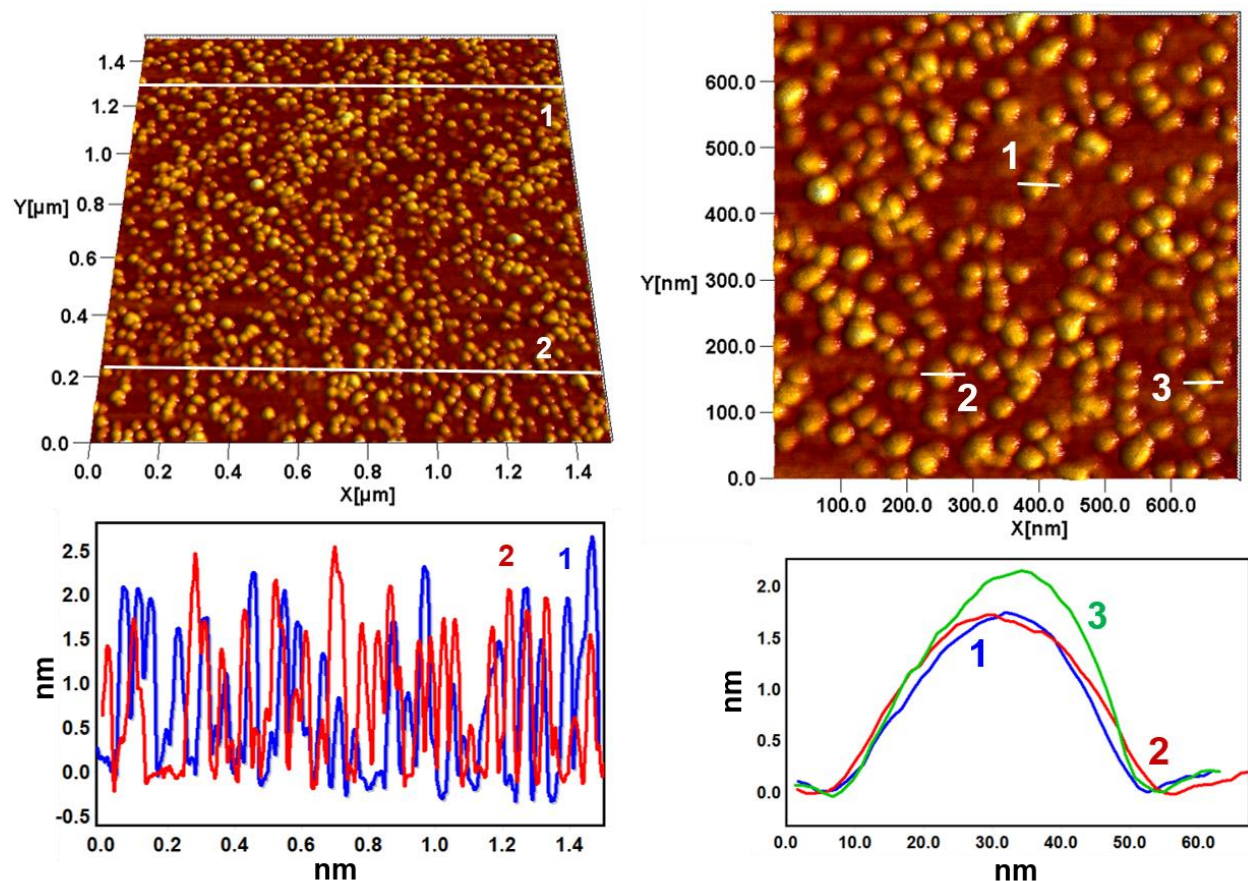
Figure 3.16. AFM images of **BarbSq6**-SPs and height histogram of SPs. Conditions: 1 µM strand, 10% EtOH, 250 mM NaCl, 10 mM PB.

3.3 Conclusions

Two novel long-wavelength phosphoramidites based on dicyanomethylene- and barbituric acid-substituted squaraine chromophores were developed. The phosphoramidites are potentially suitable for application in hybridization analysis based on fluorescence quenching.

Phosphodiester-linked squaraine trimers with oxy-, dicyanomethylene-, and barbituric-groups in the squaraine core form supramolecular polymers in aqueous ethanol solutions containing sodium chloride and phosphate buffer. The absorption spectrum of the **OSqTr**-SPs is characterized by the splitting of the long-wavelength band, while the absorption spectra of **CNSqTr**-SPs and **BarbSqTr**-SPs are broad and poorly structured. Due to precipitation and impossibility of visualization, we consider the SPs based on the squaraine trimers as not fit for further investigations and as unsuitable for biomedical applications.

The most promising way to create squaraine building blocks for SPs is to conjugate squaraine chromophores with DNA. Due to the DNA part, the Sq-SPs are well water-soluble and remain stable during and after formation. Conjugates of dicyamomethylene-squaraines with DNA form *H*-aggregates while oligonucleotides modified with oxy- and barbituric-squaraines self-assemble into SPs. The SPs are characterized by a split absorption band and an almost completely quenched fluorescence. The absence of notable fluorescence makes the SPs attractive for biological applications, such as photoacoustic imaging.

3.4 Experimental Section

*Phosphoramidite of the Dicyanomethylene Squaraine (**20**).*

Synthesis of compound **11** [178, 185].

To the solution of dibutoxycyclobut-3-ene-1,2-dione (**13**) (2.26 g, 10 mmol) and malononitrile (0.67 g, 10 mmol) in benzene (30 ml), triethylamine (1.67 ml, 12 mmol) was added dropwise. The mixture was stirred at room temperature for 30 minutes. The solvent was evaporated, the residue washed three times with diethyl ether, and dried. Yield: 3.11 g (97%).

^{1}H-NMR (300 MHz, DMSO, ppm): δ 8.84 (1H, broad s, NH), 4.59 (2H, t, J = 6.55 Hz, OCH$_2$), 3.17–3.03 (6H, m, CH$_2$CH$_3$), 1.65–1.61 (2H, m, CH$_2$), 1.45–1.29 (2H, m, CH$_2$), 1.17 (9H, t, J = 7.29 Hz, CH$_2$CH$_3$), 0.91 (3H, t, J = 7.38 Hz, CH$_2$CH$_3$).

^{13}C-NMR (75 MHz, DMSO, ppm): δ 191.31, 180.97, 180.00, 172.45, 117.80, 117.58, 71.98, 45.79, 31.55, 18.07, 13.51, 8.62.

ESI-MS (neg. MeOH): mass calc. for C$_{11}$H$_9$N$_2$O$_3^-$ = 217.0613; mass found = 217.0621.

Synthesis of compound **16**.

The preparation of the heterocyclic quaternary ammonium salt **6** is described in Chapter 2 "Experimental Section." A solution of the dicyanomethylene derivative **11** (260 mg, 0.814 mmol) and salt **6** (570 mg, 1.67 mmol) in 1-butanol (15 ml) and toluene (15 ml) was stirred at 110 °C for 15 hours. The solvents were removed under reduced pressure, and the residue was purified by column chromatography (Silica gel 60, 0–4% MeOH in CH$_2$Cl$_2$) to give the diol **16** as a green powder. R$_f$ = 0.41 (Silica gel 60, 7% MeOH in CH$_2$Cl$_2$). Yield: 280 mg (64%).

^{1}H-NMR (300 MHz, DMSO, ppm): δ 7.56 (2H, d, J = 7.37 Hz, arom H), 7.47–7.35 (4H, m, arom H), 7.25 (2H, t, J = 6.89 Hz, arom H), 6.33 (2H, s, CH), 4.31 (2H, t, J = 5.17 Hz, OH), 4.04 (4H, t, J = 7.33 Hz, NCH$_2$), 3.37 (4H, t, J = 5.62 Hz, CH$_2$OH), 1.78–1.62 (4H, m, CH$_2$), 1.69 (12H, s, 3-CH$_3$), 1.48–1.27 (12H, m, CH$_2$).

^{13}C-NMR (75 MHz, CDCl$_3$, ppm): δ 173.17, 171.92, 167.70, 166.61, 142.47, 141.89, 128.12, 124.67, 122.33, 119.23, 110.16, 89.02, 77.59, 77.16, 76.74, 62.32, 49.48, 44.41, 40.31, 32.28, 27.27, 26.62, 26.35, 25.47.

ESI-MS (neg., MeOH): mass calc., for C$_{41}$H$_{48}$N$_4$O$_3$ = 644.3726; mass found = 644.3723.

Synthesis of compound **18**.

4,4'-Dimethoxytrityl chloride (240 mg, 0.708 mmol) was added to a solution of the squaraine diol **16** (510 mg, 0.791 mmol) in anhydrous pyridine (15 ml). The mixture was stirred overnight at room temperature and under argon. The solvent was removed under reduced pressure, and the

residue was purified by column chromatography (Silica gel 60, CH_2Cl_2/EtOAc/Et_3N, 495/495/10, v/v/v). The fractions containing the product were combined and concentrated to a volume of about 2 mL. Cold (-28 °C) hexane (100 mL) was added, and the solution was kept at -28 °C for 2 hours. A green precipitate was formed, the material was filtered off, and the product was dried under high vacuum. R_f = 0.73 (Silica gel 60, 7% MeOH in CH_2Cl_2). Yield: 278 mg (41%).

^{1}H-NMR (300 MHz, DMSO, ppm): δ 7.54 (2H, d, J = 7.33 Hz, arom H), 7.45–7.12 (15H, m, arom H), 6.84 (4H, d, J = 8.92 Hz, arom H), 6.35 (1H, s, CH), 6.33 (1H, s, CH), 4.31 (1H, broad s, OH), 4.14–3.90 (4H, m, NCH_2), 3.71 (6H, s, OCH_3), 3.36 (2H, t, J = 5.6 Hz, C$\underline{H}_2$OH), 2.92 (2H, t, J = 6.29 Hz, CH_2DMT), 1.79-1.60 (4H, m, CH_2), 1.68 (6H, s, 3-CH_3), 1.67 (6H, s, 3-CH_3), 1.58–1.45 (2H, m, CH_2), 1.46–1.25 (10H, m, CH_2).

^{13}C-NMR (75 MHz, $CDCl_3$, ppm): δ 173.19, 171.99, 171.84, 167.80, 166.77, 166.67, 158.37, 145.45, 142.52, 142.51, 142.07, 141.96, 136.78, 130.09, 128.28, 128.13, 127.77, 126.64, 124.67, 124.65, 122.38, 119.27, 119.11, 113.05, 110.20, 110.11, 89.23, 89.09, 85.74, 77.58, 77.16, 76.74, 63.35, 62.43, 55.29, 49.49, 44.46, 44.44, 40.61, 32.33, 29.95, 27.39, 27.30, 26.71, 26.69, 26.38, 26.25, 25.52.

ESI-MS (neg., MeOH): mass calc. for $C_{62}H_{66}N_4O_5$ = 946.5033; mass found = 946.5039.

Synthesis of compound **20**.

2-Cyanoethyl-*N*,*N*-diisopropylchlorophosphoramidite (94 mg, 0.396 mmol) was added under argon to a solution of compound **18** (250 mg, 0.264 mmol) and diisopropylethylamine (140 µL, 0.792 mmol) in anhydrous dichloromethane (6 ml). The mixture was stirred at room temperature for 2 hours. The mixture was partially concentrated under reduced pressure and purified by column chromatography (Silica gel 60, 50% EtOAc in hexane containing 1% of Et3N). The fractions containing the product were combined and concentrated to a volume of about 2 mL. Cold (-28 °C) hexane (100 mL) was added, and the solution was kept at -28 °C for 2 hours. A green precipitate was formed, the material was filtered off, and the product was dried under high vacuum to give phosphoramidite **20**. R_f = 0.77 (Silica gel 60, EtOAc containing 1% of Et_3N). Yield: 170 mg (56%).

^{1}H-NMR (300 MHz, CDCl$_3$, ppm): δ 7.46–7.13 (15H, m, arom H), 7.03 (2H, t, J = 7.92 Hz, arom H), 6.80 (4H, d, J = 8.83 Hz, arom H), 6.51 (1H, s, CH), 6.50 (1H, s, CH), 4.07–3.93 (4H, m, NCH$_2$), 3.90–3.73 (2H, m, C$\underline{H}$CH$_3$), 3.77 (6H, s, OCH$_3$), 3.70–3.50 (4H, m, CH$_2$OP), 3.02 (2H, t, J = 6.4 Hz, CH$_2$ODMT), 2.61 (2H, t, J = 6.5 Hz, CH$_2$CN), 1.89–1.71 (4H, m, CH$_2$), 1.77 (12H, s, 3-CH$_3$), 1.68–1.55 (4H, m, CH$_2$, superimposed with water), 1.53–1.35 (8H, m, CH$_2$), 1.22–1.11 (12H, m, CHC$\underline{H}_3$).

^{13}C-NMR (75 MHz, CDCl$_3$, ppm): δ 173.18, 171.93, 171.88, 167.85, 166.78, 166.72, 158.39, 145.48, 142.52, 142.10, 142.08, 136.79, 130.10, 128.29, 128.13, 127.78, 126.65, 124.64, 122.40, 119.16, 117.83, 113.07, 110.17, 89.24, 89.21, 85.75, 77.58, 77.16, 76.74, 63.62, 63.39, 63.36, 58.55, 58.30, 55.30, 49.48, 44.47, 44.44, 43.17, 43.00, 40.75, 31.11, 31.02, 29.96, 27.39, 26.71, 26.50, 26.27, 25.84, 24.81, 24.74, 24.71, 24.64, 20.52, 20.43.

^{31}P-NMR (121 MHz, CDCl$_3$, ppm): δ 147.25.

ESI-MS (pos. MeCN): mass calc. for C$_{71}$H$_{83}$N$_6$O$_6$P = 1146.6112; mass found = 1146.6106.

*Phosphoramidite of Barbituric Squaraine (**21**).*

Synthesis of compound **12** was performed according to a published procedure [179] with modifications.

To the solution of dibutoxycyclobut-3-ene-1,2-dione (**13**) (2.00 g, 8.84 mmol) and barbituric acid (1.08 g, 8.46 mmol) in ethanol (96%, 40 ml), triethylamine (1.33 ml, 9.51 mmol) was added dropwise. The mixture was stirred at room temperature for 30 minutes. Then, water (20 ml) was added. After one hour, the solvent was evaporated, and the residue was purified by column chromatography (Silica gel 60, 0–70% MeOH in CH$_2$Cl$_2$). Fractions with λ(Abs) = 363 nm (MeOH) were collected. Yield: 1.78 g (65%).

^{1}H-NMR (300 MHz, DMSO, ppm): δ 10.52 (2H, s, NH barb), 8.94 (1H, broad s, NH of Et$_3$N), 3.11 (6H, q, J = 7.3 Hz, C$\underline{H}_2$CH$_3$), 1.18 (9H, t, J = 7.3 Hz, CH$_2$C$\underline{H}_3$).

^{13}C-NMR (75 MHz, DMSO, ppm): δ 191.89, 190.03, 177.29, 150.45, 87.93, 45.75, 8.61.

ESI-MS (neg. MeOH): mass calc. for $C_8H_3N_2O_6^- = 222.9991$; mass found = 222.9965.

Synthesis of compound **17**.

The preparation of the heterocyclic quaternary ammonium salt **6** is described in Chapter 1, "Experimental Section." The solution of the barbituric derivative **12** (300 mg, 0.922 mmol) and salt **6** (616 mg, 1.84 mmol) in 1-butanol (15 ml) and toluene (15 ml) was stirred at 110 °C for 16 hours. The solvent was evaporated under reduced pressure, and the residue was purified by column chromatography (Silica gel 60, 2–15% MeOH in CH_2Cl_2) to give the diol **17** as a blue-green powder. Yield: 400 mg (61%). $R_f = 0.26$ (Silica gel 60, 7% MeOH in CH_2Cl_2).

^{1}H-NMR (300 MHz, DMSO, ppm): δ 10.00 (2H, s, NH barb), 7.55 (2H, d, $J = 7.34$ Hz, arom H), 7.45–7.33 (4H, m, arom H), 7.28–7.18 (2H, m, arom H), 6.51 (2H, s, CH), 4.36 (2H, t, $J = 5.14$ Hz, OH), 4.05 (4H, t, $J = 7.12$ Hz, NCH_2), 3.42–3.29 (4H, m, C$\underline{H}_2$OH, superimposed with water), 1.81–1.64 (4H, m, CH_2), 1.70 (12H, s, 3-CH_3), 1.45–1.24 (12H, m, CH_2).

^{13}C-NMR (75 MHz, DMSO, ppm): δ 179.48, 175.75, 171.16, 170.78, 162.96, 151.37, 141.86, 141.70, 128.11, 124.49, 122.27, 110.99, 93.67, 86.68, 60.53, 48.80, 43.80, 40.36, 40.08, 39.80, 39.52, 39.24, 38.96, 38.69, 32.31, 26.33, 26.02, 25.03.

ESI-MS (pos. MeOH): mass calc. for $C_{42}H_{50}N_4O_6 = 706.3730$; mass found = 706.3707.

Synthesis of compound **19**.

4,4'-Dimethoxytrityl chloride (412 mg, 1.22 mmol) was added to a solution of the squaraine diol **17** (860 mg, 1.22 mmol) in anhydrous pyridine (20 ml). The mixture was stirred overnight at room temperature and under argon. The solvent was removed under reduced pressure, and the residue was purified by column chromatography (Silica gel 60, 0–5% MeOH in CH_2Cl_2/EtOAc/Et_3N, 495/495/10, v/v/v). $R_f = 0.45$ (Silica gel 60, 7% MeOH in CH_2Cl_2). Yield: 460 mg (37%).

^{1}H-NMR (300 MHz, DMSO, ppm): δ 9.99 (2H, s, NH barb), 7.55 (2H, d, $J = 7.32$ Hz, arom H), 7.45–7.12 (15H, m, arom H), 6.85 (4H, d, $J = 8.73$ Hz, arom H), 6.52 (1H, s, CH), 6.51 (1H, s, CH), 4.36 (1H, t, $J = 5.07$ Hz, OH), 4.12–3.97 (4H, m, NCH_2), 3.71 (6H, s, OCH_3), 3.37 (2H, t, J

= 5.42 Hz, C$\underline{H}_2$OH, superimposed with H_2O), 2.91 (2H, t, J = 5.82 Hz, CH_2DMT), 1.80–1.60 (4H, m, CH_2), 1.70 (6H, s, 3-CH_3), 1.68 (6H, s, 3-CH_3), 1.58–1.45 (2H, m, CH_2), 1.45–1.26 (10H, m, CH_2).

^{13}C-NMR (75 MHz, CDCl$_3$, ppm): δ 180.41, 175.55, 173.42, 173.36, 172.65, 172.34, 162.96, 158.36, 151.57, 145.44, 142.62, 142.58, 142.03, 141.86, 136.75, 130.09, 128.28, 128.08, 127.77, 126.64, 124.75, 122.34, 113.07, 110.36, 110.20, 93.94, 93.78, 86.06, 85.78, 63.25, 62.17, 55.28, 49.51, 49.45, 44.76, 32.10, 29.97, 26.97, 26.59, 26.57, 26.09, 25.30.

ESI-MS (pos. MeOH): mass calc. for $C_{63}H_{68}N_4O_8$ = 1008.5037; mass found = 1008.5052.

Synthesis of compound **21**.

2-Cyanoethyl-*N*,*N*-diisopropylchlorophosphoramidite (162 mg, 0.684 mmol) was added under argon to a solution of compound **19** (460 mg, 0.456 mmol) and diisopropylethylamine (238 µL, 1.37 mmol) in anhydrous dichloromethane (11 ml). The mixture was stirred at room temperature for 2 hours. The mixture was partially concentrated under reduced pressure and purified by column chromatography (Silica gel 60, 70–100% EtOAc in hexane containing 1% of Et$_3$N). The fractions containing the product were combined and concentrated to a volume of about 2 mL. Cold (-28 °C) hexane (100 mL) was added, and the solution was kept at -28 °C for 2 hours. A blue-green precipitate was formed, the material was filtered off, and the product was dried under high vacuum to give phosphoramidite **21**. R$_f$ = 0.63 (Silica gel 60, EtOAc containing 1% of Et$_3$N). Yield: 280 mg (51%).

^{1}H-NMR (300 MHz, CDCl$_3$, ppm): δ 7.84 (2H, s, NH barb), 7.50–7.14 (15H, m, arom H), 7.05 (2H, t, J = 7.68 Hz, arom H), 6.83 (4H, d, J = 8.75 Hz, arom H), 6.43 (2H, s, CH), 4.09–3.93 (4H, m, NCH_2), 3.93–3.74 (2H, m, C$\underline{H}CH_3$), 3.78 (6H, s, OCH_3), 3.73–3.51 (4H, m, CH_2OP), 3.05 (2H, t, J = 6.15 Hz, CH_2ODMT), 2.64 (2H, t, J = 6.42 Hz, CH_2CN), 1.92–1.69 (4H, m, CH_2), 1.76 (6H, s, 3-CH_3), 1.77 (6H, s, 3-CH_3), 1.70–1.57 (4H, m, CH_2), 1.54–1.33 (8H, m, CH_2), 1.25–1.10 (12H, m, CHC$\underline{H}_3$).

^{13}C-NMR (75 MHz, CDCl$_3$, ppm): δ 180.39, 175.42, 173.25, 173.20, 172.60, 172.45, 162.74, 158.35, 151.04, 145.43, 142.58, 142.56, 142.01, 141.95, 136.72, 130.08, 128.26, 128.06, 127.76, 126.62, 124.72, 122.32, 117.86, 113.05, 110.32, 110.26, 93.88, 85.99, 85.77, 77.58, 77.16, 76.74, 63.54, 63.32, 63.22, 58.56, 58.30, 55.26, 49.49, 49.45, 44.75, 44.66, 43.15, 42.99, 31.10, 31.01, 29.96, 26.97, 26.93, 26.84, 26.77, 26.58, 26.08, 25.62, 24.77, 24.71, 24.67, 24.62, 20.48, 20.39.

^{31}P-NMR (121 MHz, CDCl$_3$, ppm): *δ* 147.17.

ESI-MS (pos. MeOH): mass calc. for C$_{72}$H$_{85}$N$_6$O$_9$P = 1208.6116; mass found = 1208.6117.

Synthesis of the Oligophosphodiesters Containing Ring-Substituted Squaraine Dyes.

Oligophosphodiesters **CNSqTr**, **CNSq6**, **CNOSq**, **BarbSqTr**, and **BarbSq6** were prepared via automated oligonucleotide synthesis. UltraMILD procedure (GlenResearch) was applied, using the corresponding phosphoramidites, solid-supports, and reagents (Cap A). Coupling time between nucleotide and squaraine and squaraine and squaraine was increased to 3 minutes. Cleavage from the solid support and final deprotection were done by treatment with 50 mM potassium carbonate solution in methanol at room temperature for 4 hours. The oligophosphodiesters were purified by the reverse phase HPLC: column C4 polymer, 250 mm × 4.6 mm, Supelco; mobile phase A = (Et$_3$NH)OAc (0.1 M, pH 7.0), mobile phase B = MeCN, gradient 40–100% B over 15 min; elution at 40 °C; flow 0.5 ml/min.

Table 3.5. Name, sequence, chemical formula, and calculated and found mass (from the MS analysis) of the oligophosphodiesters containing ring-substituted squaraine dyes.

Name	Sequence	Chem. Formula	Exact Mass	MS Found	Yield, [nmol]
CNSqTr	(CNSq)$_3$	C$_{123}$H$_{142}$N$_{12}$O$_{13}$P$_2$	2057.0295	2057.0286	234
CNSq6	(CNSq)$_6$-CTCACGGAAG – 3'	C$_{343}$H$_{404}$N$_{65}$O$_{86}$P$_{15}$	7273.5302	7273.5490	175
CNOSq	(CNSq-OSq)$_3$-CTCACGGAAG – 3'	C$_{334}$H$_{404}$N$_{59}$O$_{89}$P$_{15}$	7129.4965	7129.5150	113
BarbSqTr	(BarbSq)$_3$	C$_{126}$H$_{146}$N$_{12}$O$_{22}$P$_2$$^{2-}$	2241.0150	2241.0176	49
BarbSq6	(BarbSq)$_6$-CTCACGGAAG – 3'	C$_{349}$H$_{416}$N$_{65}$O$_{104}$P$_{15}$	7645.5326	7646.4400	18

Chapter 4. Oligophosphodiesters Containing Trimethine Cyanine

4.1 Introduction

The aim of this project is the formation and investigation of long-wavelength absorbing supramolecular polymers from oligophosphodiesters containing cyanine chromophore.

Cyanines are one of the most widespread compounds for application in biology and medicine [188, 189]. They are used as biological labels and probes [57, 190], for fluorescence and photoacoustic imaging [191, 192], for cancer theranostics [193, 194].

Cyanines absorb and emit light in a broad spectral diapason; their absorption can be easily modified by variation of the number of vinylene groups in the chromophore system: every additional vinylene group causes a red-shift of about 100 nm (Figure 4.1). However, the prolongation of chain length results in loss of stability [195].
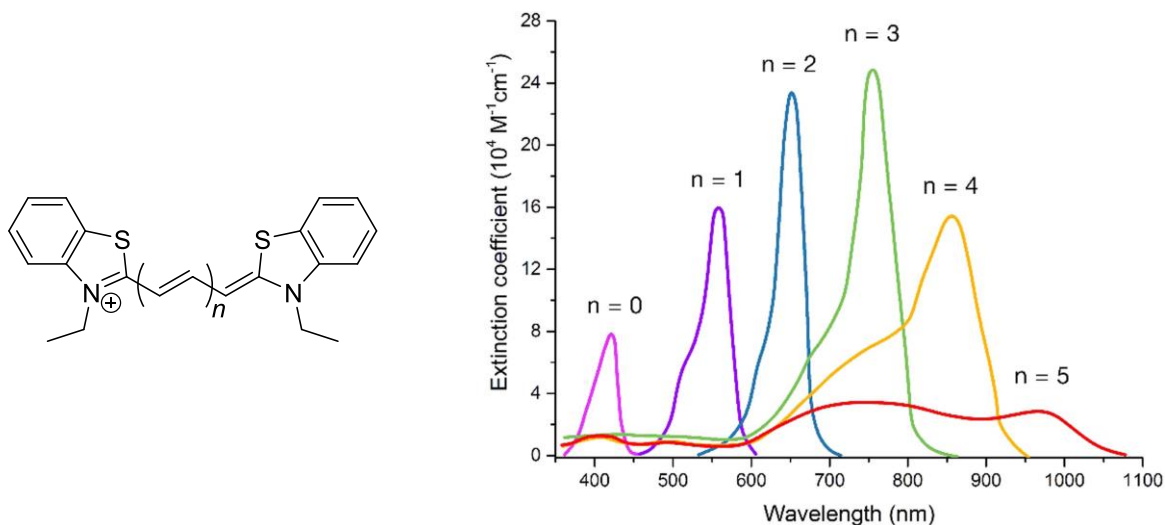
Figure 4.1. The influence of chain length (*n*) on the absorption spectra of thiacyanine monomers in methylene chloride [195].

Among commercially available cyanine phosphoramidites, arguably, trimethine cyanines are the most attractive for the preparation of the monomers for SPs using phosphoramidite chemistry. This molecule combines both long-wavelength absorption and good stability. In our work, we use

cyanine 3 phosphoramidite (Cy3) (Figure 4.2). The Cy3 molecule with absorption around 550 nm allows preparing oligophosphodiesters with spectral activity around 550 nm. Thus, we envisage SPs with absorption that differs from the squaraine chromophores.
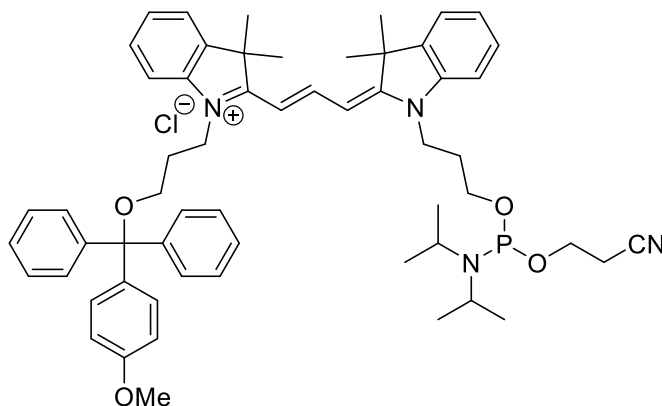
Figure 4.2. Structure of the cyanine 3 phosphoramidite [123].

The water-solubility of the cyanine chromophore is closely similar to the squaraine's [59]. Therefore, we renounce to the creation of SPs from phosphodiester-linked Cy3 homo-oligomers. Most likely, in case of formation, the SPs from the oligomers will precipitate as it is shown for squaraines in Chapter 3, section "Self-Assembly of the Phosphodiester-Linked Squaraine Trimers". Based on previous experience obtained in the way of creation SPs from squaraine oligophosphodiester, the most promising design of monomers for SPs is a combination of cyanine molecules and DNA.

In this project, we synthesize the DNA-Cy3 conjugates and study their supramolecular polymerization in aqueous ethanol solutions containing sodium chloride and phosphate buffer.

4.2 Results and Discussion

4.2.1 Synthesis of the Cy3-Modified Oligonucleotides

This section describes the synthesis of the DNA-Cy3 conjugates, which consist of ten nucleotides (CTC ACG GAA G – 3') and one (**1Cy**), three (**3Cy**), and six (**6Cy**) trimethine cyanine molecules (Figure 4.3, Table 4.1). The number before "Cy" indicates the quantity of the cyanine molecules in the oligonucleotide.

1Cy: $n = 1$

3Cy: $n = 3$

6Cy: $n = 6$
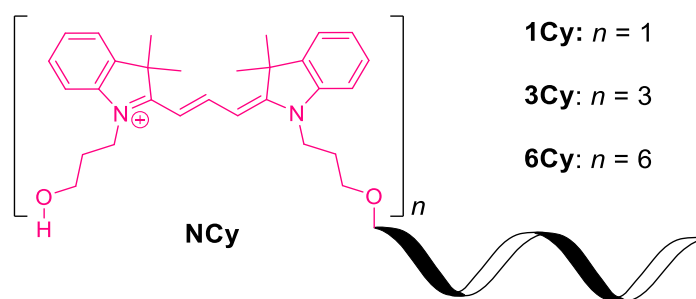
Figure 4.3. Structure of the Cy3-modified oligonucleotides.

Table 4.1. Name, structure, and yield of oligophosphodiesters containing Cy3 chromophore.

Name	Sequence	Yield, %
1Cy	Cy3-CTC ACG GAA G – 3'	27
3Cy	Cy3-Cy3-Cy3-CTC ACG GAA G – 3'	14
6Cy	Cy3-Cy3-Cy3-Cy3-Cy3-Cy3-CTC ACG GAA G – 3'	1.2

The synthesis of the Cy3-modified oligonucleotides was performed via the phosphoramidite approach. Cyanine 3 phosphoramidite for the synthesis was purchased from GlenResearch. Following the recommendations of GlenResearch [123], nucleotide monomers with base-labile protecting groups (acetyl-protected dC, isopropyl-phenoxyacetyl protected dG, and phenoxyacetyl-protected dA) and ammonium hydroxide as deprotection solution (r.t., two hours) were used for the synthesis.

The yield of the Cy3-modified oligonucleotides dramatically decreases with the increasing length of the cyanine part. Thus, the oligonucleotide with one cyanine molecule **1Cy** was synthesized with a yield of 27%, while the yield of **6Cy** containing six cyanines was about 1%. This phenomenon can be caused by one of the following reasons: 1) the Cy3 molecules decompose during the synthesis or deprotected or 2) the coupling efficiency decreases with the prolongation of the cyanine chain.

To study the chemical stability of Cy3 in deprotection solutions, the trimethine chromophore was treated separately with the solution of 30% NH₄OH and solution of 50 mM K₂CO₃ in methanol. During the treatment, the absorption of the chromophore was almost unchanged (Figure 4.4). Consequently, the studied deprotection solutions do not destroy the Cy3 chromophore.
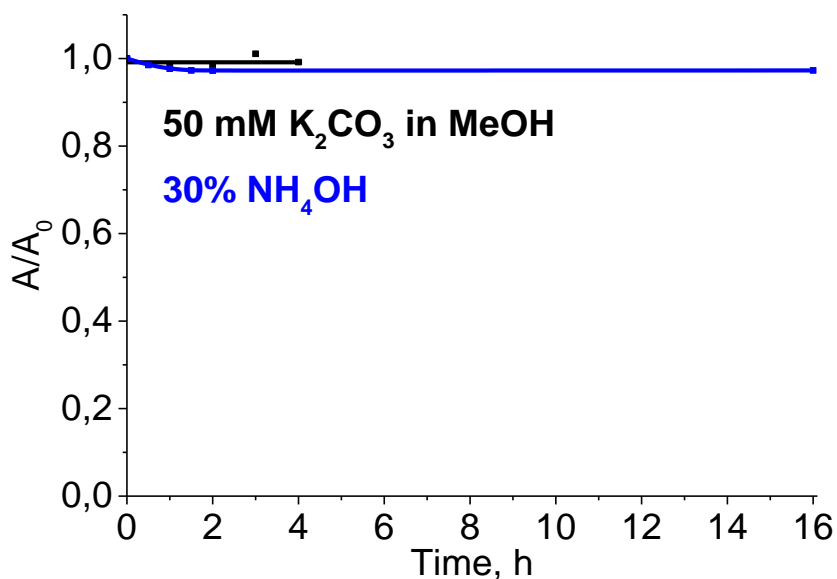
Figure 4.4. The decay of the long-wavelength absorption band of Cy3 chromophore during the treatment with concentrated aqueous NH₄OH (blue) and 50 mM K₂CO₃ in methanol (black) at room temperature. A/A₀ – relative absorbance, where A₀ is the absorption intensity at the starting point, and A is the absorption intensity at the time-point.

The data (average stepwise yields and overall yields) obtained from the DNA synthesizer in the course of the synthesis of oligonucleotide **6Cy** reveals that after incorporating the second cyanine, the yield of every new addition decreases noticeably. HPLC analyses conducted for crude **6Cy** (sample after synthesis and deprotection) contain few intense peaks (Figure 4.5). According to

ESI-MS data (Table 4.2), the peak with the highest retention time corresponds to the target sequence **6Cy**, while peaks with shorter retention time suggest the presence of strands with smaller numbers of cyanine molecules in the analyzed mixture. Consequently, a reduced coupling efficiency of cyanines, starting from the third Cy3, is the main reason for the low yield of **6Cy**.
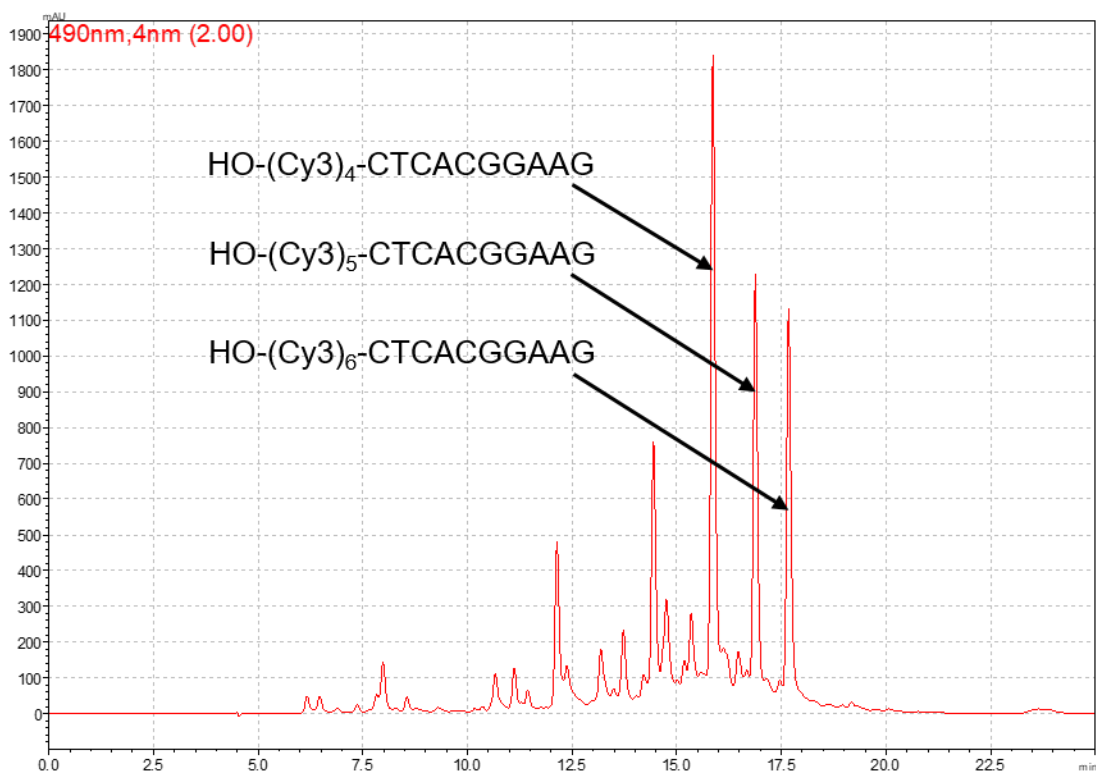
Figure 4.5. HPLC of the crude mixture obtained after the synthesis and deprotection of **6Cy**.

Table 4.2. Name, structure, and MS data for the identified products obtained in the synthesis of **6Cy**.

Name	Structure	MS calc.	MS found
4Cy	HO-(Cy3)$_4$-CTC ACG GAA G – 3'	5064.5226	5064.5200
5Cy	HO-(Cy3)$_5$-CTC ACG GAA G – 3'	5571.7634	5571.7580
6Cy	HO-(Cy3)$_6$-CTC ACG GAA G – 3'	6079.0041	6079.0046

4.2.2 Self-Assembly of the Cy3-Modified Oligonucleotides

In the beginning, we studied spectral-luminescence properties of the Cy3-modified oligonucleotides in ethanol. Absorption and fluorescence characteristics are given in Table 4.3, absorption and emission spectra are shown in Figure 4.6.

Table 4.3. Spectral properties of the Cy3-modified oligonucleotides in ethanol, $c = 1\,\mu M$, $\lambda(\text{Ext}) = 500$ nm.

Name	Structure	$\lambda(\text{Abs})$, nm	$\lambda(\text{Fl})$, nm	Q.Y., %
1Cy	Cy3-CTC ACG GAA G – 3'	260, 553	566	42
3Cy	(Cy3)$_3$-CTC ACG GAA G – 3'	260, 553	569	23
6Cy	(Cy3)$_6$-CTC ACG GAA G – 3'	260, 553	572	16
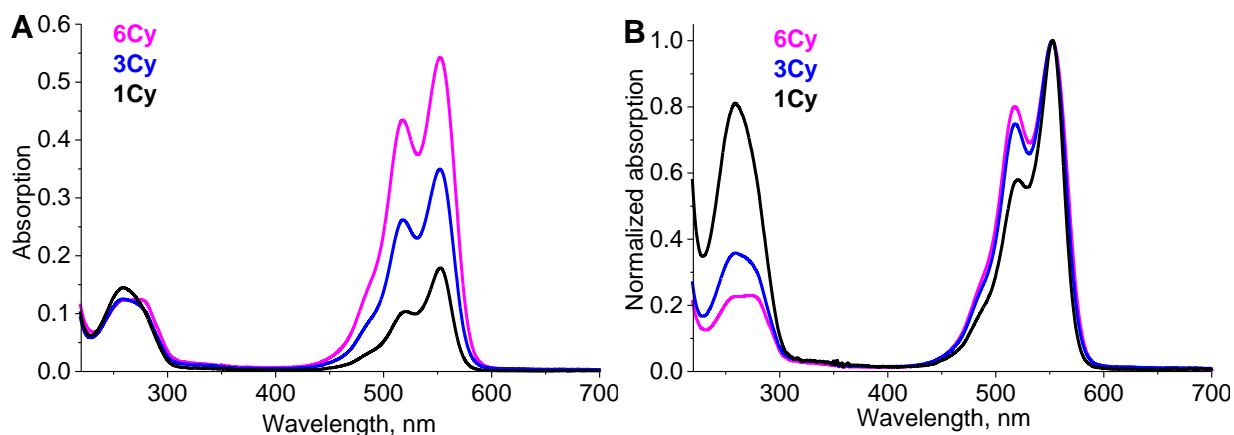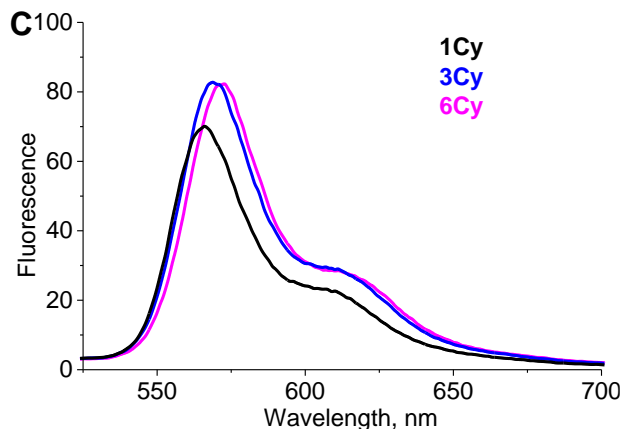
Figure 4.6. Absorption (A) normalized absorption (B) and fluorescence (C) spectra of the Cy3-DNA conjugates **1Cy** (black), **3Cy** (blue), and **6Cy** (magenta). Conditions: 1 µM strand, ethanol.

In the long-wavelength region, Cy3-modified oligonucleotides absorb light at 553 nm (Figure 4.6A) and emit at 566–572 nm (Figure 4.6C). The absorption spectra of **1Cy**, **3Cy**, and **6Cy** also contain a short-wavelength band at 260 nm caused by electron transitions in the nucleotide part ($\varepsilon \approx 112\,000$ M^{-1} cm^{-1}) and the cyanine part ($\varepsilon \approx 4\,930$ M^{-1} cm^{-1} for one cyanine unit). Prolongation of the length of the cyanine segment leads to quenching of the fluorescence: the quantum yield decreases from 42% for **1Cy** to 16% for **6Cy**. The fluorescence quenching and the arising of a new blue-shifted band in the UV-Vis spectrum (518 nm) superimposed with the short-wavelength shoulder (Figure 4.6B) are signs of aggregation in *H*-type. Most likely, the aggregation occurs due to intramolecular folding.

In aqueous ethanol solutions (1 µM strand, 100 mM NaCl, 10 mM PB), the absorption spectrum of **6Cy** shows the presence of a new short-wavelength *H*-band (about 510 nm). Upon changing the ethanol concentration from 0% to 30%, an increase of absorptivity is observed. Starting from 35% of EtOH in the mixture, the intensity of the *H*-band decreases, and the intensity of the main band increases (Figure 4.7). Changing the concentration of **6Cy** (up to 10 µM) or the concentration of NaCl (up to 500 mM) does not lead to the formation of new types of aggregates.
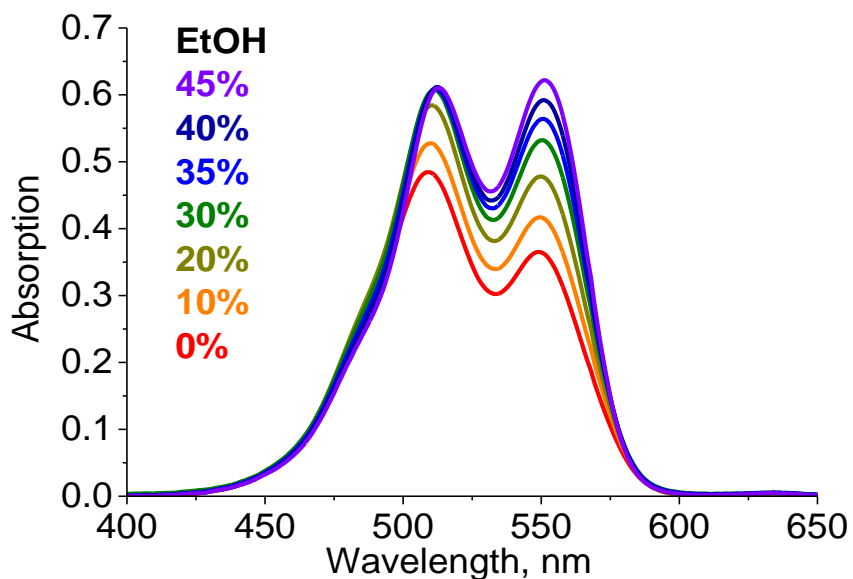
Figure 4.7. Absorption spectra of the oligonucleotide **6Cy** depending on the concentration of ethanol in the aqueous solution. Conditions: 1 μM **6Cy**, 10 mM PB, 100 mM NaCl.

The oligonucleotide **6Cy** does not show signs of SP formation. Thus, under the heating-cooling runs, the spectrum only slightly changes and has a non-sigmoidal shape (Figure 4.8).
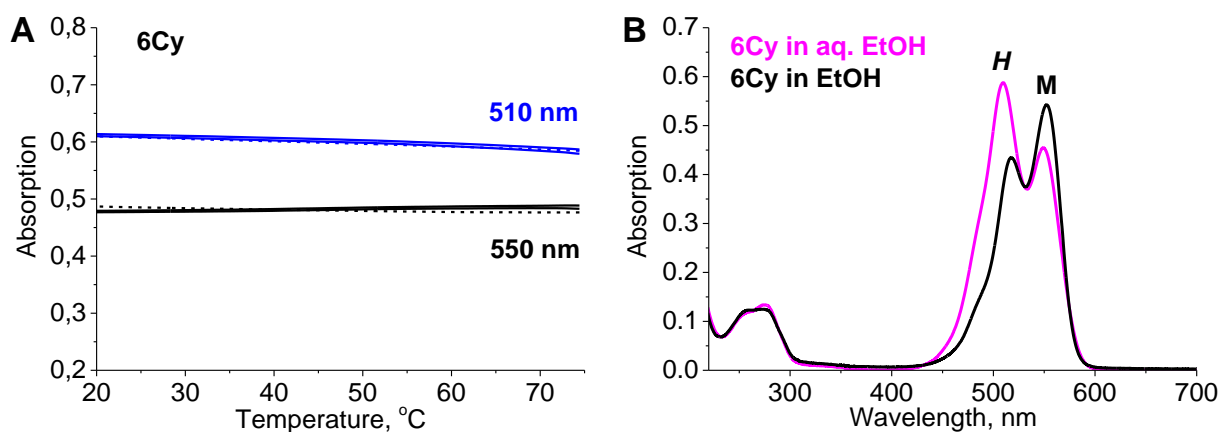
Figure 4.8. A: Cooling (solid lines) and heating (dashed lines) runs (rate: 0.5 °C/min) for the oligonucleotide **6Cy** recorded at 510 nm (blue) and 550 nm (black), showing the absence of self-assembly processes. B: Absorption spectrum of **6Cy** in ethanol (black) and aqueous media (magenta). Conditions: 1 μM **6Cy**, 15% EtOH, 100 mM NaCl, 10 mM PB.

The DNA-cyanines conjugates **3Cy** and **1Cy** containing shorter cyanine segments than **6Cy** form *H*-aggregates (**3Cy**) (Figure 4.9A) or do not show aggregation (**1Cy**) (Figure 4.9B). For both **3Cy**

and **1Cy**, the thermal experiments conducted in aqueous ethanol solutions show no signs of supramolecular polymerization.
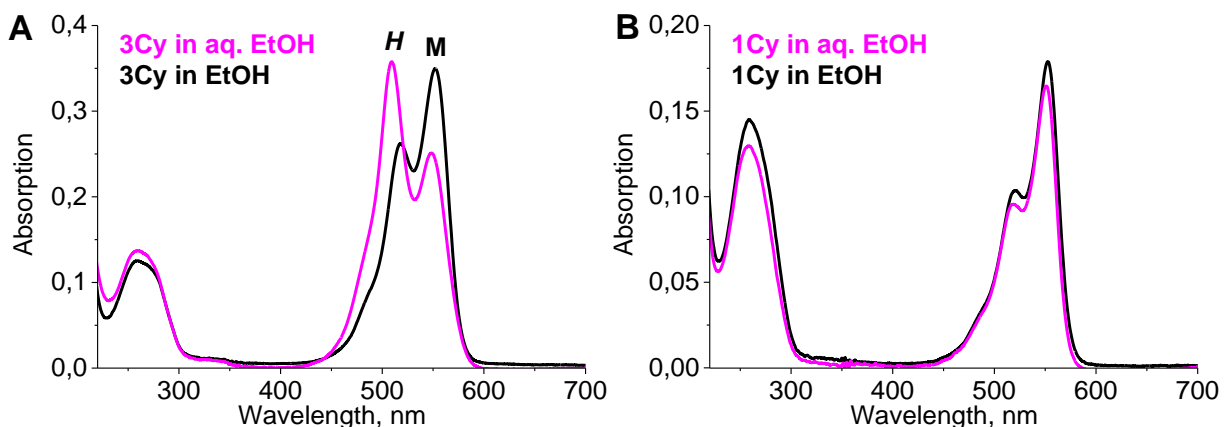
Figure 4.9. Absorption spectra of **3Cy** (A) and **1Cy** (B) measured in ethanol (black) and aqueous media (magenta). Conditions: 1 μM strand, 15% EtOH, 100 mM NaCl, 10 mM PB.

4.3 Conclusions

Cyanine-modified oligonucleotides **NCy**, consisting of ten nucleotides and varied numbers of trimethine cyanine molecules (N = 1, 3, 6), were synthesized. Increasing the length of the cyanine part dramatically decreases the yield of the oligonucleotide.

Depending on the length of the cyanine segment, the Cy3-modified oligonucleotides form *H*-aggregates (N = 3 or 6) or do not show aggregation (N = 1). Like the *H*-aggregates of all squaraine oligophosphodiesters studied in this work, the *H*-aggregates of trimethine cyanine-modified oligonucleotides reveal no supramolecular polymerization.

Due to low yields of DNA-cyanine conjugates with prolonged chromophore segments, we consider these compounds as not fit for further investigations.

4.4 Experimental Section

Cy3-modified oligonucleotides **1Cy**, **3Cy**, and **6Cy** were prepared via automated oligonucleotide synthesis on a 394-DNA/RNA synthesizer (*Applied Biosystems*). UltraMild CE phosphoramidites,

UltraMild supports, and special Cap Mix A (THF/Pyridine/Pac$_2$O) were used for the synthesis. Coupling time between nucleotide and cyanine and cyanine and cyanine was increased to 3 minutes. Cleavage from the solid support and final deprotection were done by treatment with 30% NH$_4$OH at room temperature for two hours. The oligonucleotides were purified by reverse-phase HPLC: column C4 polymer, 250 mm $\times$ 4.6 mm, Supelco, mobile phase A = (Et$_3$NH)OAc (0.1 M, pH 7.0), mobile phase B = MeCN; flow 1 ml/min. Elution at 50 °C. Gradient 0–30% B over 20 min for **1Cy** and 10 – 60% B over 20 min for **3Cy** and **6Cy**.

Table 4.4. Name, sequence, chemical formula, and calculated and found mass (from the MS analysis) of the oligophosphodiesters containing Cy3 molecule.

Name	Sequence	Chem. Formula	Exact Mass	MS found	Yield, [nmol]
1Cy	Cy3-CTC ACG GAA G – 3'	$C_{126}H_{158}N_{43}O_{60}P_{10}{}^{+}$	3542.8005	3542.7923	267
3Cy	(Cy3)$_3$-CTC ACG GAA G – 3'	$C_{184}H_{230}N_{47}O_{68}P_{12}{}^{3+}$	4557.2819	4557.2699	144
6Cy	(Cy3)$_6$-CTC ACG GAA G – 3'	$C_{271}H_{338}N_{53}O_{80}P_{15}{}^{6+}$	6079.0041	6079.0046	12

Chapter 5. Cy3-Modified Oligonucleotides for Studying Excitons

This part of the work was performed in collaboration with the Department of Biological Engineering, Massachusetts Institute of Technology [196].

5.1 Introduction

Light-harvesting and molecular electronics applications require systems with controllable excitons. Control over excitons is possible in structures where molecular components are organized with nanoscale precision. DNA represents a platform where chromophores can be arranged with nanoscale precision and, thus, excitonic chromophore systems can be designed, engineered, and studied.

Structural DNA nanotechnologies give access not only to the DNA duplexes but also to more complexly organized double-crossover tiles (DX-tiles) (Figure 5.1), which also can serve as a nanoscale platform for the arrangement of chromophores. DX tiles are at least twice as rigid as duplexes due to inter-duplex crosslinking that couples bending, twisting, and stretching modes [197, 198].
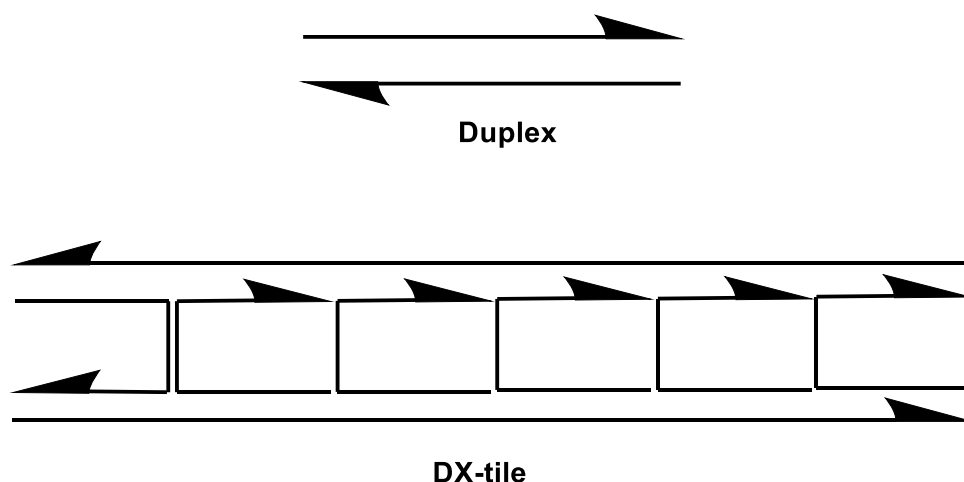
Figure 5.1. The organization of oligonucleotides in DNA duplex and DX-tile.

In the original work [196], excitons of trimethine cyanines (Cy3) (for structure of chromophore see Figure 4.2) formed from one or two cyanine molecules inserted into DNA duplex or DX-tile scaffold were investigated. Part of this work was the synthesis of Cy3-modified ligonucleotides.

5.2 Synthesis of the Cy3-Modified Oligonucleotides

The structures of the Cy3-modified oligonucleotides **S1–S18** used for the studying of excitons are shown in Table 5.1. The strands are varied in the number of cyanine molecules (1 or 2) and their position in the strand as well as in the length of the oligonucleotide. The synthesis of a sufficiently large number of the Cy3-modified oligonucleotides gave us enough data based on which we can make conclusions about the yields of the oligonucleotides and the reactivity of the cyanine molecule.

Table 5.1. Name, structure, and yield of the Cy3-modified oligonucleotides **S1–S18**.

Name	Sequence	Yield, %
S1	5' – TTCGGGCCTCGCCCC-Cy3-T-CAC – 3'	23
S2	5'– TTCGGGCCTCGCCCC-Cy3-Cy3-CAC – 3'	19
S3	5' – TCGCCTGGGCGATAC-Cy3-T-CCC – 3'	32
S4	5' – TCGCCTGGGCGATAC-Cy3-Cy3-CCC – 3'	22
S5	5' – CTGGACGCTCGCCGC-Cy3-T-CTC – 3'	26
S6	5' – CTGGACGCTCGCCGC-Cy3-Cy3-CTC – 3'	20
S7	5' – AAGTTCAGCGCCGGA-Cy3-T-CGA – 3'	23
S8	5' – AAGTTCAGCGCCGGA-Cy3-Cy3-CGA – 3'	9.6
S9	5' – TGCACTCTCG-Cy3-T-Cy3-TGACCGAGCT – 3'	20
S10	5' – TGCACTCTCG-Cy3-T-T-Cy3-TGACCGAGCT – 3'	20
S11	5' – TGCACTCTCG-Cy3-T-T-T-Cy3-TGACCGAGCT – 3'	20
S12	5' – TAGGGCGTGGGGGTCAC-Cy3-T-CAG – 3'	6.8
S13	5' – TAGGGCGTGGGGGTCAC-Cy3-Cy3-CAG – 3'	4.9
S14	5' – TAGGGCGTGGGGGTC-Cy3-T-ACCAG – 3'	12
S15	5' – TAGGGCGTGGGGGTC-Cy3-Cy3-ACCAG – 3'	3.4
S16	5' – GCCGCTTCTCCTGGACGCTCTCGCCTGGGCGATAC-Cy3-TCCC – 3'	14
S17	5' – TCGCCTGGGCGATAC-Cy3-TCCCGCCGCTTCTCCTGGACGCTC – 3'	12
S18	5' – TCGCCTGGGCGATAC-Cy3-Cy3-TCCCGCCGCTTCTCCTGGACGCTC – 3'	6.4

The syntheses of oligonucleotides **S1–S18** were performed using nucleotide monomers with base labile protecting groups (acetyl-protected dC, isopropyl-phenoxyacetyl protected dG, and phenoxyacetyl-protected dA). This was necessary for deprotection in UltraMild conditions (50 mM K_2CO_3 in MeOH, r.t., four hours or aqueous 30% NH_4OH, r.t., two hours). We found that Cy3-modified oligonucleotides containing 1 or 2 cyanine units and 20–25 building blocks (**S1–S15**) can be easily deprotected and cleaved from the support in the methanolic solution of potassium carbonate, while oligonucleotides built from 40–41 units (**S16–S18**) must be deprotected in aqueous solution due to their low solubility in methanol.

The incorporation of the second Cy3 molecule leads to a noticeable decrease in the yield of modified oligonucleotides. The average yield calculated for sequences **S1**, **S3**, **S5**, and **S7** with one cyanine is 26%, while the average yield for analogous strands **S2**, **S4**, **S6**, and **S8** containing two cyanines is 18%.

The nucleotide composition strongly affects the yield of the oligonucleotide as well. Thus, sequences **S12–S15** contain ten guanosine nucleotides, five of which are placed in a row. As a result, the average yield calculated for **S12–S15** is 8%, while the average yield of **S1–S4** oligonucleotides, which have almost the same length as **S12–S15** and a corresponding number of Cy3 molecules, is 24%.

In conclusion, about 20 Cy3-modified oligonucleotides with different lengths (20–25 and 42 units) and the number of cyanines (1 or 2 molecules) were synthesized. Their yields depending on the number of cyanines and composition of the nucleotides, were investigated.

5.3 Experimental Section

Cy3-modified oligonucleotides **S1–S18** were prepared via automated oligonucleotide synthesis on a 394-DNA/RNA synthesizer (*Applied Biosystems*). UltraMild CE phosphoramidites, UltraMild supports, and special Cap Mix A (THF/Pyridine/Pac$_2$O) were used for the synthesis. Coupling times between nucleotide and cyanine, cyanine and cyanine, and cyanine and nucleotide were increased to 3 minutes. Cleavage from the solid support and final deprotection were done by

treatment with 50 mM potassium carbonate solution in methanol at room temperature for four hours (oligonucleotides **S16–S18** were deprotected in 30% NH$_4$OH at room temperature for two hours). The oligonucleotides were purified by the reverse-phase HPLC: column C4 polymer, 250 mm × 4.6 mm, Supelco, mobile phase A = (Et$_3$NH)OAc (0.1 M, pH 7.0), mobile phase B = MeCN. Gradient 0–35% B over 22 min; flow 1 ml/min; elution at 40 °C.

Table 5.2. Name, sequence, chemical formula, and calculated and found mass (from the MS analysis) of the oligophosphodiesters containing Cy3 molecule.

Name	Sequence	Chem. Formula	Exact Mass	MS found
S1	5'– TTCGGGCCTCGCCCCCy3TCAC – 3'	$C_{209}H_{269}N_{65}O_{119}P_{19}^+$	6181.2005	6181.2006
S2	5' – TTCGGGCCTCGCCCCCy3Cy3CAC – 3'	$C_{228}H_{292}N_{65}O_{116}P_{19}^{2+}$	6384.3952	6384.4048
S3	5' – TCGCCTGGGCGATACCy3TCCC – 3'	$C_{211}H_{269}N_{69}O_{118}P_{19}^+$	6245.2179	6245.2266
S4	5' – TCGCCTGGGCGATACCy3Cy3CCC – 3'	$C_{230}H_{292}N_{69}O_{115}P_{19}^{2+}$	6448.4126	6448.4244
S5	5' – CTGGACGCTCGCCGCCy3TCTC – 3'	$C_{210}H_{269}N_{67}O_{119}P_{19}^+$	6221.2067	6221.2106
S6	5' – CTGGACGCTCGCCGCCy3Cy3CTC – 3'	$C_{229}H_{292}N_{67}O_{116}P_{19}^{2+}$	6424.4013	6424.4092
S7	5' – AAGTTCAGCGCCGGACy3TCGA – 3'	$C_{214}H_{268}N_{78}O_{114}P_{19}^+$	6342.2581	6342.2702
S8	5'– AAGTTCAGCGCCGGACy3Cy3CGA – 3'	$C_{233}H_{291}N_{78}O_{111}P_{19}^{2+}$	6545.4528	6545.4652
S9	5' – TGCACTCTCGCy3TCy3TGACCGAGCT – 3'	$C_{261}H_{331}N_{77}O_{135}P_{22}^{2+}$	7384.5619	7384.5704
S10	5' – TGCACTCTCGCy3TTCy3TGACCGAGCT – 3'	$C_{271}H_{344}N_{79}O_{142}P_{23}^{2+}$	7688.6080	7688.6132
S11	5' – TGCACTCTCGCy3TTTCy3TGACCGAGCT –3'	$C_{281}H_{357}N_{81}O_{149}P_{24}^{2+}$	7992.6540	7992.6711
S12	5' – TAGGGCGTGGGGGTCACCy3TCAG – 3'	$C_{235}H_{293}N_{87}O_{129}P_{21}^+$	7047.3526	7047.3574
S13	5' – TAGGGCGTGGGGGTCACCy3Cy3CAG – 3'	$C_{254}H_{316}N_{87}O_{126}P_{21}^{2+}$	7250.5473	7250.5596
S14	5' – TAGGGCGTGGGGGTCCy3TACCAG – 3'	$C_{235}H_{293}N_{87}O_{129}P_{21}^+$	7047.3526	7047.3628
S15	5' – TAGGGCGTGGGGGTCCy3Cy3ACCAG – 3'	$C_{254}H_{316}N_{87}O_{126}P_{21}^{2+}$	7250.5473	7250.5524
S16	5' – GCCGCTTCTCCTGGACGCTCTCGCCT-GGGCGATACCy3TCCC – 3'	$C_{402}H_{514}N_{136}O_{242}P_{39}^+$	12325.1856	12325.2096
S17	5' – TCGCCTGGGCGATACCy3TCCCGCCGC-TTCT CCTGGACGCTC – 3'	$C_{402}H_{514}N_{136}O_{242}P_{39}^{2+}$	12325.1856	12325.1908
S18	5' – TCGCCTGGGCGATACCy3Cy3TCCCGCCG CTTCTCCTGGACGCTC – 3'	$C_{421}H_{537}N_{136}O_{239}P_{39}^{2+}$	12528.3803	12528.4114

References

[1] T. F. A. de Greef, E. W. Meijer. *Nature*, 2008, **453**, 171–173.

[2] L. Yang, X. Tan, Z. Wang, X. Zhang. *Chem. Rev.*, 2015, **115**, 7196–7239.

[3] R. G. Jones, C. K. Ober, P. Hodge, P. Kratochvíl, G. Moad, M. Vert. *Pure Appl. Chem.*, 2013, **85**, 463–492.

[4] T. Aida, E.W. Meijer. *Isr. J. Chem.*, 2020, **60**, 33–47.

[5] T. F. A. De Greef, M. M. J. Smulders, M. Wolffs, A. P. H. J. Schenning, R. P. Sijbesma, E. W. Meijer. *Chem. Rev.*, 2009, **109**, 5687–5754.

[6] M. M. J. Smulders, M. M. L. Nieuwenhuizen, T. F. A. de Greef, P. van der Schoot, A. P. H. J. Schenning, E. W. Meijer. *Chem. Eur. J.*, 2010, **16**, 362–367.

[7] D. Zhao, Jeffrey S. Moore. *Org. Biomol. Chem.*, 2003, **1**, 3471–3491.

[8] Y. Dorca, J. Matern, G. Fernández, L. Sánchez. *Isr. J. Chem.*, 2019, **59**, 869–880.

[9] F. Li, X. Li, Y. Wang, X. Zhang. *Angew. Chem. Int. Ed.*, 2019, **58**, 17994–18002.

[10] Y. Wang, J. Chou, Y. Sun, S. Wen, S. Vasilescu, H. Zhang. *Mater. Sci. Eng. C*, 2019, **101**, 650–659.

[11] Y. Cui, D. Tao, X. Huang, G. Lu, C. Feng. *Langmuir*, 2019, **35**, 3134–3142.

[12] Y. Dorca, E. E. Greciano, J. S. Valera, R. Gómez, L. Sánchez. *Chem. Eur. J.*, 2019, **25**, 5848–5864.

[13] X. Zhou, Q. Jin, L. Zhang, Z. Shen, L. Jiang, M. Liu. *Small*, 2016, **12**, 4743–4752.

[14] T. Shimizu, M. Masuda, H. Minamikawa. *Chem. Rev.*, 2005, **105**, 1401–1443.

[15] Y. Gong, Q. Hu, C. Wang, L. Zang, L. Yu. *Langmuir*, 2016, **32**, 421–427.

[16] X. Zhang, Y. Dai, X. Chen, R. Zhuo. *Macromol. Rapid Commun.*, 2016, **37**, 888–893.

[17] Y. Zhua, B. Yanga, S. Chena, J. Du. *Prog. Polym. Sci.*, 2017, **64**, 1–22.

[18] A. M. Cassell, C. L. Asplund, J. M. Tour. *Angew. Chem. Int. Ed.*, 1999, **38**, 2403–2405.

[19] Y. Zheng, H. Zhou, D. Liu, G. Floudas, M. Wagner, K. Koynov, M. Mezger, H.-J. Butt, T. Ikeda. *Angew. Chem. Int. Ed.*, 2013, **52**, 4845–4848.

[20] F. Herbst, D. Döhler, P. Michael, W. H. Binder. *Macromol. Rapid Commun.*, 2013, **34**, 203–220.

[21] J. Hentschel, A. M. Kushner, J. Ziller, Z. Guan. *Angew. Chem. Int. Ed.*, 2012, **51**, 10561–10565.

[22] X. Ma, H. Tian. *Acc. Chem. Res.*, 2014, **47**, 1971–1981.

[23] X. Yan, F. Wang, B. Zheng, F. Huang. *Chem. Soc. Rev.*, 2012, **41**, 6042–6065.

[24] B. Rybtchinski. *ACS Nano*, 2011, **5**, 6791–6818.

References

[25]   P. Cordier, F. Tournilhac, C. Soulié-Ziakovic, L. Leibler. *Nature*, 2008, **451**, 977–980.

[26]   A. M. Levine, S. Biswas, A. B. Braunschweig. *Nanoscale Adv.*, 2019, **1**, 3858–3869.

[27]   F. Würthner, Z. Chen, F. J. Hoeben, P. Osswald, C. C. You, P. Jonkheijm, J. V. Herrikhuyzen, A. P. Schenning, P. P. van der Schoot, E. W. Meijer, E. H. Beckers, S. C. Meskers, R. A. Janssen. *J. Am. Chem. Soc.*, 2004, **126**, 10611–10618.

[28]   Y. Yanagisawa, Y. Nan, K. Okuro, T. Aida. *Science*, 2018, **359**, 72–76.

[29]   A. Blanazs, S. P. Armes, A. J. Ryan. *Macromol. Rapid Commun.*, 2009, **30**, 267–277.

[30]   J. Lia, X. J. Loh. *Adv. Drug Deliv. Rev.*, 2008, **60**, 1000–1017.

[31]   X. Jin, L. Zhu, B. Xue, X. Zhu, D. Yan. *Natl. Sci. Rev.*, 2019, **6**, 1128–1137.

[32]   Y. Hu, M. Y. Chai, W. T. Yang, F. J. Xu. *Bioconjug. Chem.*, 2013, **24**, 1049–1056.

[33]   H. Hu, H.-Q. Song, B.-R. Yu, Q. Cai, Y. Zhu, F-J. Xu. *Polym. Chem.*, 2015, **6**, 2466–2477.

[34]   P. Y. W. Dankers, T. M. Hermans, T. W. Baughman, Y. Kamikawa, R. E. Kieltyka, M. M. C. Bastings, H. M. Janssen, N. A. J. M. Sommerdijk, A. Larsen, M. J. A. van Luyn, A. W. Bosman, E. R. Popa, G. Fytas, E. W. Meijer. *Adv. Mater.*, 2012, **24**, 2703–2709.

[35]   T. Wan, Y. Chen, Q. Pan, X. Xu, Y. Kang, X. Gao, F. Huang, C. Wu, Y. Ping. *J. Control. Release*, 2020, **322**, 236–247.

[36]   L. Wang, P.-P. Yang, X.-X. Zhao, H. Wang. *Nanoscale*, 2016, **8**, 2488–2509.

[37]   Y. Wu, G. Xu, X. Jin, X. Zhu. *Sci. China Mater.*, 2018, **61**, 1444–1453.

[38]   P. Y. W. Dankers, M. C. Harmsen, L. A. Brouwer, M. J. A. van Luyn, E. W. Meijer. *Nat. Mater.*, 2005, **4**, 568–574.

[39]   L. Saunders, P. X. Ma. *Macromol. Biosci.*, 2019, **19**, 1800313.

[40]   J.-A.Yang, J. Yeom, B. W. Hwang, A. S. Hoffman, S. K. Hahn. *Prog. Polym. Sci.*, 2014, **39**, 1973–198.

[41]   S. Piluso, A. H. Soultan, J. Patterson. *Curr. Pharm. Design.*, 2017, **23**, 281–294.

[42]   J. Song, Q. Cheng, S. Zhu, R. C. Stevens. *Biomed. Microdevices*, 2002, **4**, 213–221.

[43]   R. Dong, Y. Zhou, X. Huang, X. Zhu, Y. Lu, J. Shen. *Adv. Mater.*, 2015, **27**, 498–526.

[44]   M. J. Webber, E. A. Appel, E. W. Meijer, R. Langer. *Nat. Mater.*, 2016, **15**, 13–26.

[45]   E. Krieg, M. M. C. Bastings, P. Besenius, B. Rybtchinski. *Chem. Rev.*, 2016, **116**, 2414–2477.

[46]   A. Mishra, R. K. Behera, P. K. Behera, B. K. Mishra, G. B. Behera. *Chem. Rev.*, 2000, **100**, 1973–2011.

[47]   L. Beverina, M. Sassi. *Synlett*, 2014, **25**, 477–490.

[48]   U. Mayerhöffer, M. Gsänger, M. Stolte, B. Fimmel, F. Würthner. *Chem. Eur. J.*, 2013, **19**, 218–232.

[49] O. S. Kolosova, S. V. Shishkina, V. Marks, G. Gellerman, I. V. Hovor, A. L. Tatarets, E. A. Terpetschnig, L. D. Patsenker. *Dyes Pigm.*, 2019, **163**, 318–329.

[50] S. H. Kim, S. H. Hwang, J. J. Kim, C. M. Yoon, S. R. Keum. *Dyes Pigm.*, 1998, **37**, 145–154.

[51] G. de Miguel, M. Marchena, M. Zitnan, S. S. Pandey, S. Hayaseb, A. Douhal. *Phys. Chem. Chem. Phys.*, 2012, **14**, 1796–1805.

[52] L. Tong, P. Bi-Xian. *Dyes Pigm.*, 1999, **43**, 73–76.

[53] E. Terpetschnig, H. Szmacinski, J. R. Lakowicz. *Anal. Chim. Acta*, 1993, **282**, 633–641.

[54] R. B. Mujumdar, L. A. Ernst, S. R. Mujumdar, C. J. Lewis, A. S. Waggoner. *Bioconjug. Chem.*, 1993. 4, 105-111.

[55] J. L. Bricks, A. D. Kachkovskii, Y. L. Slominskii, A. O. Gerasov, S. V. Popov. *Dyes Pigm.*, 2015, **121**, 238–255.

[56] C. Sun, W. Du, B. Wang, B. Dong, B. Wang. *BMC Chem.*, 2020, **14**, 21.

[57] M. S. T. Gonçalves. *Chem. Rev.*, 2009, **109**, 190–212.

[58] R. R. Gupta, L. Strekowski. Heterocyclic Polimethine dyes. Synthesis, Properties and Applications. In Topics in Heterocyclic Chemistry. Volume 14. Springer. 2008.

[59] L. I. Markova, E. A. Terpetschnig, L. D. Patsenker. *Dyes Pigm.*, 2013, **99**, 561–570.

[60] Y. Xu, Z. Li, A. Malkovskiy, S. Sun, Y. Pang. *J. Phys. Chem. B*, 2010, **114**, 8574–8580.

[61] H. Chen, M. S. Farahat, K.-Y. Law, D. G. Whitten. *J. Am. Chem. Soc.*, 1996, **118**, 2584–2594.

[62] A. Kaczmarek-Kedziera, D. Kedziera. *Theor. Chem. Acc.*, 2016, **135**, 214.

[63] E. S. Emerson, M. A. Conlin, A. E. Rosenoff, K. S. Norland, H. Rodriguez, D. Chin, G. R. Bird. *J. Phys. Chem.*, 1967, **71**, 2396–2403.

[64] F. Würthner, T. E. Kaiser, C. R. Saha-Möller. *Angew. Chem. Int. Ed.*, 2011, **50**, 3376–3410.

[65] J. J. McEwen, K. J. Wallace. *Chem. Commun.*, 2009, 6339–6351.

[66] M. Kasha. *Radiation Research*, 1963, **20**, 55–71.

[67] R. S. Stoll, N. Severin, J. P. Rabe, S. Hecht. *Adv. Mater.*, 2006, **18**, 1271–1275.

[68] K. Jyothish, M. Hariharan, D. Ramaiah. *Chem. Eur. J.*, 2007, **13**, 5944–5951.

[69] M. E. Stawasz, D. L. Sampson, B. A. Parkinson. *Langmuir*, 2000, **16**, 2326–2342.

[70] Z. Yan, S. Guang, H. Xu, X. Su, X. Jia, X. Liu. *RSC Adv.*, 2013, **3**, 8021–8027.

[71] J. M. Malicka, A. Sandeep, F. Monti, E. Bandini, M. Gazzano, C. Ranjith, V. K. Praveen, A. Ajayaghosh, N. Armaroli. *Chem. Eur. J.*, 2013, **19**, 12991–13001.

[72] S. Yagi, Y. Hyodo, M. Hirose, H. Nakazumi, Y. Sakurai, A. Ajayaghosh. *Org. Lett.*, 2007, **9**, 1999–2002.

References

[73] A. Ajayaghosh, P. Chithra, R. Varghese, K. P. Divya. *Chem. Commun.*, 2008, 969–971.

[74] P. Chithra, R. Varghese, K. P. Divya, A. Ajayaghosh. *Chem. Asian J.*, 2008, **3**, 1365–1373.

[75] U. Mayerhöffer, F. Würthner. *Chem. Sci.*, 2012, **3**, 1215–1220.

[76] U. Mayerhöffer, F. Würthner. *Angew. Chem. Int. Ed.*, 2012, **51**, 5615–5619.

[77] S. Das, K. G. Thomas, K. J. Thomas, V. Madhavan. *J. Phys. Chem.*, 1996, **100**, 17310–17315.

[78] S. Bujosa, E. Castellanos, A. Frontera, C. Rotger, A. Costa, B. Soberats. *Org. Biomol. Chem.*, 2020, **18**, 888–894.

[79] D. Zhang, Y.-X. Zhao, Z.-Y. Qiao, U. Mayerhöffer, P. Spenst, X.-J. Li, F. Würthner, H. Wang. *Bioconjug. Chem.*, 2014, **25**, 2021–2029.

[80] R. Feng, W. Shi, D. Wang, J. Wen, H. Li, S. Sun, Y. Xu. *Sci. Rep.*, 2017, **7**, 43491.

[81] C. Luo, Q. X. Zhou, W. H. Lei, J. G. Wang, B. W. Zhang, X. S. Wang. *Supramol. Chem.*, 2011, **23**, 662–668.

[82] O. Wörzund, G. Scheibe. *Naturforschg.*, 1969, **21 b**, 381–390.

[83] B. Birkan, D. Güllen, S. Özcelik. *Phys. Chem. B*, 2006, **110**, 10805–10813.

[84] V. V. Prokhorov, O. M. Perelygina, S. I. Pozin, E. I. Mal'tsev, A. V. Vannikov. *J. Phys. Chem. B*, 2015, **119**, 15046–15053.

[85] B. Schade, A. K. Singh, V. Wycisk, J. L. Cuellar-Camacho, H. von Berlepsch, R. Haag, C. Böttcher. *Chem. Eur. J.*, 2020, **26**, 6919–6934.

[86] J. Wang, L. Zeng, D. Ding, X. Li, H. Zhang, H. Zhao, J. Fan, W. Zhang, Y. He. *Phys. Chem. Chem. Phys.*, 2011, **13**, 16741–16747.

[87] K. C. Hannah, B. Armitage. *Acc. Chem. Res.*, 2004, **37**, 845–853.

[88] T. D. Slavnova, A. K. Chibisov, H. Görner. *J. Phys. Chem. A*, 2005, **109**, 4758–4765.

[89] E. E. Jelley. *Nature*, 1936, **138**, 1009–1010.

[90] G. Scheibe, L. Kandler, H. Ecker. *Naturwissenschaften*, 1937, **25**, 75–75.

[91] S. Kirstein, S. Daehne. *Int. J. Photoenergy*, 2006, 1–21, 20363.

[92] C. Didraga, A. Pigzlys, P. R. Hania, H. von Berlepsch, K. Duppen, J. Knoester. *J. Phys. Chem. B*, 2004, **108**, 14976–14985.

[93] E. K. Walker, D. A. V. Bout, K. J. Stevenson. *J. Phys. Chem. C*, 2011, **115**, 2470–2475.

[94] D. Bousmail, P. Chidchob, H. F. Sleiman. *J. Am. Chem. Soc.*, 2018, **140**, 9518–9530.

[95] Y. Xiang, E. Moulin, E. Buhler, M. Maaloum, G. Fuks, N. Giuseppone. *Langmuir*, 2015, **31**, 7738–7748.

[96] Y. Mai, A. Eisenberg. *Chem. Soc. Rev.*, 2012, **41**, 5969–5985.

[97] G. Pan, X. Jin, Q. Mou, C. Zhang. *Chin. Chem. Lett.*, 2017, **28**, 1822–1828.

[98]   G.-Y. Pan, H.-R. Jia, Y.-X. Zhu, F.-G. Wu. *Nanoscale*, 2018, **10**, 2115–2127.

[99]   Z. Ruan, L. Liu, L. Fu, T. Xing, L. Yan. *Polym. Chem.*, 2016, **7**, 4411–4418.

[100] F. A. Aldaye, A. L. Palmer, H. F. Sleiman. *Science*, 2008, **321**, 1795–1799.

[101] N. C. Seeman, H. F. Sleiman. *Nature Rev. Materials*, 2017, **3**, 17068.

[102] J. Watson, F. Crick. *Nature*, 1953, **171**, 737–738.

[103] S. Neidle. Principles of Nucleic Acid Structure. Academic Press. 2008. Copyright © 2008 Elsevier Inc. All rights reserved, 302 p.

[104] E. T. Kool. *Chem. Rev.*, 1997, **97**, 1473–1488.

[105] Methods in Molecular Biology. Vol. 20 Protocols for Oligonucleotides and Analogs. Edited by S. Agrawal. Copyright 01993 Humana Press Inc., Totowa, NJ.

[106] R. Eritja. *Int. J. Pept. Res. Ther.*, 2007, **13**, 53–68.

[107] S. L. Beaucage, M. H. Caruthers. *Tetrahedron Lett.*, 1981, **22**, 1859–1862.

[108] M. H. Caruthers. *Biochem. Soc. Trans.*, 2011, **39**, 575–580.

[109] S. L. Beaucage, R. P. Iyer. *Tetrahedron*, 1993, **49**, 1925–1963.

[110] J. Micklefield. *Curr. Med. Chem.*, 2001, **8**, 1157–1179.

[111] V. L. Malinovskii, D. Wenger, R. Häner. *Chem. Soc. Rev.*, 2010, **39**, 410–422.

[112] Y. Saitoa, R. H. E. Hudson. *J. Photochem. Photobiol. C,* 2018, **36**, 48–73.

[113] C. Brotschi, G. Mathis, C. J. Leumann. *Chem. Eur. J.*, 2005, **11**, 1911–1923.

[114] Y. R. Baker, D. Traoré, P. Wanat, A. Tyburn, A. H. El-Sagheer, T. Brown. *Tetrahedron*, 2020, **76**, 130914.

[115] M. Meng, B. Schmidtgall, C. Ducho. *Molecules*, 2018, **23**, 2941.

[116] C. B. Winiger, S. M. Langenegger, O. Khorev, R. Häner. *Beilstein J. Org. Chem.*, 2014, **10**, 1589–1595.

[117] B. Mullah, A. Andrus. *Tetrahedron Lett.*, 1997, **38**, 5751–5754.

[118] W. Wang, W. Wan, H.-H. Zhou, S. Niu, A. D. Q. Li. *J. Am. Chem. Soc.*, 2003, **125**, 5248–5249.

[119] F. A. Aldaye, H. F. Sleiman. *Angew. Chem. Int. Ed.*, 2006, **45**, 2204–2209.

[120] C. D. Bösch, E. Abay, S. M. Langenegger, M. Nazari, A. Cannizzo, T. Feurer, R. Häner. *Helv. Chim. Acta*, 2019, **102**, e1900148.

[121] A. A. Ouahabi, L. Charles, J.-F. Lutz. *J. Am. Chem. Soc.*, 2015, **137**, 5629–5635.

[122] R. Häner, F. Garo, D. Wenger, V. L. Malinovskii. *J. Am. Chem. Soc.*, 2010, **132**, 7466–7471.

[123] Products for DNA Research. 2020 catalog. GlenResearch.

[124] L. I. Markova, V. L. Malinovskii, L. D. Patsenker, R. Häner. *Org. Biomol. Chem.*, 2012, **10**, 8944–8947.

[125] E. Stulz. *Chem. Eur. J.*, 2012, **18**, 4456–4469.

[126] M. Vybornyi, Y. Vyborna, R. Häner. *Chem. Soc. Rev.*, 2019, **48**, 4347–4360.

[127] D. Han, S. Pal, J. Nangreave, Z. Deng, Y. Liu, H. Yan. *Science*, 2011, **332**, 342–346.

[128] Y. He, T. Ye, M. Su, C. Zhang, A. E. Ribbe, W. J., C. Mao. *Nat. Lett.*, 2008, **452**, 198–202.

[129] B. Wei, M. Dai, P. Yin. *Nature*, 2012, **485**, 623–627.

[130] C. K. McLaughlin, G. D. Hamblin, H. F. Sleiman. *Chem. Soc. Rev.*, 2011, **40**, 5647–5656.

[131] S. M. Langenegger, R. Häner. *ChemBioChem*, 2005, **6**, 2149–2152.

[132] T. G. W. Edwardson, K. M. M. Carneiro, C. K. McLaughlin, C. J. Serpell, H. F. Sleiman. *Nat. Chem.*, 2013, **5**, 868–875.

[133] Z. Li, Y. Zhang, P. Fullhart, C. A. Mirkin. *Nano Lett.*, 2004, **4**, 1683–1687.

[134] Y. Vyborna, M. Vybornyi, R. Häner. *Chem. Commun.*, 2017, **53**, 5179–5181.

[135] H. Yu, M. Sabetti, R. Häner. *Chem. Asian J.*, 2018, **13**, 968–971.

[136] M. Vybornyi, A. Rudnev, R. Häner. *Chem. Mater.*, 2015, **27**, 1426–1431.

[137] C. D. Bösch, S. M. Langenegger, R. Häner. *Angew. Chem. Int. Ed.*, 2016, **55**, 9961–9964.

[138] Y. Vyborna, M. Vybornyi, A. V. Rudnev, R. Häner. *Angew. Chem. Int. Ed.*, 2015, **54**, 7934–7938.

[139] C. D. Bösch, J. Jevric, N. Bürki, M. Probst, S. M. Langenegger, R. Häner. *Bioconjug. Chem.*, 2018, **29**, 1505–1509.

[140] M. Vybornyi, A. Rudnev, S. M. Langenegger, T. Wandlowski, G. Calzaferri, R. Häner. *Angew. Chem. Int. Ed.*, 2013, **52**, 11488–11493.

[141] M. Kownacki, S. M. Langenegger, S.-X. Liu, R. Häner. *Angew. Chem. Int. Ed.*, 2019, **58**, 751–755.

[142] Y. Vyborna, S. Altunbas, M. Vybornyi, R. Häner. *Chem. Commun.*, 2017, **53**, 12128–12131.

[143] Y. Vyborna, M. Vybornyi, R. Häner. *Bioconjug. Chem.*, 2016, **27**, 2755–2761.

[144] S. E. Boiadjiev, D. A. Lightner. *Monatsh. Chem.*, 2005, **136**, 489–508.

[145] Y. L. Lyubchenko, L. S. Shlyakhtenko. *Proc. Natl. Acad. Sci. USA*, 1997, **94**, 496-501.

[146] Y. L. Lyubchenko, L. S. Shlyakhtenko, T. Ando. *Methods*, 2011, **54**, 274–283.

[147] C. Gude, W. Rettig. *J. Phys. Chem. A*, 2000, **104**, 8050–8057.

[148] H. Koga, E. Tokunaga, M. Hidaka, Y. Umemura, T. Saito, A. Isogai, T. Kitaoka. *Chem. Commun.*, 2010, **46**, 8567–8569.

References

[149] W. K. Cho, J. K. Lee, S. M. Kang, Y. S. Chi, H.-S. Lee, I. S. Choi. *Chem. Eur. J.*, 2007, **13**, 6351–6358.

[150] K. M. McMahon, R. K. Mutharasan, S. Tripathy, D. Veliceasa, M. Bobeica, D. K. Shumaker, A. J. Luthi, B. T. Helfand, H. Ardehali, C. A. Mirkin, O. Volpert, S. Thaxton. *Nano Lett.,* 2011, **11**, 1208–1214.

[151] S. N. Barnaby, A. Lee, C. A. Mirkin. *PNAS*, 2014, **111**, 9739–9744.

[152] K. Isozaki, T. Ochiai, T. Taguchi, K. Nittoh, K. Miki. *Appl. Phys. Lett.*, 2010, **97**, 221101.

[153] J. R. Dunklin, G. T. Forcherio, D. K. Roper. *Opt. Mater. Express*, 2014, **4**, 375–383.

[154] P. Zhao, N. Li, D. Astruc. *Coord. Chem. Rev.*, 2013, **257**, 638–665.

[155] L. Li, Md. Nurunnabi, Md. Nafiujjaman, Y. Lee, K. M. Huh. *J. Control. Release*, 2013, **171**, 241–250.

[156] S. J. Chadwick, D. Salah, P. M. Livesey, M. Brust, M. Volk. *J. Phys. Chem. C*, 2016, **120**, 10647–10657.

[157] A. Bucharskaya, G. Maslyakova, G. Terentyuk, A. Yakunin,Y. Avetisyan, O. Bibikova, E. Tuchina, B. Khlebtsov, N. Khlebtsov, V. Tuchin. *Int. J. Mol. Sci.*, 2016, **17**, 1295.

[158] X. Huang, P. K. Jain, I. H. El-Sayed, M. A. El-Sayed. *Lasers Med. Sci*. 2008, **23**, 217–228.

[159] S. Ahn, S. Y. Jung, S. J. Lee. *Molecules*, 2013, **18**, 5858–5890.

[160] D. Kim, S. Park, J. H. Lee, Y. Y. Jeong, S. Jon. *J. Am. Chem. Soc.*, 2007, **129**, 7661–7665.

[161] P. Ghosh, G. Han, M. De, C. K. Kim, V. M. Rotello. *Adv. Drug Deliv. Rev.*, 2008, **60** 1307–1315.

[162] S. Rana, A. Bajaj, R. Mout, V. M. Rotello. *Adv. Drug Deliv. Rev.*, 2012, **64**, 200–216.

[163] K. Saha, S. S. Agasti, C. Kim, X. Li, V. M. Rotello. *Chem. Rev.*, 2012, **112**, 2739–2779.

[164] E. Boisselier, D. Astruc. *Chem. Soc. Rev.*, 2009, **38**, 1759–1782.

[165] N. Elahi, M. Kamali, M. H. Baghersa. *Talanta*, 2018, **184**, 537–556.

[166] D. A. Handley. Colloidal Gold: Principles, Methods and Applications. 1989. Vol. 1 (Hayat, M. A., Ed.). Academic press, San Diego.

[167] J. Turkevich, P. C. Stevenson, J. Hillie. *Discuss. Faraday Soc.*, 1951, **11**, 55–75.

[168] Z. Liang, J. Zhang, L. Wang, S. Song, C. Fan, G. Li. *Int. J. Mol. Sci.*, 2007, **8**, 526–532.

[169] W. Haiss, N. T. K. Thanh, J. Aveyard, D. G. Fernig. *Anal. Chem.*, 2007, **79**, 4215–4221.

[170] J. Sharma, R. Chhabra, C. S. Andersen, K. V. Gothelf, H. Yan, Y. Liu. *J. Am. Chem. Soc.*, 2008, **130**, 7820–7821.

[171] T. Zhang, P. Chen, Y. Sun, Y. Xing, Y. Yang, Y. Dong, L. Xu, Z. Yang, D. Liu. *Chem. Commun.*, 2011, **47**, 5774–577.

[172] M. Brust, M. Walker, D. Bethell, D. J. Schiffrin, R. Whyman. *J. Chem. Soc., Chem. Commun.,* 1994, **7**, 801–802.

[173] C. A. Mirkin, R. L. Letsinger, R. C. Mucic, J. J. Storhoff. *Nature*, 1996, **382**, 607–609.

[174] S. J. Hurst, A. K. R. Lytton-Jean, C. A. Mirkin. *Anal. Chem.*, 2006, **78**, 8313–8318.

[175] A. L. Tatarets, I. A. Fedyunyaeva, E. Terpetschnig, L. D. Patsenker. *Dyes Pigm.*, 2005, **64**, 125–134.

[176] A. L. Tatarets, I. A Fedyunyayeva, T. S. Dyubko, Y. A. Povrozin, A. O. Doroshenko, E. A Terpetschnig, L. D. Patsenker. *Anal. Chim. Acta*, 2006, **570**, 214–223.

[177] K. Ilina, W. M. MacCuaig, M. Laramie, J. N. Jeouty, L. R. McNally, M. Henary. *Bioconjug. Chem.*, 2020, **31**, 194–213.

[178] D. dos Santos Pisoni, C. L. Petzhold, M. P. de Abreu, F. S. Rodembusch, L. F. Campo. *C. R. Chimie*, 2012, **15**, 454–462.

[179] I. V. Hovor, O. S. Kolosova, E. V. Sanin, O. M. Obukhova, A. L. Tatarets, E. A. Terpetschnig, L. D. Patsenker. *Dyes Pigm.*, 2019, **170**, 107567.

[180] B. Jin, X. Zhang, W. Zheng, X. Liu, J. Zhou, N. Zhang, F. Wang, D. Shangguan. *Anal. Chem.*, 2014, **86**, 7063–7070.

[181] O. Langmar, D. Saccone, A. Amat, S. Fantacci, G. Viscardi, C. Barolo, R. D. Costa, D. M. Guldi. *ChemSusChem*, 2017, **10**, 2385–2393.

[182] J. Wu, D. Yang, Q. Wang, L. Yang, H. Sasabe, T. Sano, J. Kido, Z. Lu, Y. Huang. *J. Mater. Chem. A*, 2018, **6**, 5797–5806.

[183] K. T. Mahmudov, M. N. Kopylovich, A. M. Maharramov, M. M. Kurbanova, A. V. Gurbanov, A. J. L. Pombeiro. *Coord. Chem. Rev.*, 2014, **265**, 1–37.

[184] E. Lima, O. Ferreira, V. S. D. Gomes, A. O. Santos, R. E. Boto, J. R. Fernandes, P. Almeida, S. M. Silvestre, L. V. Reis. *Dyes Pigm.*, 2019, **167**, 98–108.

[185] R. I. Zubatyuk, V. N. Baumer, A. L. Tatarets, L.D. Patsenker, O.V. Shishkin. *Acta Crystallogr.*, 2004, **E60**, 2252–2254.

[186] S. F. Völker, A. Schmiedel, M. Holzapfel, K. Renziehausen, V. Engel, C. Lambert. *J. Phys. Chem. C*, 2014, **118**, 17467–17482.

[187] J. Clayden, N. Greeves, S. Warren, P. Wothers. Organic chemistry. Oxford. University Press. 2001–2005.

[188] A. P. Gorka, R. R. Nani, M. J. Schnermann. *Org. Biomol. Chem.*, 2015, **13**, 7584–7598.

[189] H. Ihmels, D. Otto. *Top. Curr. Chem.*, 2005, **258**, 161–204.

[190] L. Yuan, W. Lin, K. Zheng, L. He, W. Huang. *Chem. Soc. Rev.*, 2013, **42**, 622–661.

[191] J. O. Escobedo, O. Rusin, S. Lim, R. M. Strongin. *Curr. Opin. Chem. Biol.*, 2010. **14**, 64–70.

[192] J. Zhang, Z. Qiao, P. Yang, J. Pan, L. Wang, H. Wang. *Chin. J. Chem.*, 2015, **33**, 35–52.

References

[193] P. Bhattarai, Z. Dai. *Adv. Healthcare Mater.*, 2017, **6**, 1700262.

[194] Y. Chen, L. Li, W. Chen, H. Chen, J. Yin. *Chin. Chem. Lett.*, 2019, **30**, 1353–1360.

[195] J. L. Bricks, Y. L. Slominskii, I. D. Panas, A. P Demchenko. *Methods Appl. Fluoresc.*, 2018, **6**, 012001.

[196] S. M. Hart, W. J. Chen, J. L. Banal, W. P. Bricker, A. Dodin, L. Markova, Y. Vyborna, A. P. Willard, R. Häner, M. Bath, G. S. Schlau-Cohen. Engineering couplings for exciton transport using synthetic DNA scaffolds. In progress.

[197] X. Li, X. Yang, J. Qi, N. C. Seeman. *J. Am. Chem. Soc.*, 1996, **118**, 6131–6140.

[198] P. Sa-Ardyen, A. V. Vologodskii, N. C. Seeman. *Biophys. J.*, 2003, **84**, 3829–3837.

Appendices

General Methods and Procedures

^{1}H-NMR, ^{13}C-NMR, and ^{31}P-NMR spectra were measured on a *Bruker Avance 300* spectrometer in DMSO or CDCl$_3$ using a signal of remaining non-deuterium solvent as an internal standard.

Mass spectrometry was performed with an *Applied Biosystems* MDS-Sciex QTRAP LC/MS/MS system and LTQ Orbitrap XL system.

Absorption spectra and extinction coefficients (ε) were recorded in 1-cm quartz cells at 20 °C (if not indicated else) on *Varian Cary-100 Bio*-UV-VIS spectrophotometer equipped with a *Varian Cary*-block temperature controller.

Emission spectra and quantum yields (Q.Y.s) were measured in 1-cm quartz cells at 20 °C on a *Varian Cary Eclipse* fluorescence spectrophotometer equipped with a *Varian Cary*-block temperature controller.

CD spectra were recorded on a *JASCO J-715* spectropolarimeter using quartz cuvettes with an optical path of 1 cm.

Atomic force microscopy (AFM) measurements were conducted on a *Nanosurf FlexAFM* using tapping mode AFM probes (Budget Sensors). Unmodified mica was purchased from PLANO GmbH. The following procedure for sample deposition was applied: 30 µL of sample were transferred onto the mica, after 3 min the solution was removed, the surface was rinsed (3 times) with 0.5 mL Milli-Q water and dried with a stream of argon gas.

Transmission electron microscopy (TEM) was performed on *ANA FEI Tecnai Spirit* Transmission electron microscope provided by Microscopy Imaging Center (MIC), University of Bern, Switzerland. Samples were deposited on the carbon-coated copper grids that were purchased from Agar Scientific. The procedure of deposition: 5 µL of sample were transferred onto the grid, after 5 min the solution was removed, the grid was rinsed (3 times) with 5 µL Milli-Q water, 5 µL of aqueous uranyl acetate were added to the sample and after 5 min the solution was removed.

Reversed-phase HPLC purification and analysis of the oligophosphodiesters were carried out on a *LC-20AT / SPD-M20A* system (Shimadzu, Kyoto, Japan).

Reagents and solvents for the synthesis of the squaraine phosphoramidites were purchased from commercial suppliers: Acros Organics, Fluka, and Sigma Aldrich.

The preparation of the phosphate buffer (PB) (0.1 M, pH = 7.0): 60 mL $Na_2HPO_4 \cdot 2H_2O$ (17.8 g/L) and 40 mL KH_2PO_4 (13.61 g/L) were mixed.

Concentrations of the oligonucleotides were determined based on the molar absorptivities. For the calculation of the molar absorptivities, values $\varepsilon_{260}(Sq) = 11\ 000\ M^{-1}\ cm^{-1}$, $\varepsilon_{260}(A) = 15\ 060\ M^{-1}\ cm^{-1}$, $\varepsilon_{260}(T) = 8\ 560\ M^{-1}\ cm^{-1}$, $\varepsilon_{260}(G) = 12\ 180\ M^{-1}\ cm^{-1}$, and $\varepsilon_{260}(C) = 7\ 100\ M^{-1}\ cm^{-1}$ were applied.

To measure the molar absorptivity of squaraine, the diol (~ 10 mg) was dissolved in 50 mL of absolute ethanol. The stock solution was diluted (1 to 100), and the absorbance was measured in a 1-cm standard quartz cell. The extinction coefficients were calculated according to the Beer-Lambert law. The ε of the dye was independently measured three times, and the average value was taken.

For the determination of the quantum yields, the integrated relative intensities of the samples were measured against Sulfo-Cyanine5 carboxylic acid or Sulfo-Cyanine3 carboxylic acid (*Lumiprobe*) (quantum yield, Cy5 = 28% and Cy3 = 10% in water) as the reference. The emission spectra of the solutions were recorded, and the quantum yields of the samples were determined according to the formula:

Q.Y. = Q.Y.ref · (F/Fref) · (Aref/A) · (n²/n²ref),

where *F* and *Fref* are the integrated areas of the fluorescence spectra, *A* and *Aref* are the absorbance at the excitation wavelength, and *n* and *n ref* are the refraction indices of solvents used for the sample under examination and the reference, respectively.

NMR- and Mass-Spectra of the Compounds 6–12 and 16–21

Compound **6**:
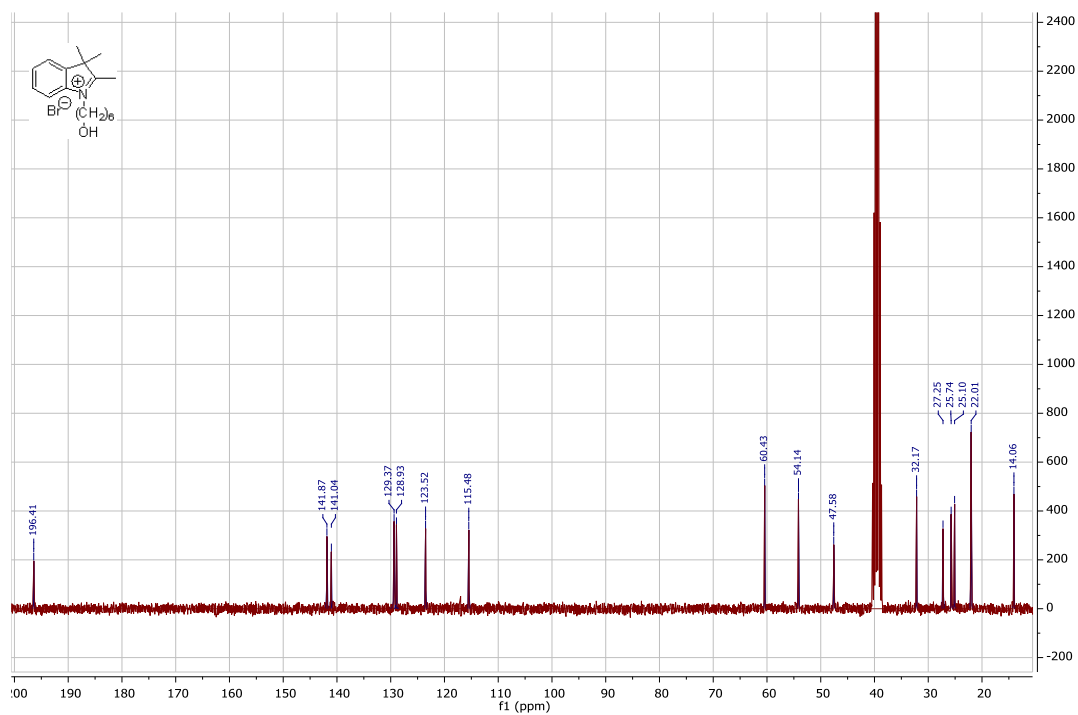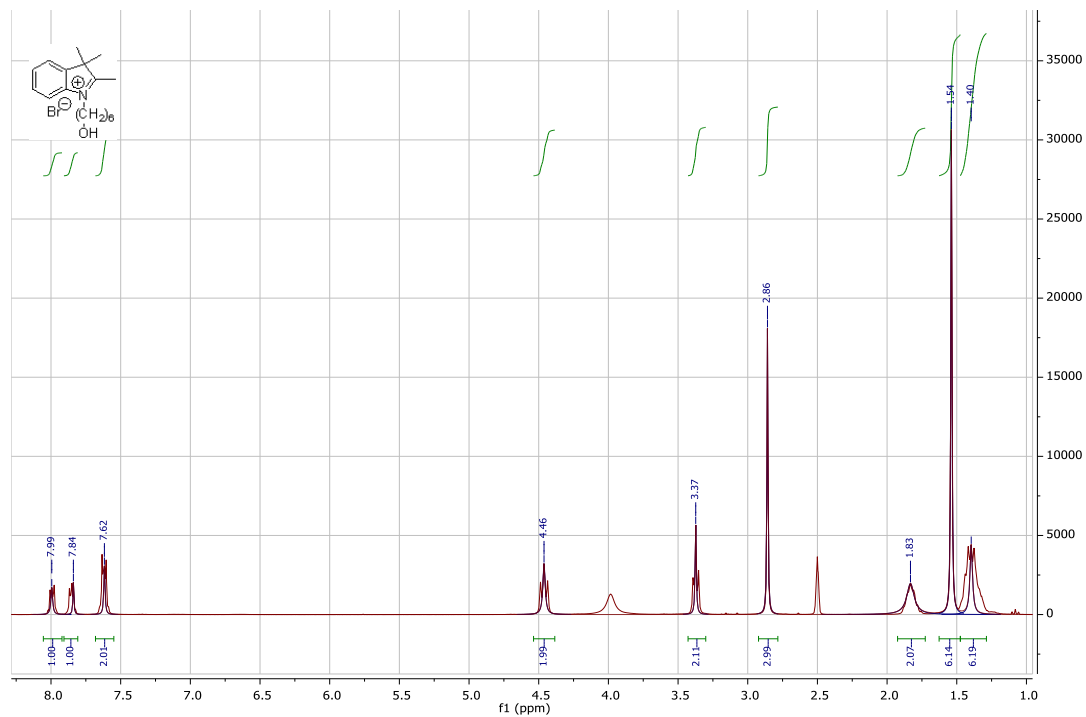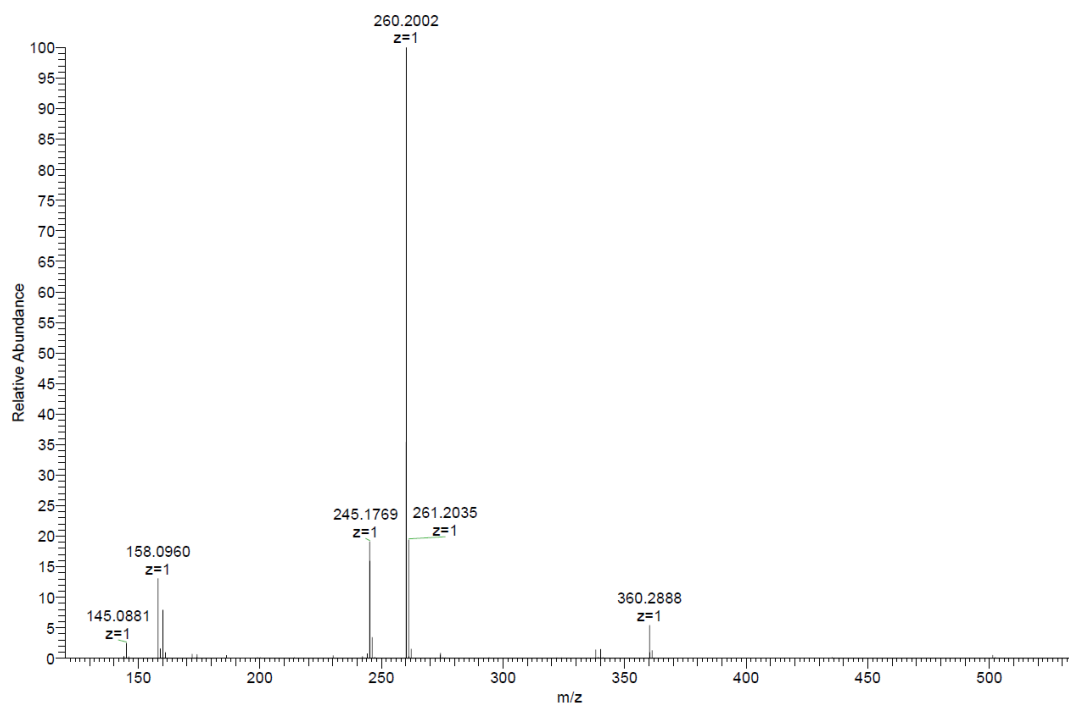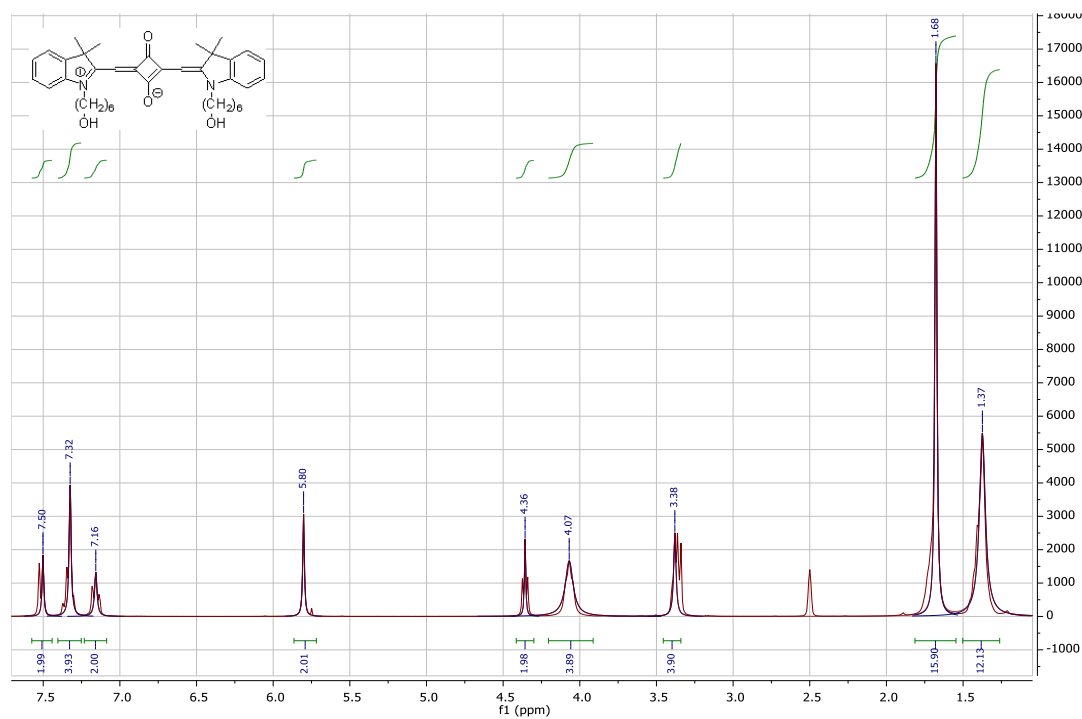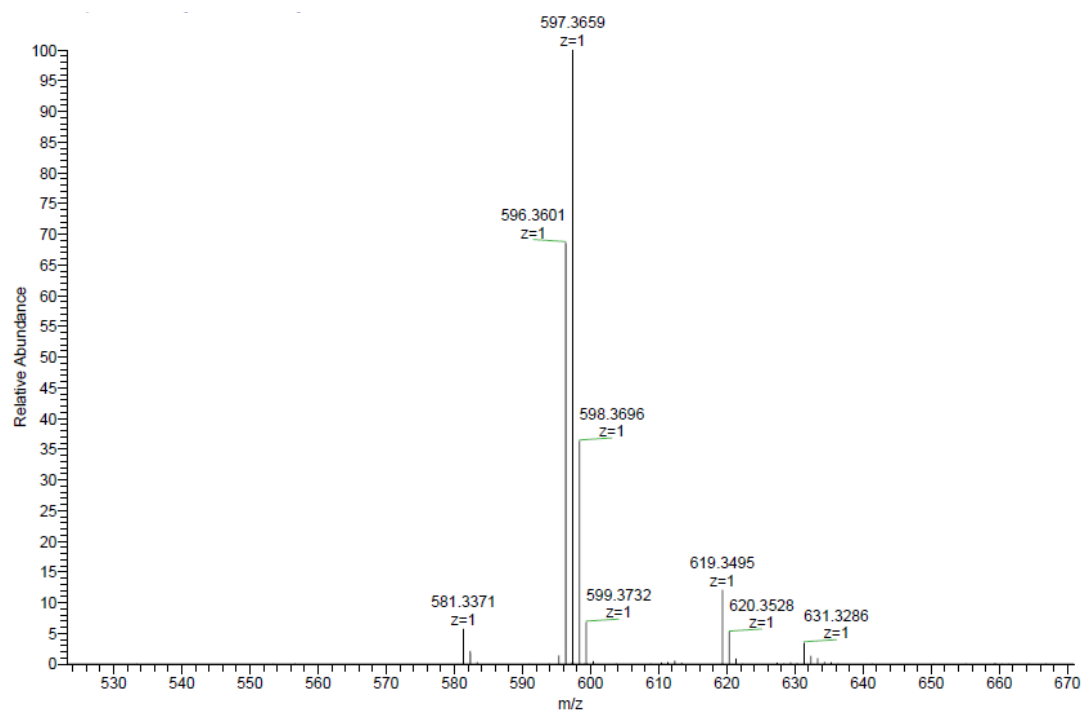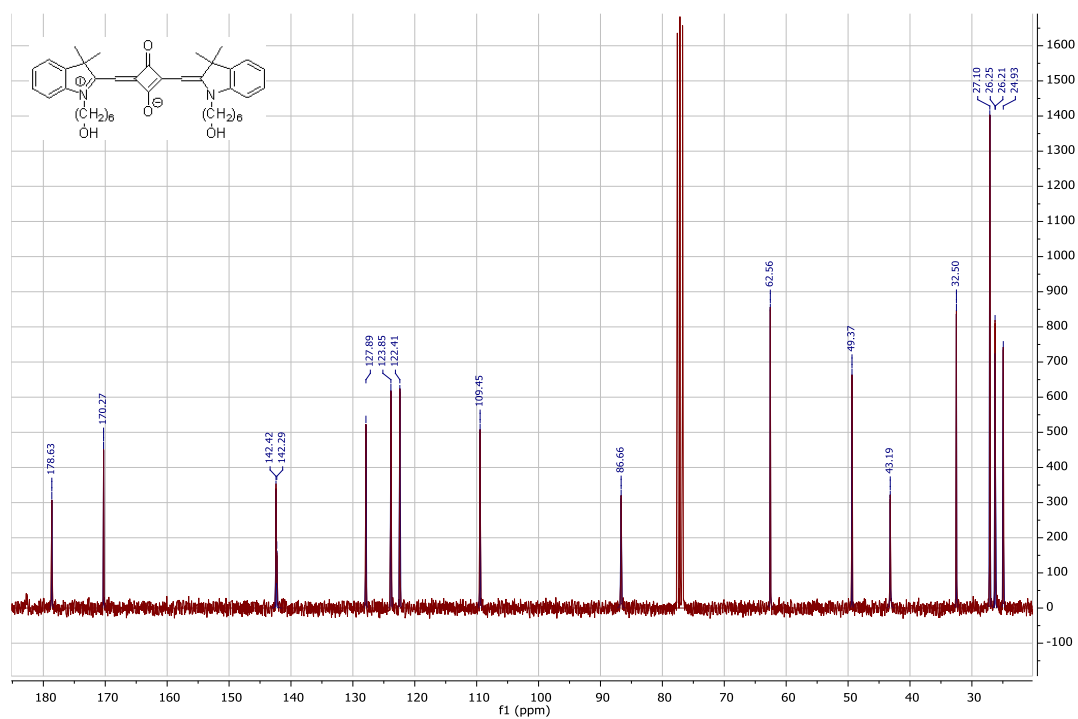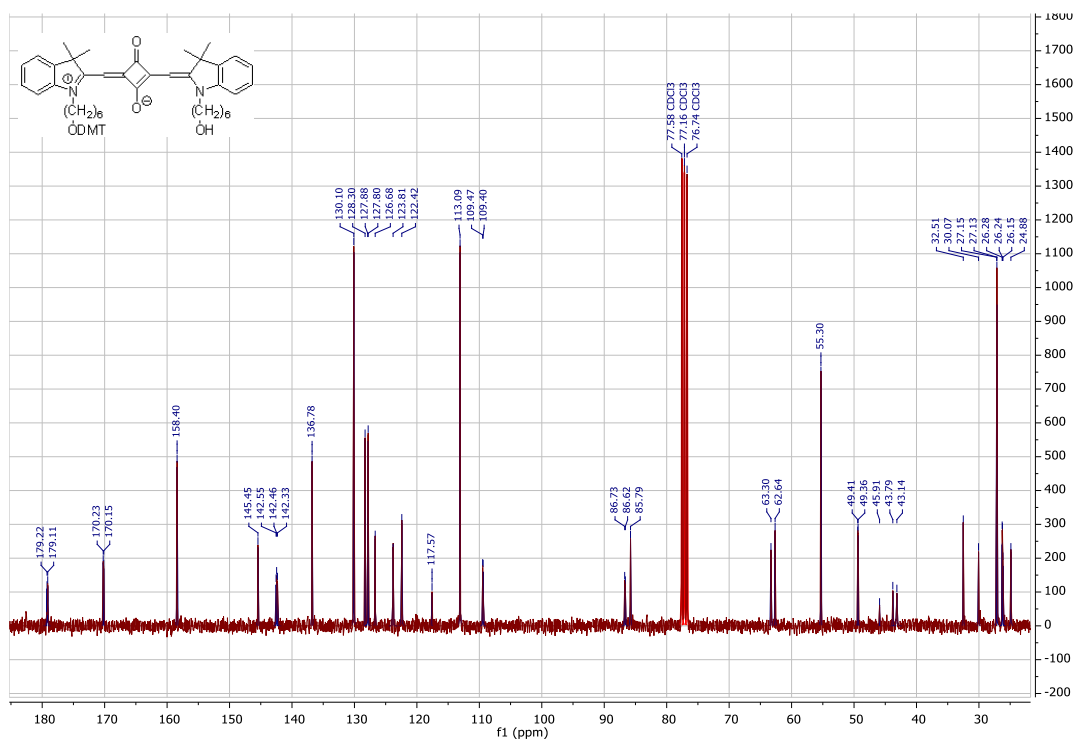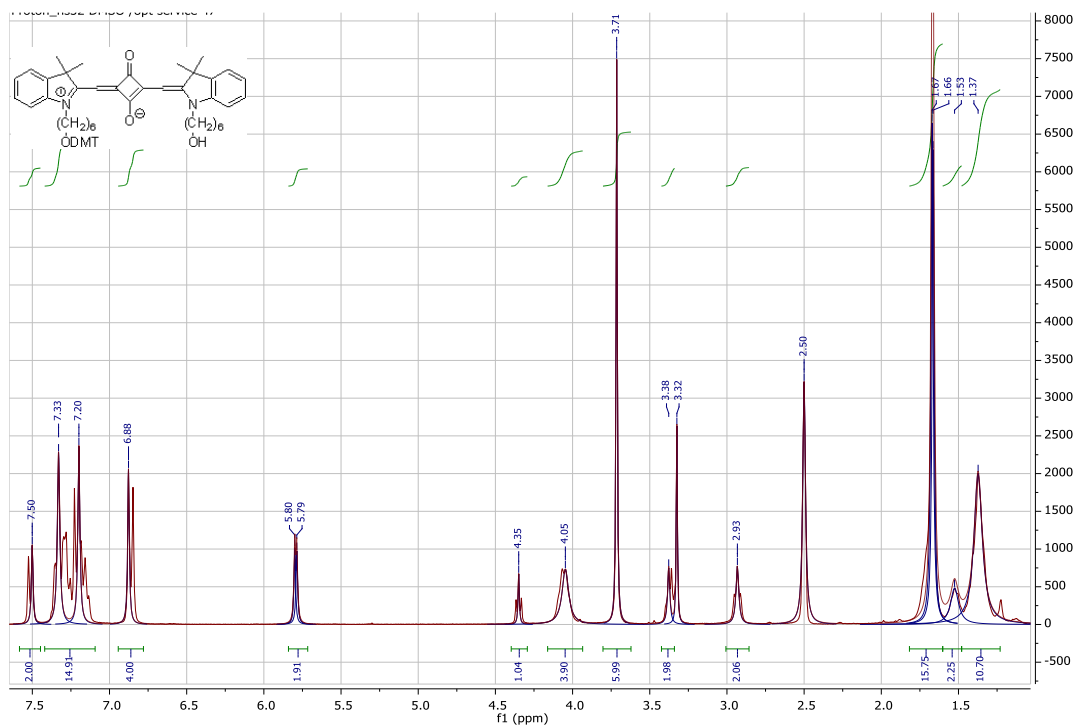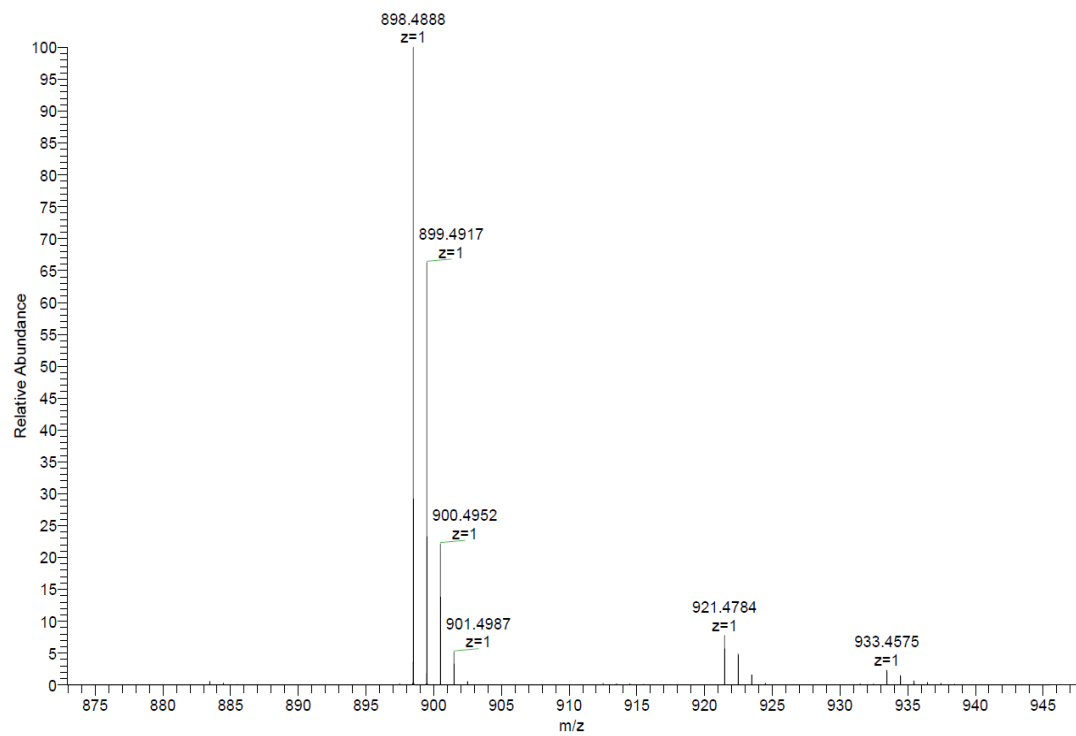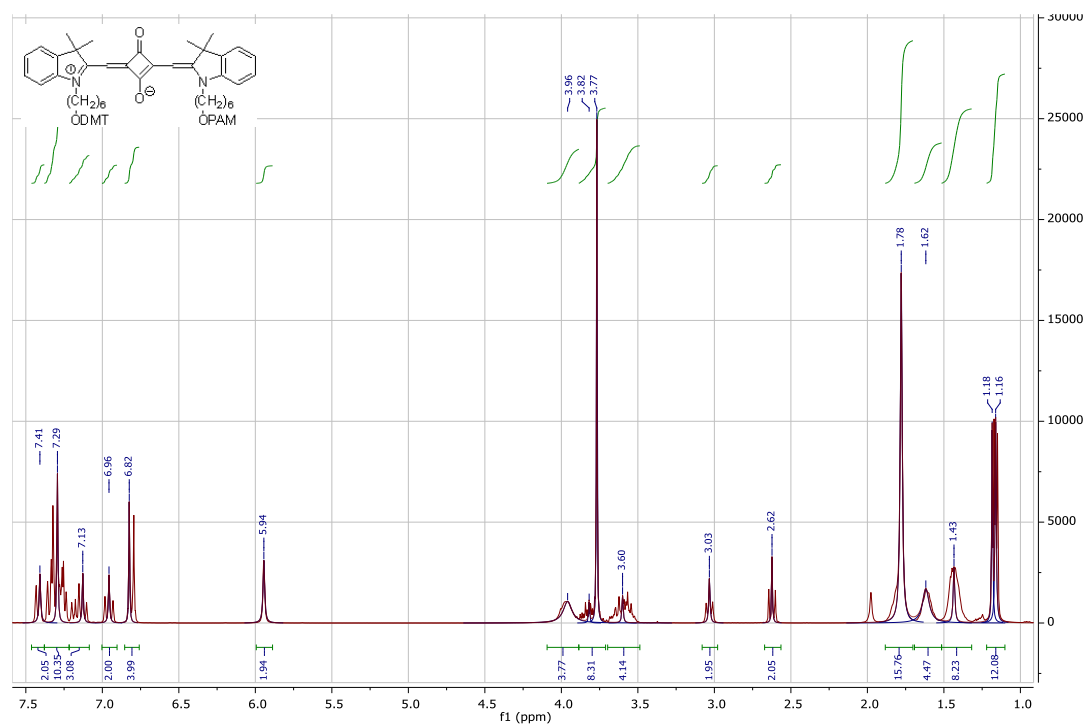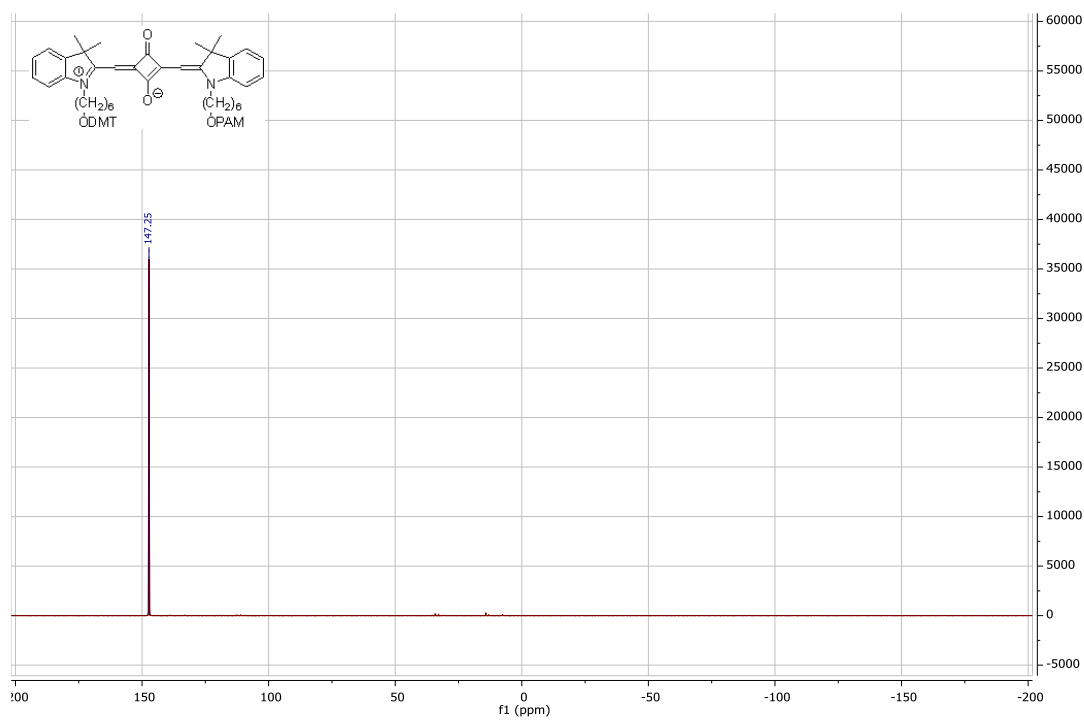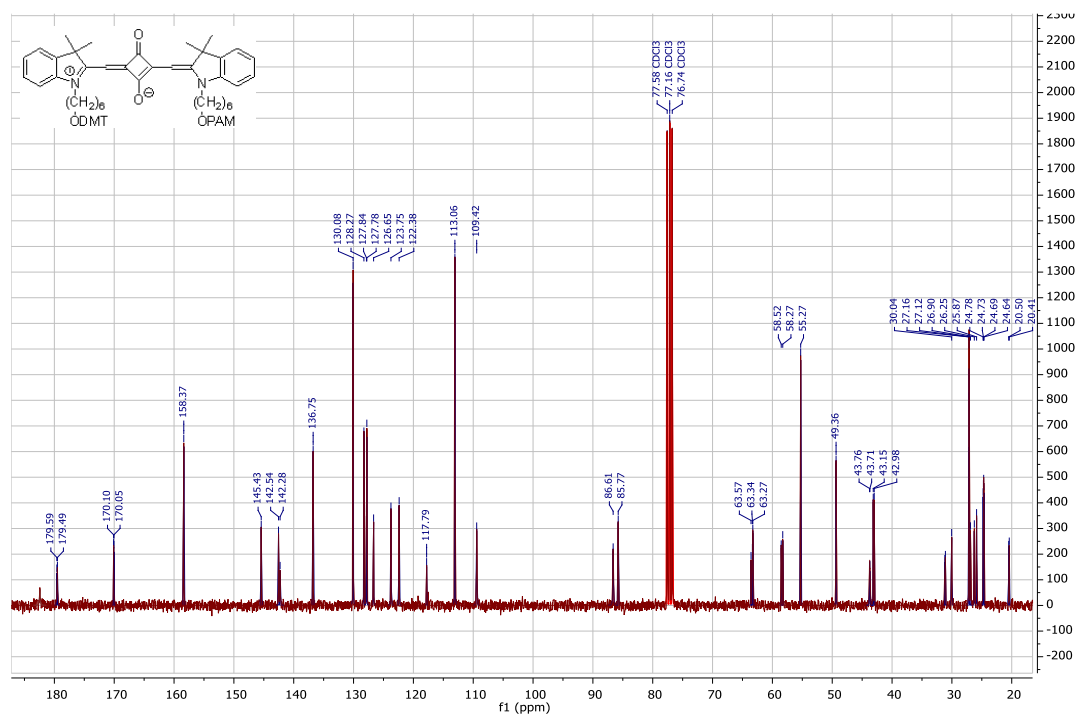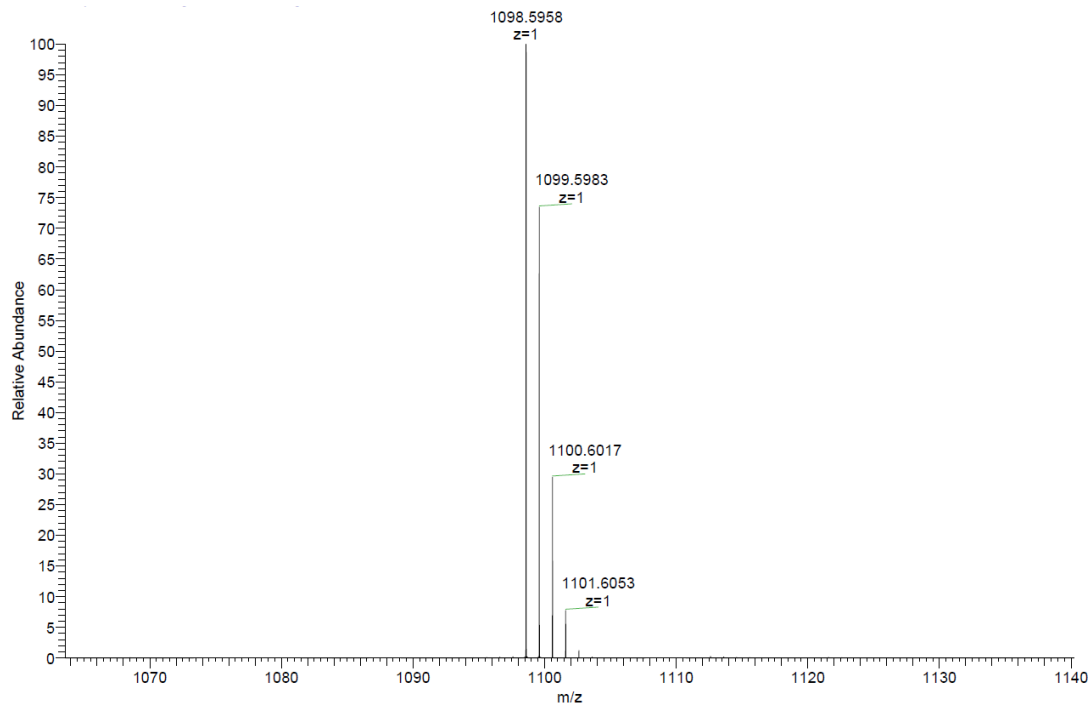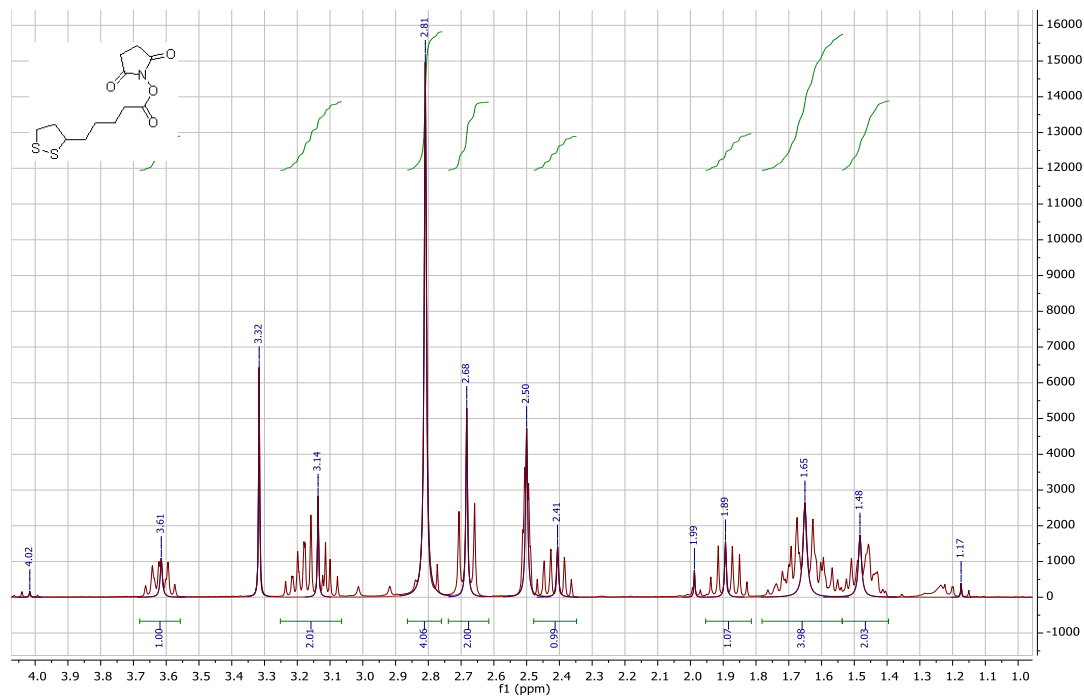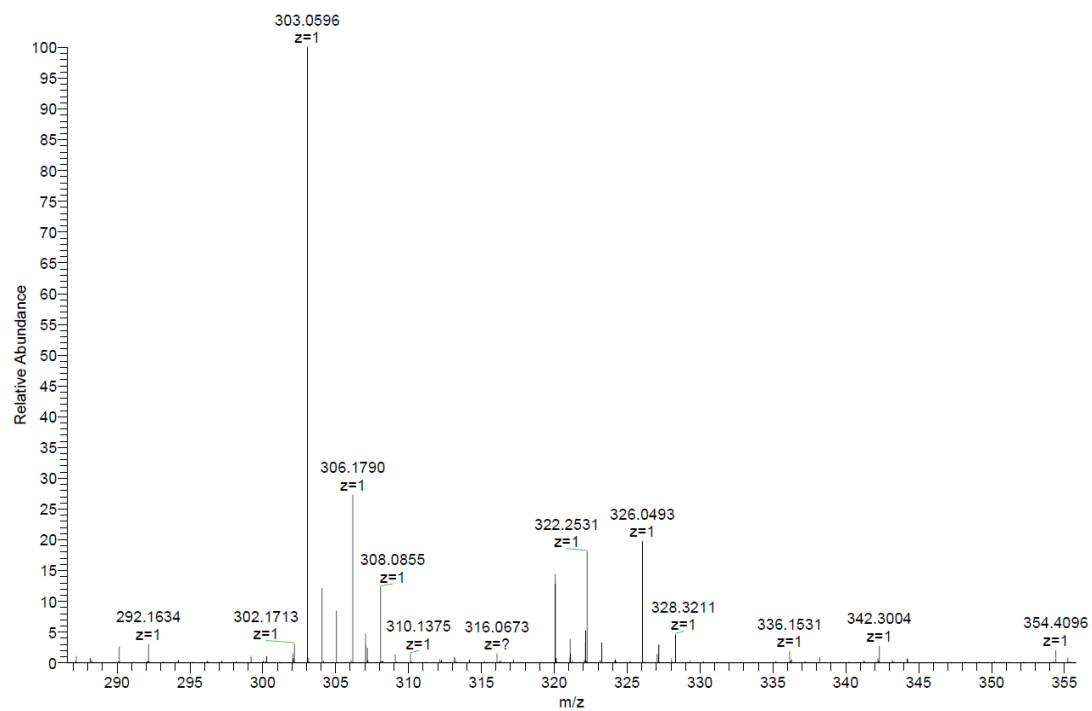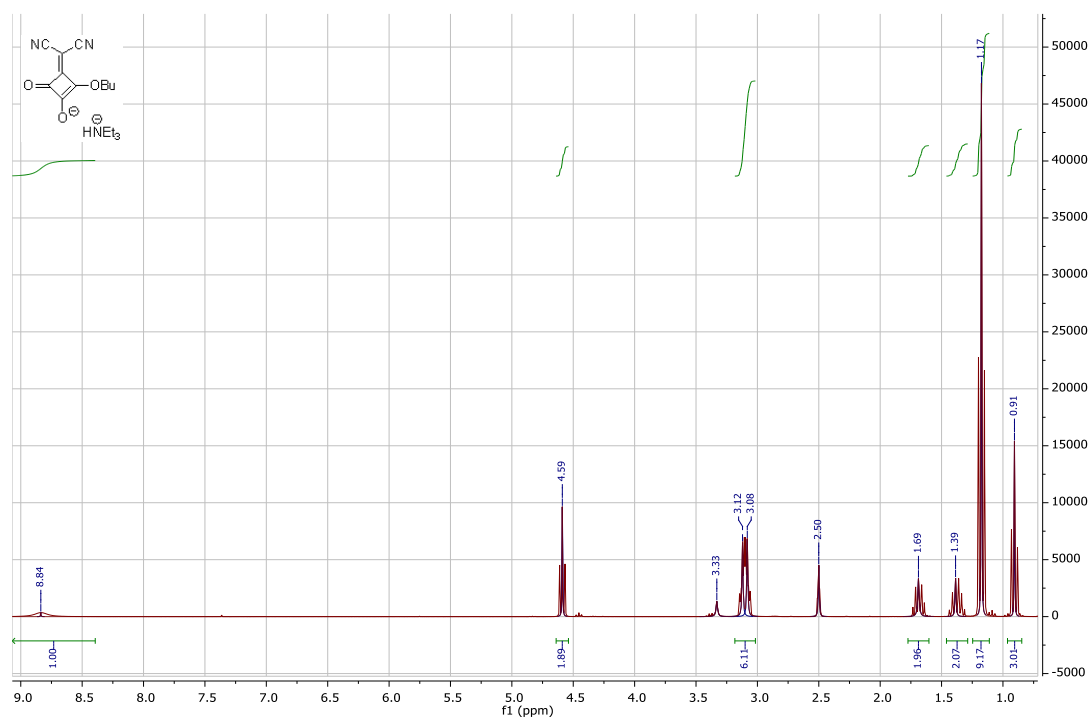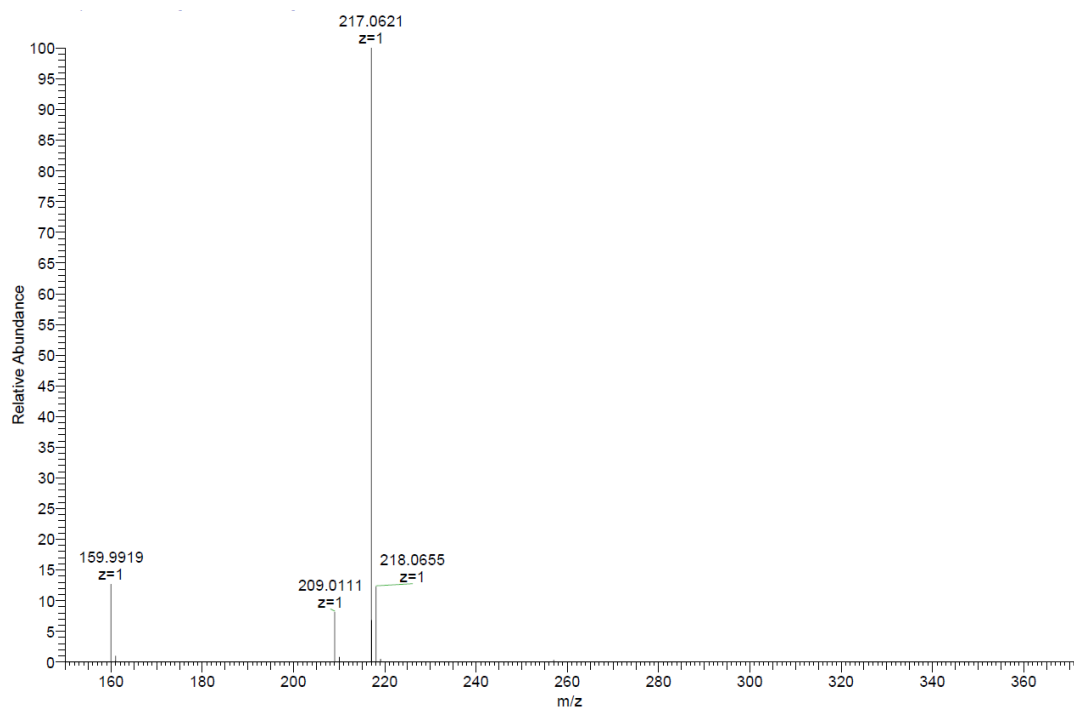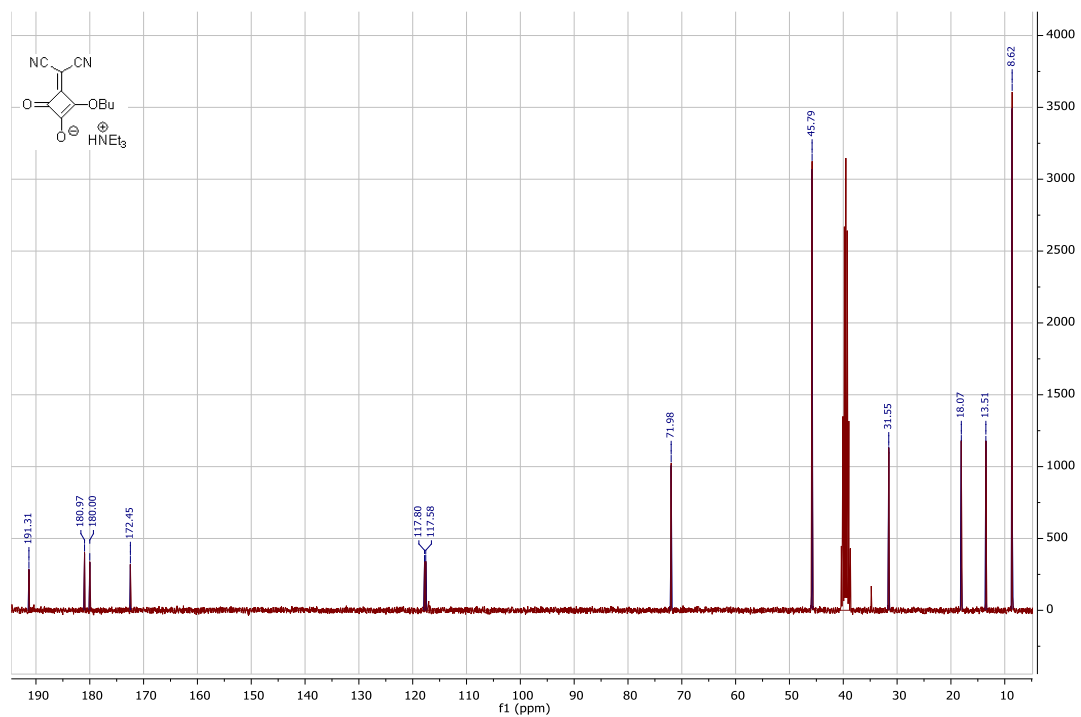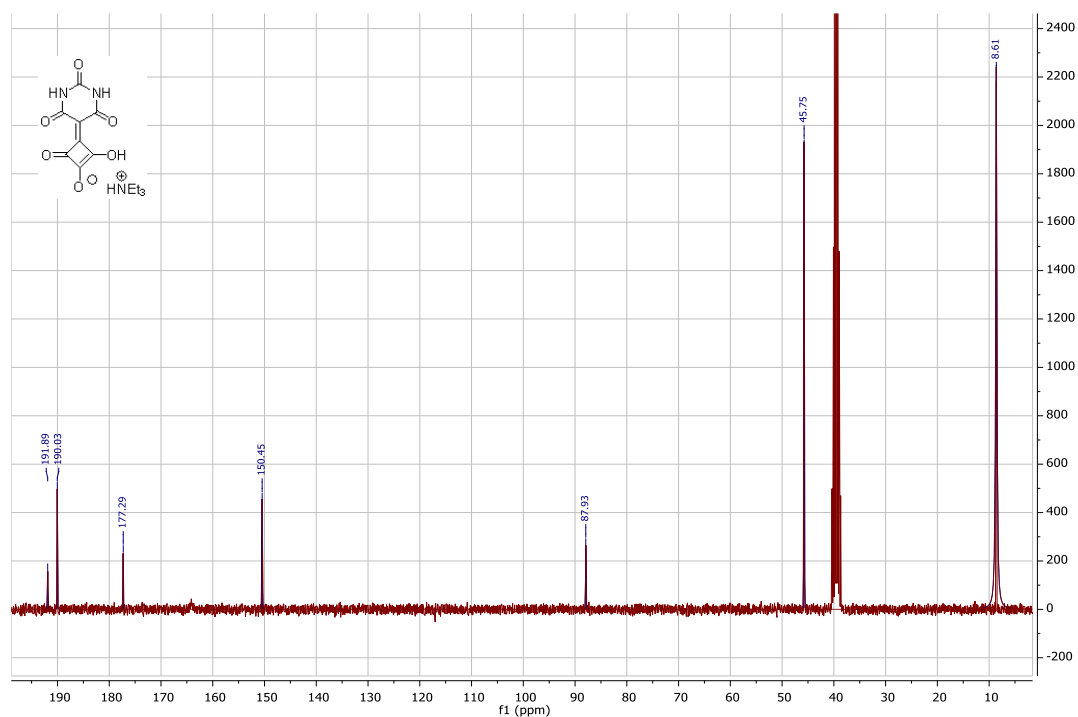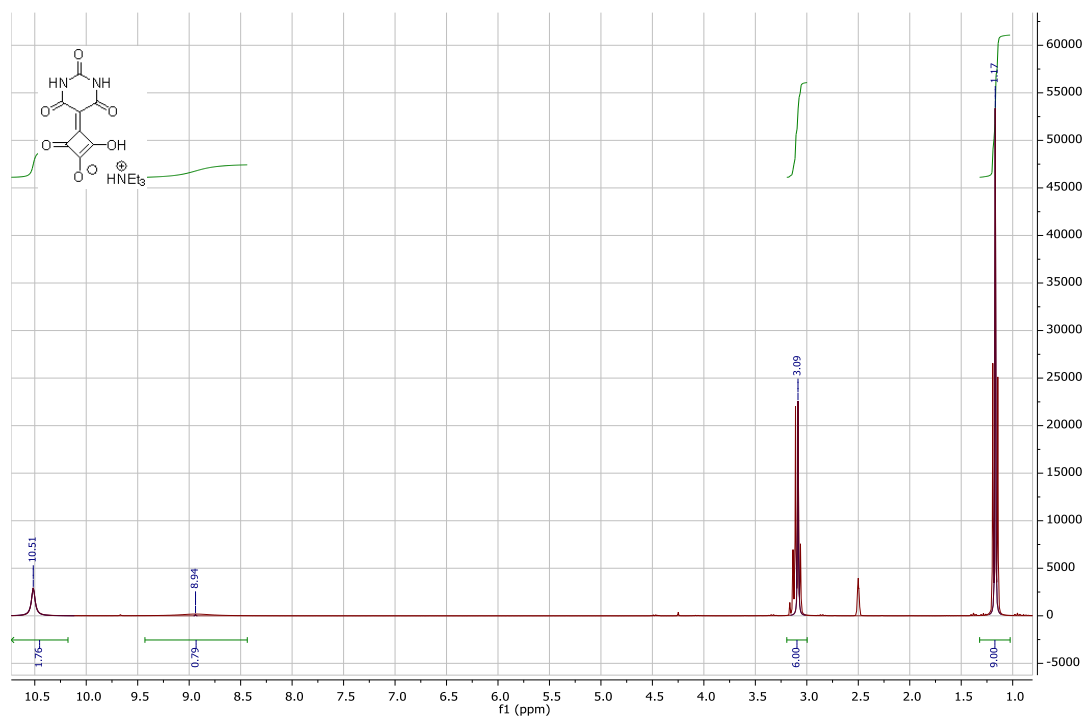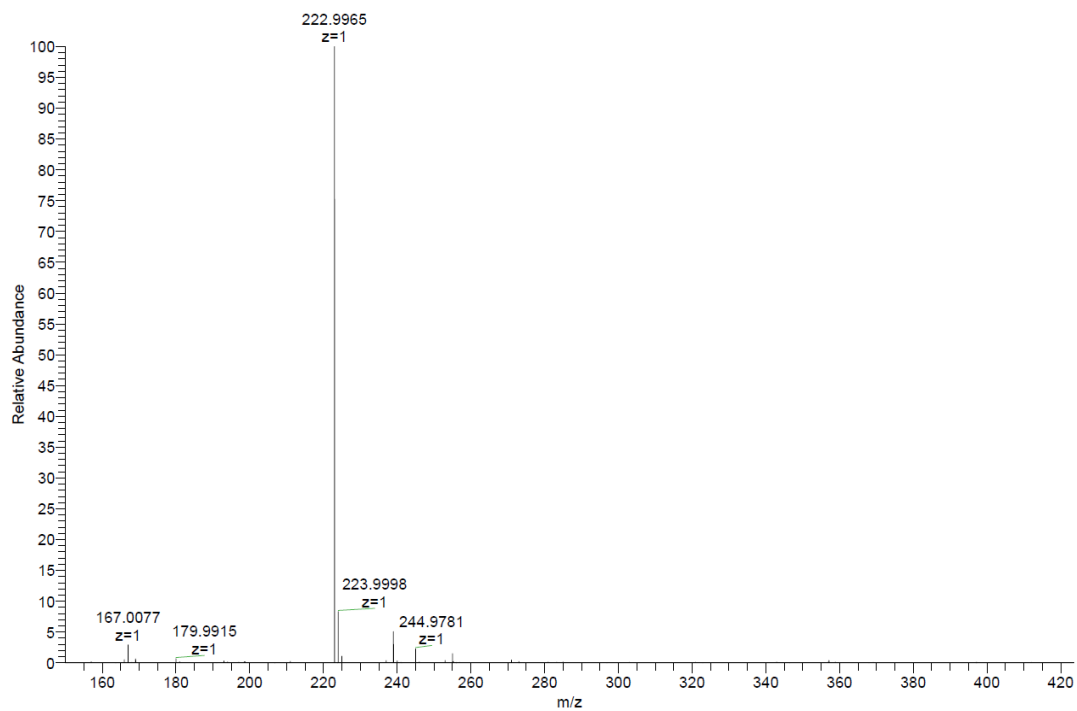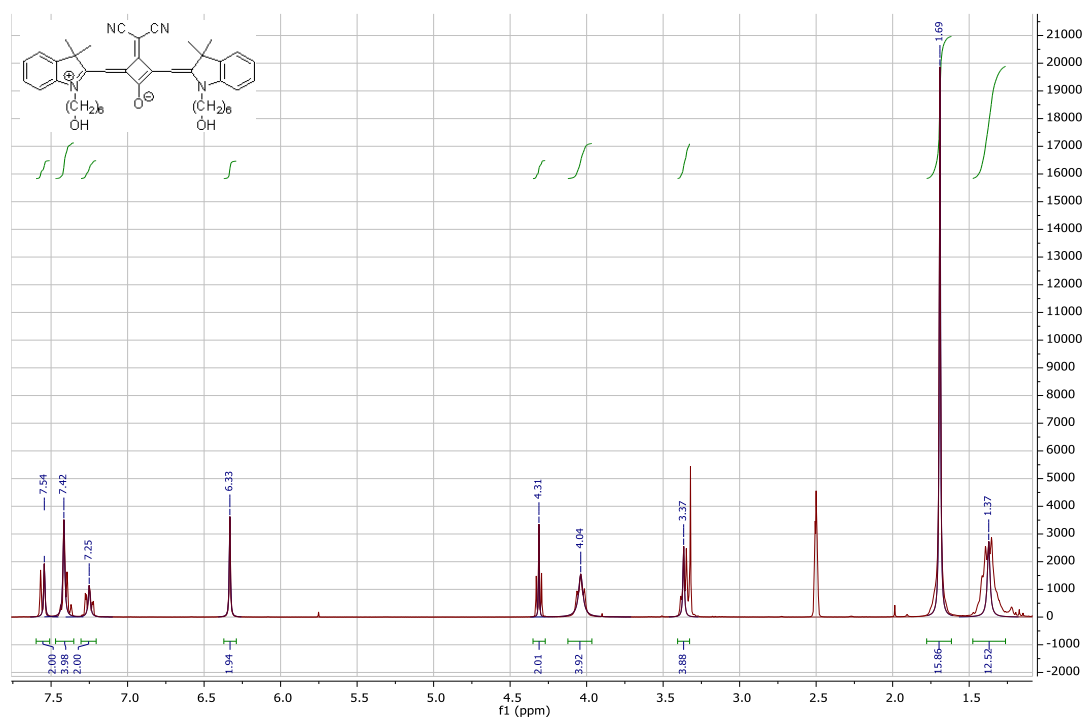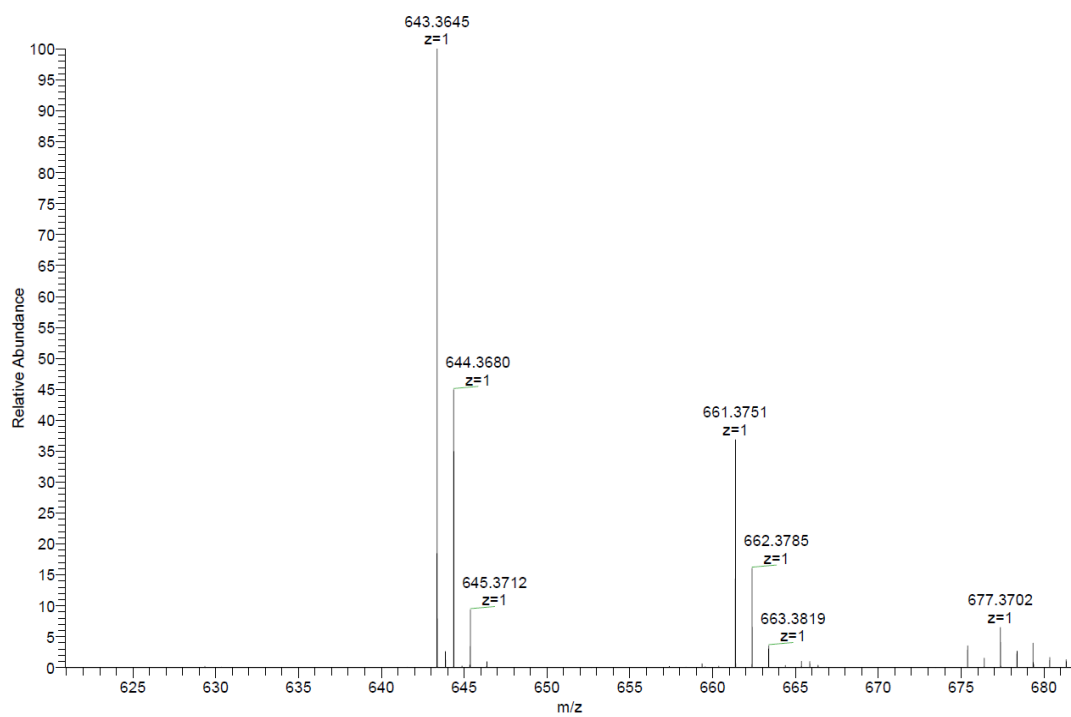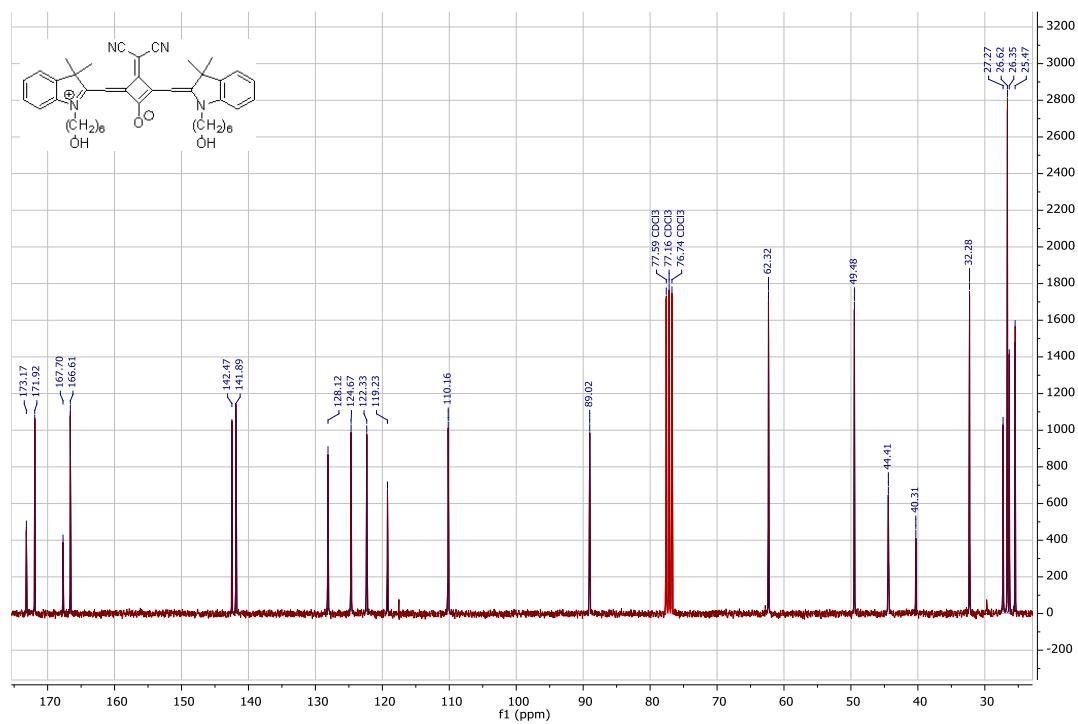
Compound **7**:
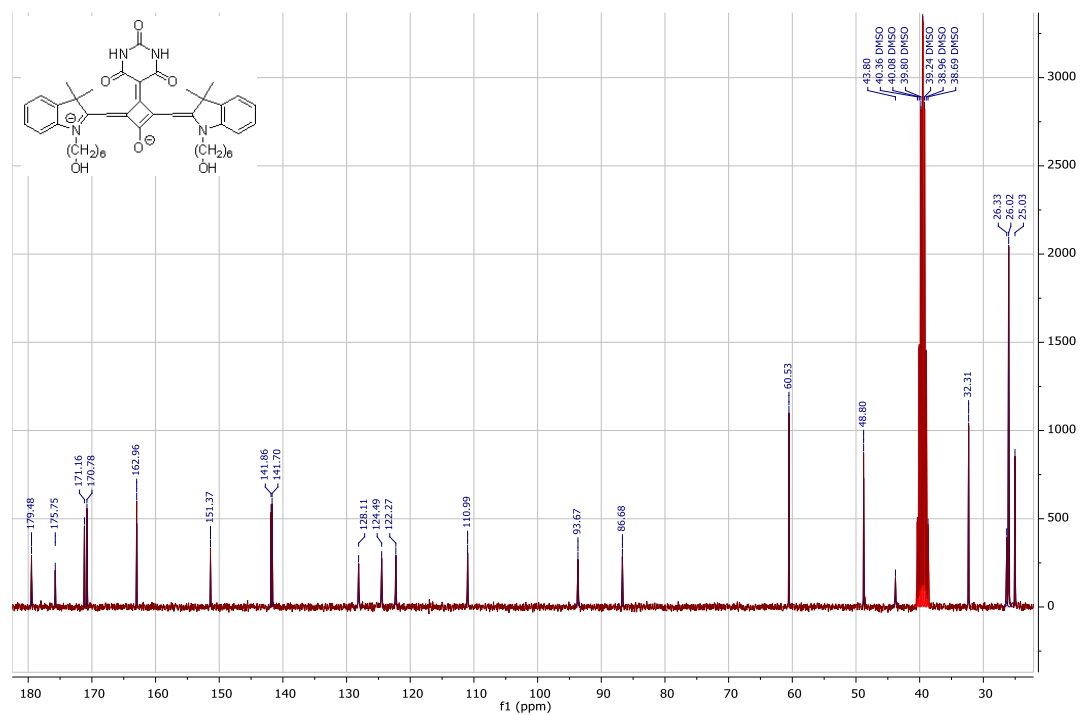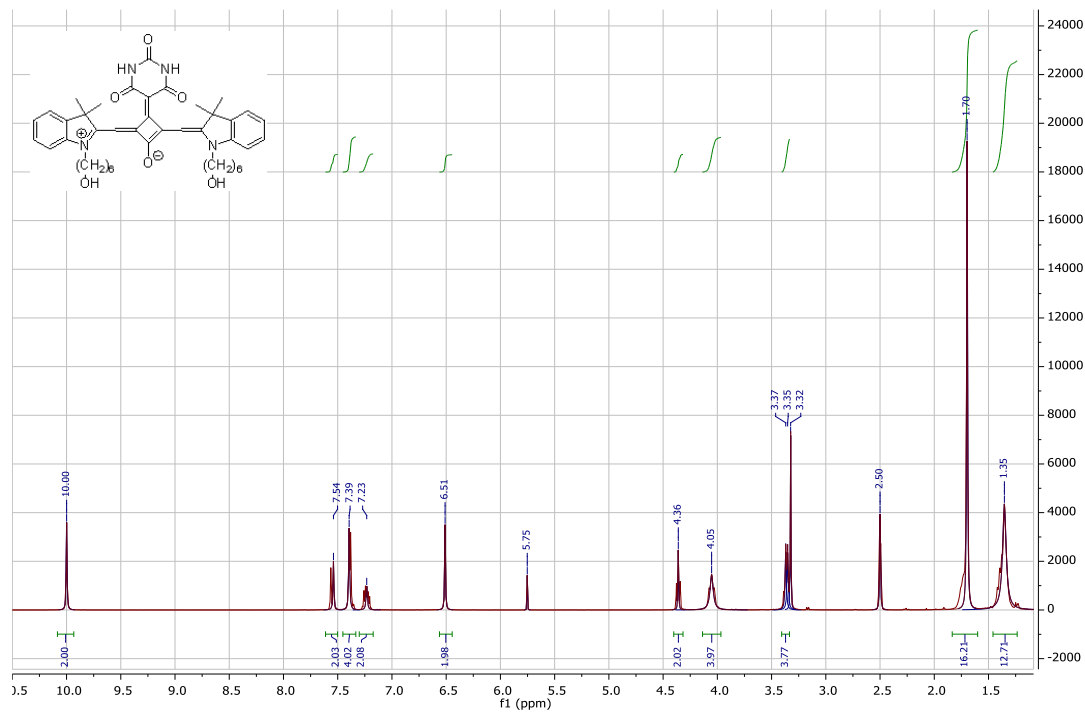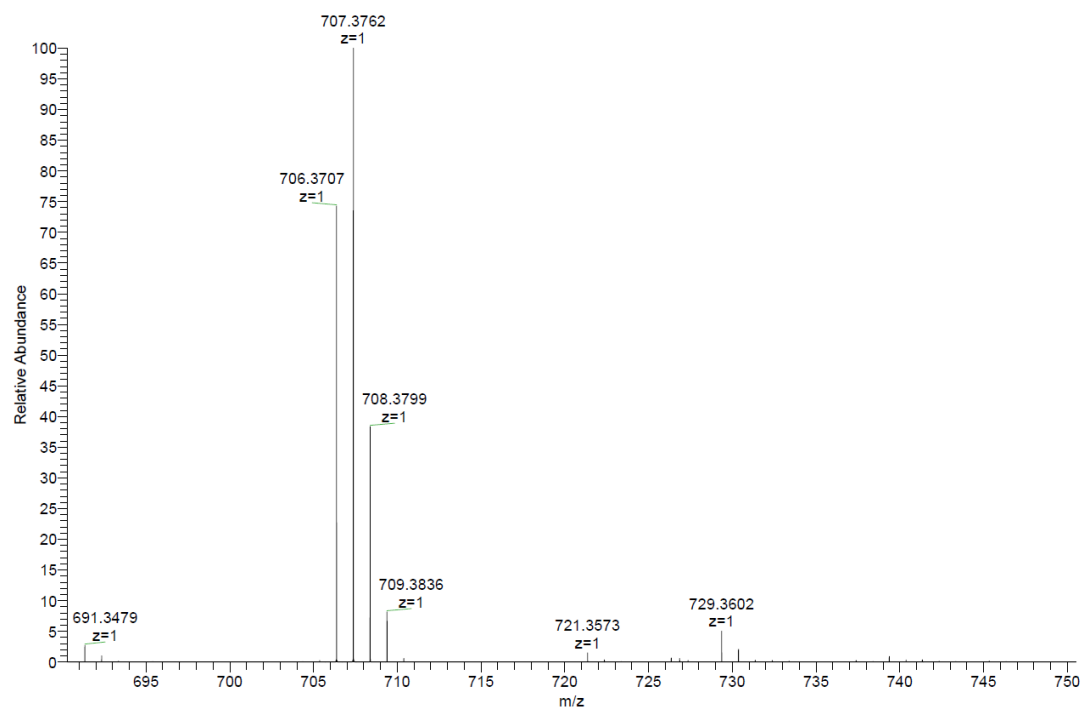
Compound **8**:
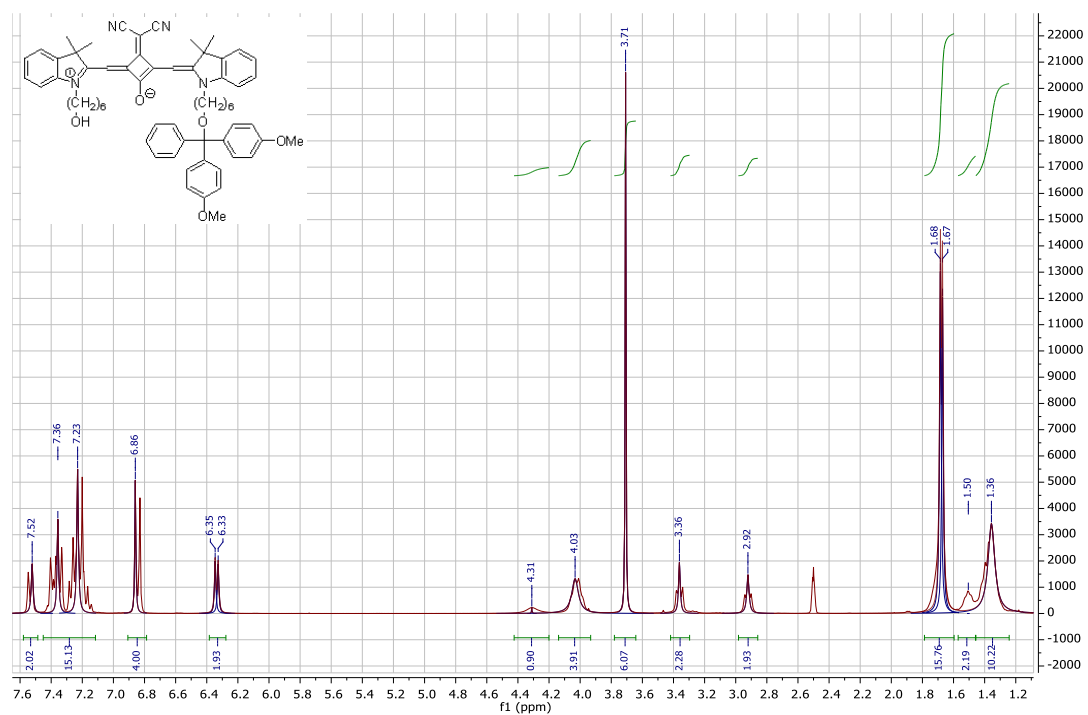
Compound **9**:
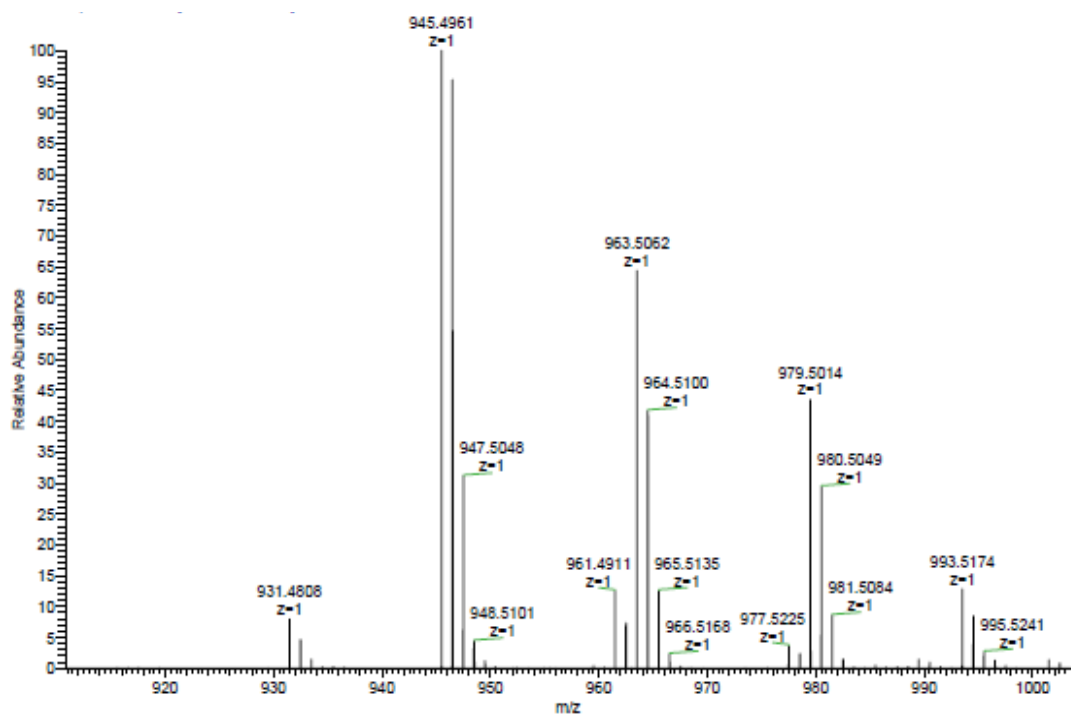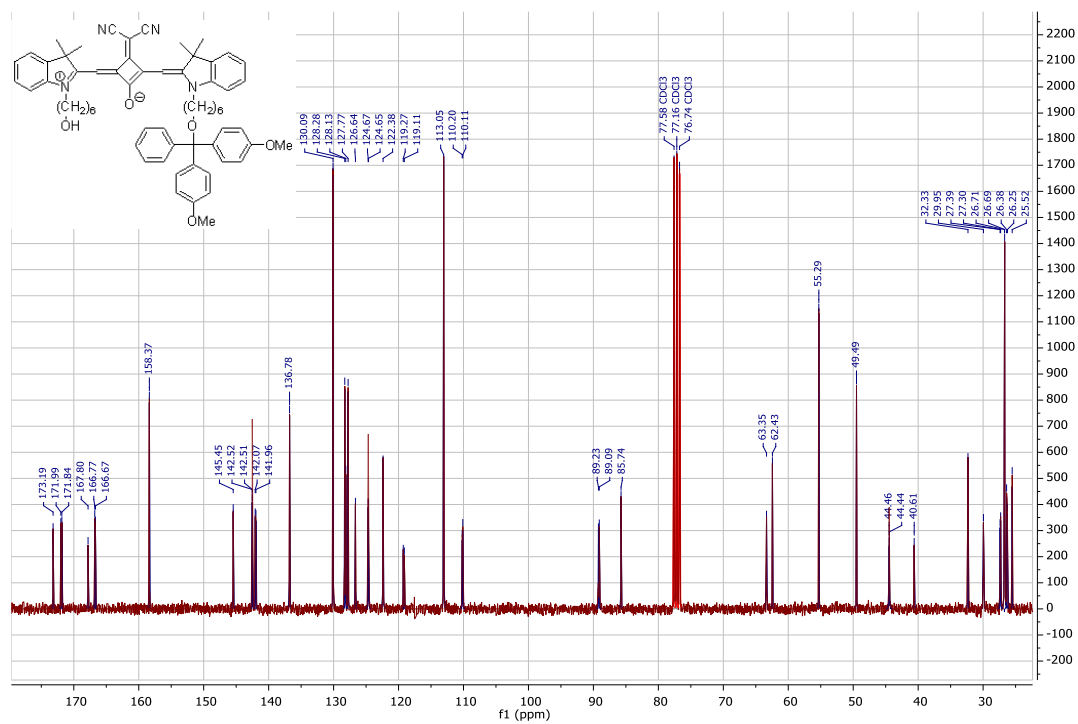
Compound **10**:
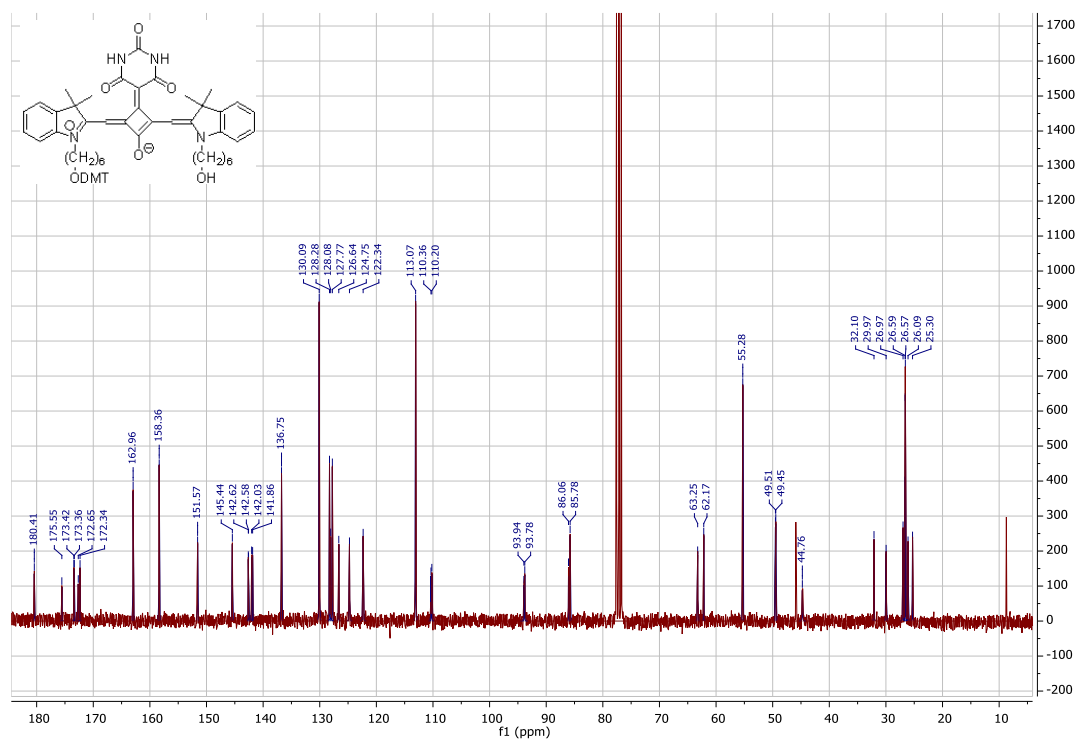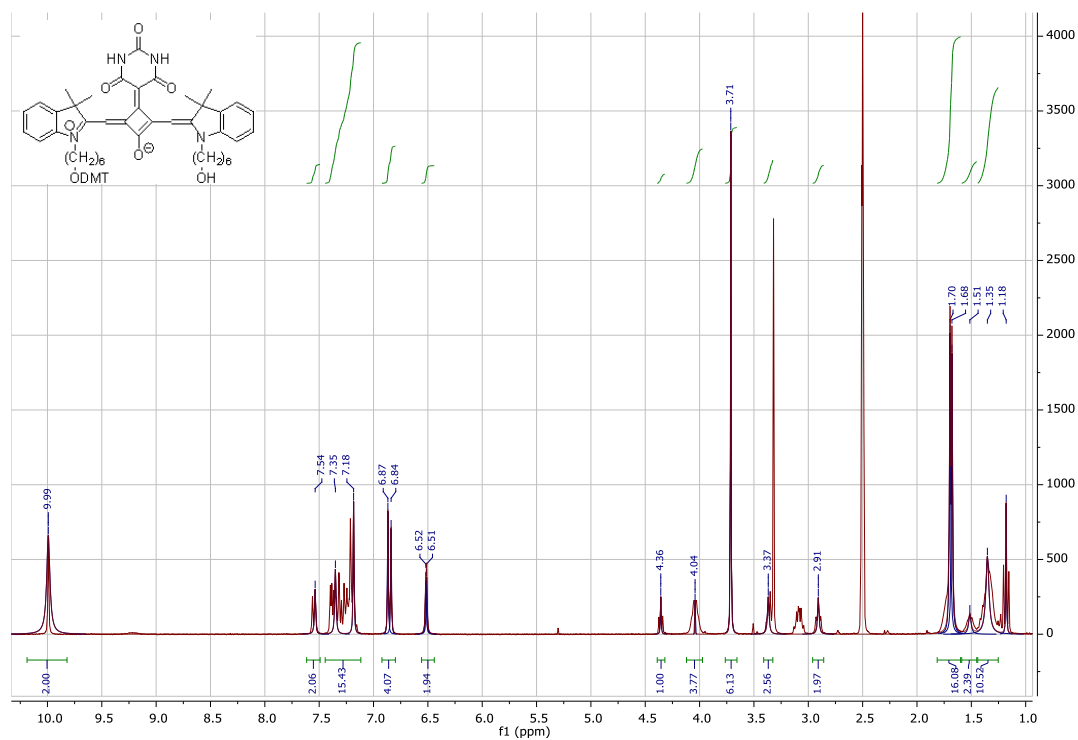
Compound **11**:
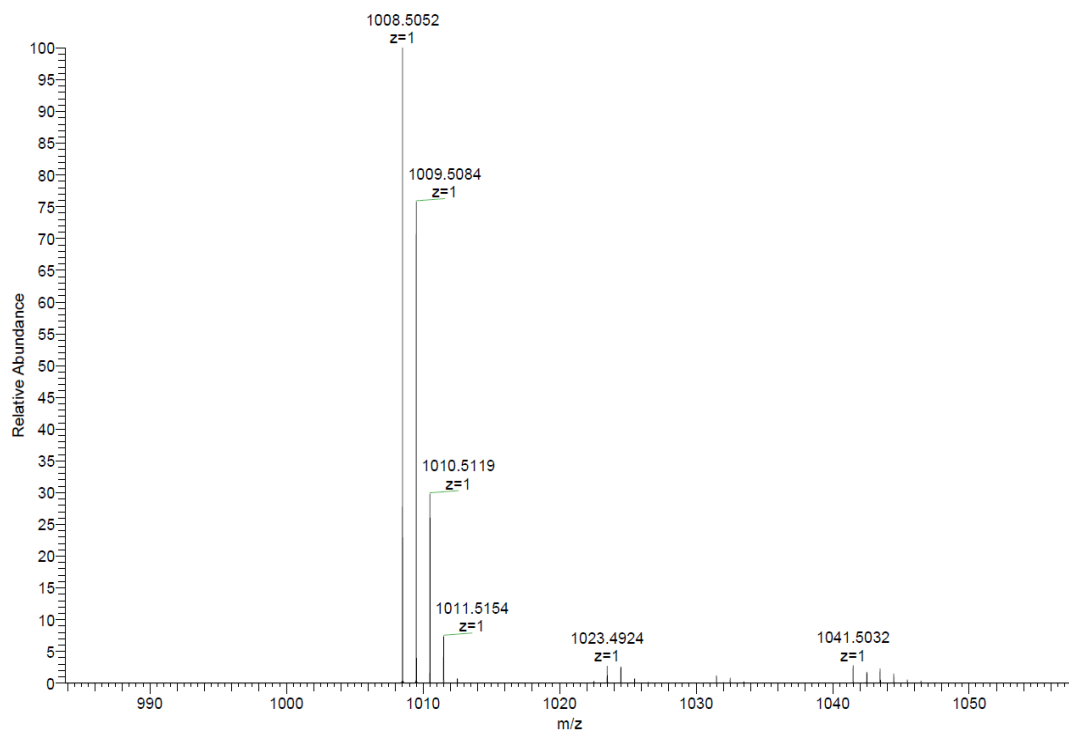
Compound **12**:
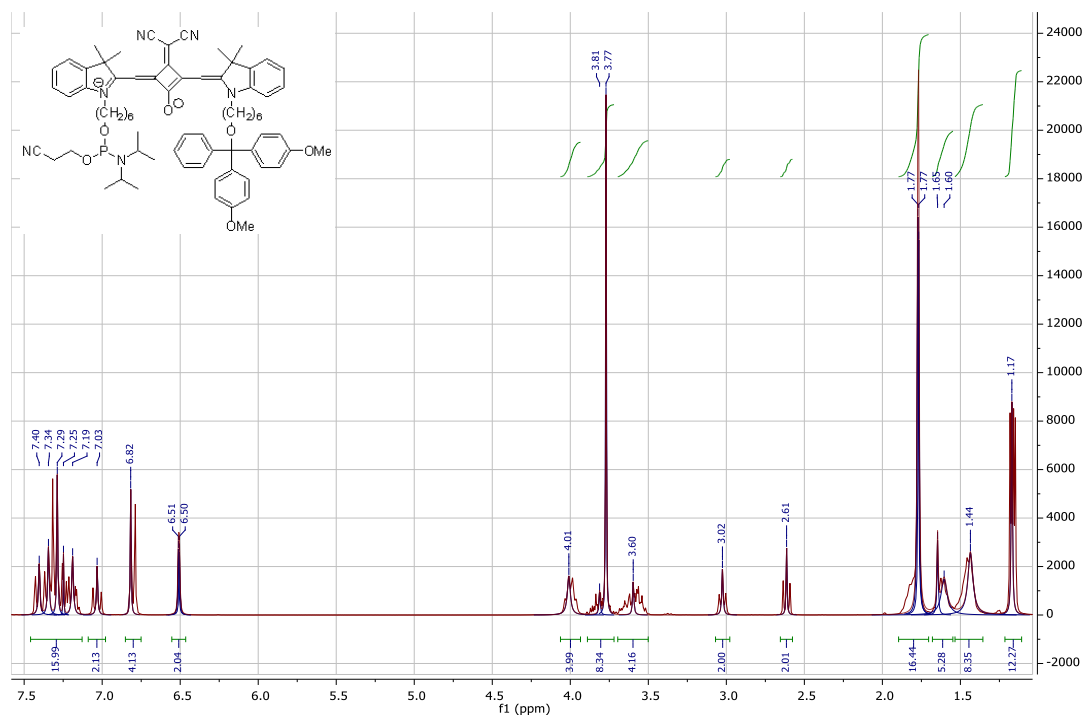
Compound **16**:
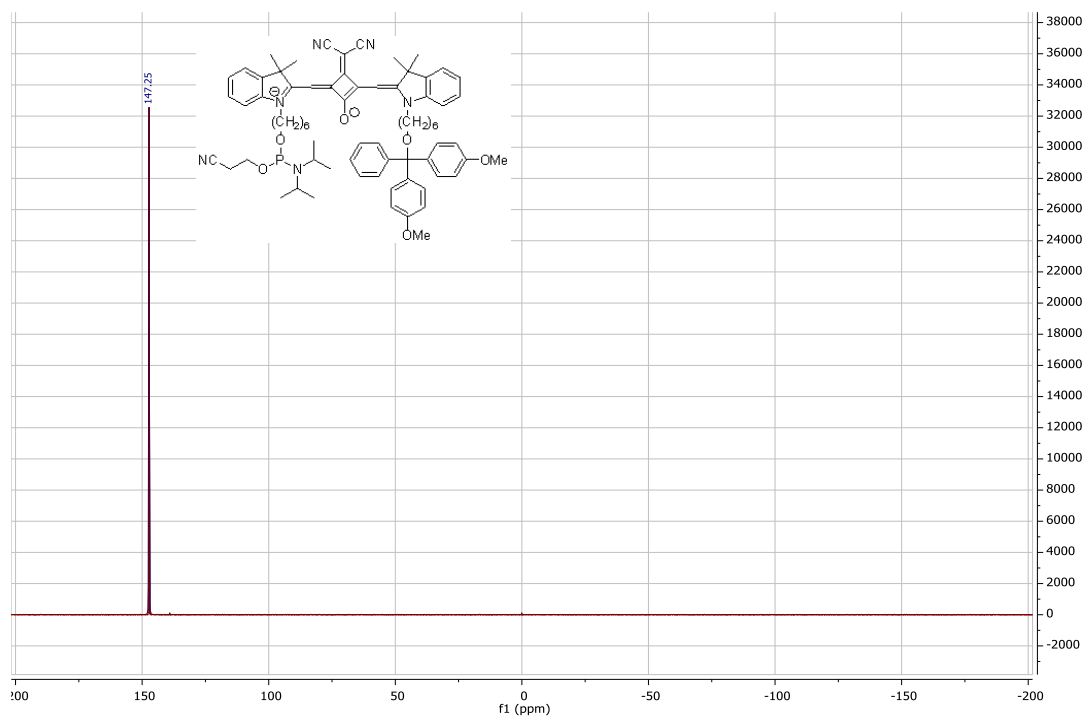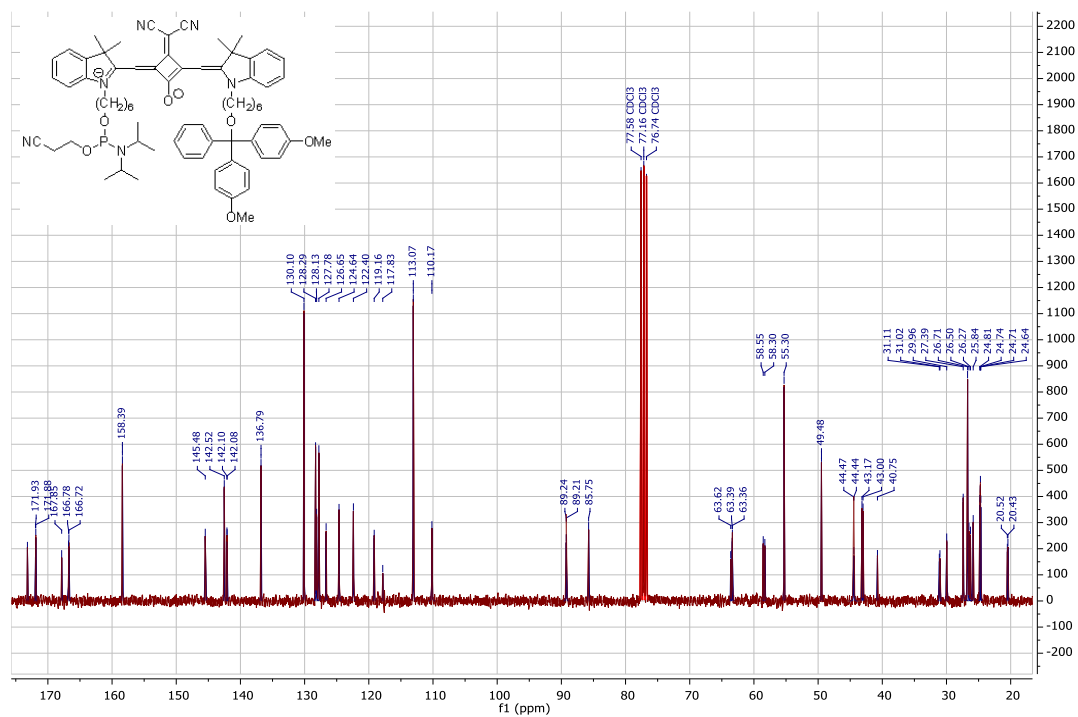
Compound **17**:
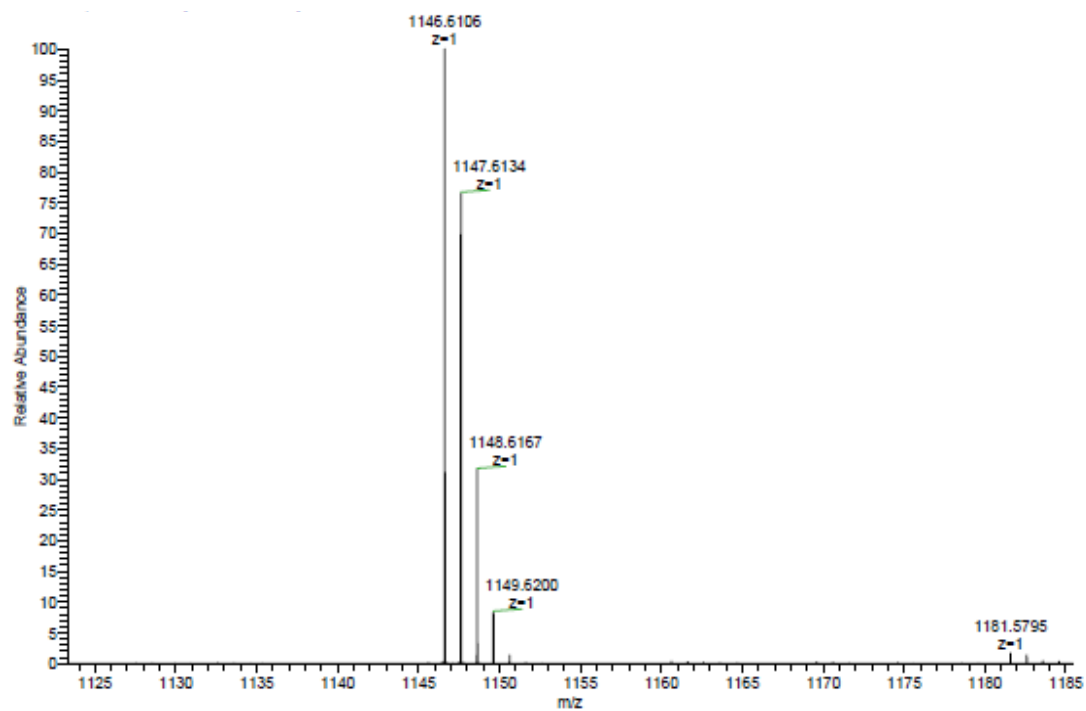
Compound **18**:

Compound **19**:

Compound **20**:

Compound **21**:
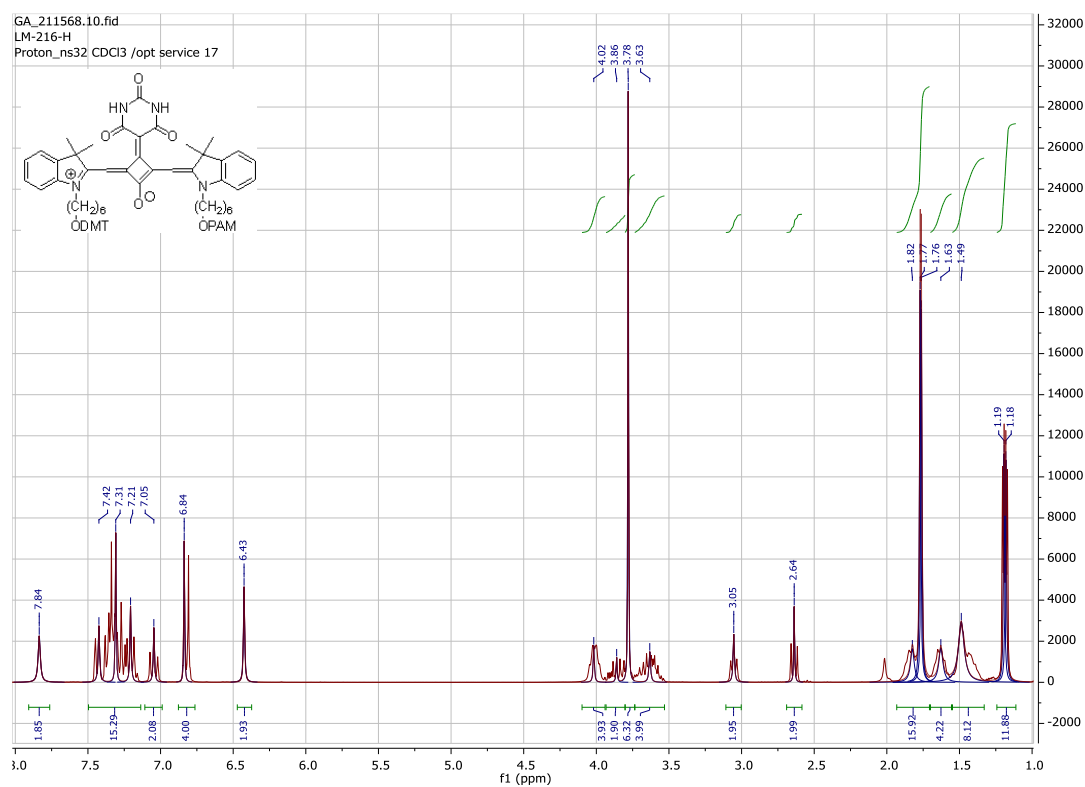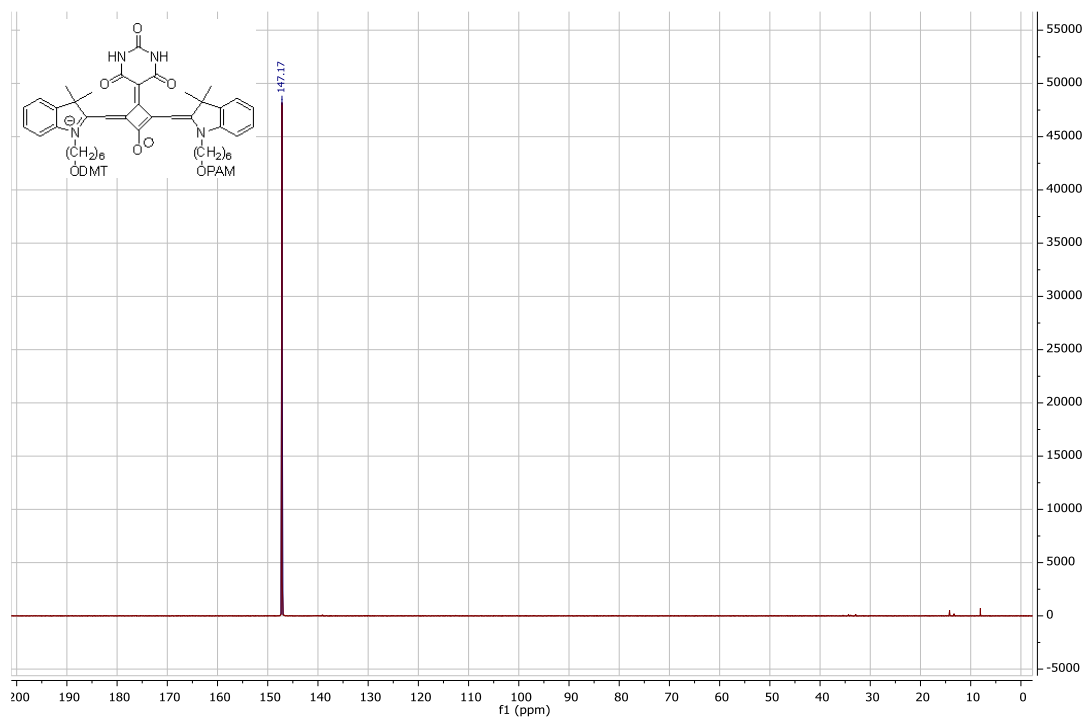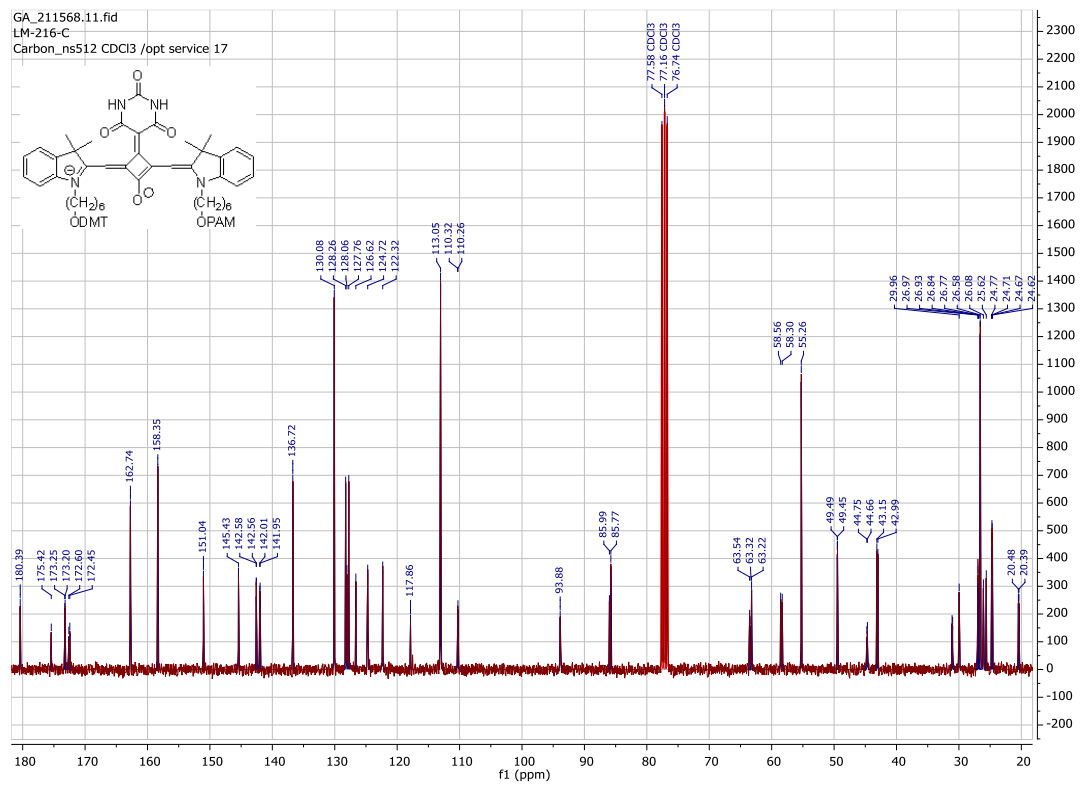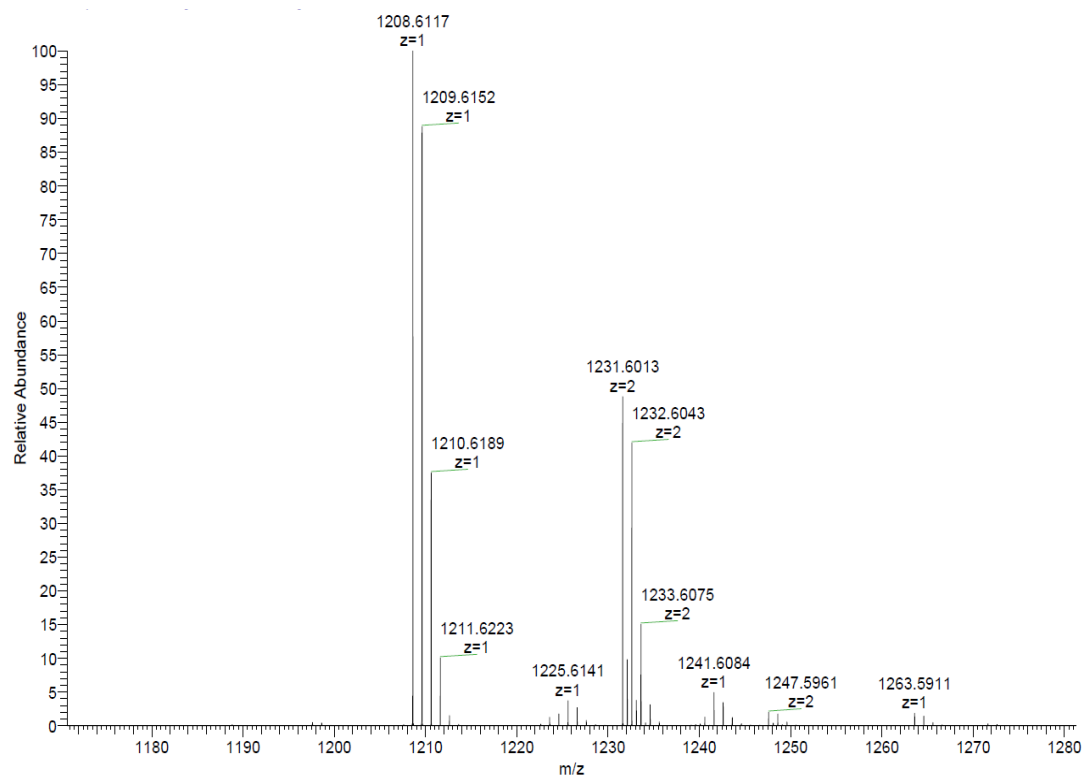
MS and HPLC of the Oligophosphodiesters

Homo-oligomer **SqTr** (ESI-MS data: positive mode, MeOH):
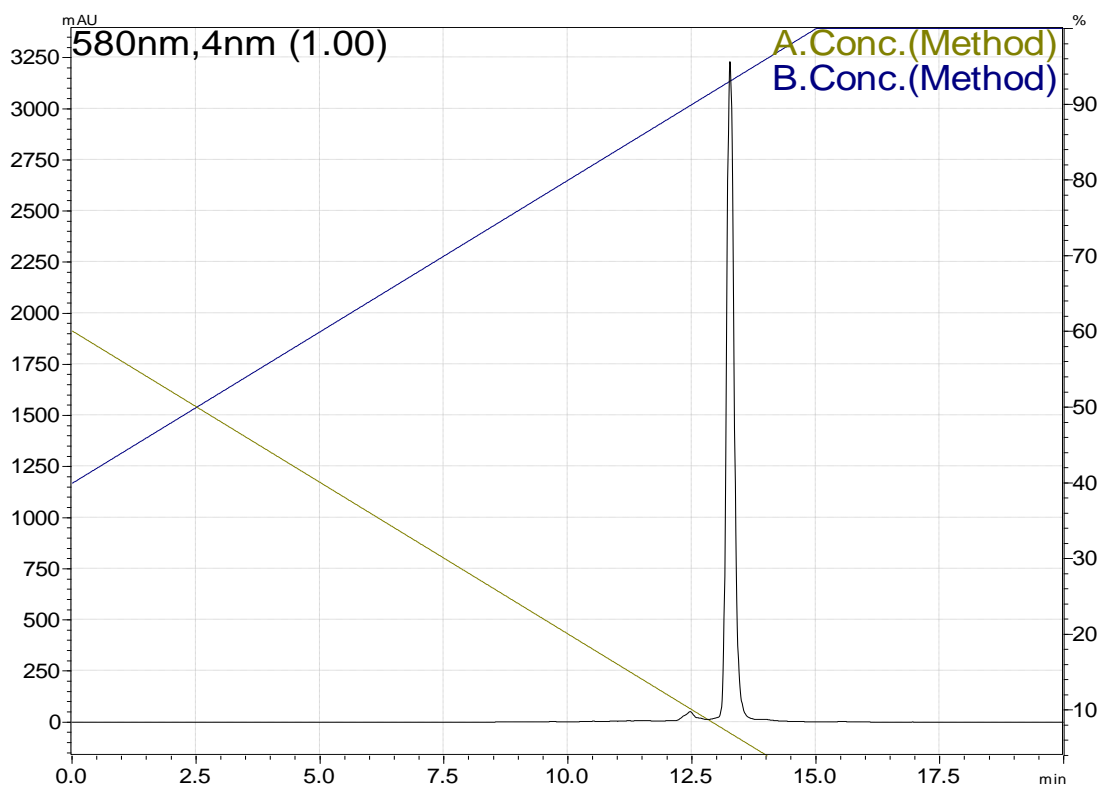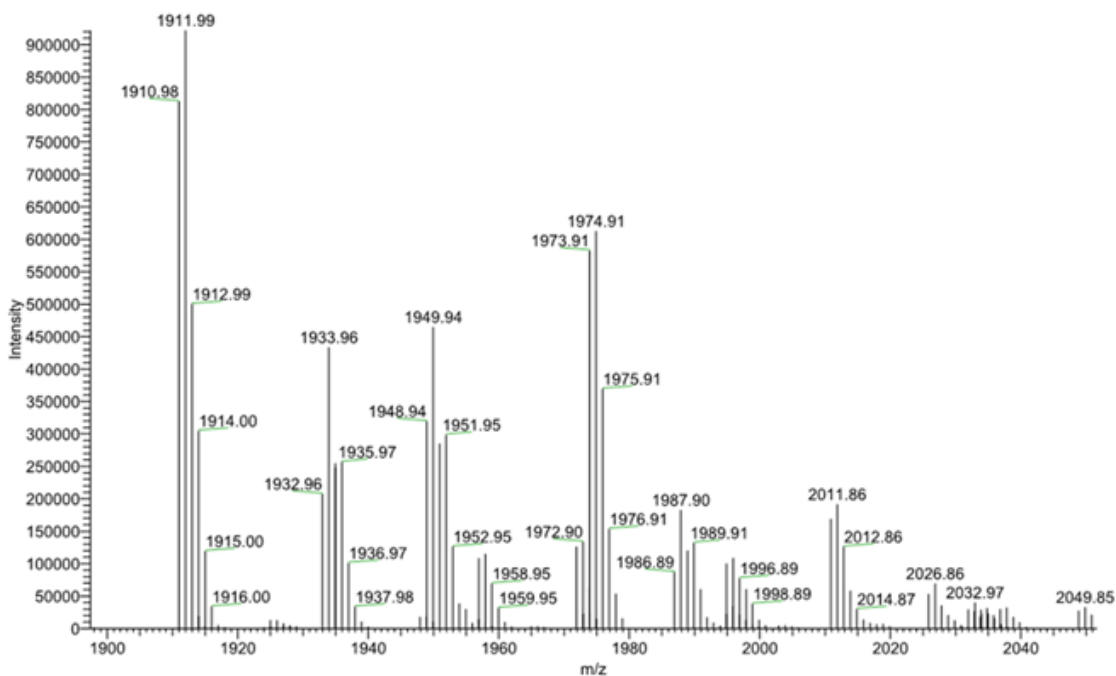
Homo-oligomer **SqHex** (ESI-MS data: positive mode, MeOH):
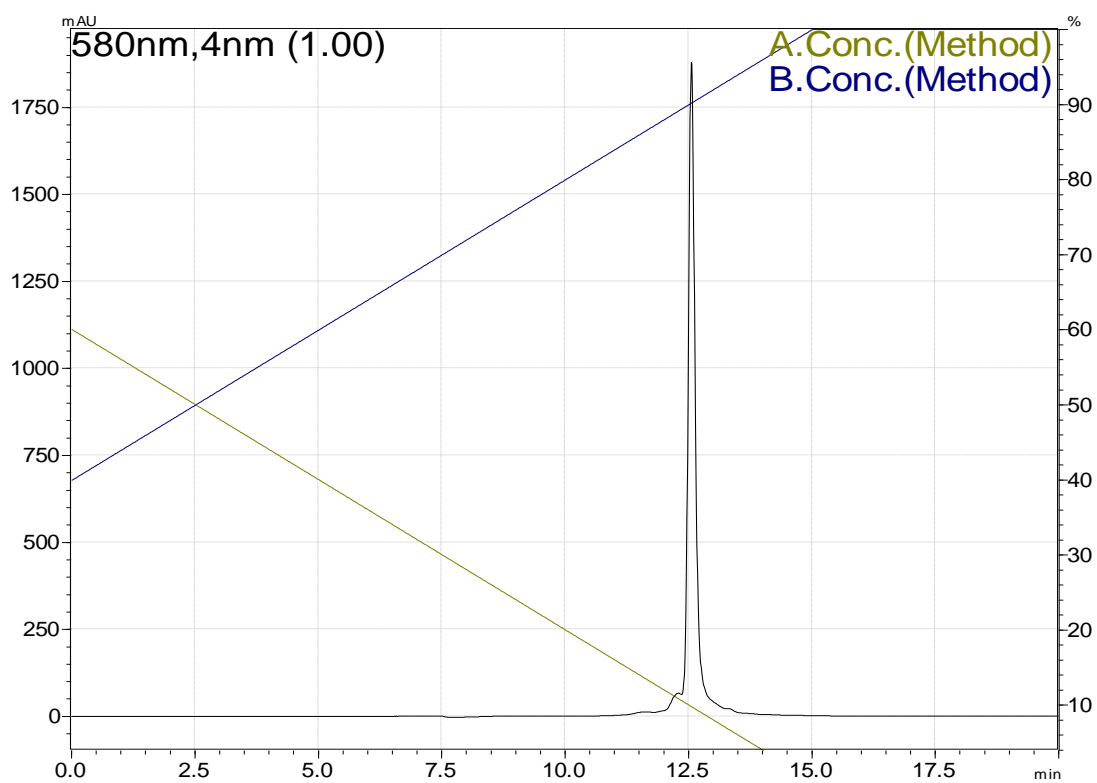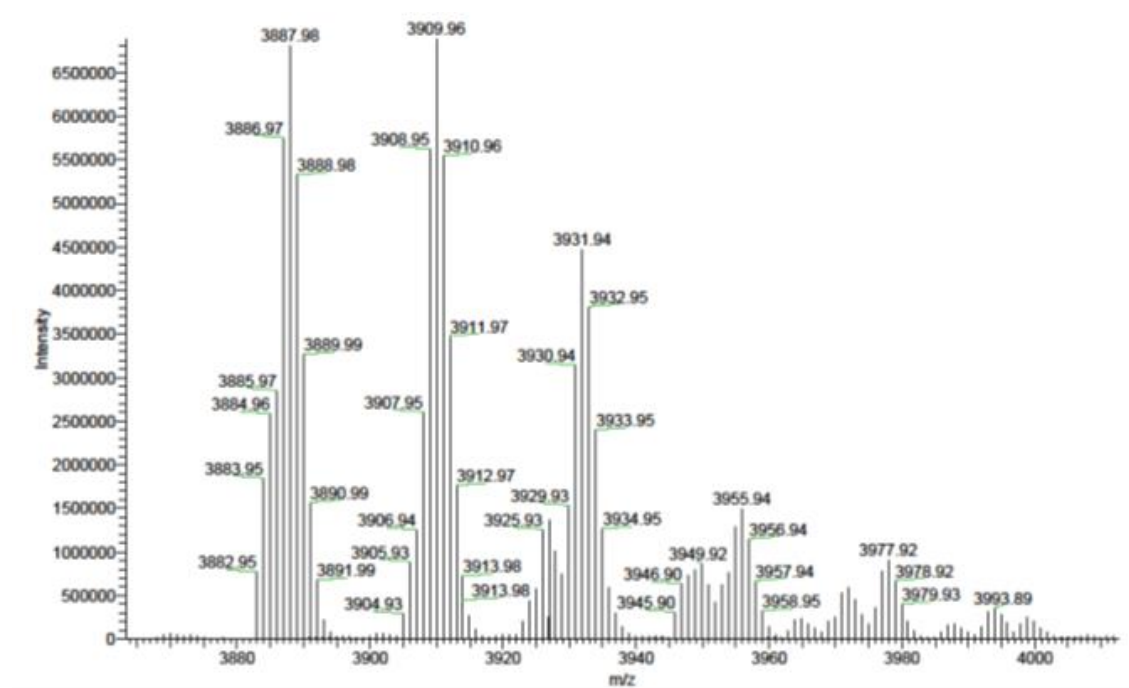
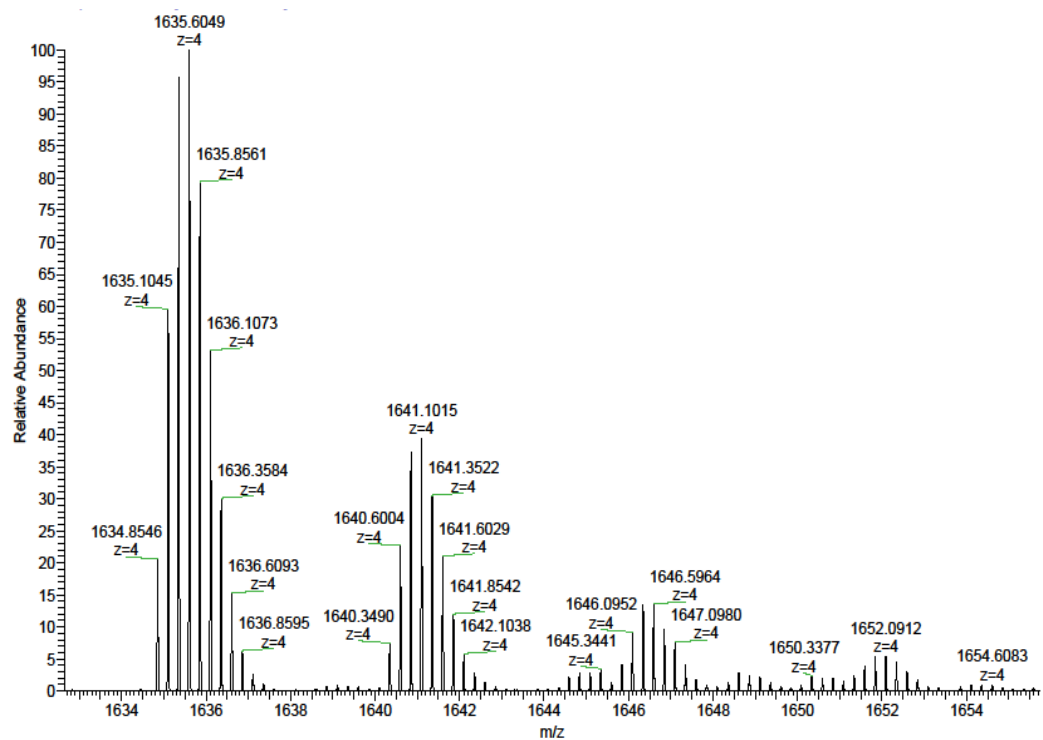Oligonucleotide **Sq1** (ESI-MS data: negative mode, MeCN/(Et$_3$NH)OAc):
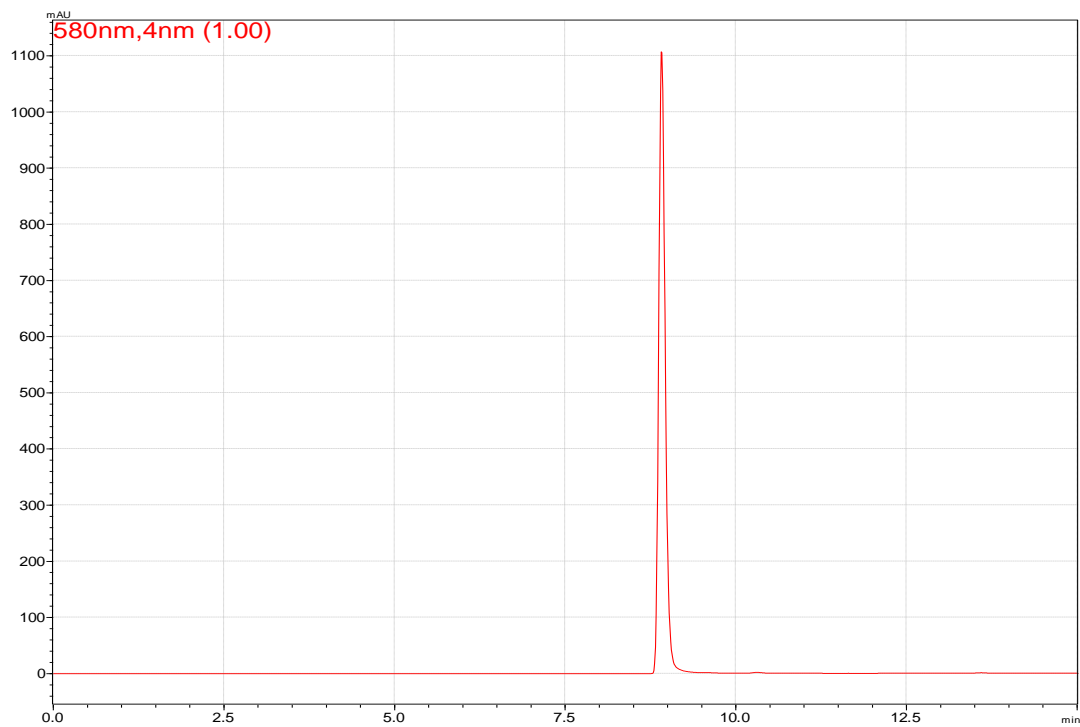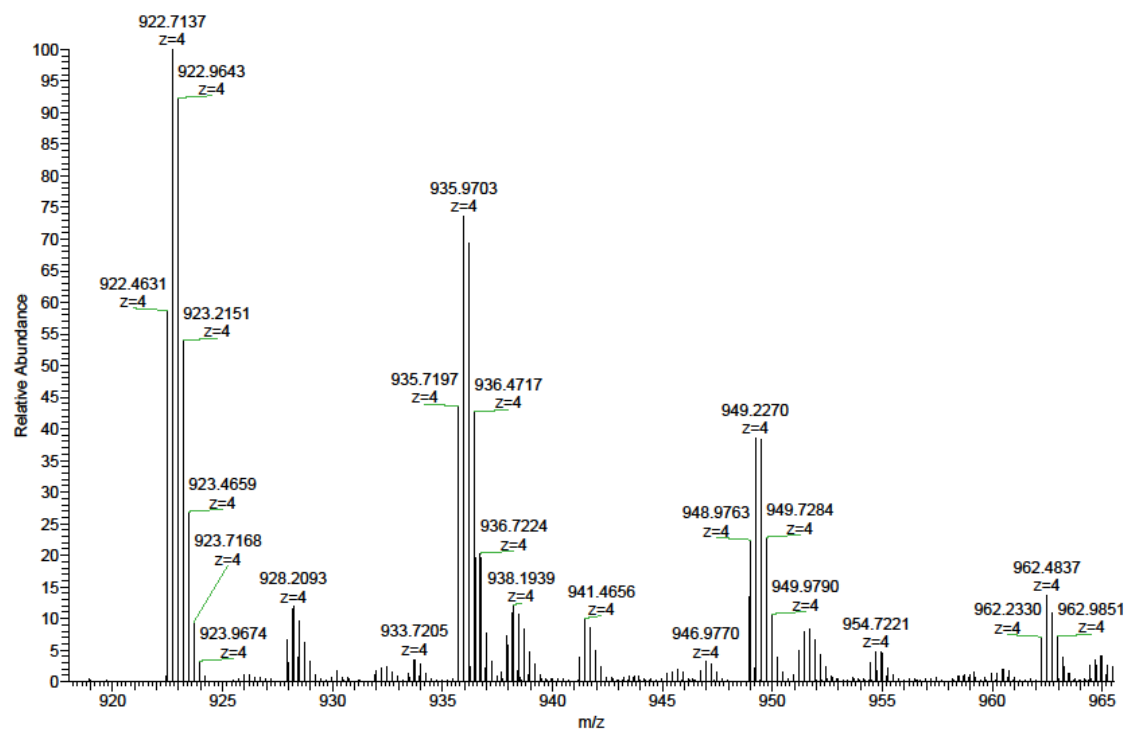
Oligonucleotide **cSq1** (ESI-MS data negative mode, MeCN/(Et₃NH)OAc):
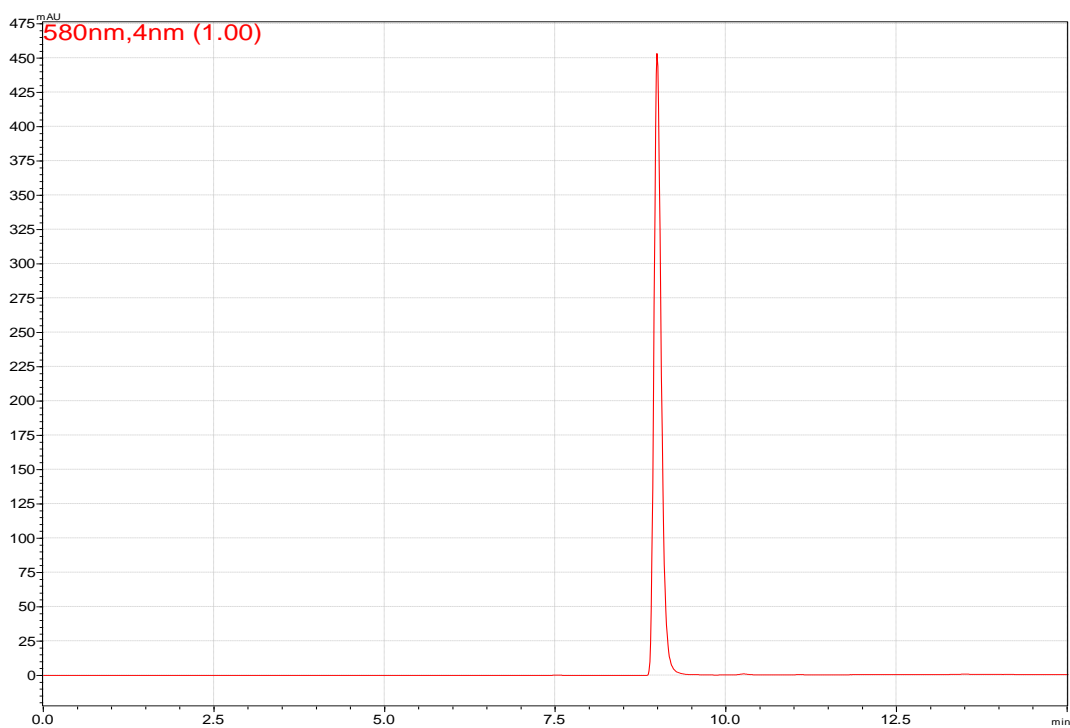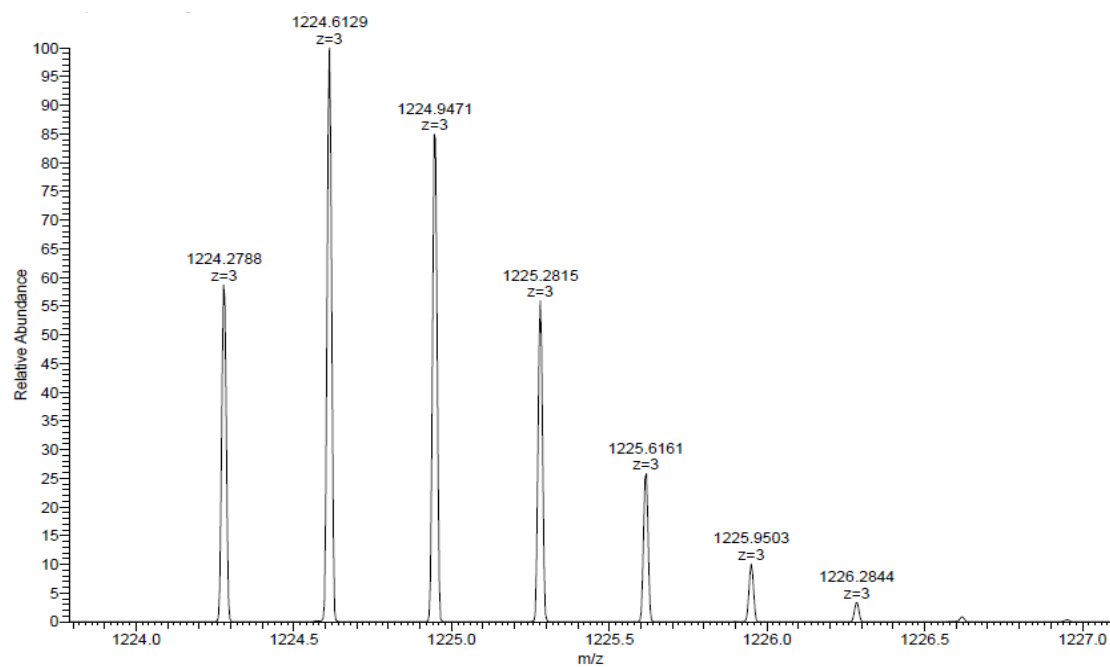
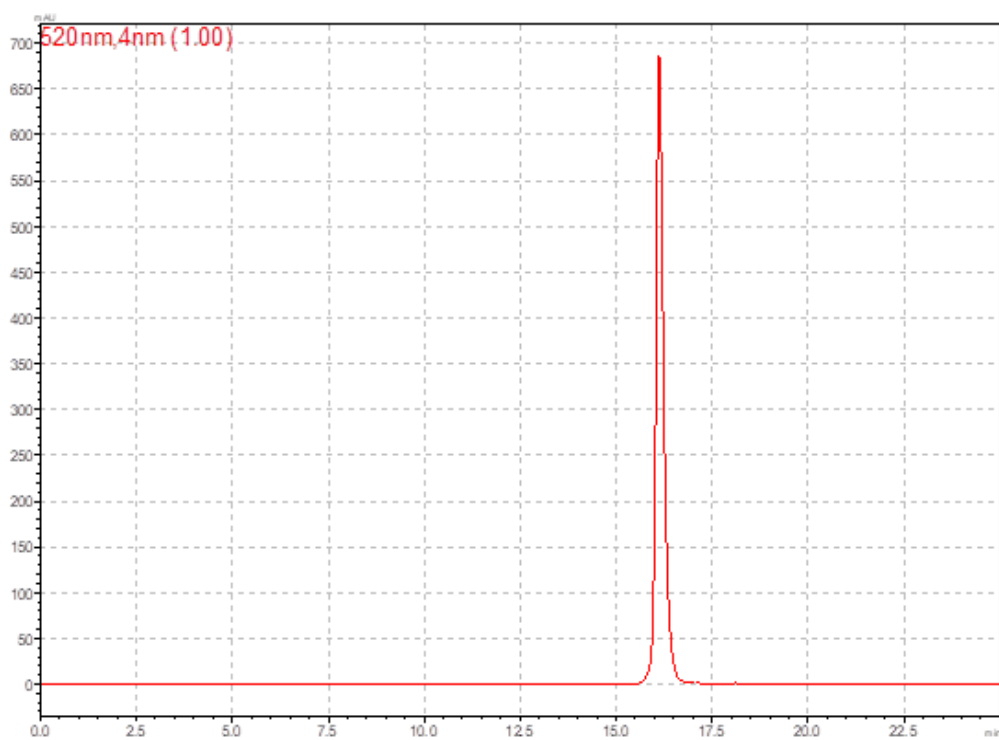Oligonucleotide **Sq3** (ESI-MS data: negative mode, MeCN/(Et₃NH)OAc):
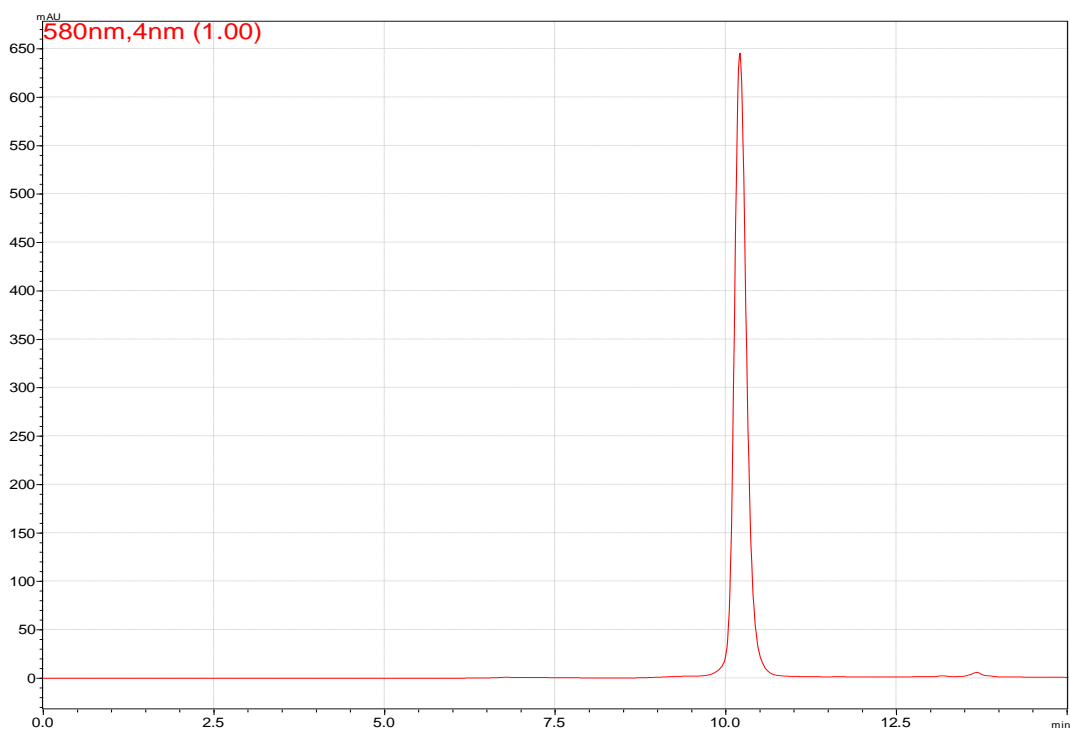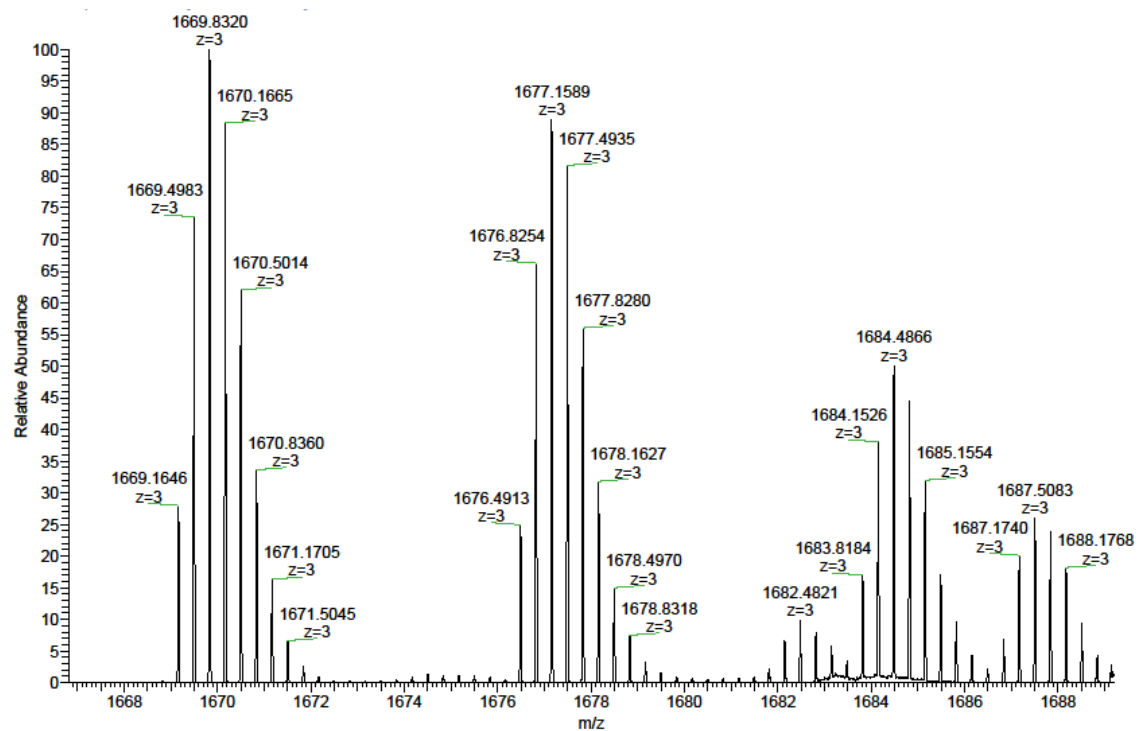
Oligonucleotide **cSq3** (ESI-MS data: negative mode, MeCN/(Et$_3$NH)OAc):
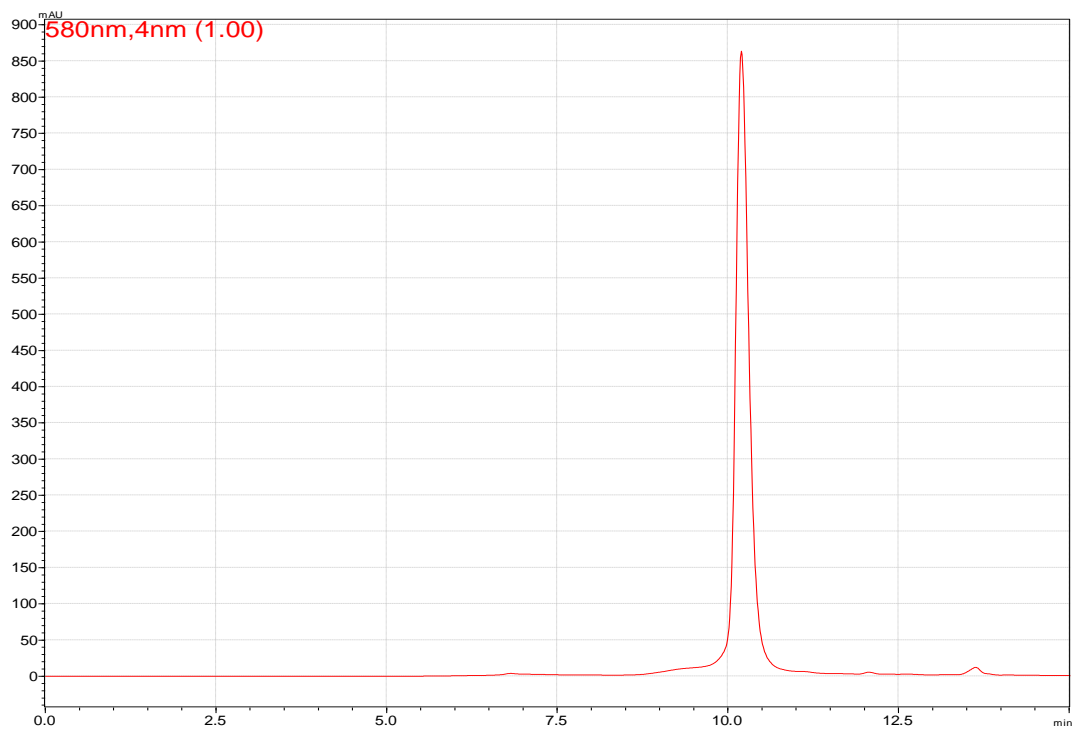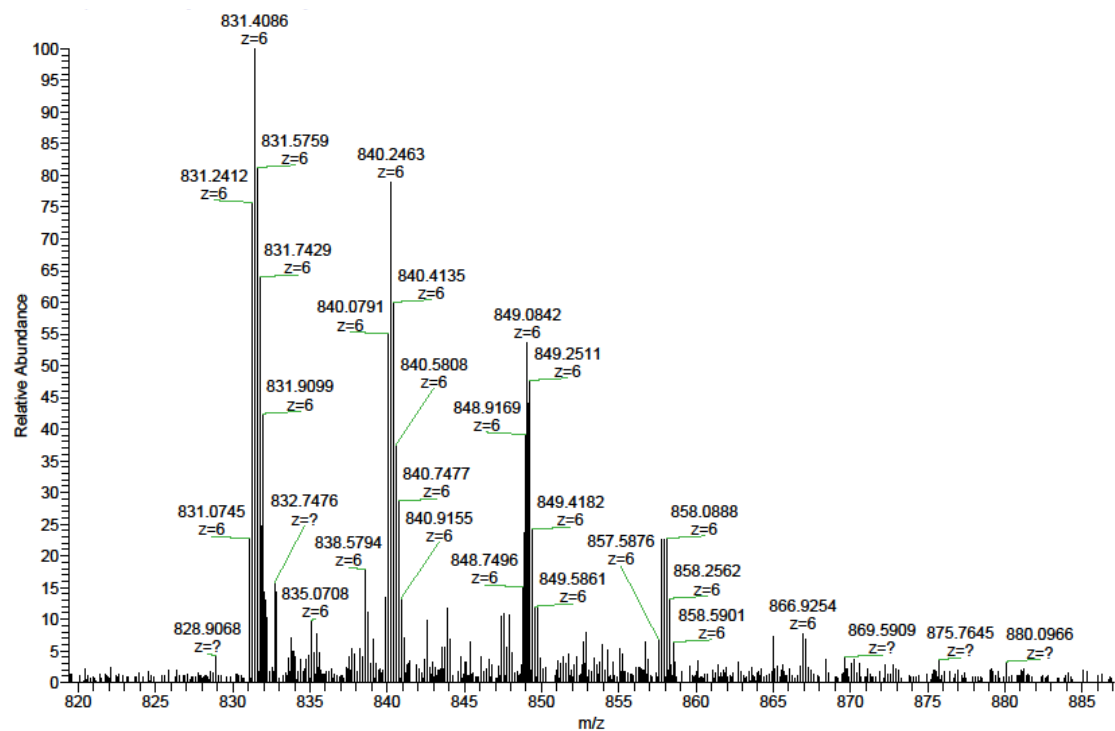
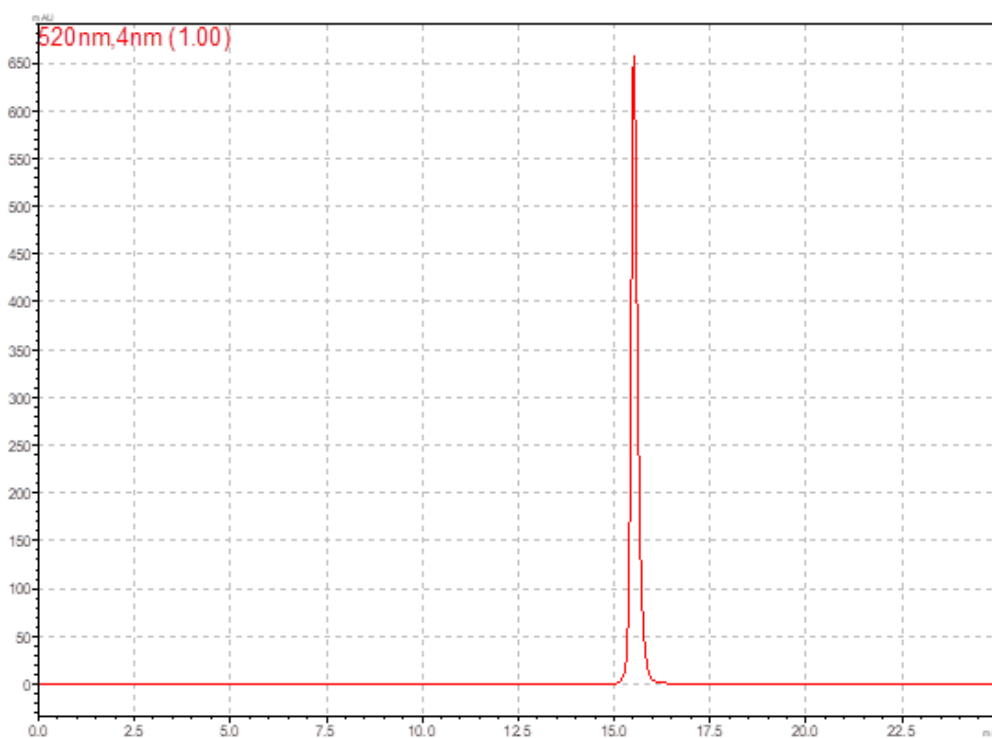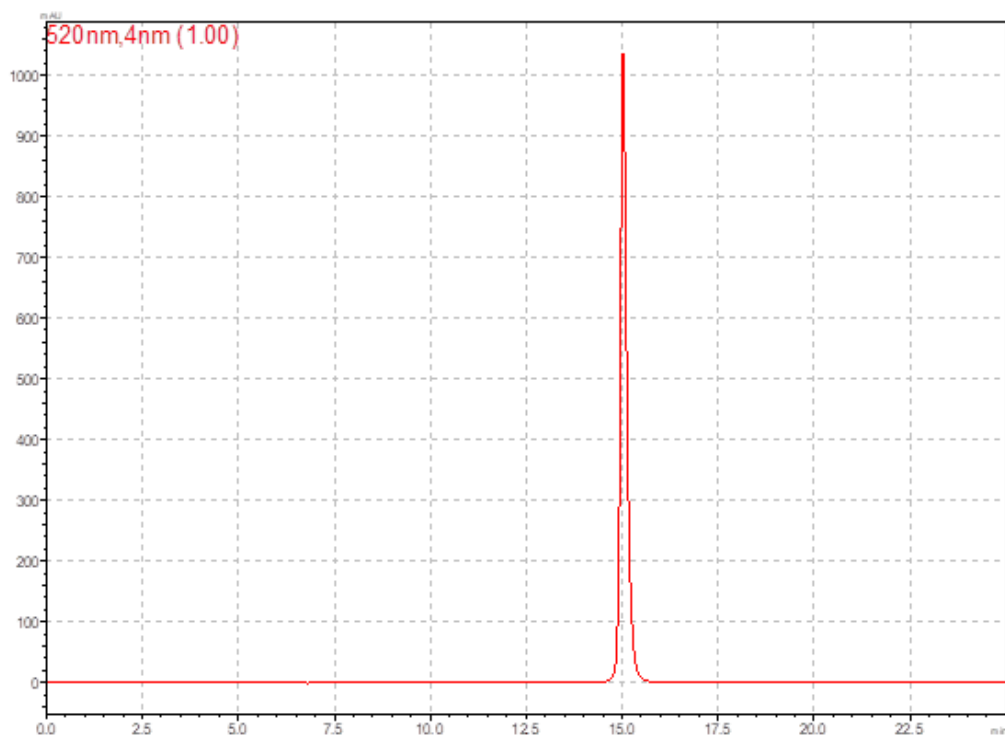Oligonucleotide **Sq6** (ESI-MS data: negative mode, MeCN/(Et$_3$NH)OAc):
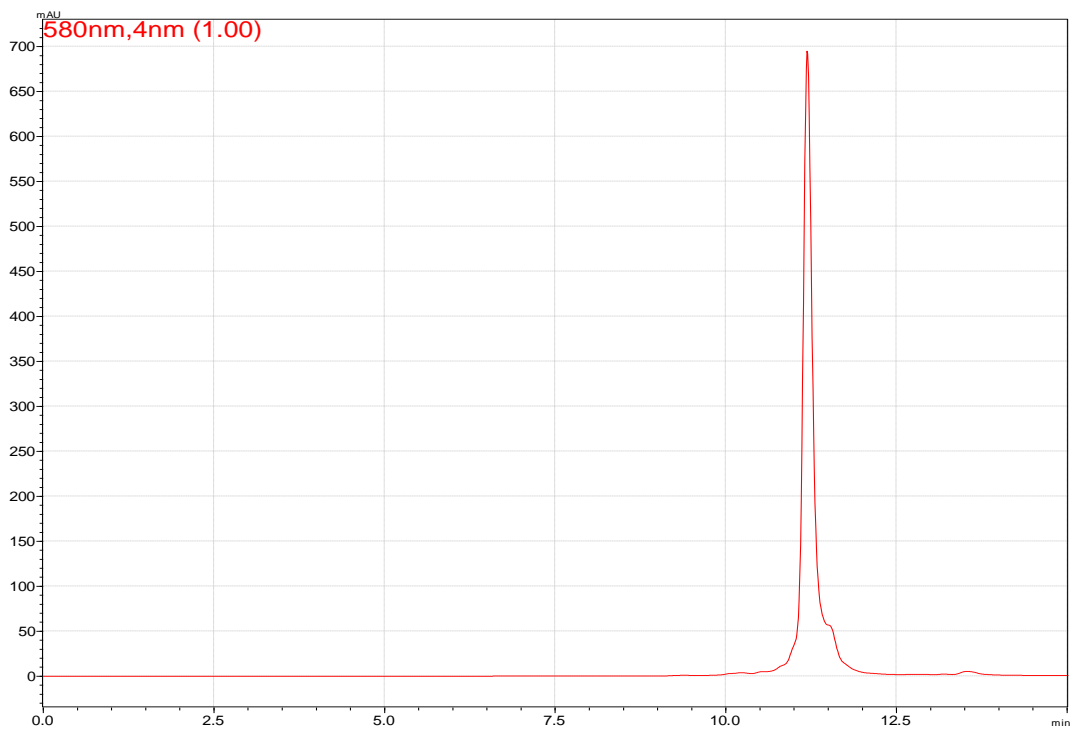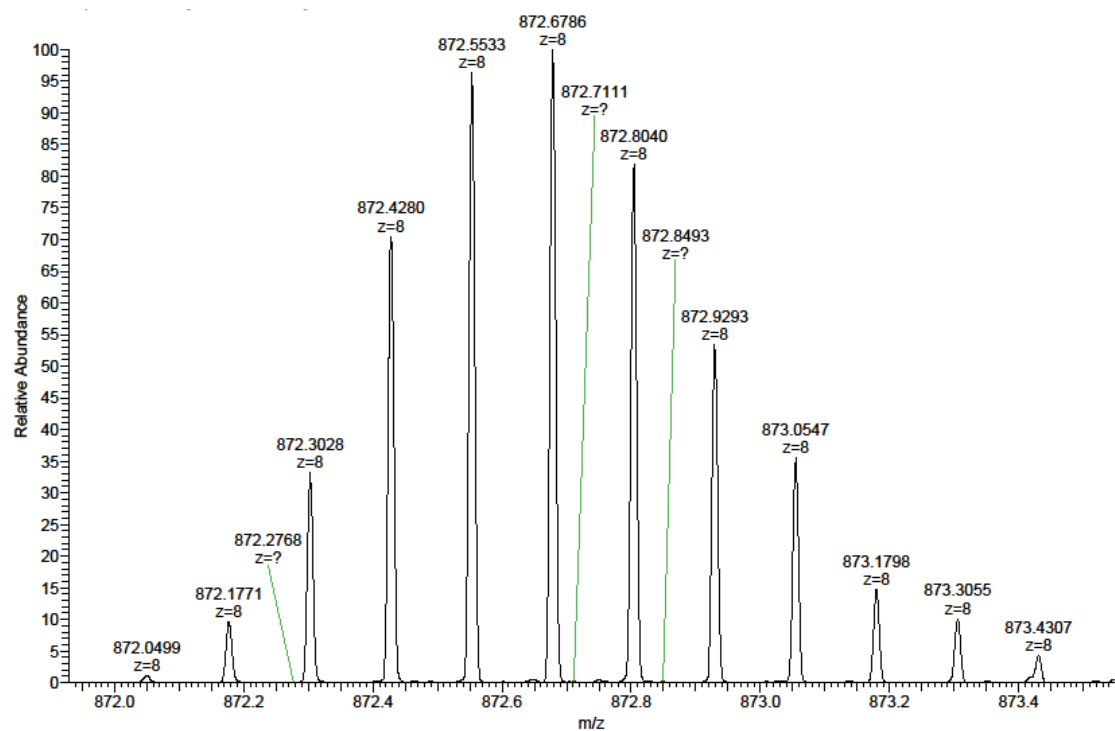
Oligonucleotide **cSq6** (ESI-MS data: negative mode, MeCN/(Et$_3$NH)OAc):
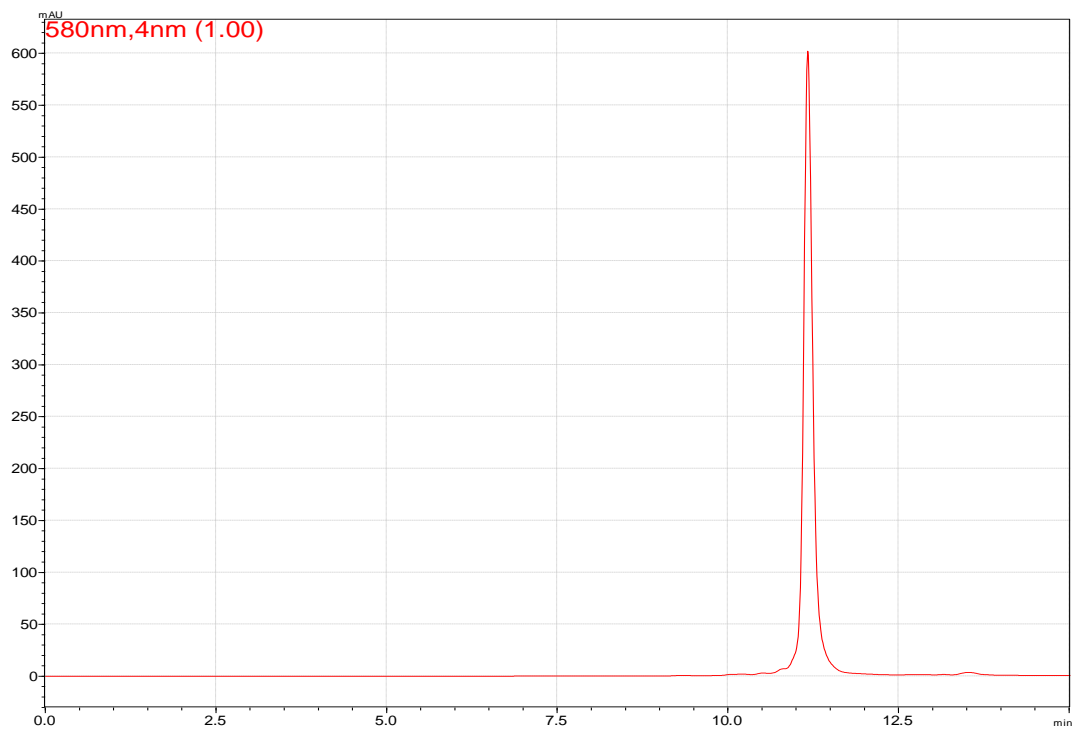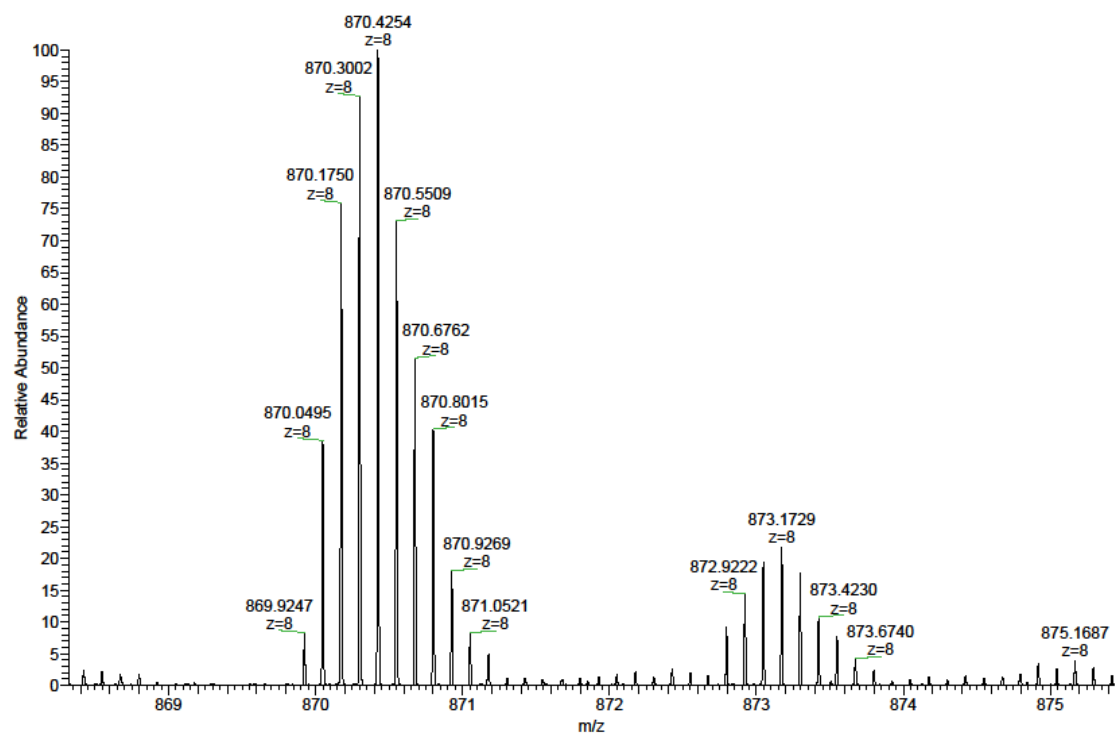
Oligonucleotide **Sq3-ON20** (ESI-MS data: negative mode, MeOH):
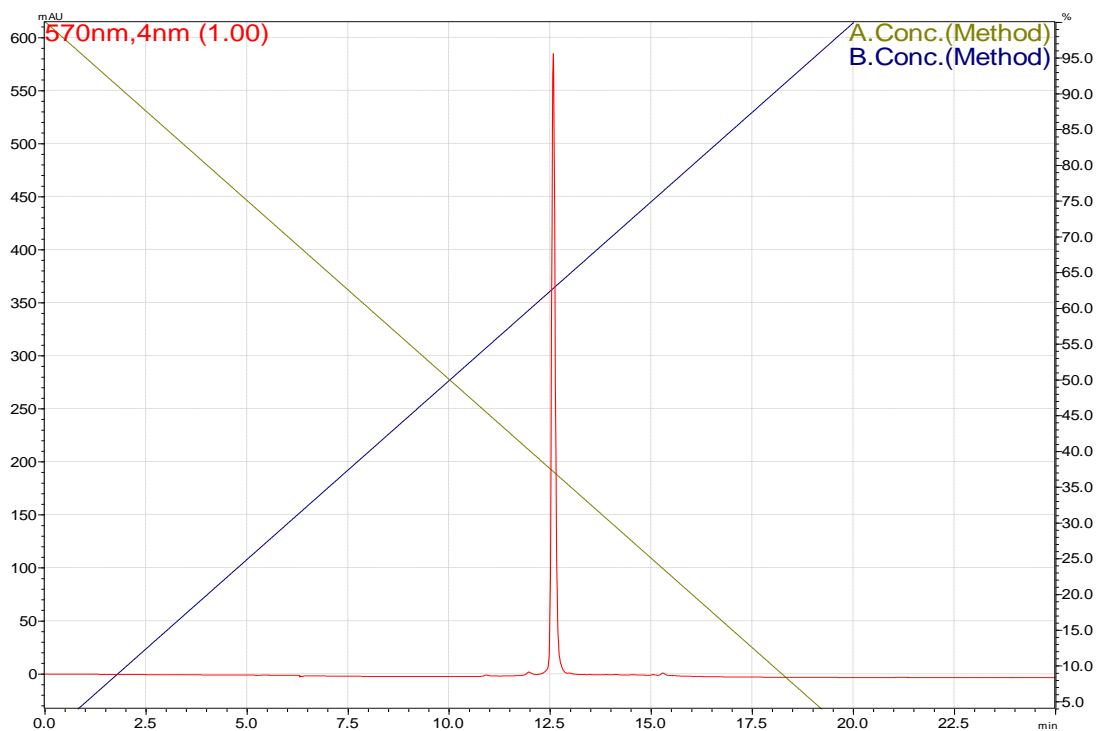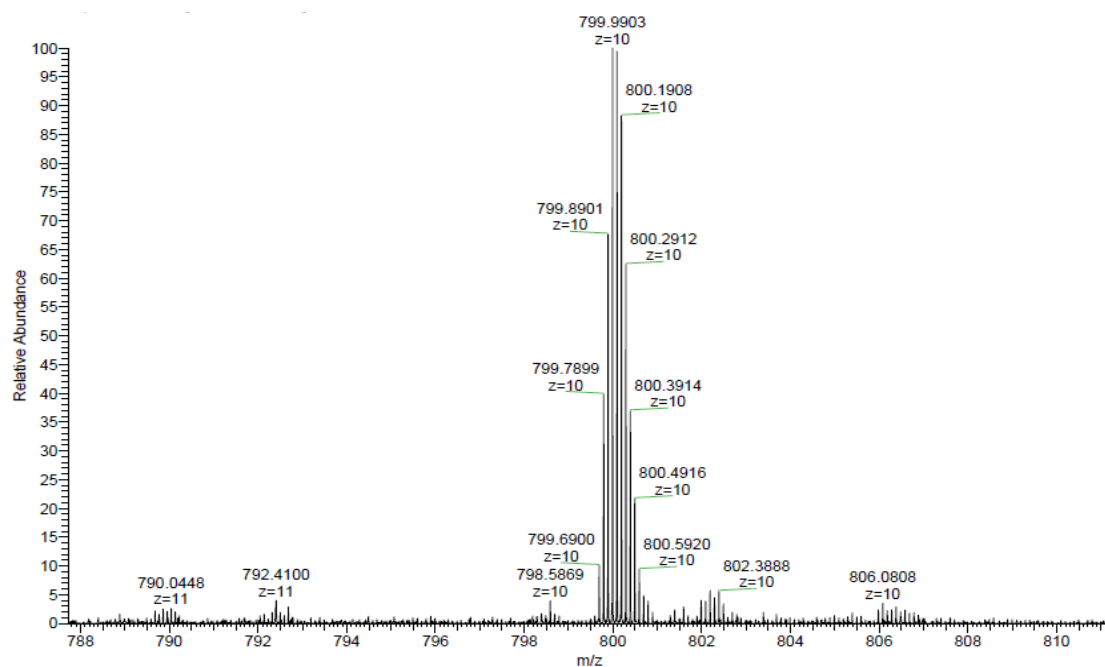
Oligonucleotide **cSq3-ON20** (ESI-MS data: negative mode, MeOH):
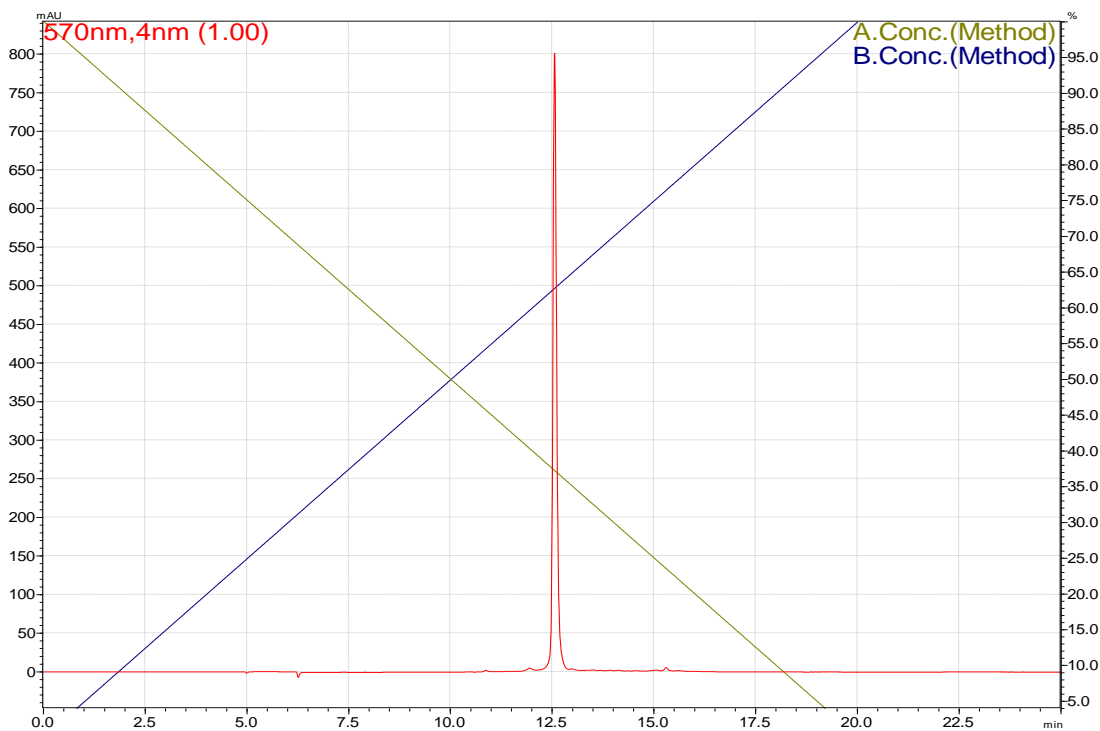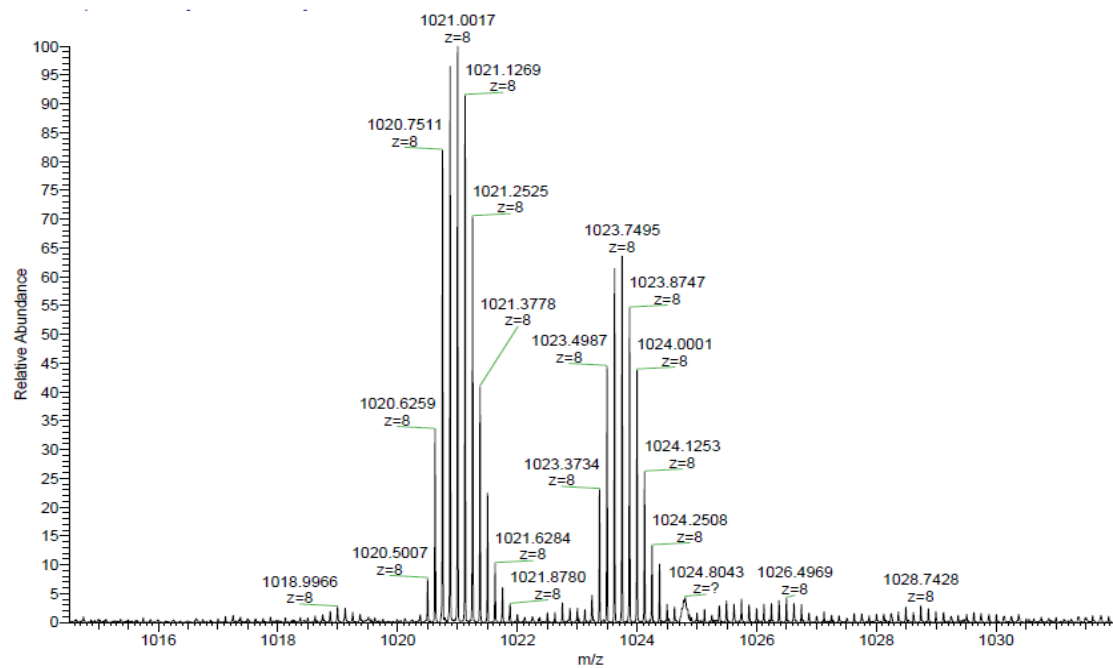
Oligonucleotide **Sq6-NH2** (ESI-MS data: negative mode, MeOH):
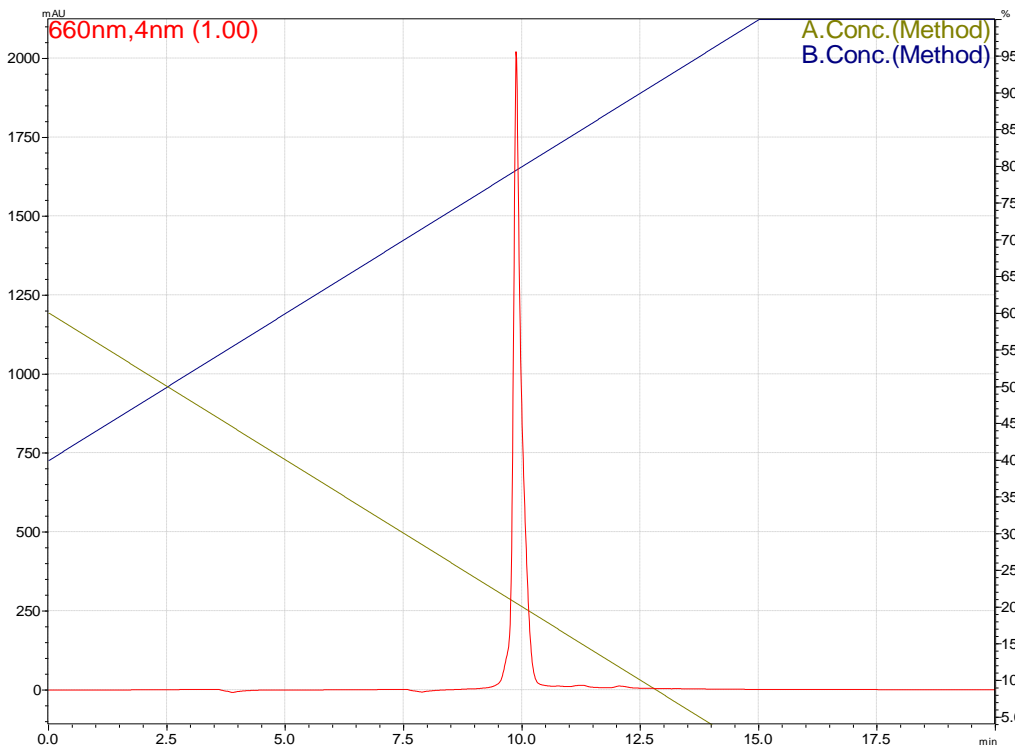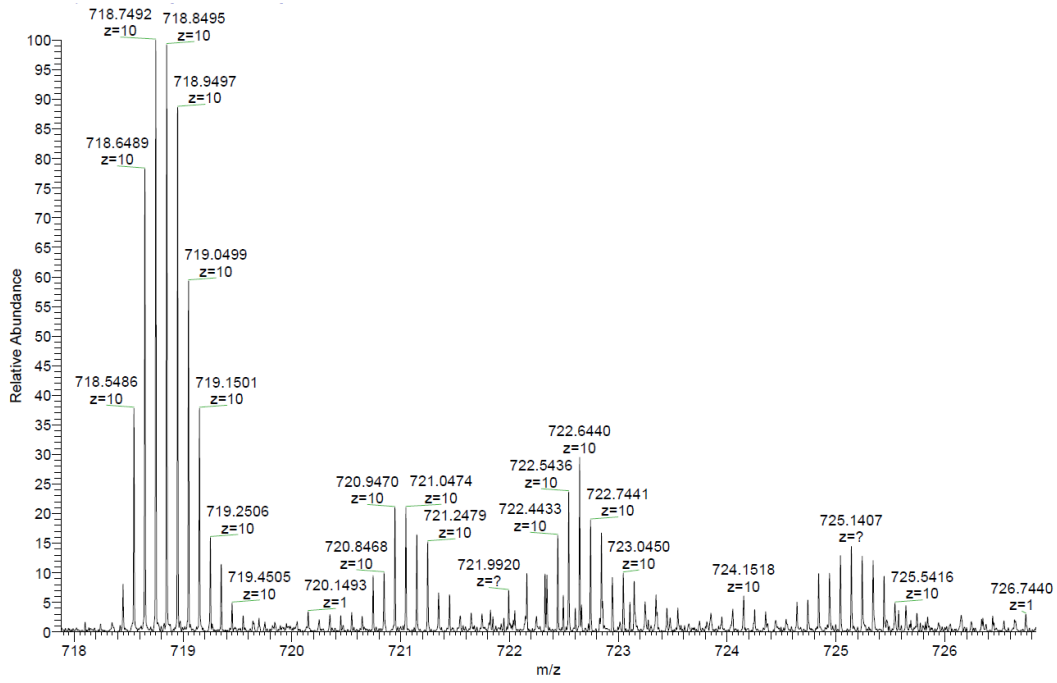
Oligonucleotide **Sq6T10-NH2** (ESI-MS data: negative mode, MeOH):
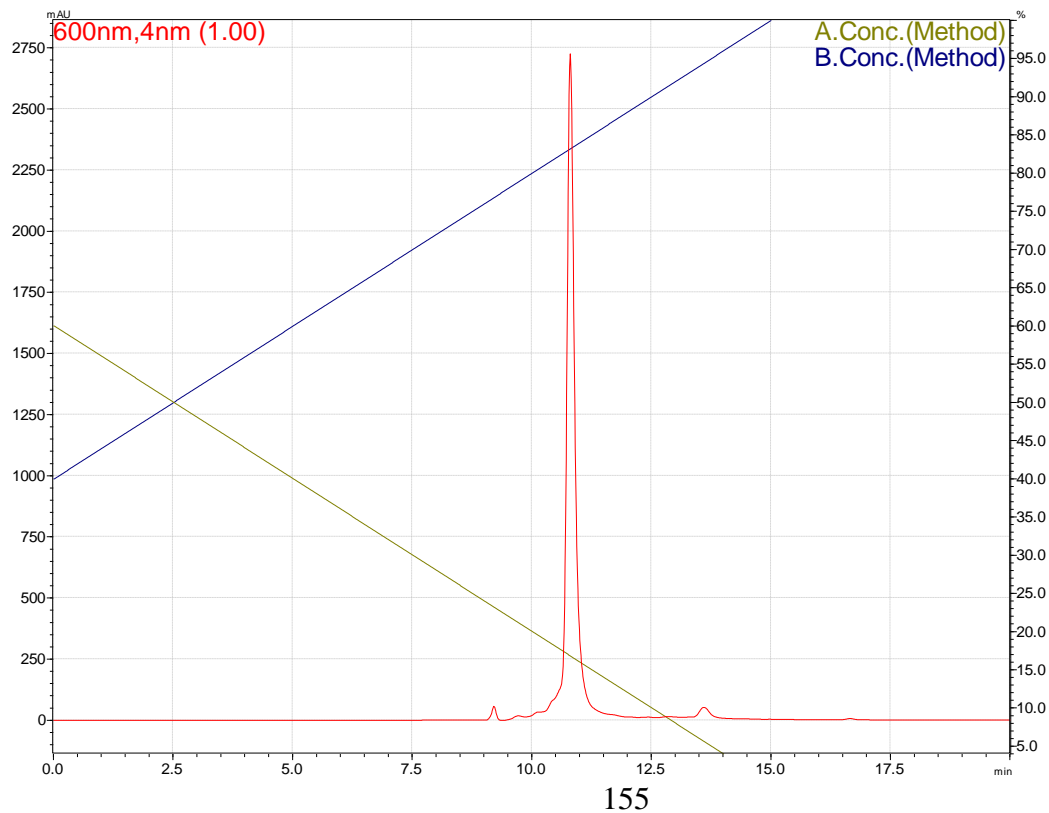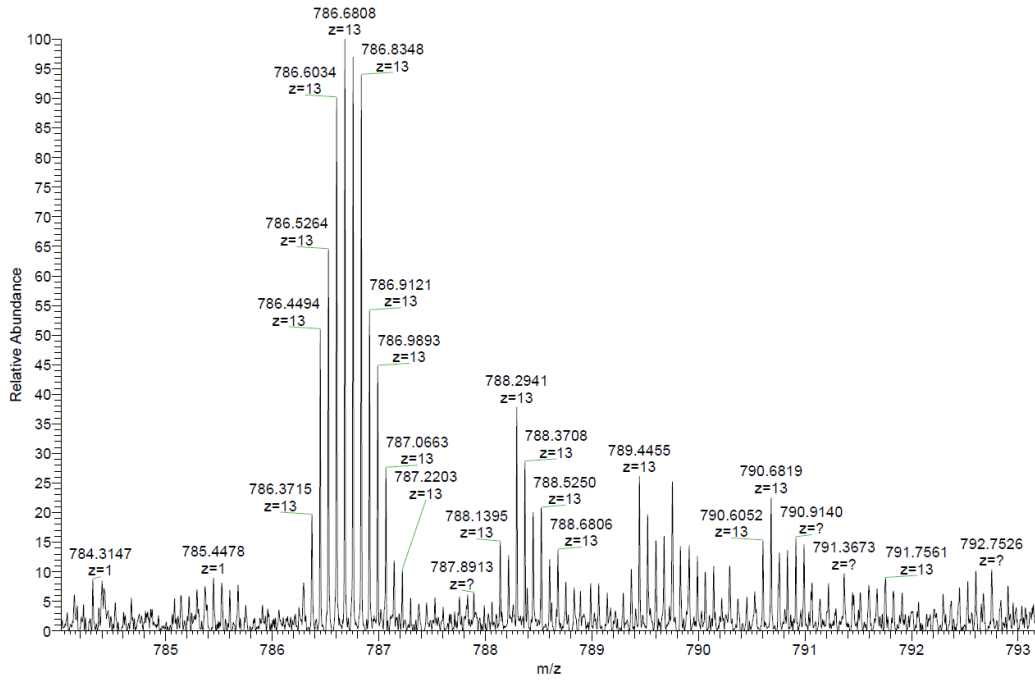
Oligonucleotide **Sq6-SS** (ESI-MS data**:** negative mode, MeOH):
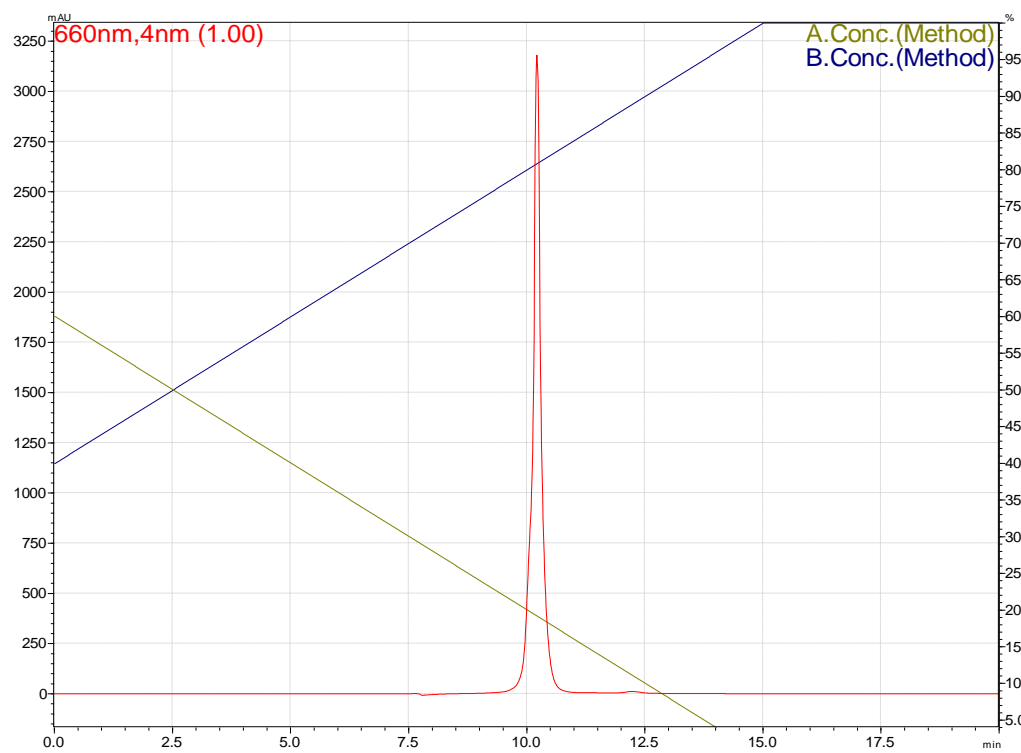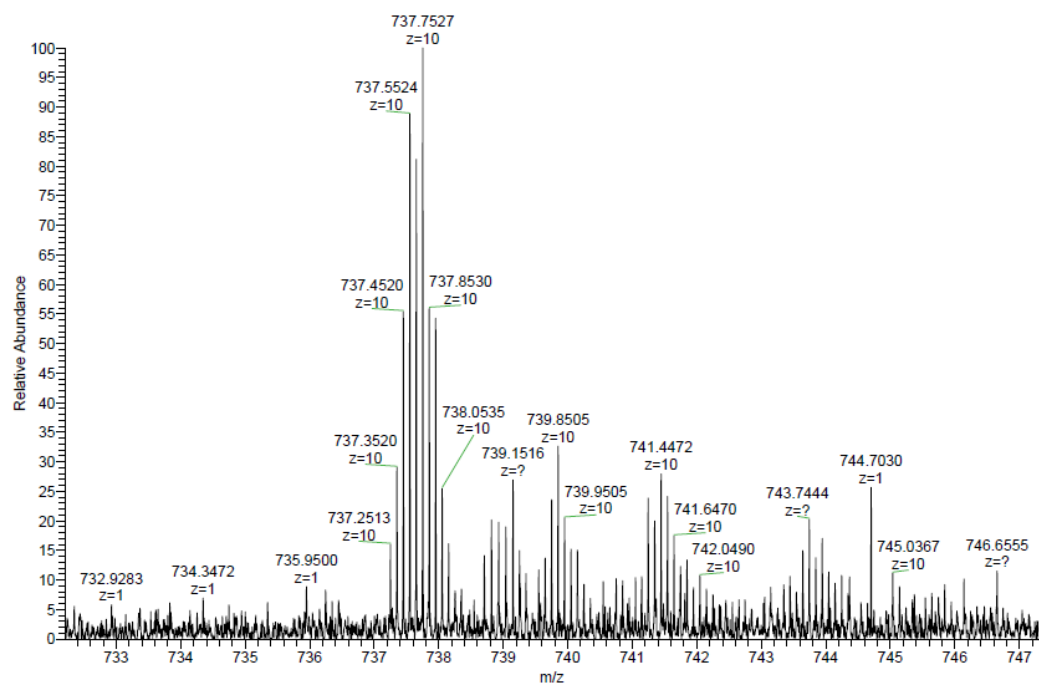
Oligonucleotide **Sq6T10-SS** (ESI-MS data: negative mode, MeOH):
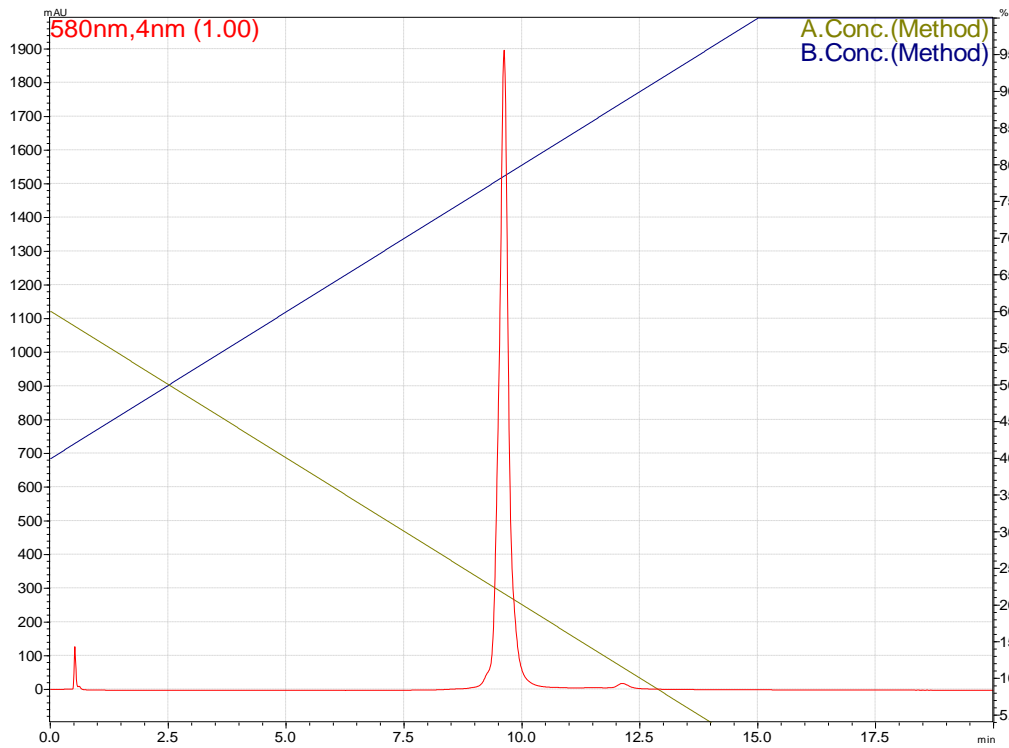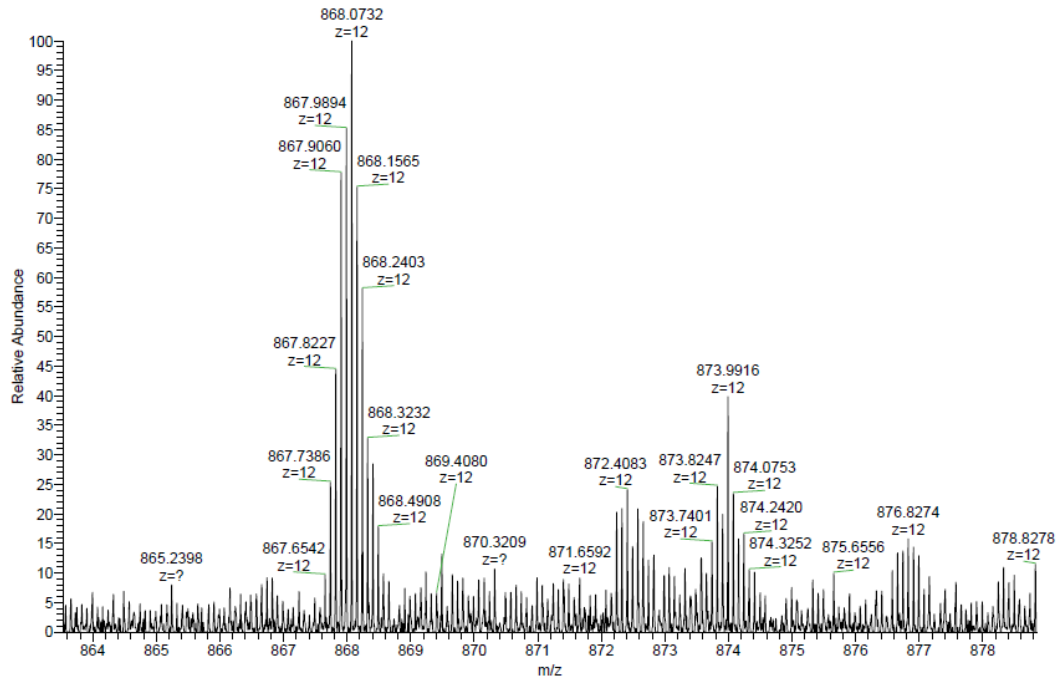
Oligonucleotide **T6-SS** (ESI-MS data: negative mode, MeOH):
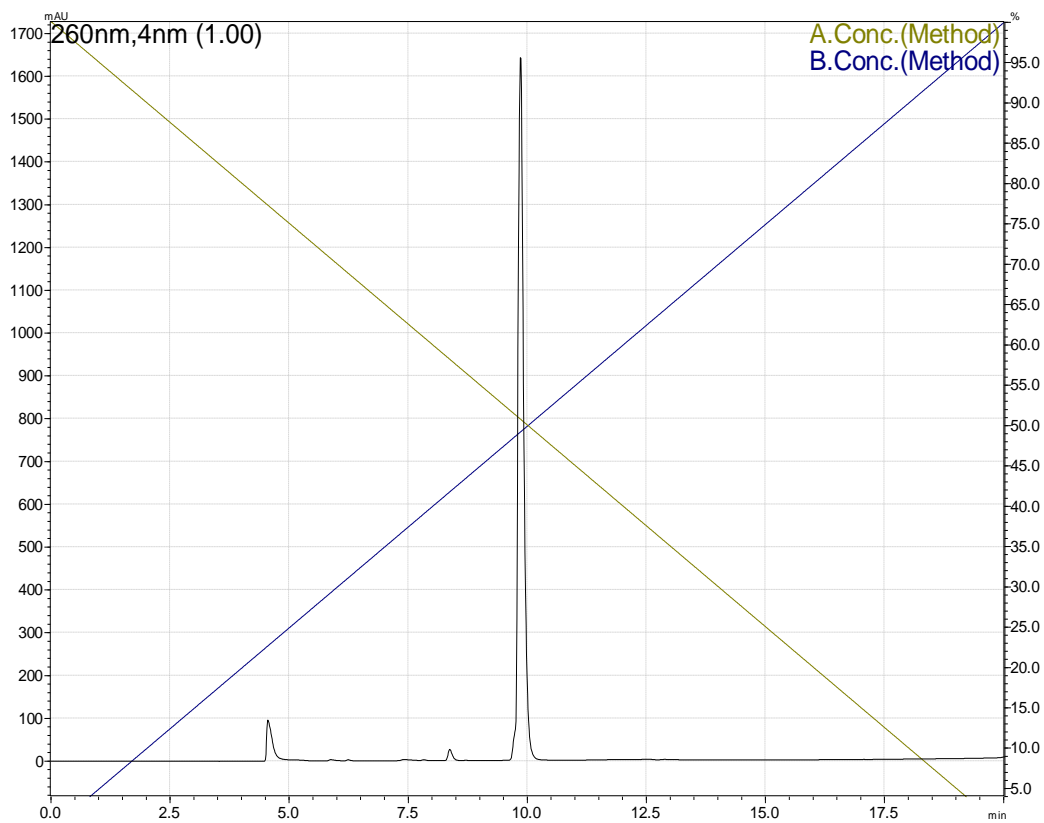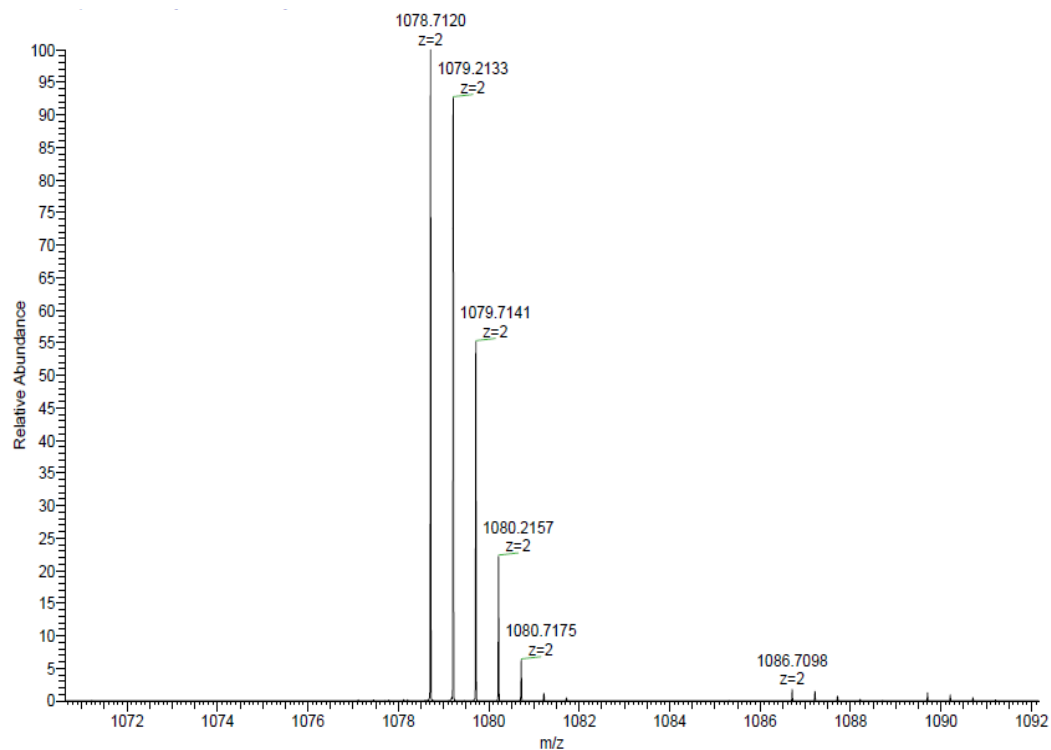
Oligonucleotide **cNM-SS** (ESI-MS data: negative mode, MeOH):
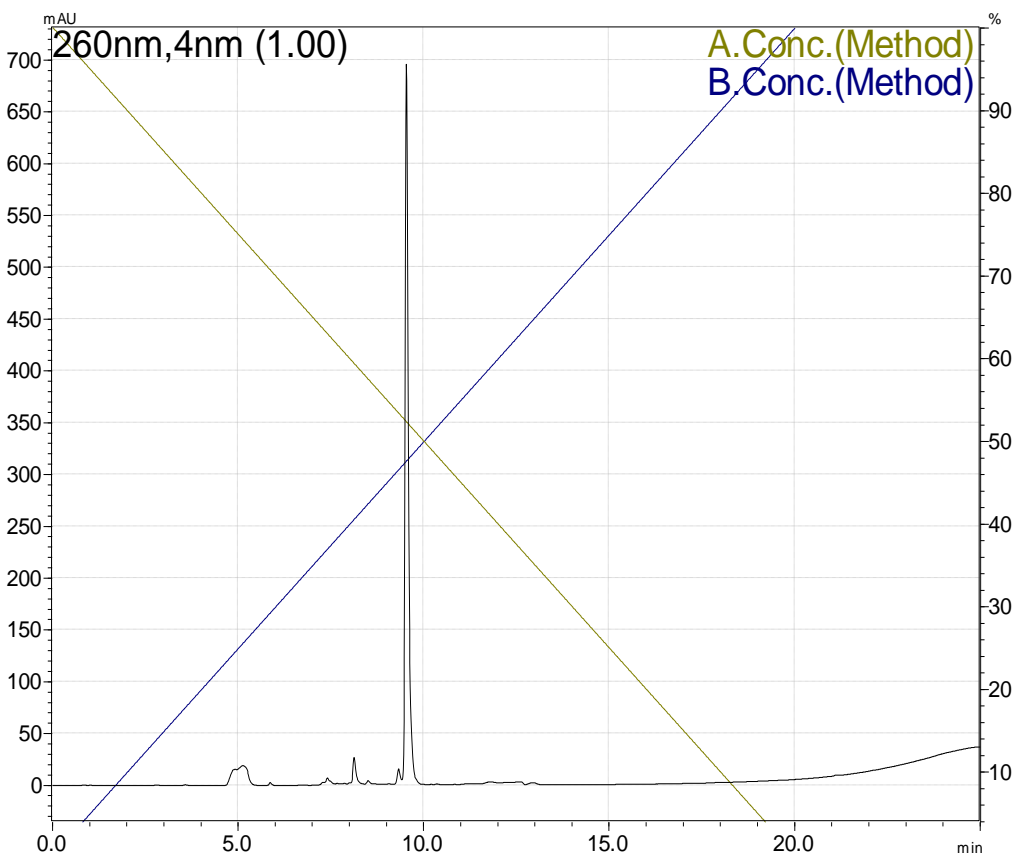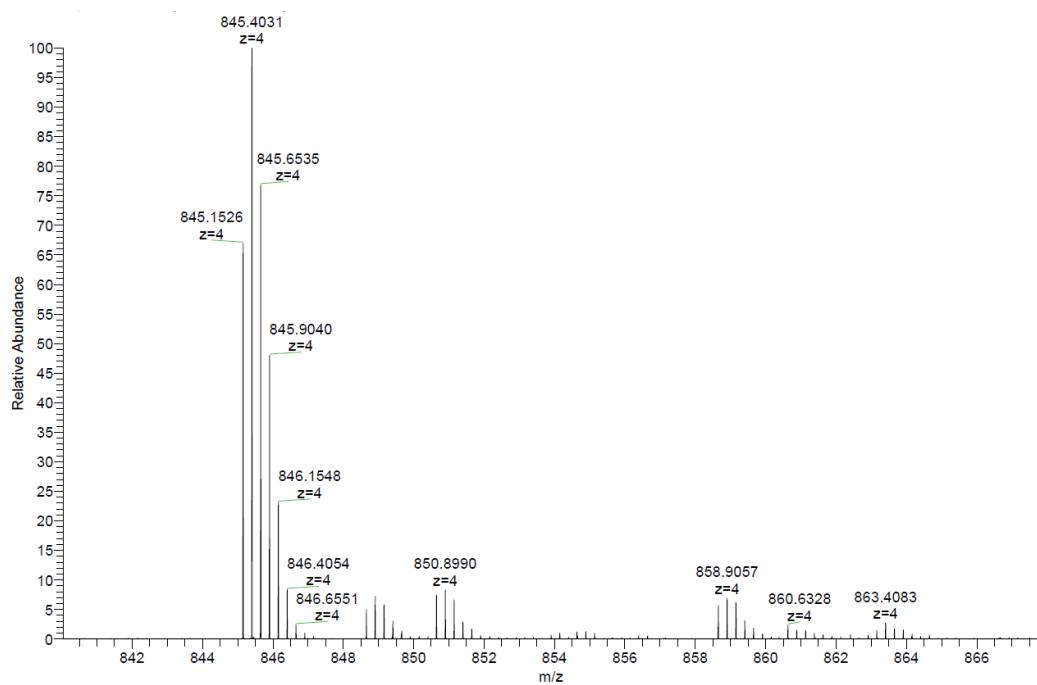
Oligonucleotide **NC-SS** (ESI-MS data: negative mode, MeOH):
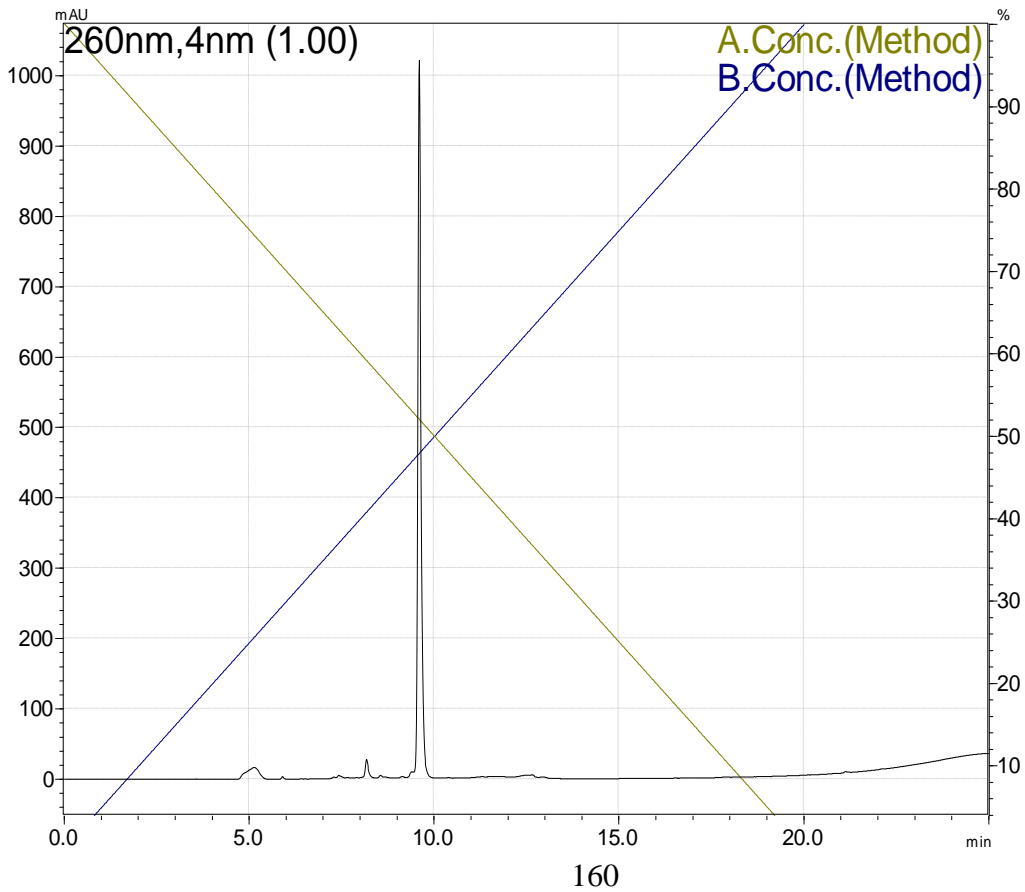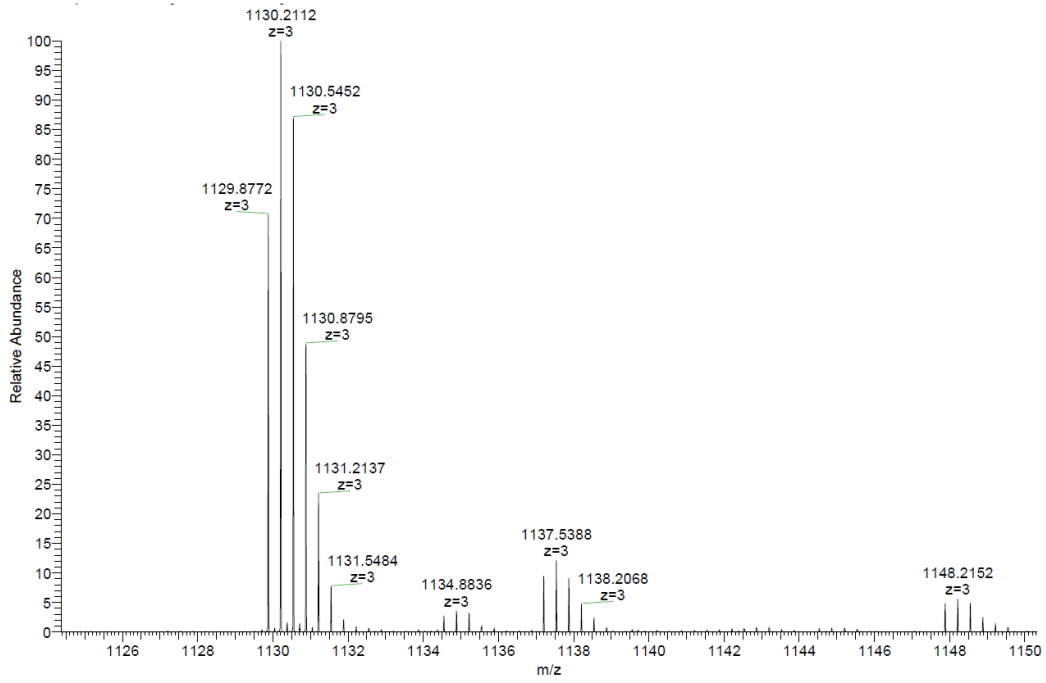
Oligonucleotide **cNMT10-SS** (ESI-MS data: negative mode, MeOH):
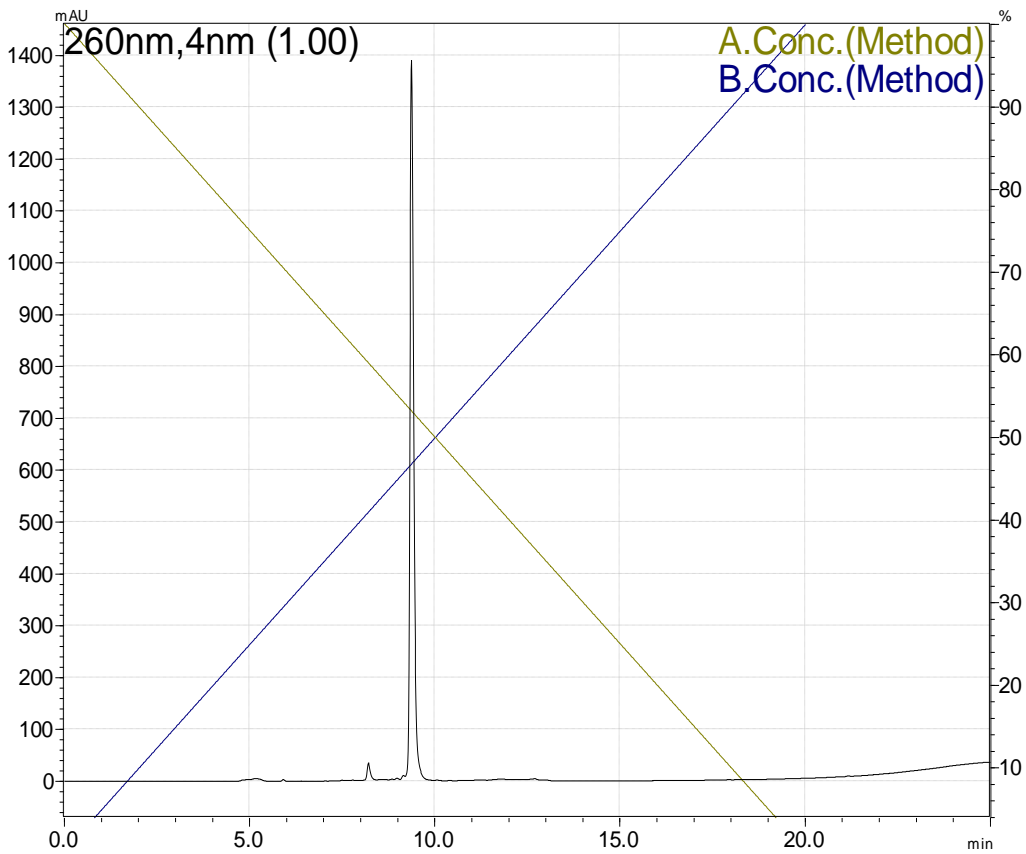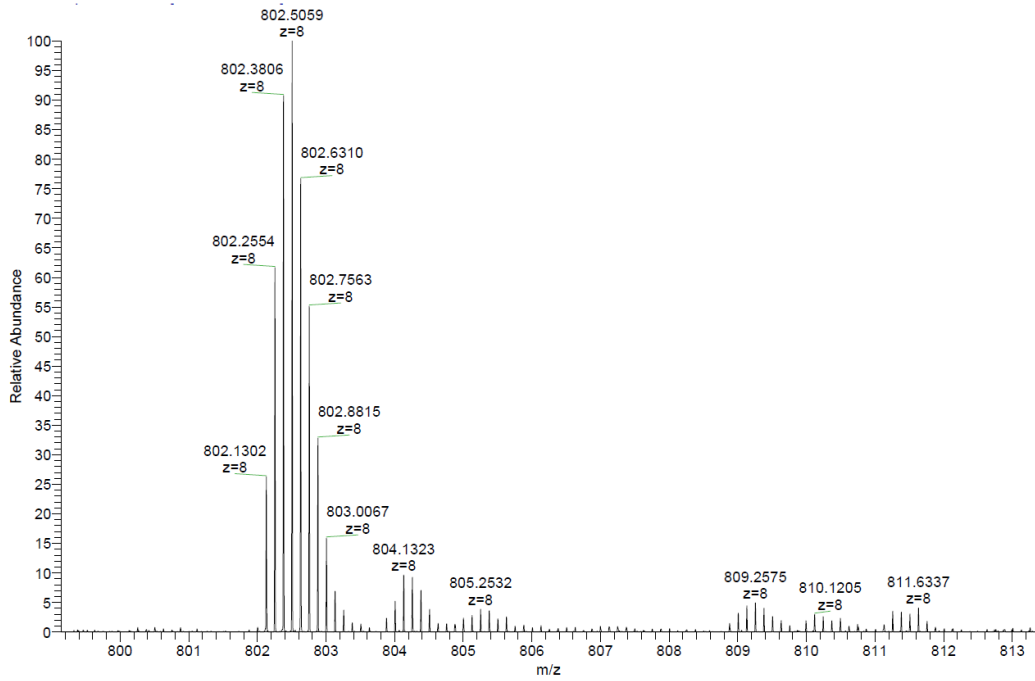
Oligonucleotide **NCT10-SS** (ESI-MS data: negative mode, MeOH):
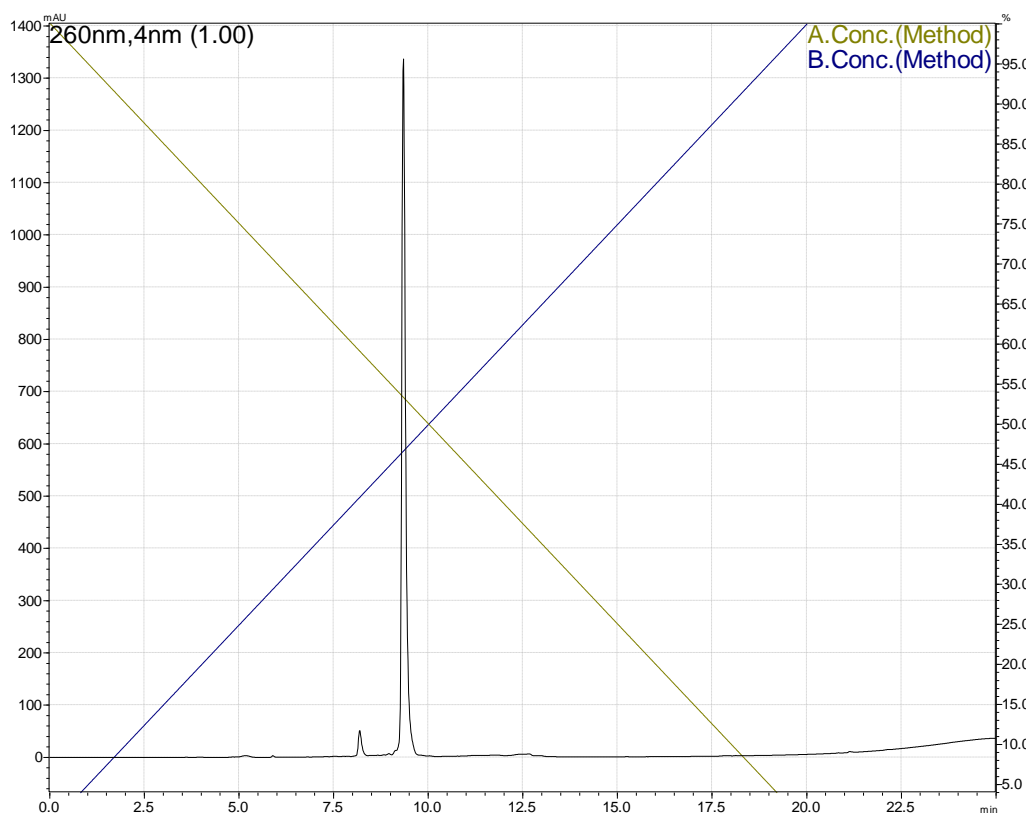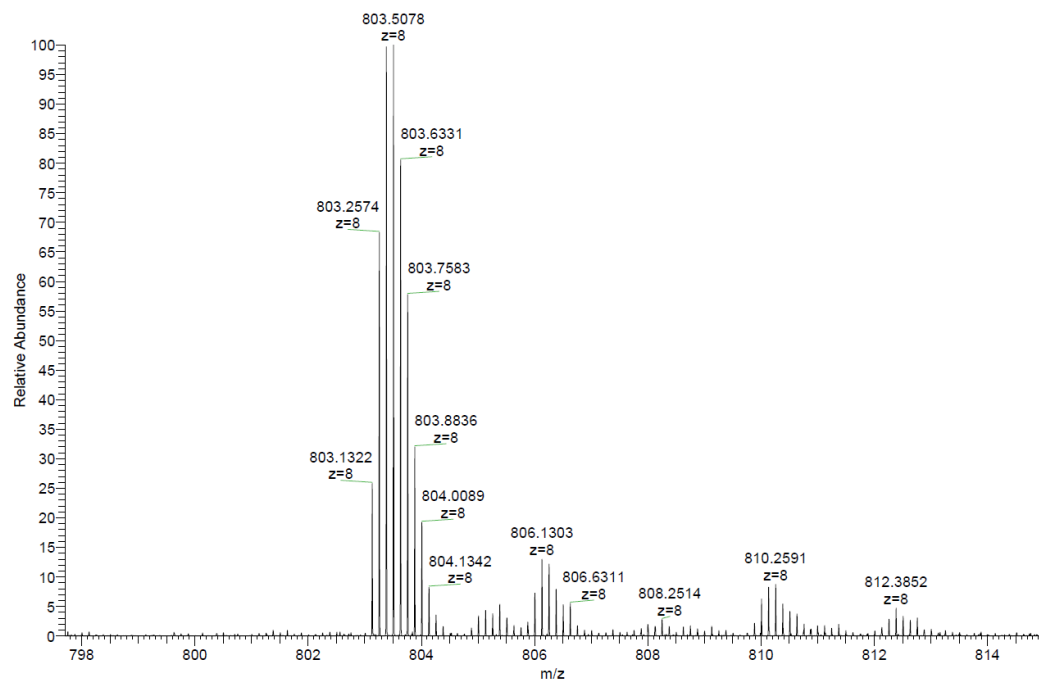
Homo-oligomer **CNSqTr** (ESI-MS: negative mode, MeOH):
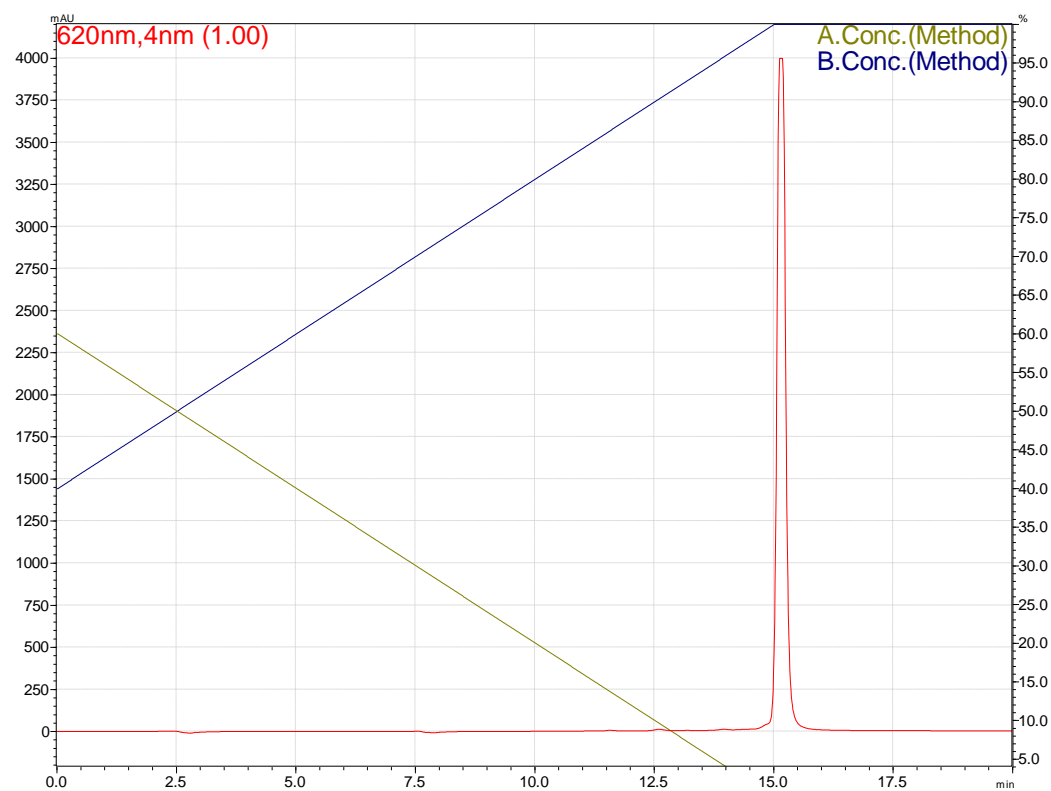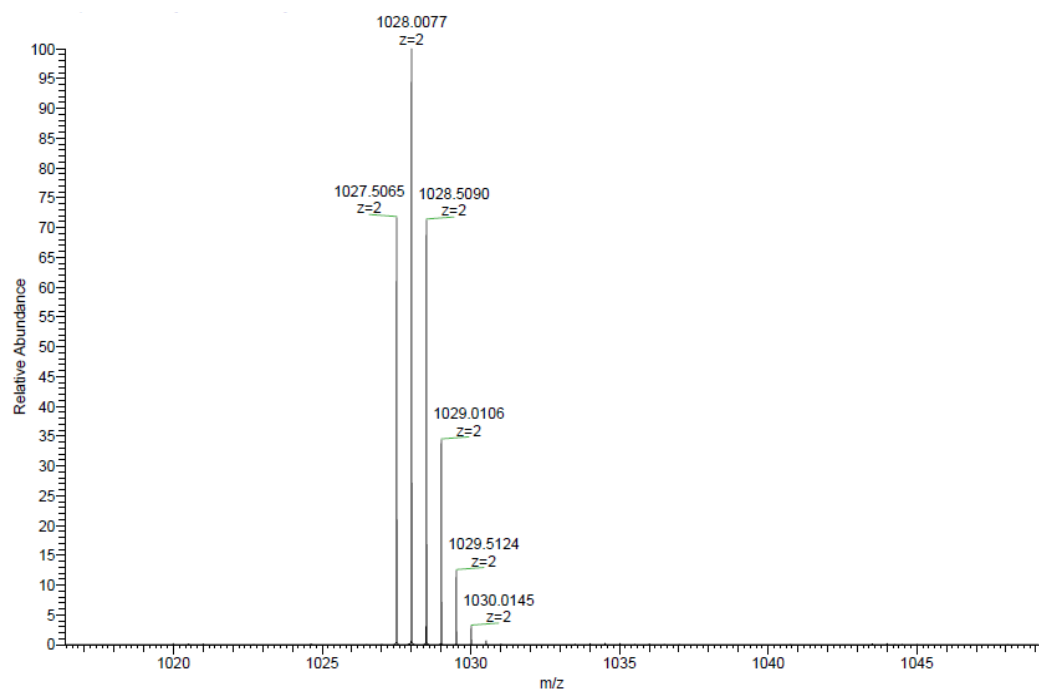
Oligonucleotide **CNSq6** (ESI-MS: negative mode, MeOH):
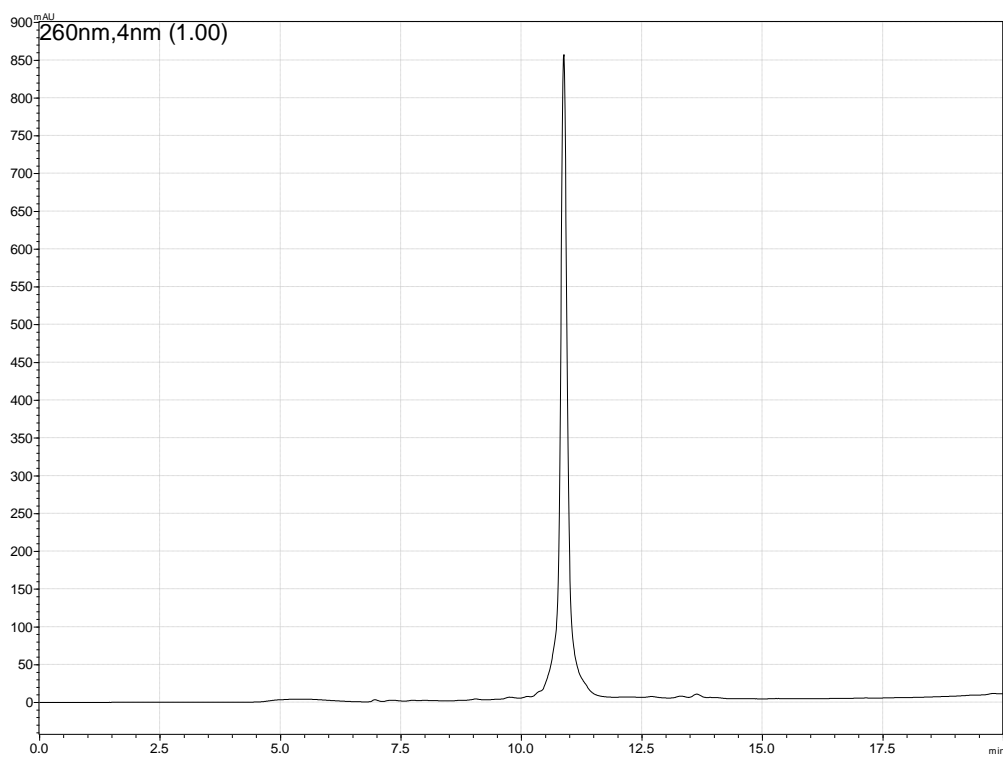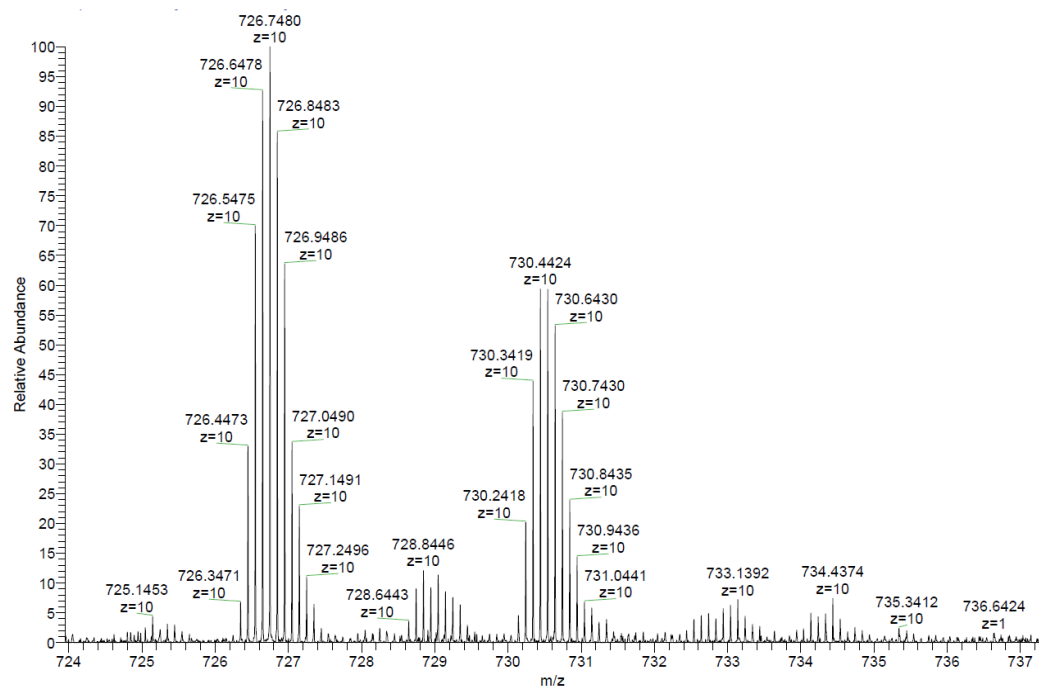
Oligonucleotide **CNOSq** (ESI-MS: negative mode, MeOH):
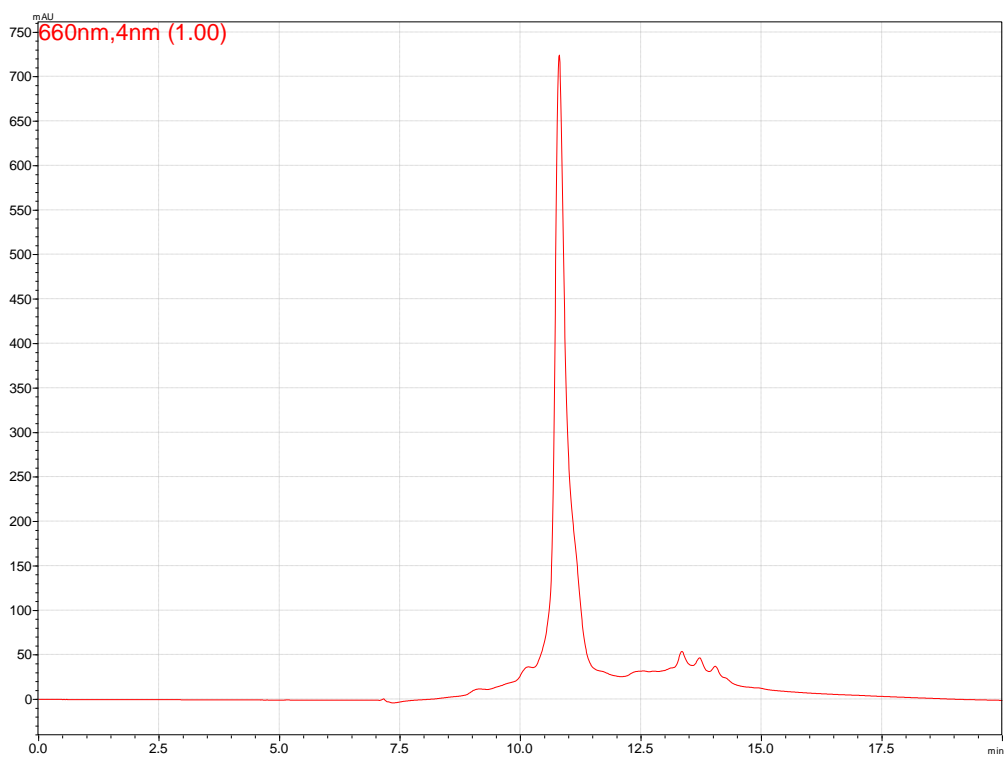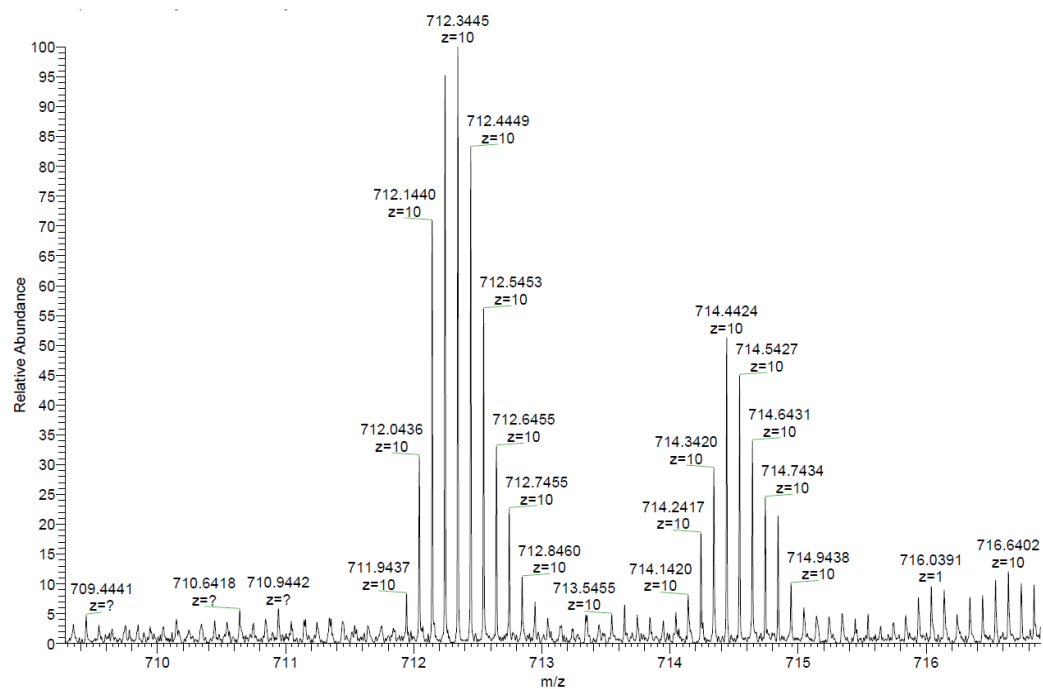
Homo-oligomer **BarbSqTr** (ESI-MS: positive mode, MeOH):
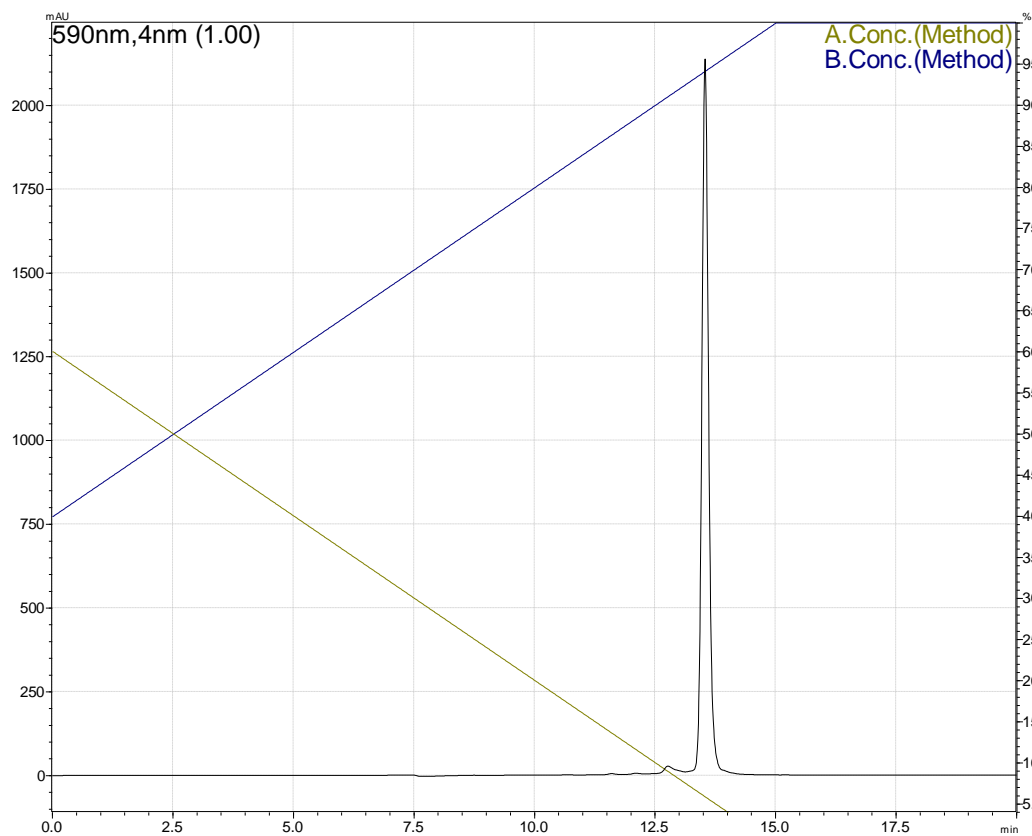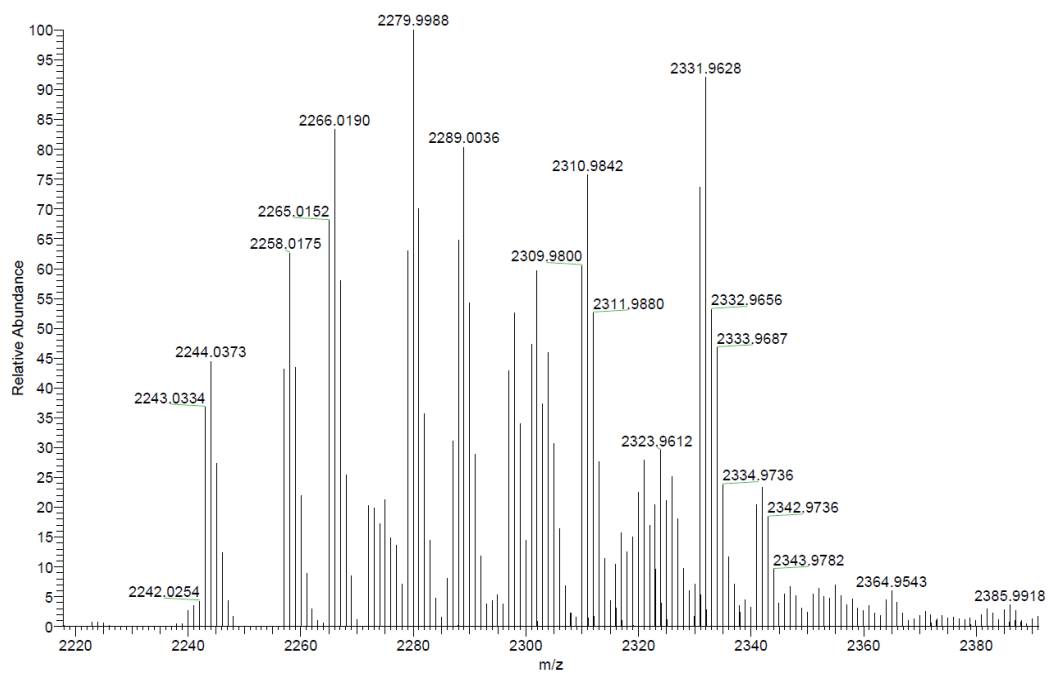
Oligonucleotide **BarbSq6** (ESI-MS: negative mode, MeOH):
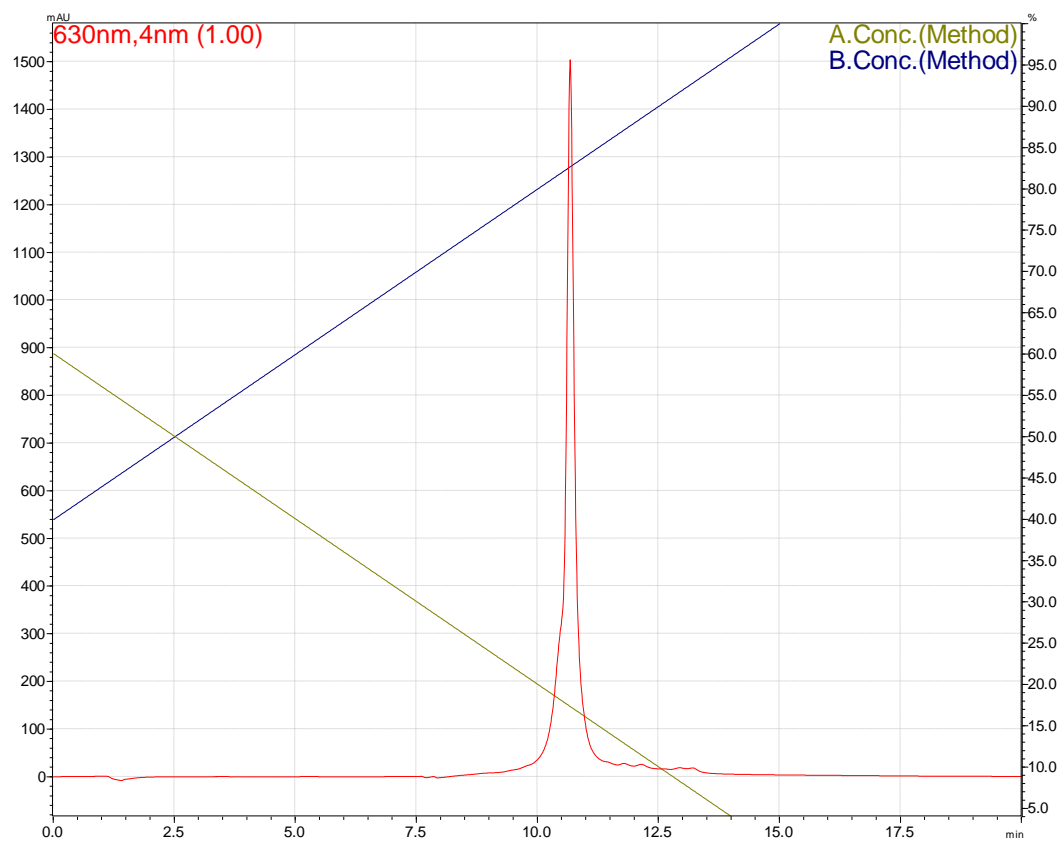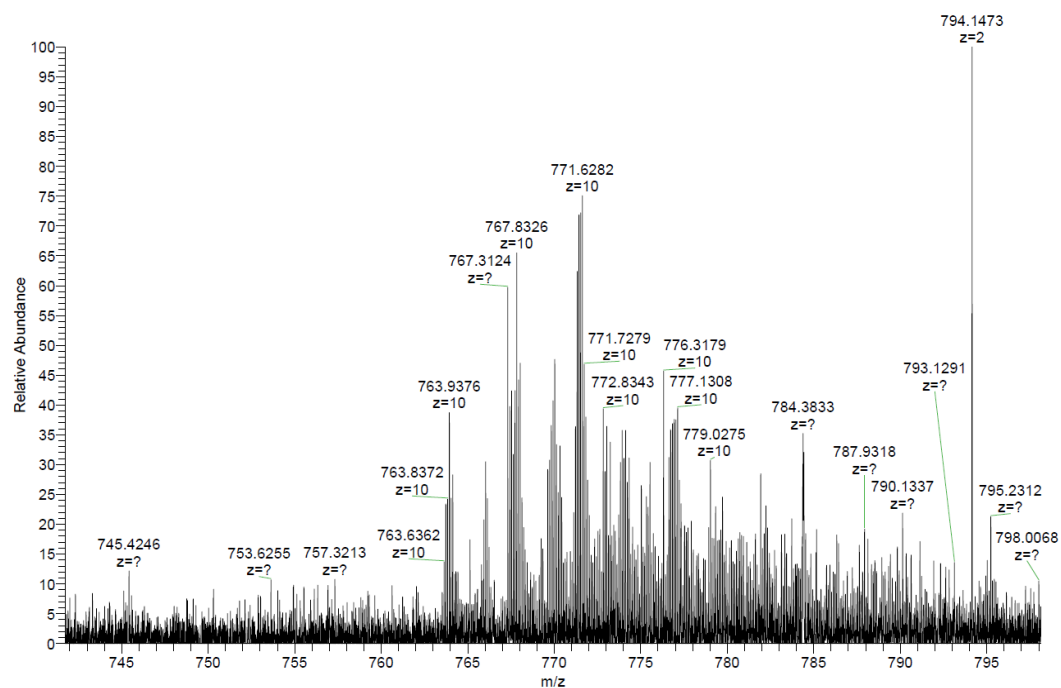
Oligonucleotide **1Cy** (ESI-MS: negative mode, MeOH):
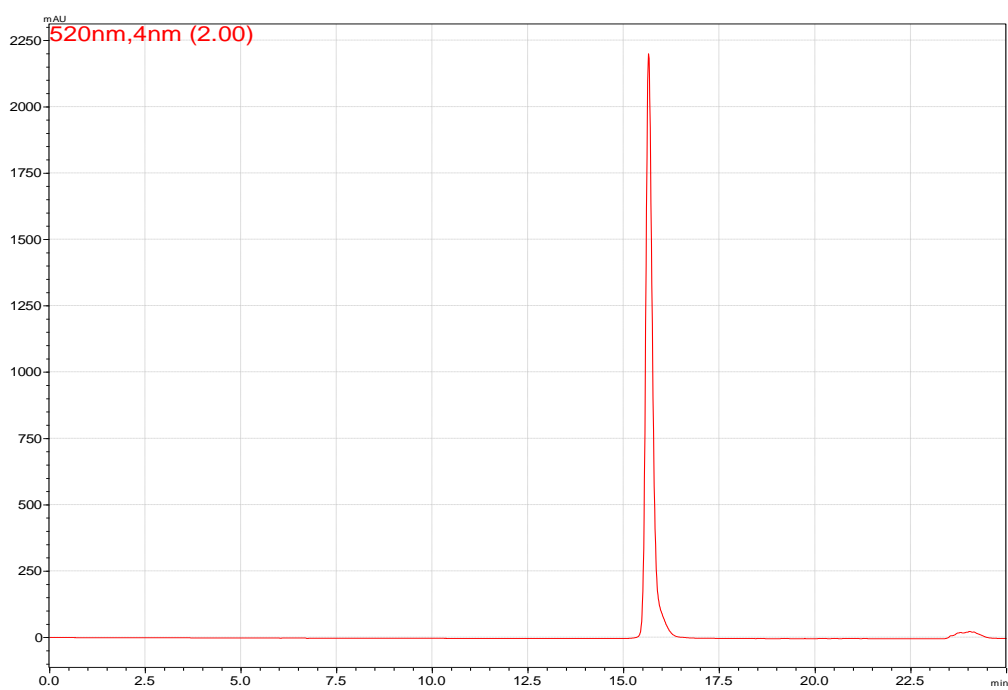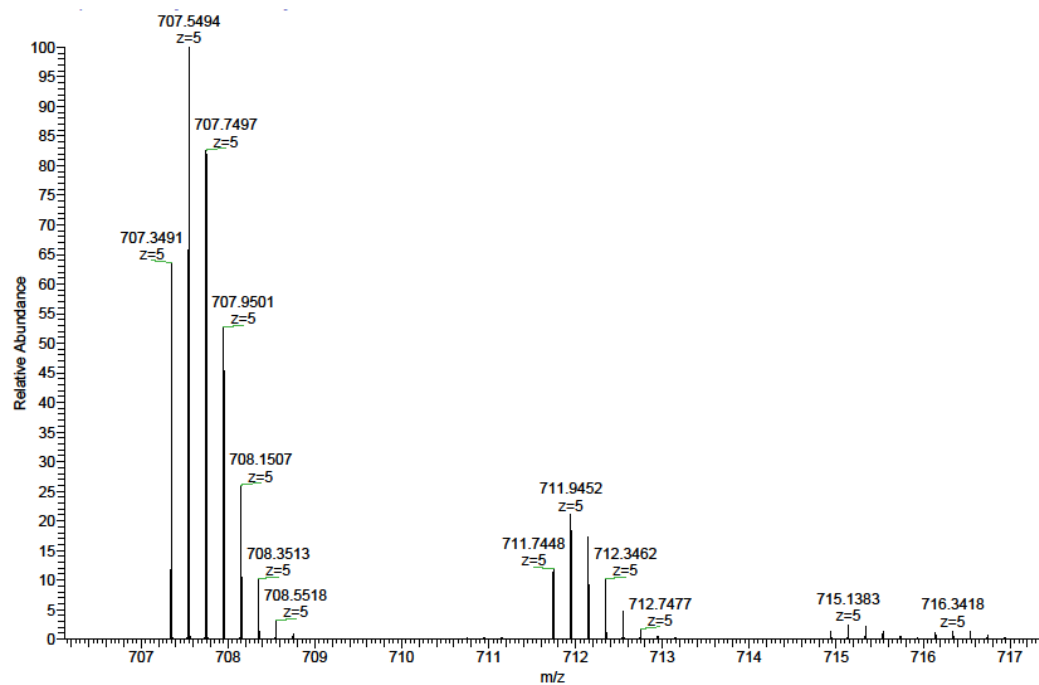
Oligonucleotide **3Cy** (ESI-MS: negative mode, MeOH):
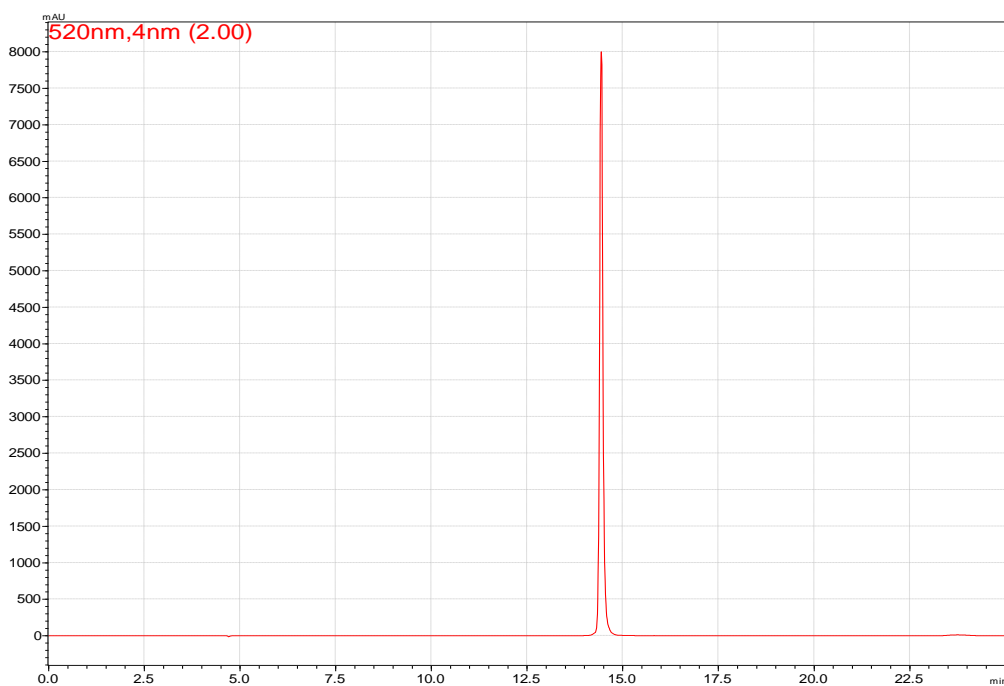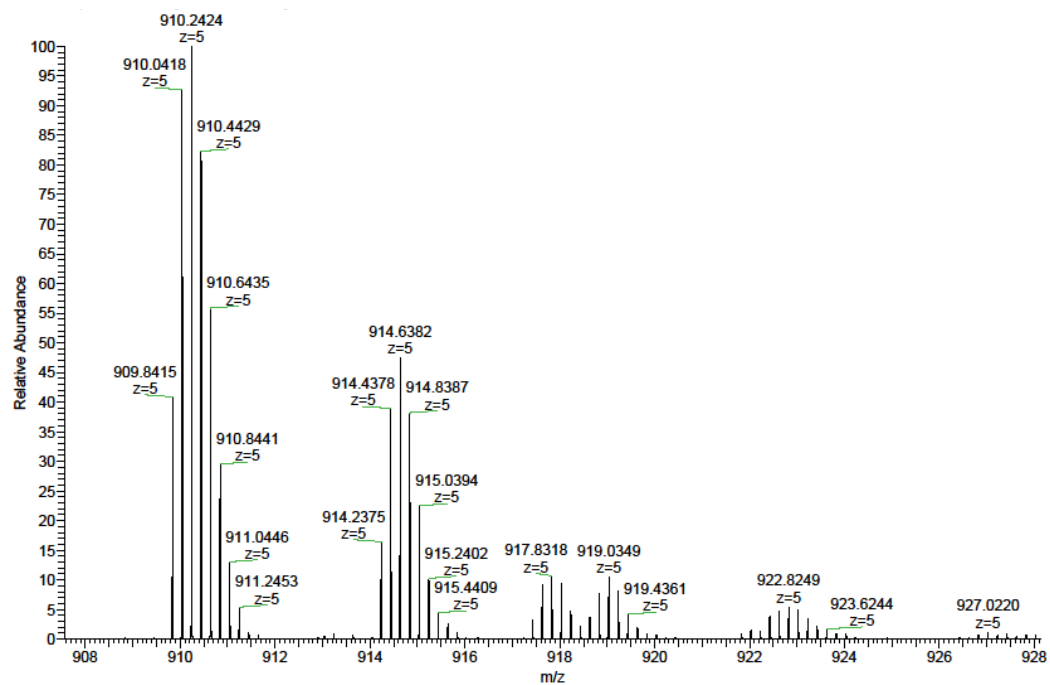
Oligonucleotide **6Cy** (ESI-MS: negative mode, MeOH):
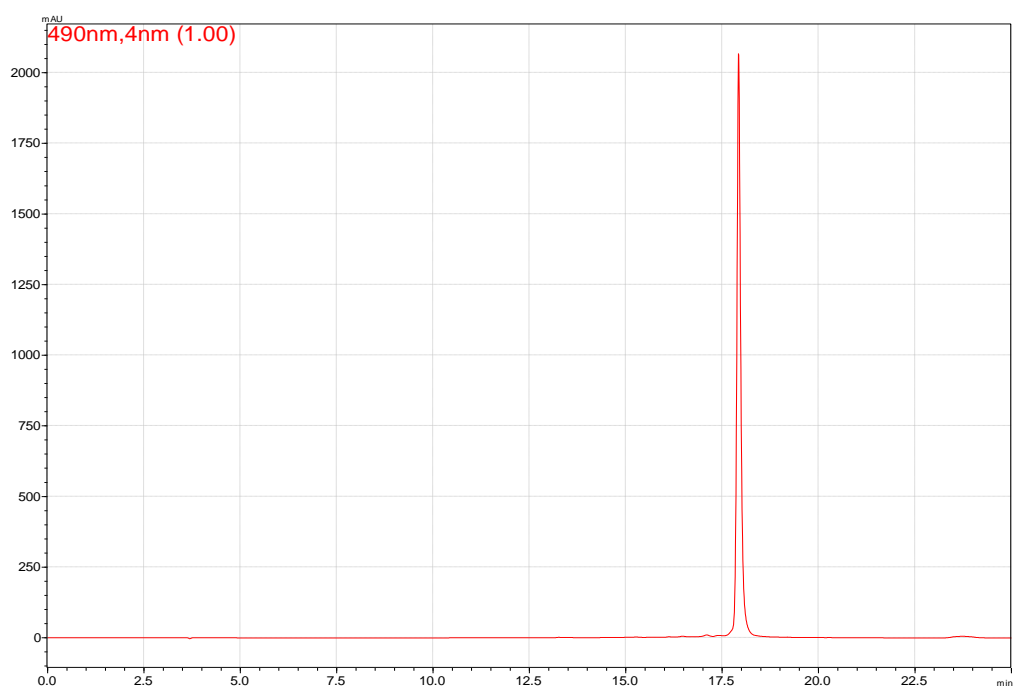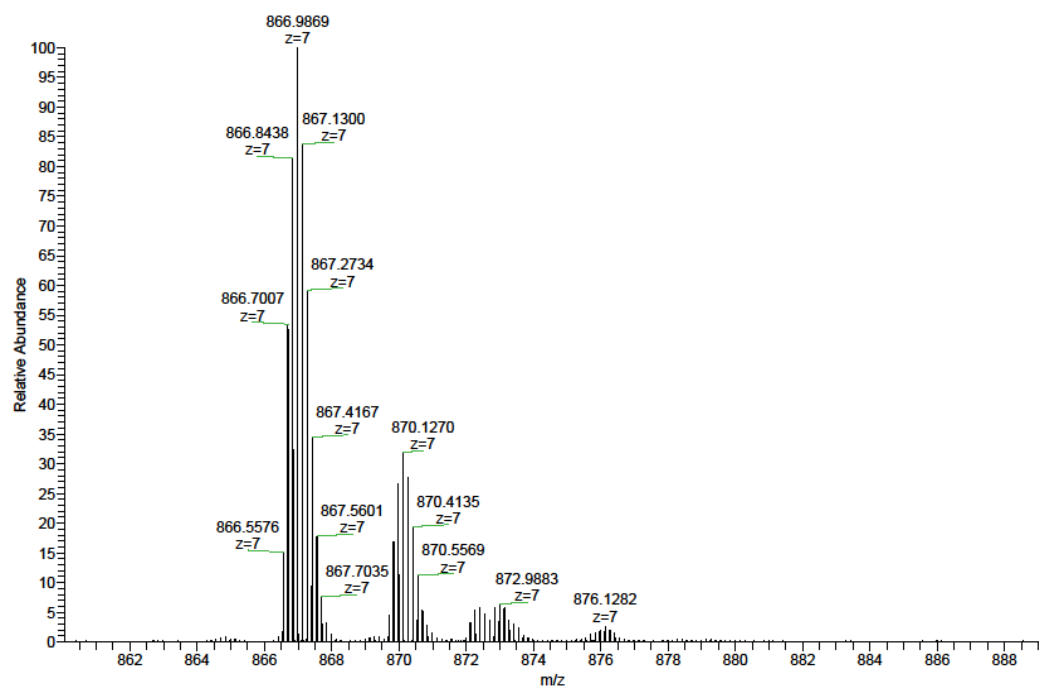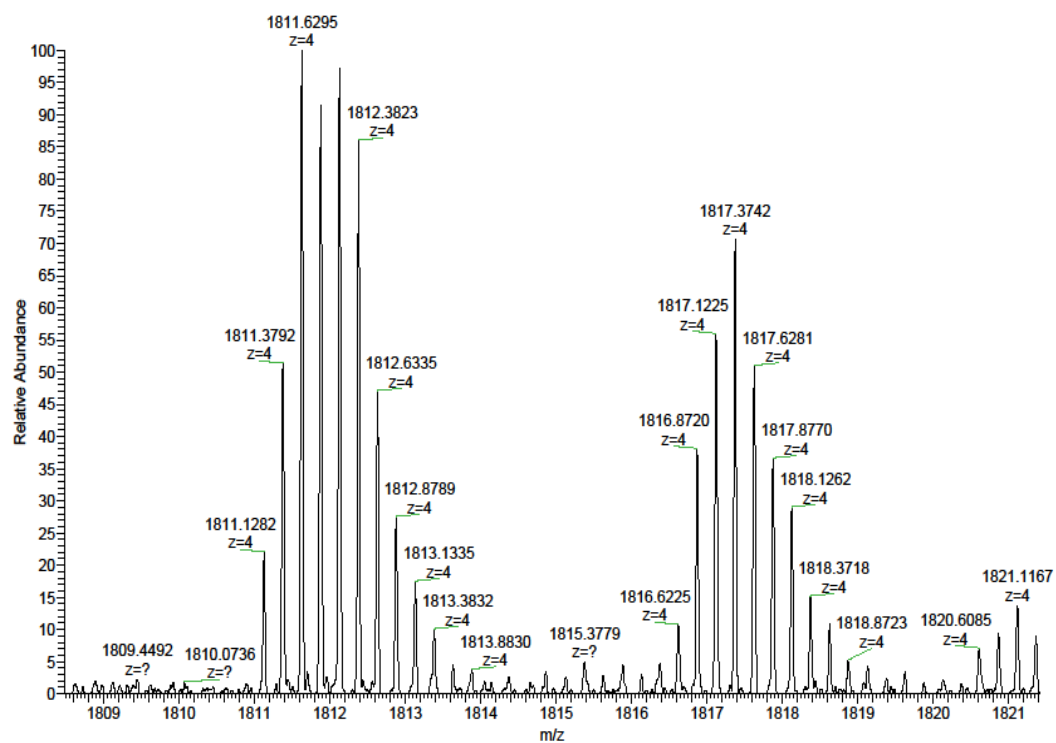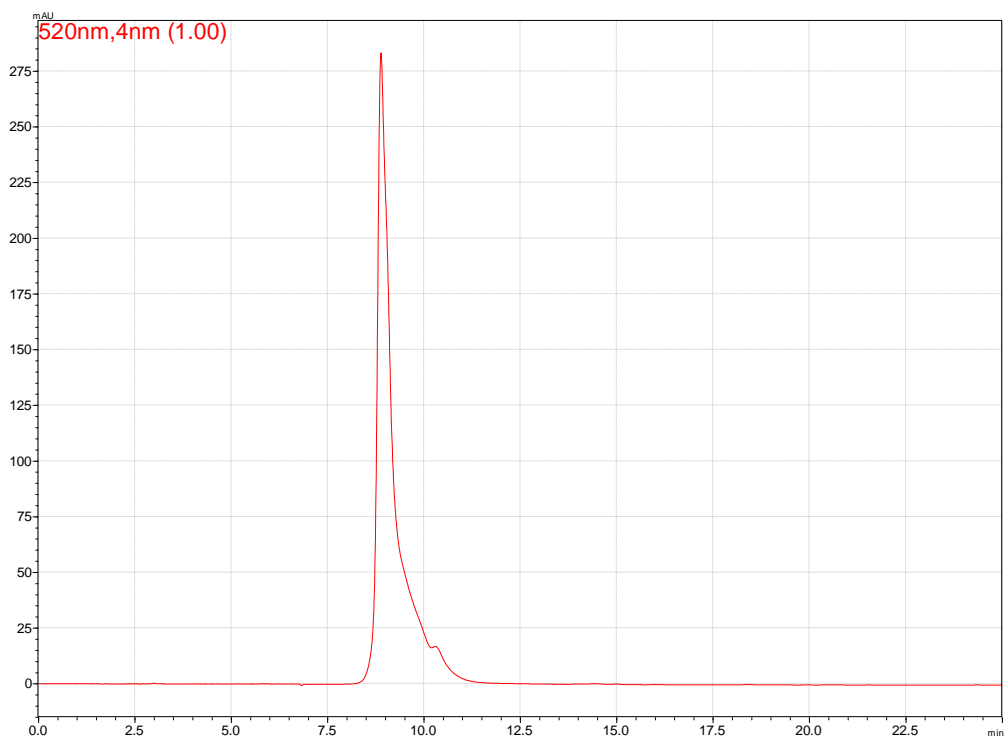
Oligonucleotide **S1** (ESI-MS: negative mode, MeCN/(Et₃NH)OAc):
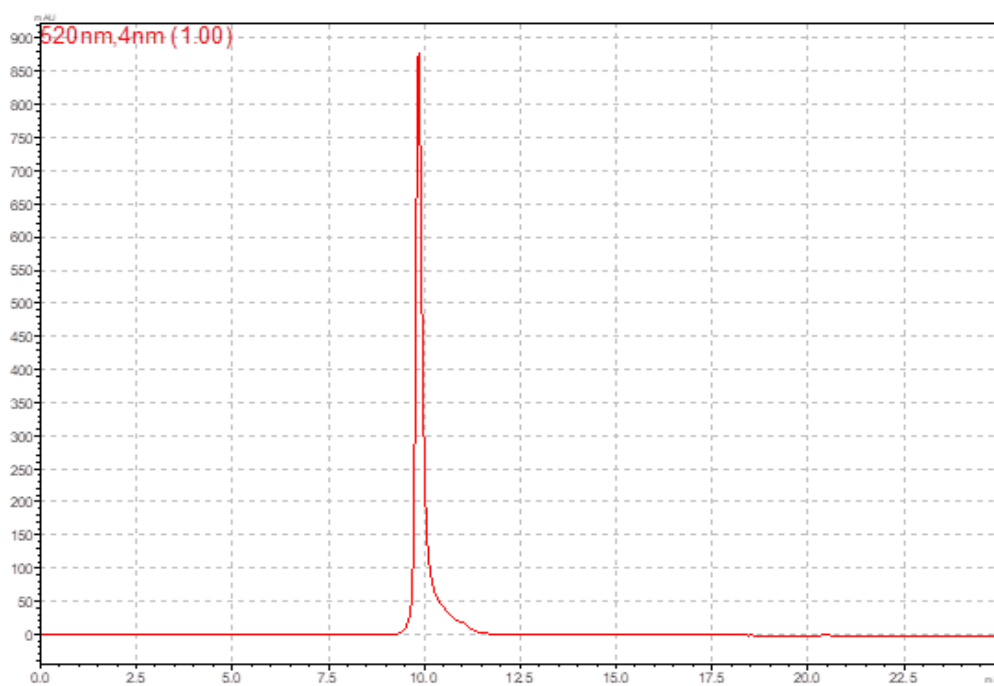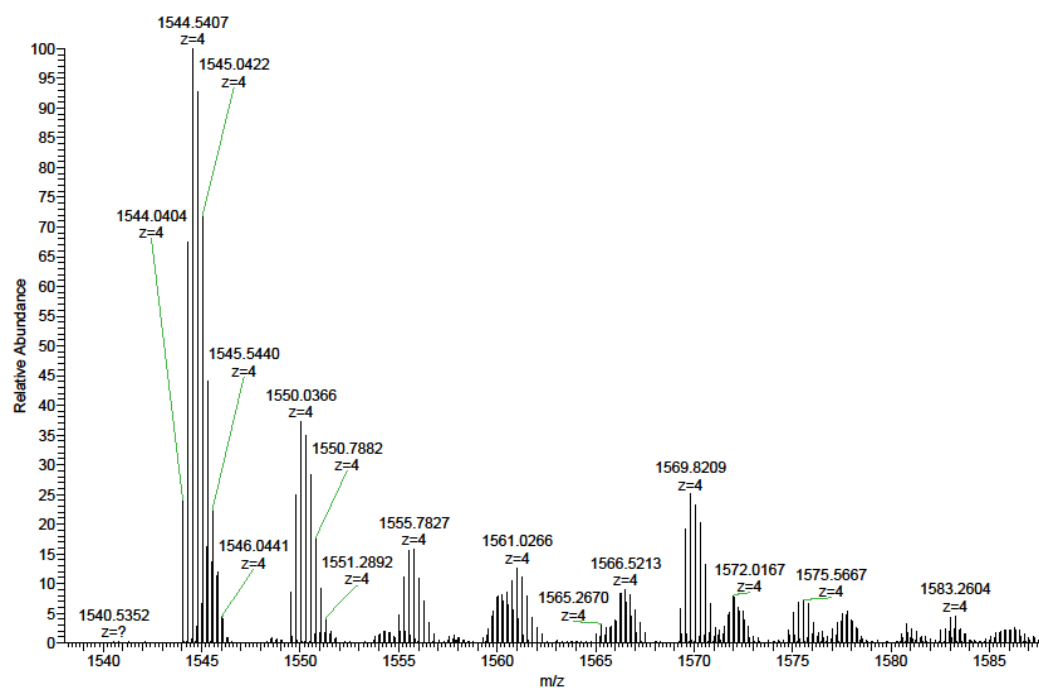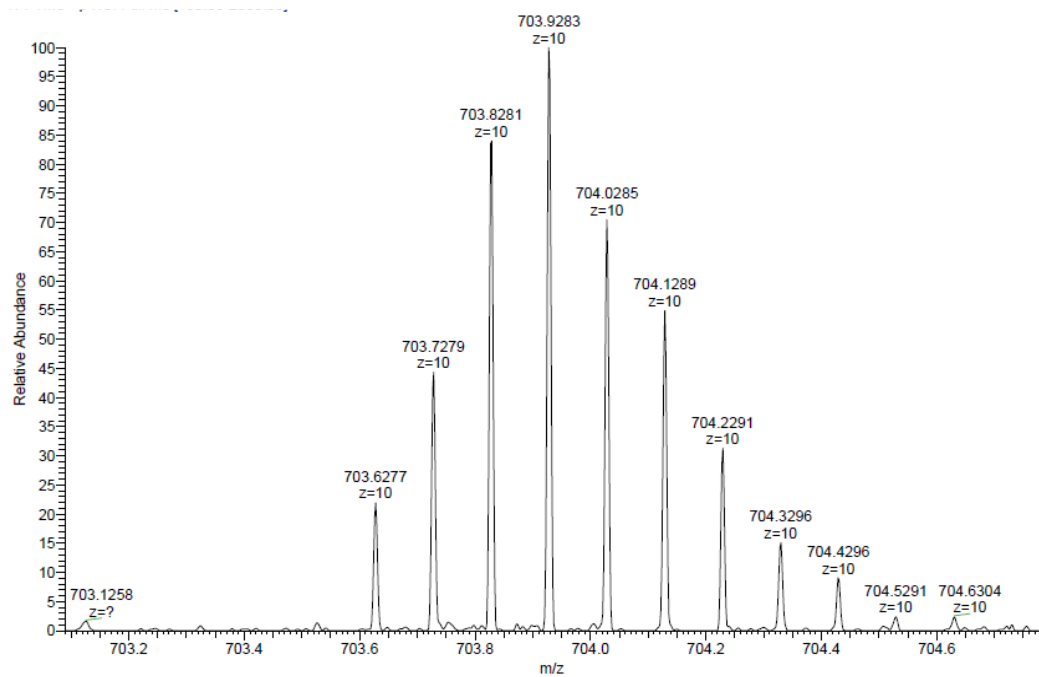
Oligonucleotide **S2** (ESI-MS: negative mode, MeCN/(Et$_3$NH)OAc):
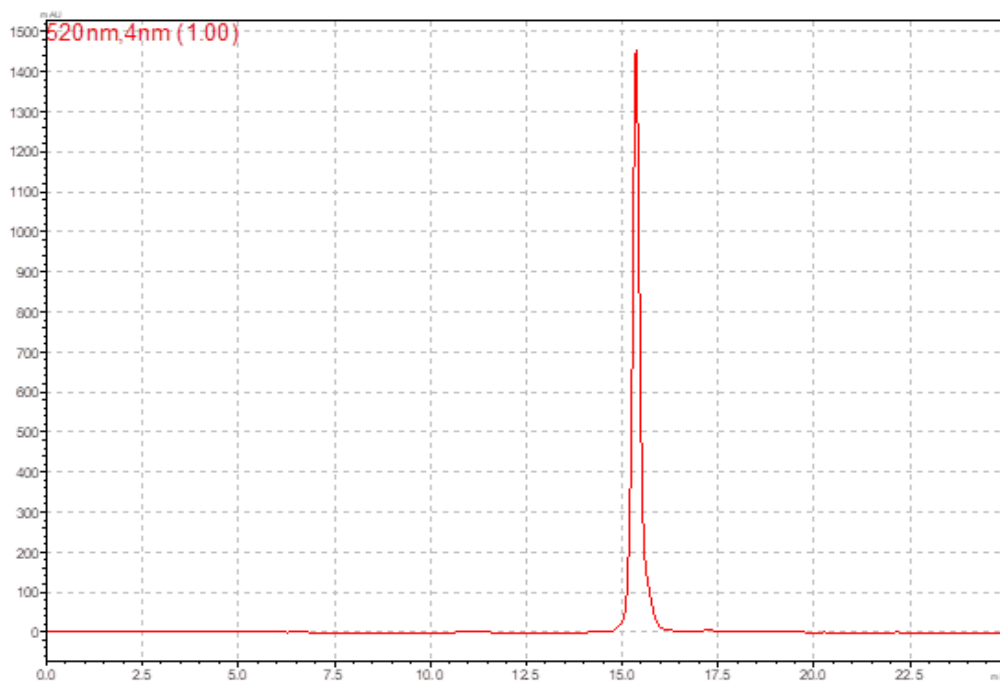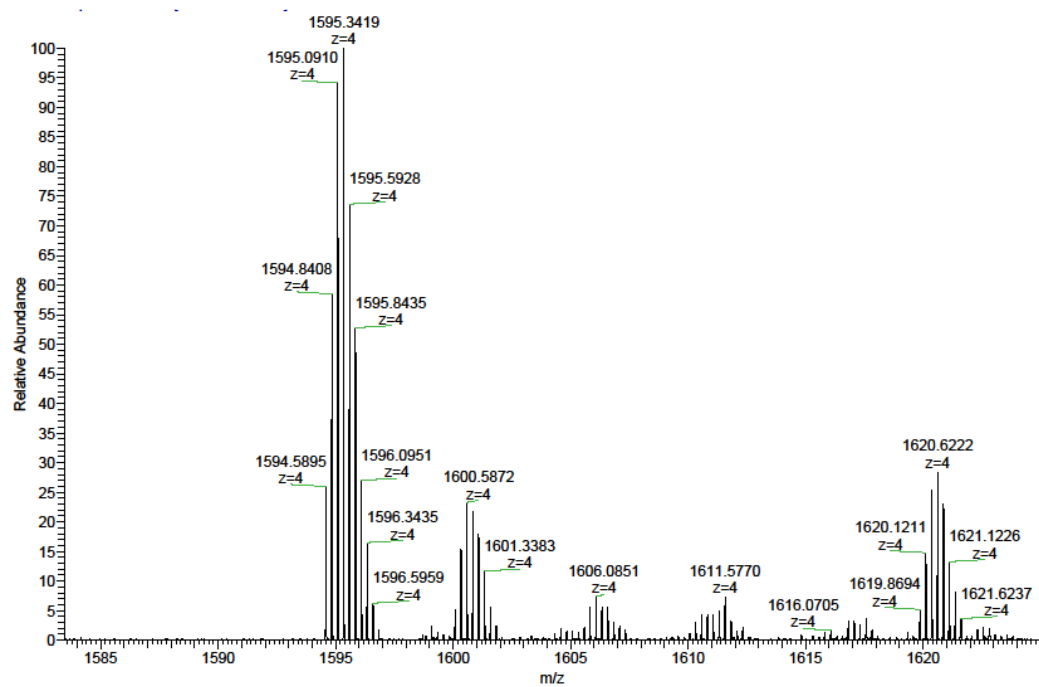
Oligonucleotide **S3** (ESI-MS: negative mode, MeCN/(Et₃NH)OAc):
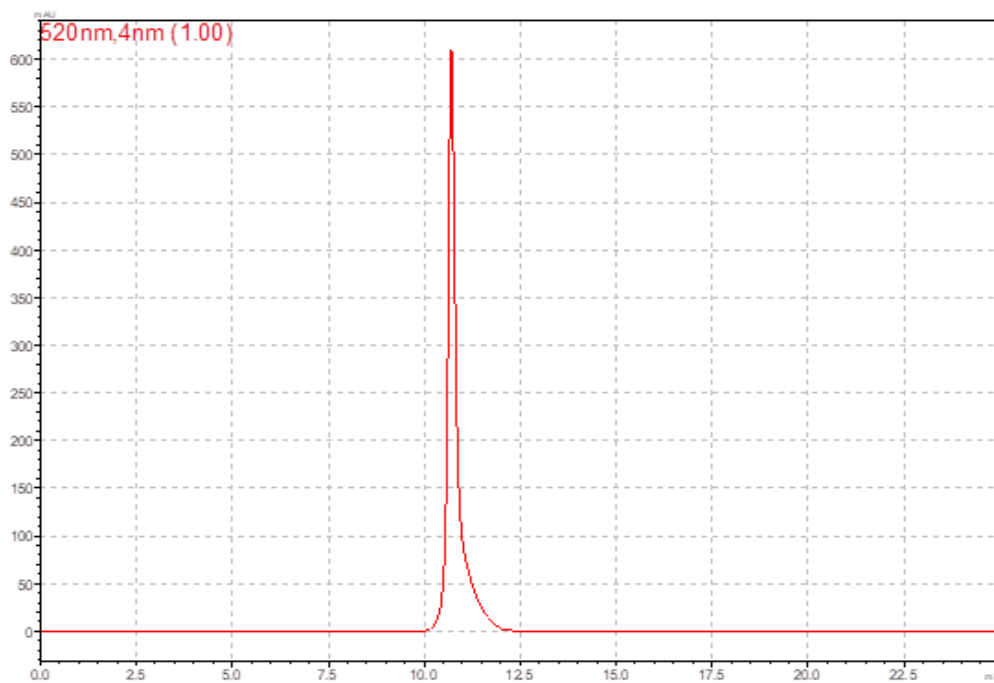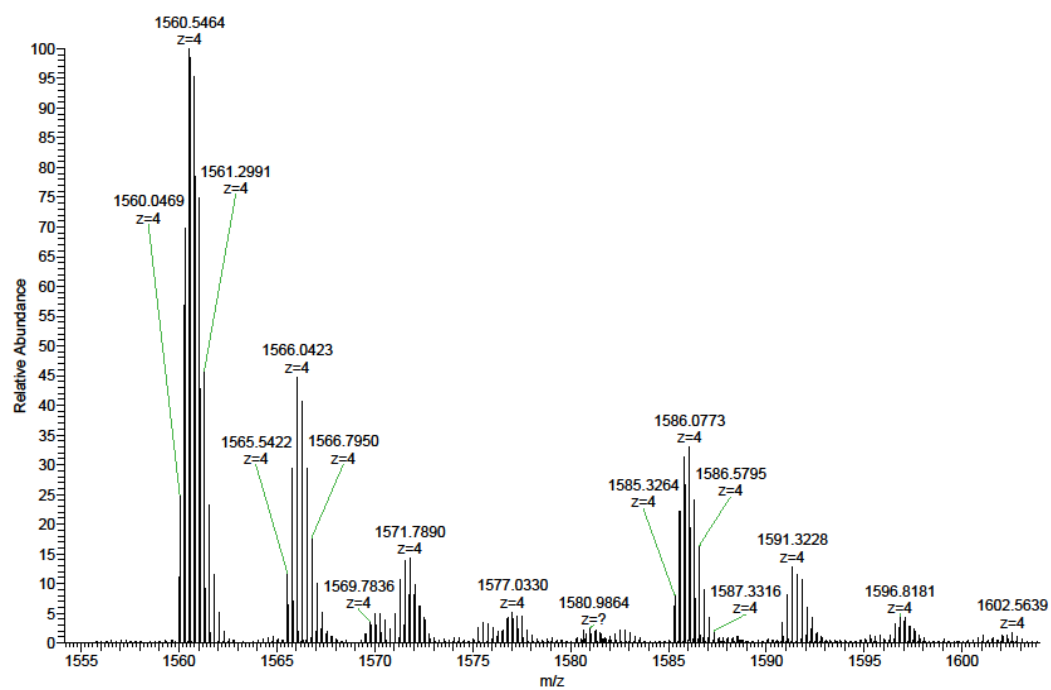
Oligonucleotide **S4** (ESI-MS: negative mode, MeCN/(Et₃NH)OAc):
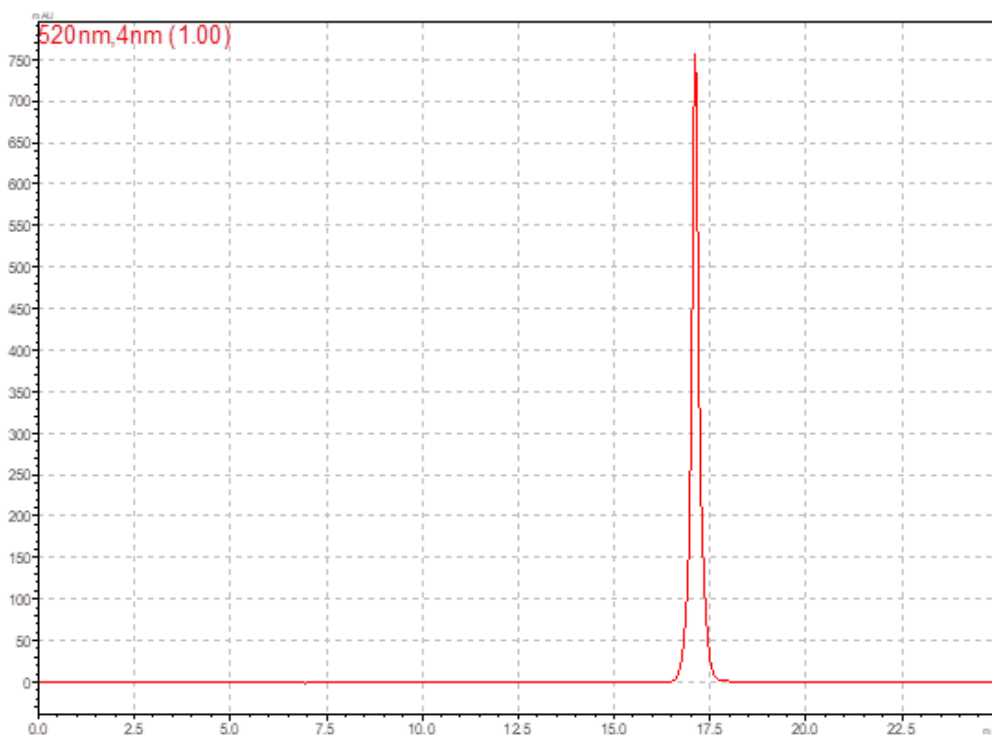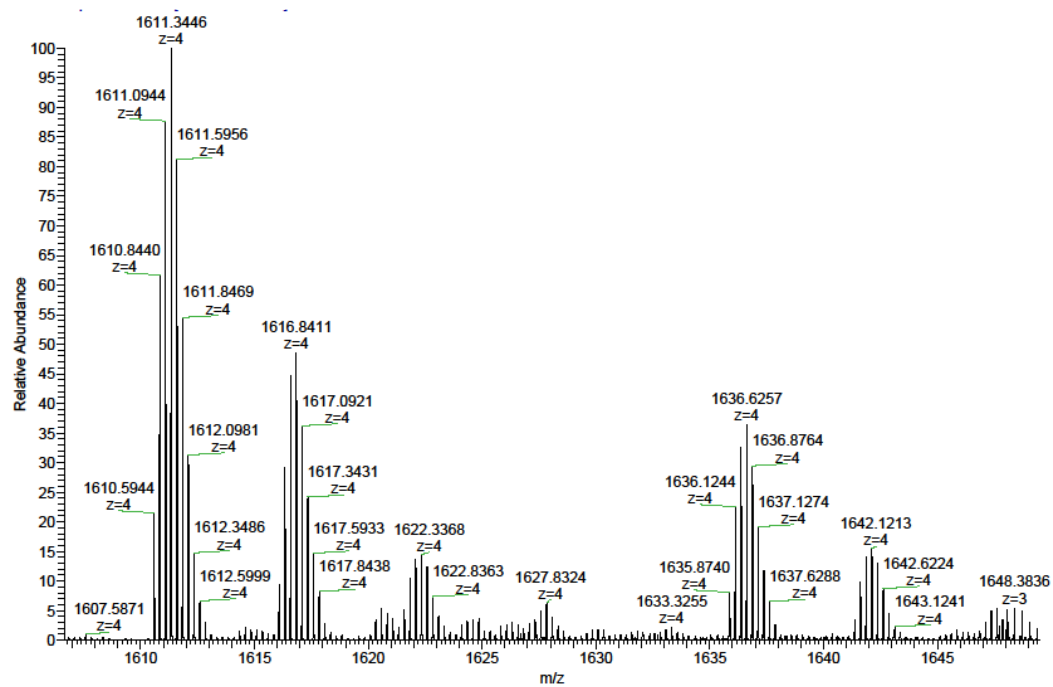
Oligonucleotide **S5** (ESI-MS: negative mode, MeCN/(Et$_3$NH)OAc):
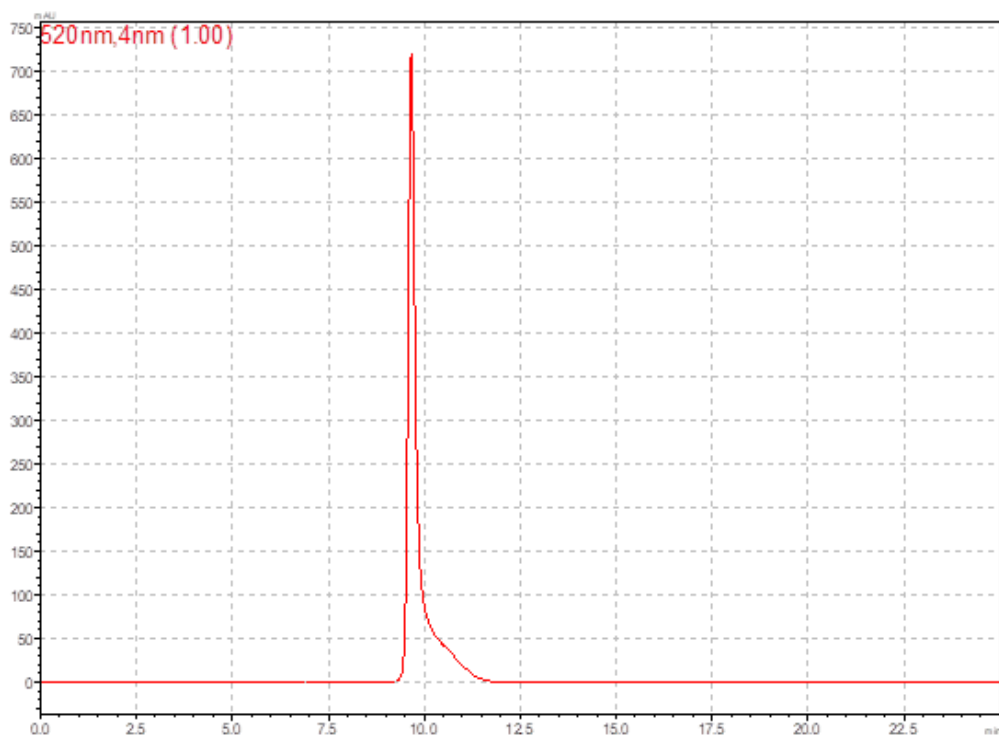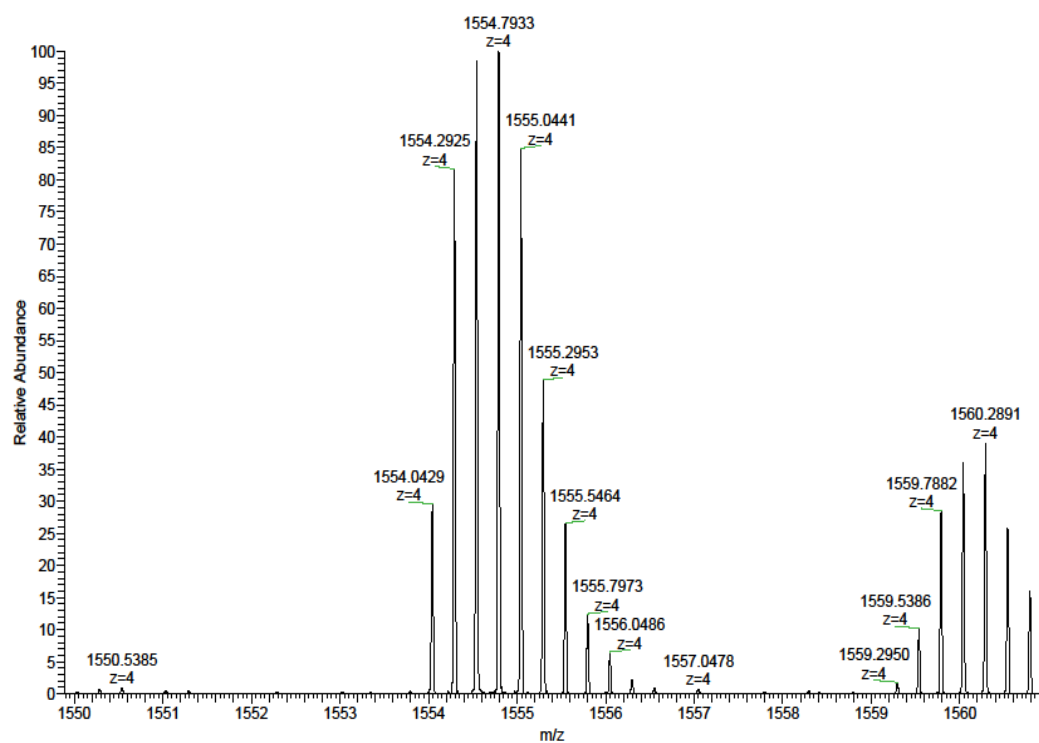
Oligonucleotide **S6** (ESI-MS: negative mode, MeCN/(Et₃NH)OAc):
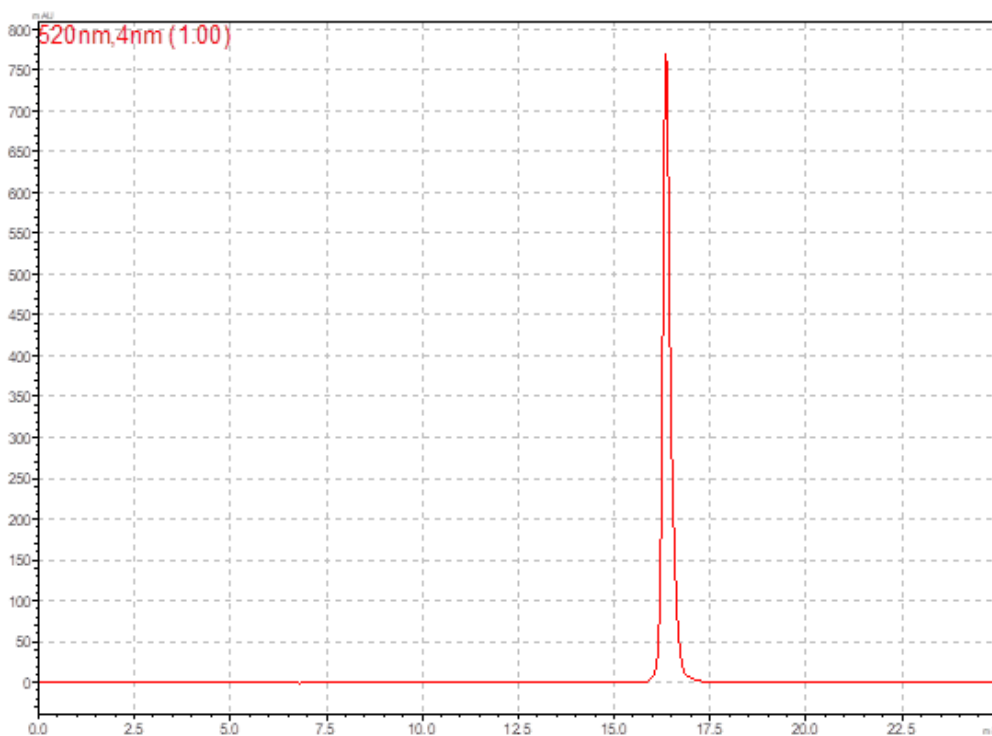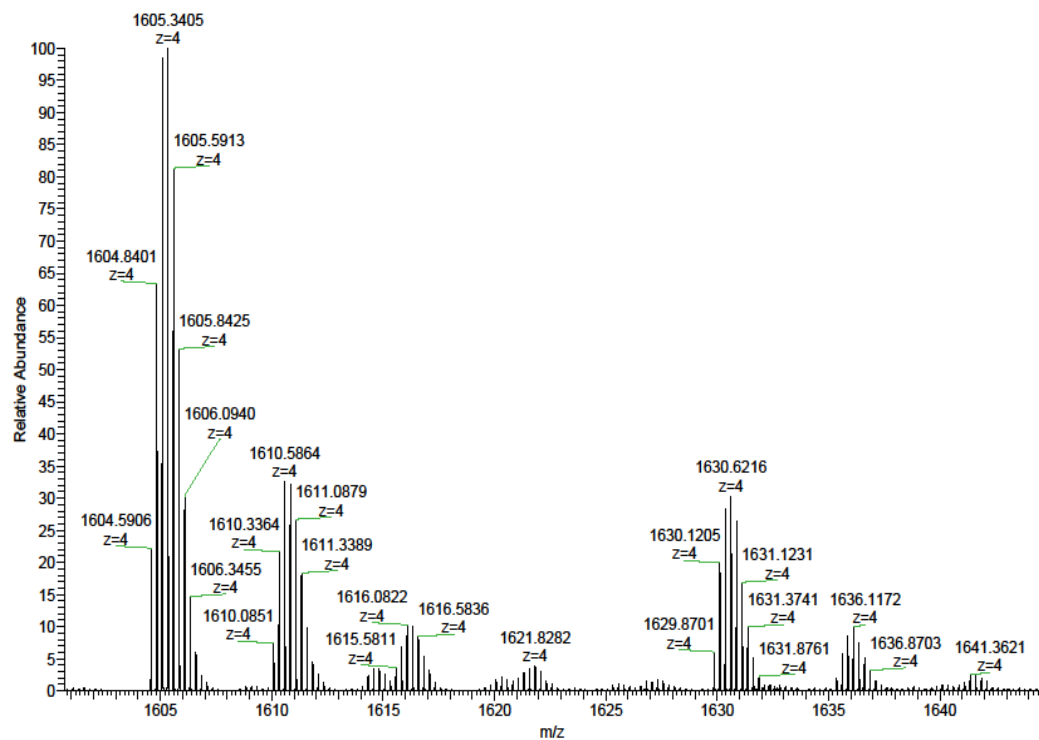
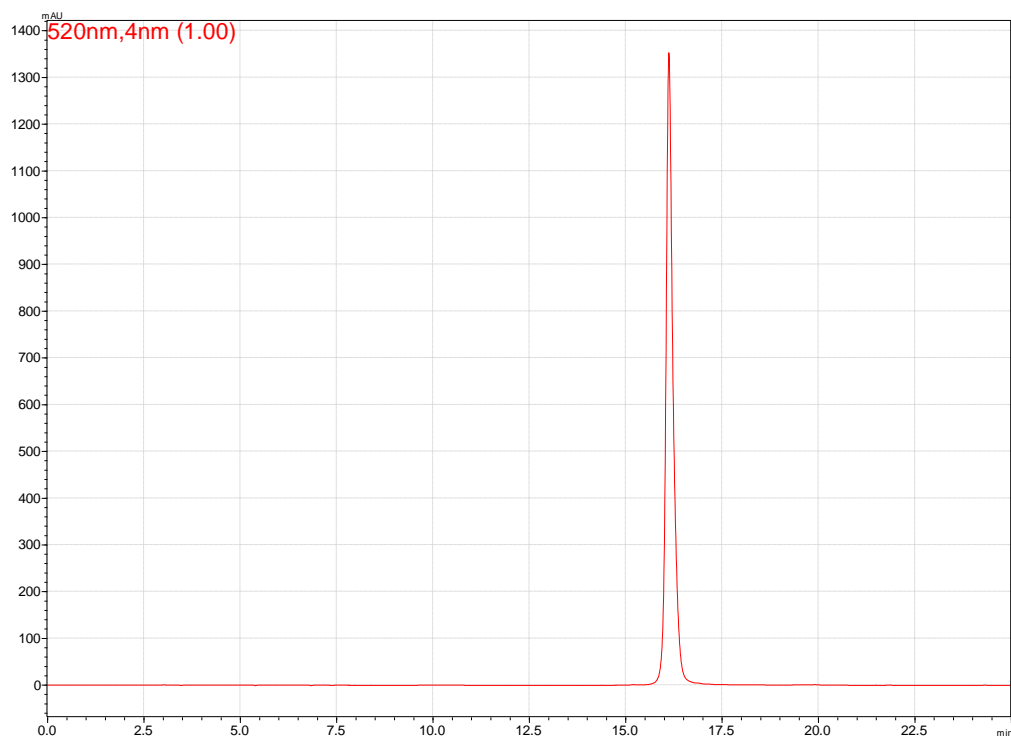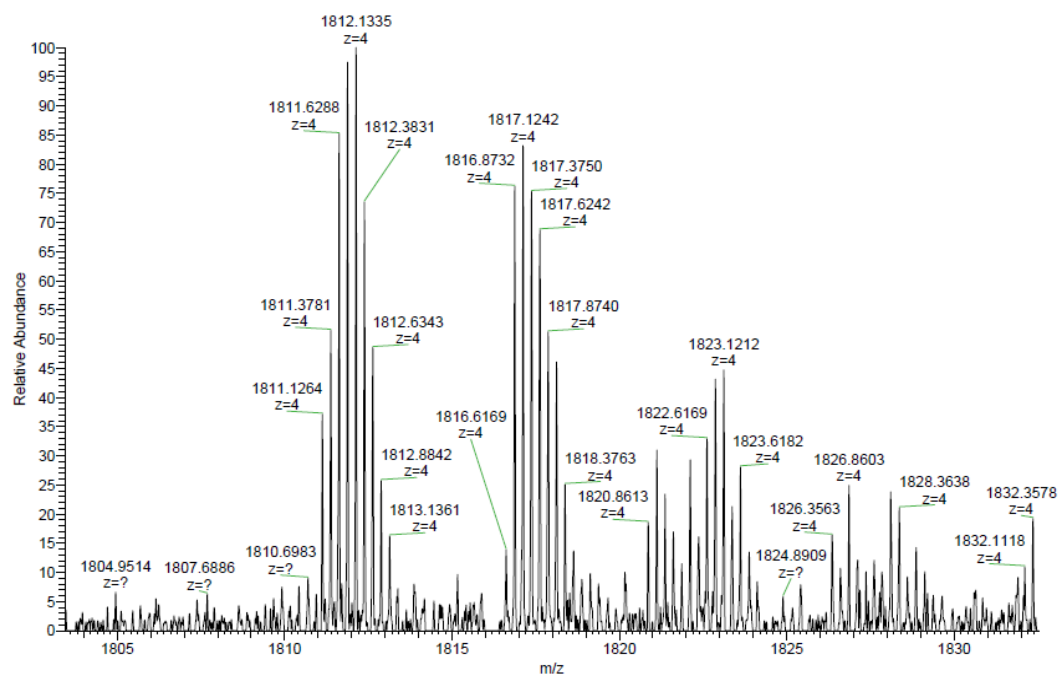Oligonucleotide **S7** (ESI-MS: negative mode, MeCN/(Et₃NH)OAc):
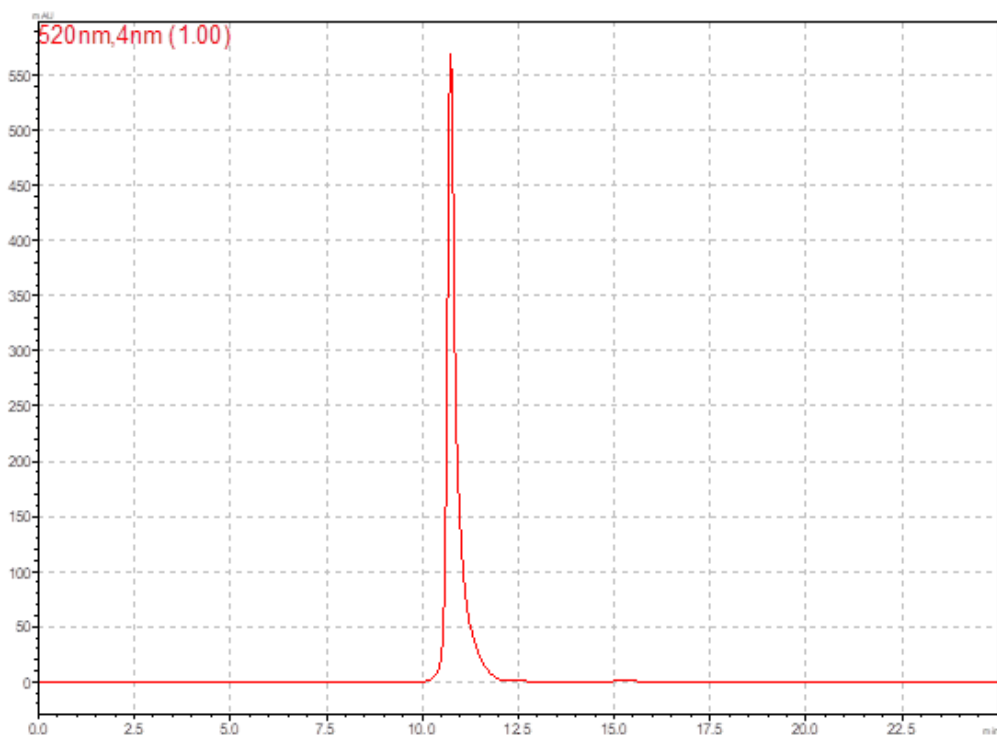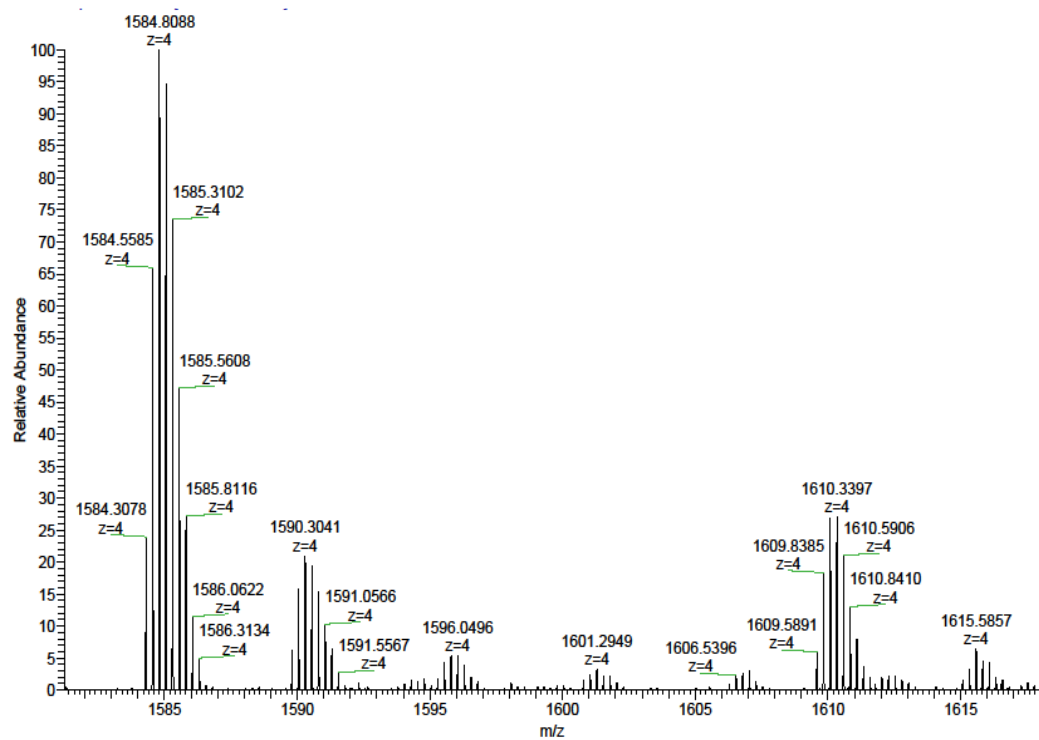
Oligonucleotide **S8** (ESI-MS: negative mode, MeCN/(Et$_3$NH)OAc):
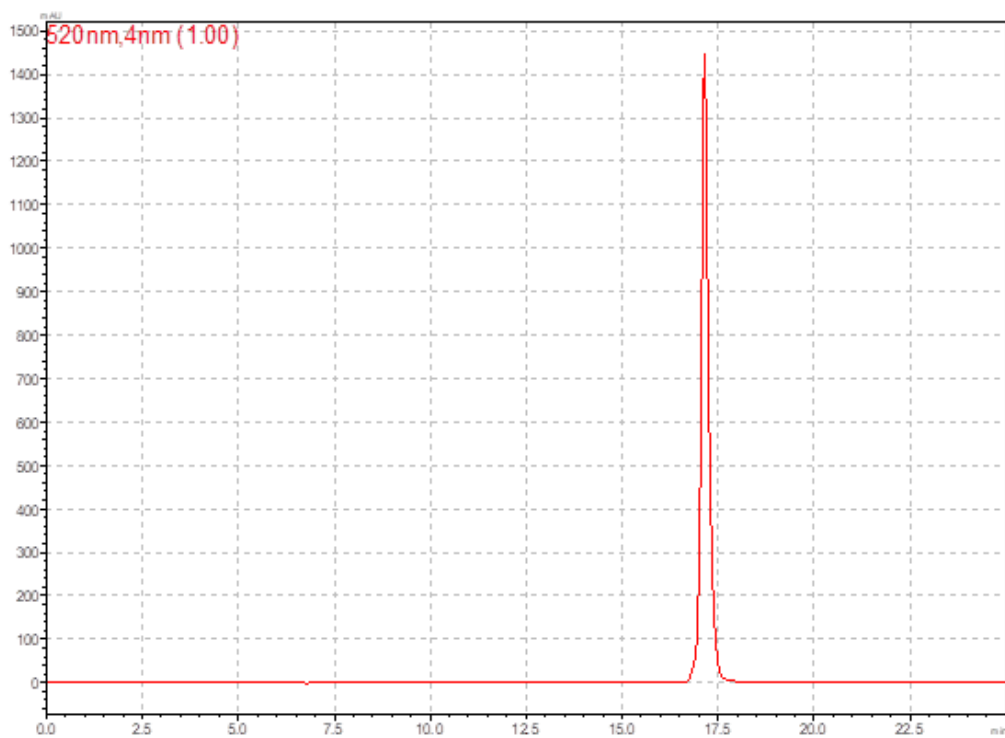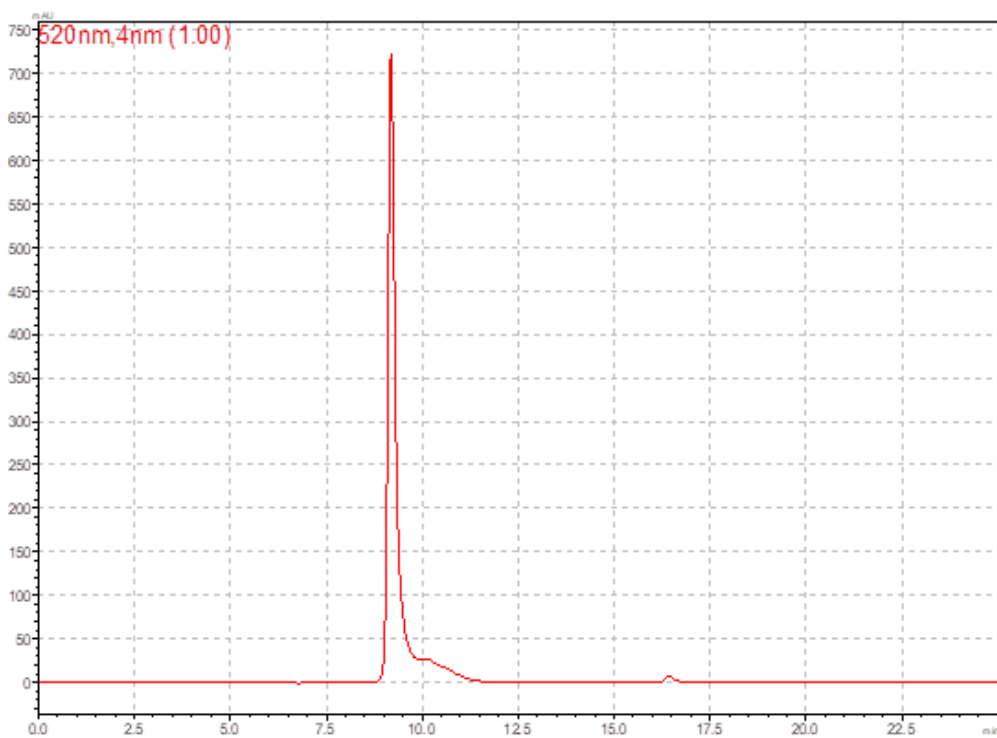
Oligonucleotide **S9** (ESI-MS: negative mode, MeCN/(Et₃NH)OAc):
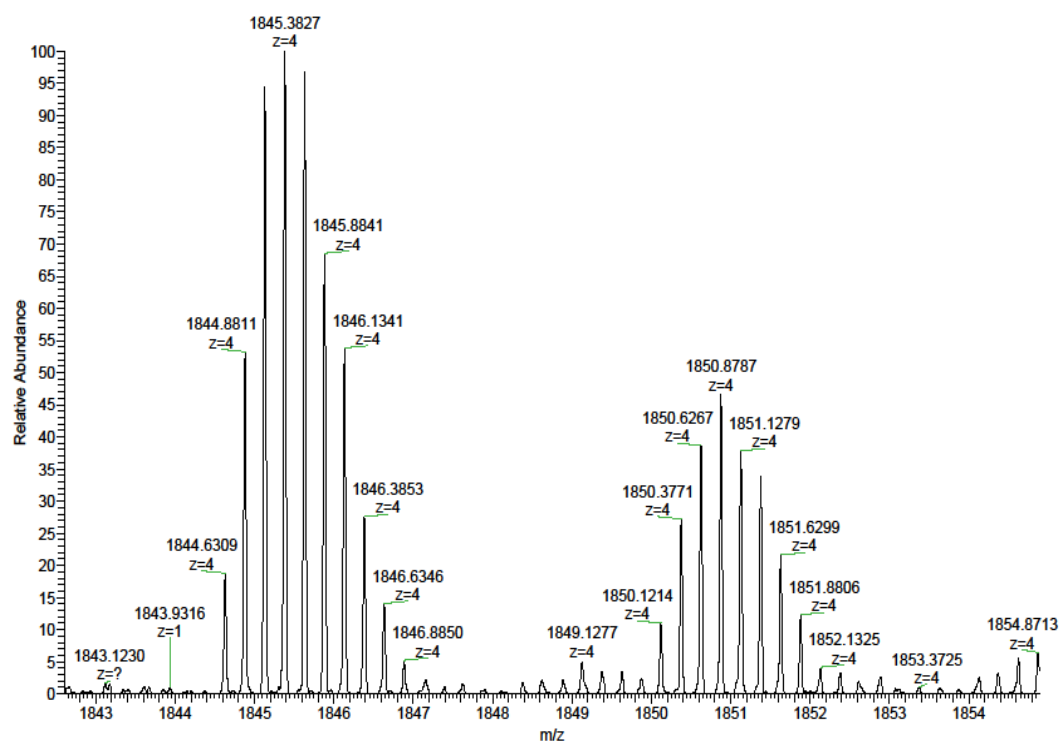
Oligonucleotide **S10** (ESI-MS: negative mode, MeCN/(Et₃NH)OAc):
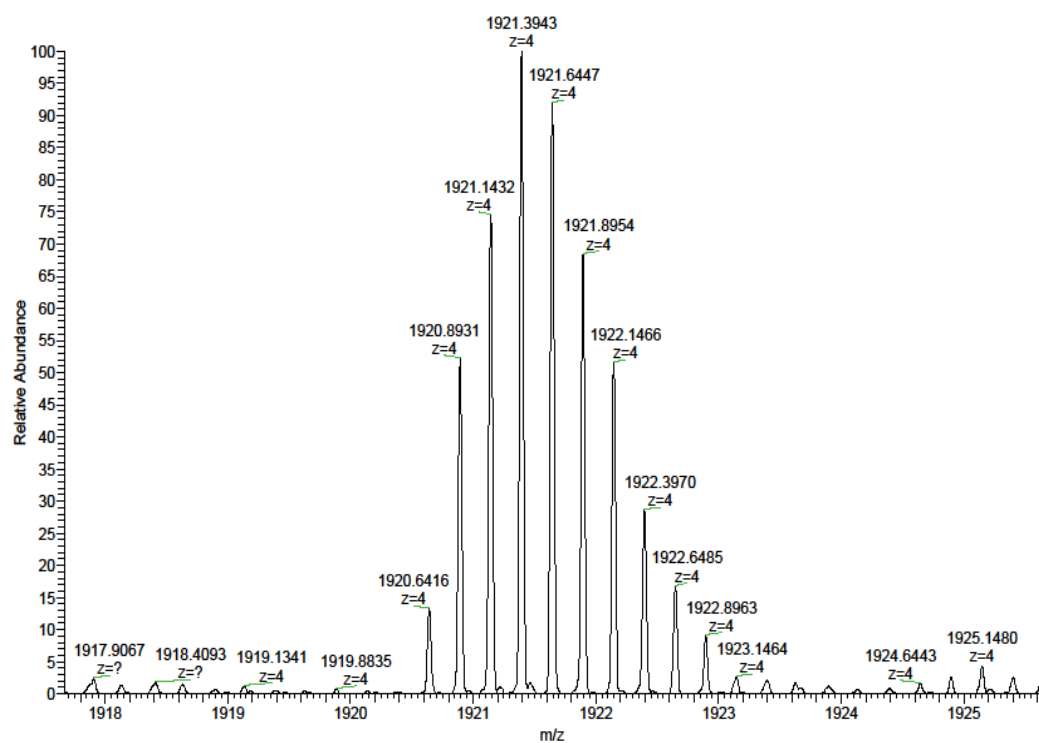
Oligonucleotide **S11** (ESI-MS: negative mode, MeCN/(Et₃NH)OAc):
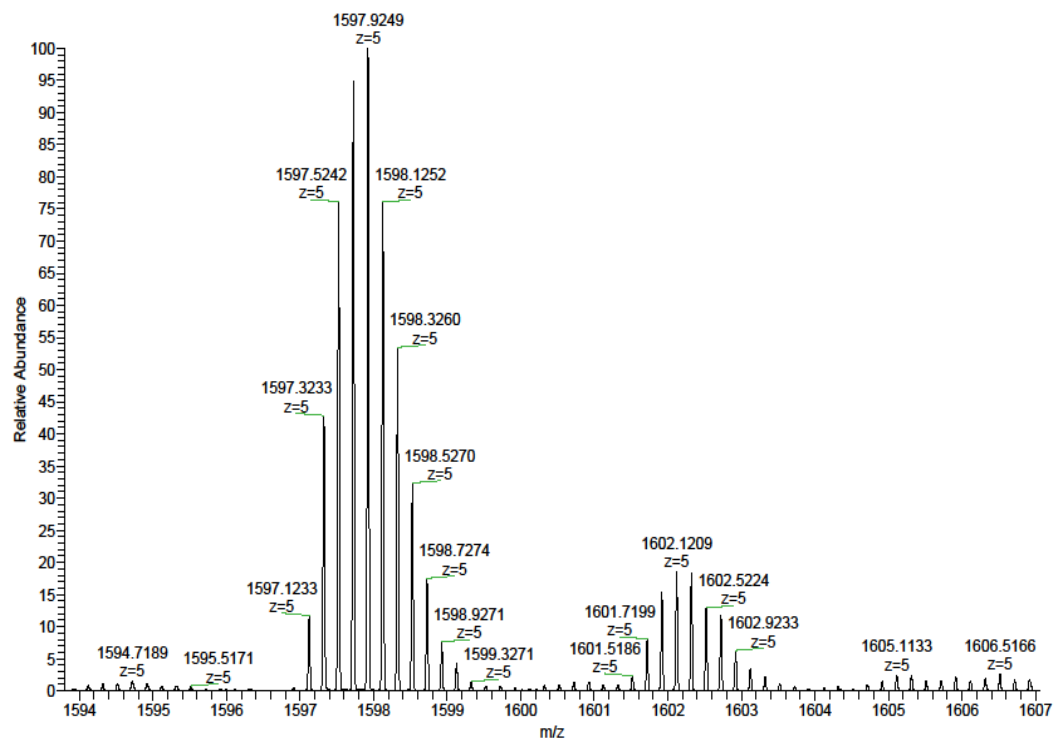
Oligonucleotide **S12** (ESI-MS: negative mode, MeCN/(Et₃NH)OAc):
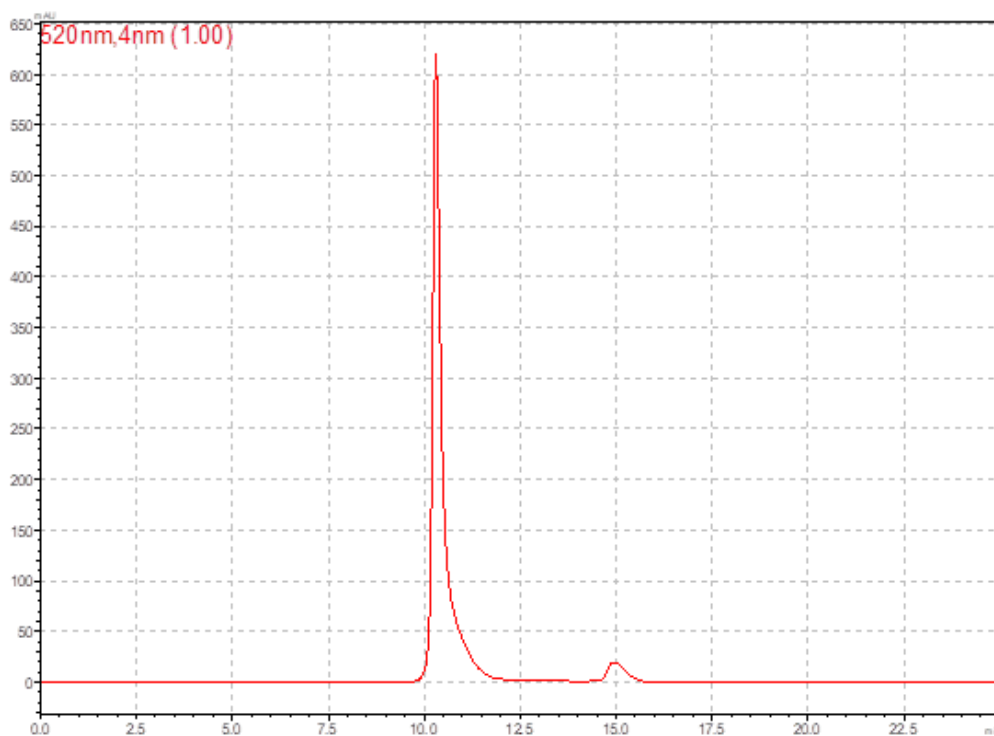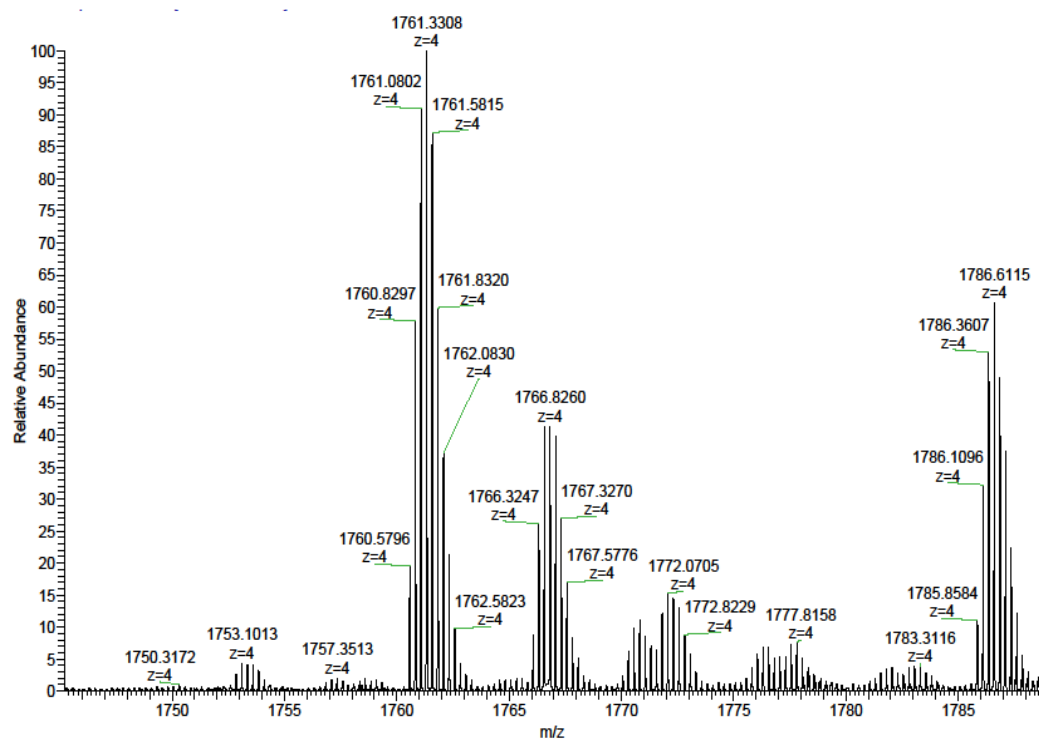
Oligonucleotide **S13** (ESI-MS: negative mode, MeCN/(Et₃NH)OAc):
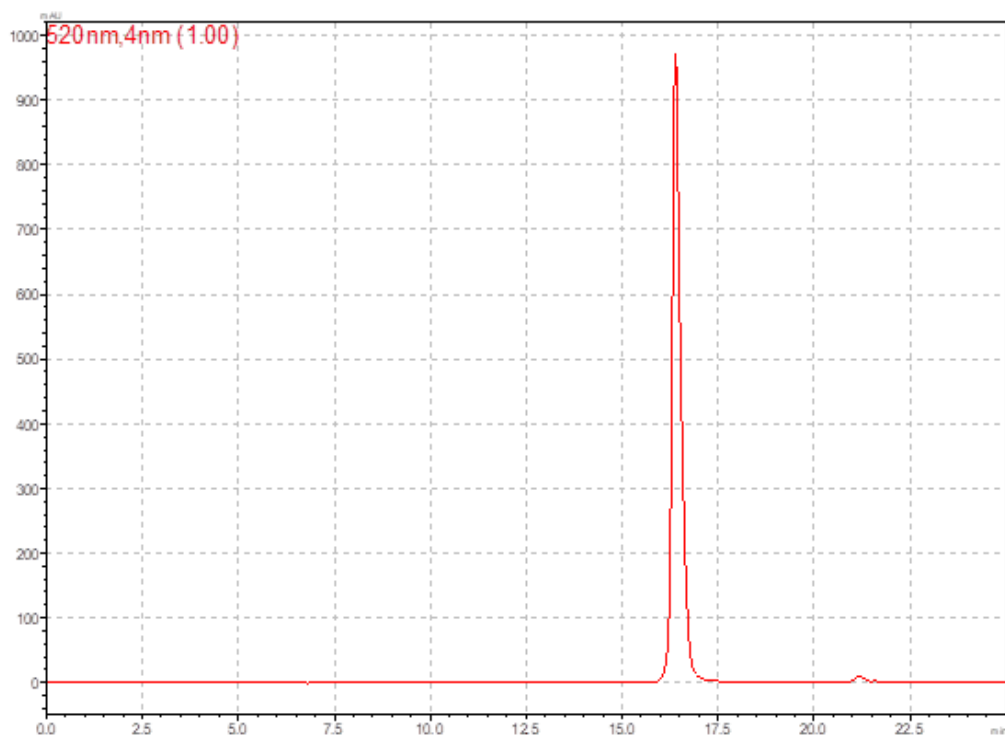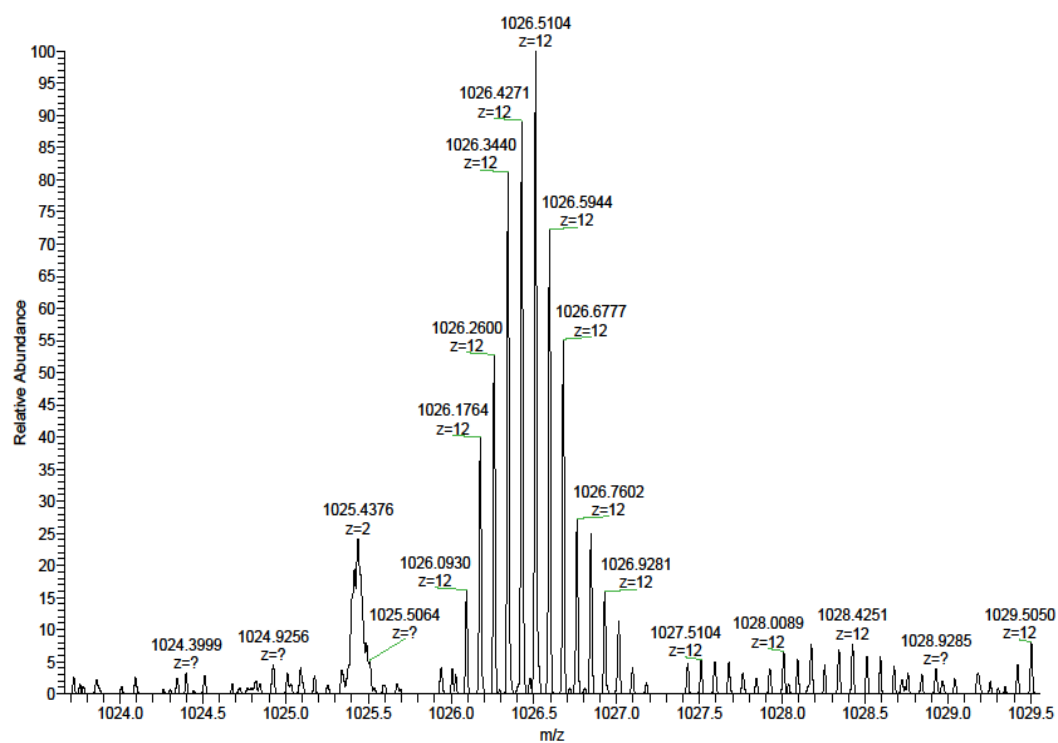
Oligonucleotide **S14** (ESI-MS: negative mode, MeOH):
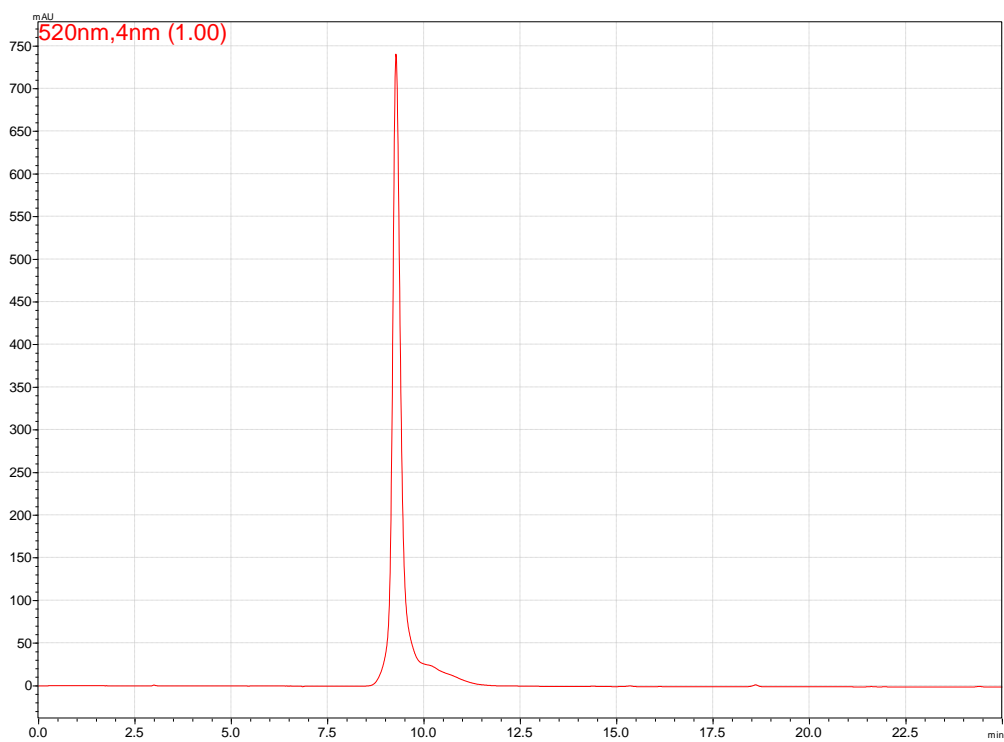
Oligonucleotide **S15** (ESI-MS: negative mode, MeCN/(Et₃NH)OAc):

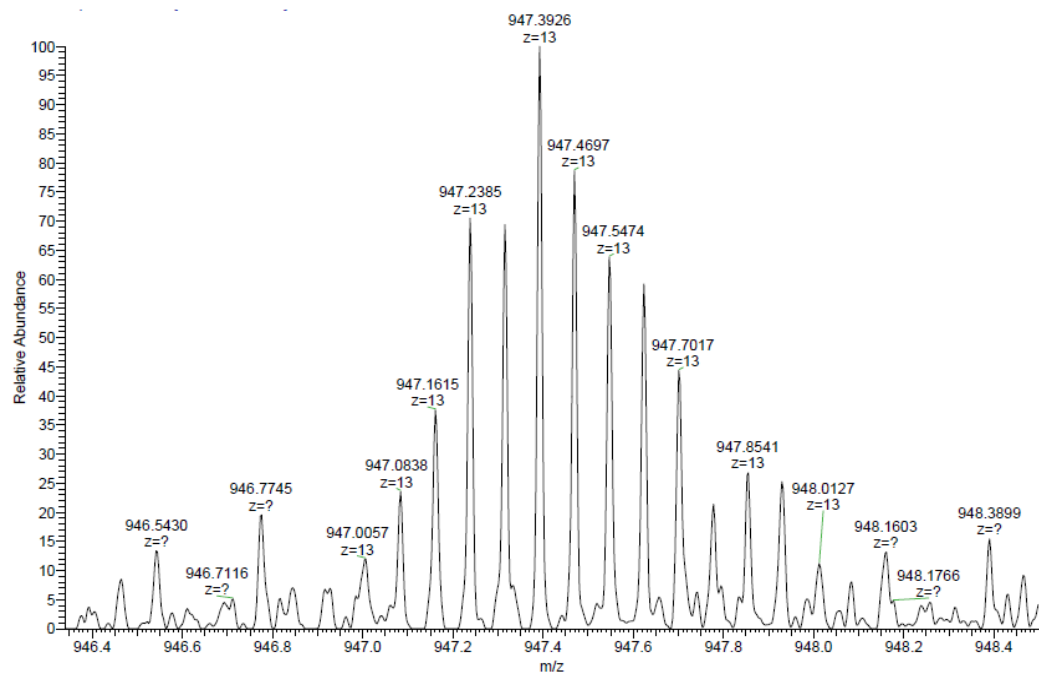Oligonucleotide **S16** (ESI-MS: negative mode, MeCN/(Et₃NH)OAc):

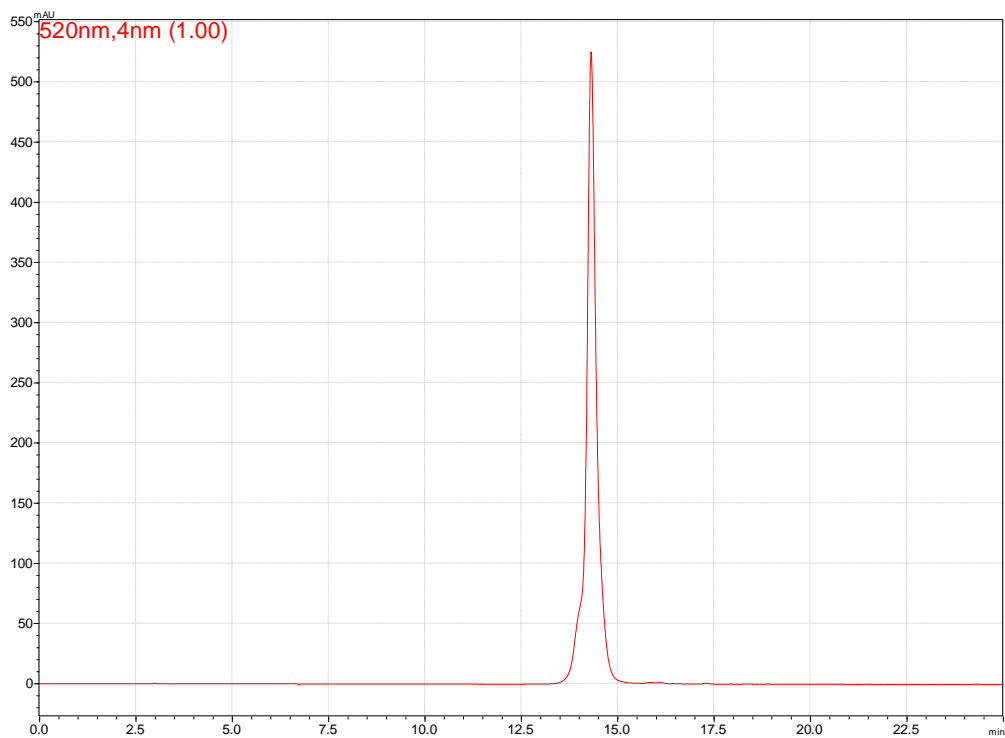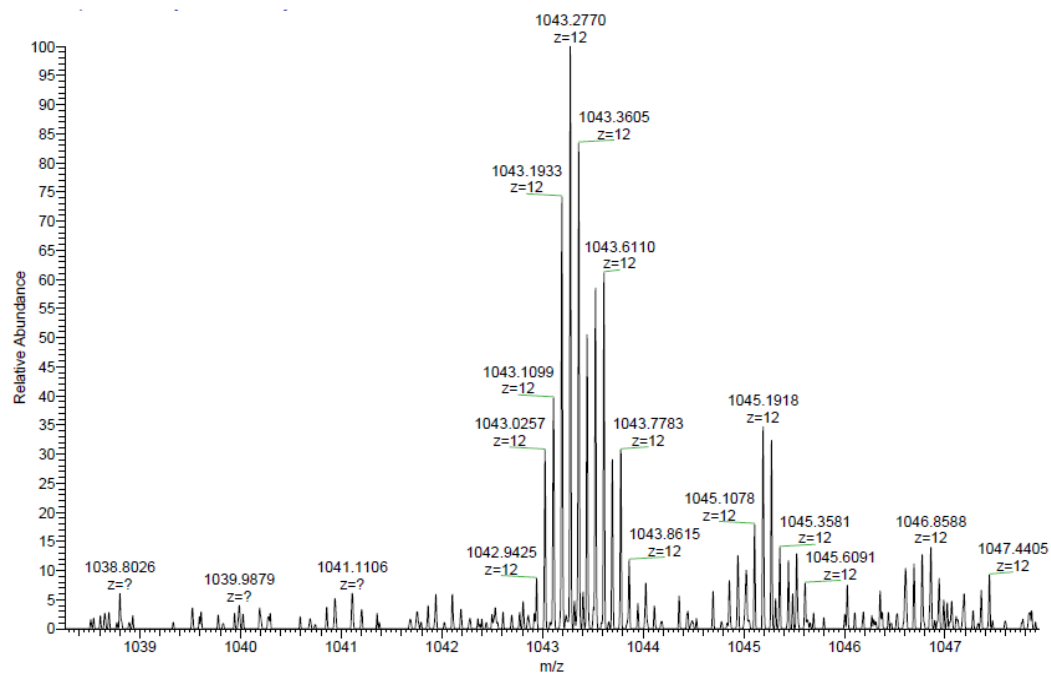Oligonucleotide **S17** (ESI-MS: negative mode, MeOH):

Oligonucleotide **S18** (ESI-MS: negative mode, MeOH):

Declaration of consent

on the basis of Article 18 of the PromR Phil.-nat. 19

Name/First Name: Markova Larysa

Registration Number: 15-140-411

Study program: Chemistry and Molecular Sciences

Bachelor ☐ Master ☐ Dissertation ☒

Title of the thesis: Supramolecular Polymers from Oligophosphodiesters Containing Squaraine or Cyanine Chromophores

Supervisor: Prof. Dr. Robert Häner

I declare herewith that this thesis is my own work and that I have not used any sources other than those stated. I have indicated the adoption of quotations as well as thoughts taken from other authors as such in the thesis. I am aware that the Senate pursuant to Article 36 paragraph 1 litera r of the University Act of September 5th, 1996 and Article 69 of the University Statute of June 7th, 2011 is authorized to revoke the doctoral degree awarded on the basis of this thesis. For the purposes of evaluation and verification of compliance with the declaration of originality and the regulations governing plagiarism, I hereby grant the University of Bern the right to process my personal data and to perform the acts of use this requires, in particular, to reproduce the written thesis and to store it permanently in a database, and to use said database, or to make said database available, to enable comparison with theses submitted by others.

Place/Date

Signature

Curriculum Vitae

Larysa Markova

Personal Information

Date and place of birth	July 22, 1983, Kharkiv, Ukraine
Address	Gewerbestrasse 20, Bern CH-3012, Switzerland
Phone	+41767199251
E-mail	larysya.markova@gmail.com

Education

2016 – present	Ph.D. student, the group of Prof. Robert Häner, Department of Chemistry and Biochemistry, University of Bern, Switzerland.
2004 – 2006	M.Sc. in Chemical Science, Department of Technology of Organic Compounds of National Technical University "Kharkiv Polytechnical Institute," Kharkiv, Ukraine.
2000 – 2004	B.Sc. in Chemical Science, Department of Technology of Organic Compounds of National Technical University "Kharkiv Polytechnical Institute," Kharkiv, Ukraine.

Publications

Markova L.I., Terpetschnig E.A., Patsenker L.D. Comparison of a Series of Hydrophilic Squaraine and Cyanine Dyes for Use as Biological Labels. Dyes and Pigments, 2013, 99, 561–570.

Markova L.I., Malinovskii V.L., Patsenker L.D., Häner R. J- vs. H-type Assembly: Pentamethine Cyanine (Cy5) as a Near-IR Chiroptical Reporter. Chem. Commun., 2013, 49, 5298–5300.

Markova L.I., Fedyunyayeva I.A., Povrozin Y.A., Semenova O.M., Khabuseva S.U., Terpetschnig E.A., Patsenker L.D. Water-Soluble Indodicarbocyanine Dyes Based on 2,3-Dimethyl-3-(4-sulfobutyl)-3H-indole-5-sulfonic acid. Dyes and Pigments. 2013, 96, 535–546.

Markova L.I., Malinovskii V.L., Patsenker L.D., Häner R. Synthesis and Properties of Squaraine-Modified DNA. Org. Biomol. Chem., 2012, 10, 8944–8947.

Povrozin Y.A., Markova L.I., Tatarets A.L., Sidorov V.I., Terpetschnig E.A., Patsenker L.D. Near-Infrared, Dual-Ratiometric Fluorescent Label for Measurement of pH. Anal. Biochem., 2009, 390, 136–140.